P-09-49

Site investigation SFR

Hydrogeological modelling of SFR Data review and parameterisation of model version 0.1

Johan Öhman
Golder Associates AB

Sven Follin
SF GeoLogic AB

January 2010

Svensk Kärnbränslehantering AB
Swedish Nuclear Fuel
and Waste Management Co

Box 250, SE-101 24 Stockholm
Phone +46 8 459 84 00

ISSN 1651-4416
SKB P-09-49

Site investigation SFR

Hydrogeological modelling of SFR Data review and parameterisation of model version 0.1

Johan Öhman
Golder Associates AB

Sven Follin
SF GeoLogic AB

January 2010

Keywords: P-report SKBDoc id 1243761, Review statement SKBDoc id 1243509, SFR, Structural data, Hydraulic data, Parameterisation, Transmissivity, Deformation zones, Hydraulic conductivity, Rock mass, Spatial variability, Depth dependence, Project SFR extension.

Abstract

The primary objective of the ongoing hydrogeological investigations at SFR is to develop a description of the hydrogeological system inside the SFR regional model domain. The descriptive model should provide preliminary parameter values to a mathematical flow model, which will be for safety assessment and design analyses. This document reports the results gained by a compilation and re-interpretation of existing hydraulic data. The compilation and re-interpretation of the hydraulic data was based on a preliminary version of the updated bedrock geological model by /Curtis et al. 2009/. Aspects that impose uncertainty both in the hydrogeological conceptual description and its mathematical implementation and performance, such as poor data quality and data coverage in combination with spatial variability, are also discussed.

Sammanfattning

Huvudsyftet med de pågående hydrogeologiska undersökningarna vid SFR är att utveckla en beskrivning av de hydrogeologiska förhållandena inom det regionala modellområdet för SFR. Den beskrivande modellen innefattar en preliminär parameterisering av en matematisk flödesmodell, som ska användas för säkerhets- och konstruktionsanalyser. Föreliggande rapport redovisare resultaten från en sammanställning och omtolkning av befintliga hydrauliska data. Arbetet som utförts baserar sig på en preliminär version av den uppdaterade berggrundsmodellen som är under utveckling av /Curtis et al. 2009/. Rapporten tar även upp olika omständigheter som på ett eller annat sätt skapar osäkerheter i den beskrivande modellen och parameteriseringen av den matematiska modellen, som exempelvis låg datakvalitet och låg täckningsgrad (datadensitet) i kombination med spatial variabilitet.

Contents

1 Introduction

1.1 Background

In 1987, the first stage of a final repository for low and intermediate level radioactive operational waste (SFR) was constructed and taken into operation. An investigation programme for its future extension was initiated in 2008 by the Swedish Nuclear Fuel and Waste Management Company (SKB). This extension of SFR is necessitated by the pending decommissioning of the closed reactors Barsebäck, Studsvik and Ågesta, the additional amounts of operational waste associated with the extended operating time of the remaining nuclear power plants, as well as the future decommission of running nuclear power plants Oskarshamn, Forsmark, and Ringhals /SKB 2008/.

This document reports the results gained by a compilation and re-interpretation of existing hydraulic data, which is one of the activities performed within the ongoing site investigation programme at SFR, which involves the disciplines: geology, rock mechanics, hydrogeology and hydrogeochemistry. The work reported here was carried out in accordance with activity plan AP SFR-08-022.The controlling documents for performing this activity are listed in Table 1-1. Both the activity plan and the method descriptions are SKB's internal controlling documents.

Table 1-1. Controlling documents for the performance of the activity reported here.

Activity plan	**Number**	**Version**
Platsmodellering, Hydrogeologi version 0.1	AP SFR-08-022	1.0
Method descriptions	**Number**	**Version**
Hantering av data och modeller inom Projekt SFR -utbyggnad - delprojekt undersökningar	SKB MD SDU-203	2.0
Hantering av primärdata vid platsundersökningar	SKB MD SDK-508	

1.2 Objectives

The primary objective of the ongoing hydrogeological investigations at SFR is to develop a description of the hydrogeological system inside the SFR regional domain (Figure 1-1). Specifically, the descriptive model should provide parameter values to a *groundwater flow model*, which will be used by Safety Assessment and Design for predictions. In addition to the new data gathered from the ongoing hydrogeological investigations at SFR, the hydrogeological description should also comprise, to the extent possible, the huge amount of hydrogeological information available from the constructions of the Forsmark nuclear power plant and the existing SFR /Carlsson et al. 1986, 1987, Axelsson and Mærsk Hansen 1997, Axelsson et al. 2002, Holmén and Stigsson 2001/, as well as from the nearby site investigations for a deep repository for high level spent nuclear fuel /Follin et al. 2007b/.

A second objective is to provide feedback to the overall SFR field investigation programme /SKB 2008/ and to bring attention to important conceptual uncertainties that need to be resolved in time due. It is imperative that the contributing disciplines (geology, rock mechanics, hydrogeology, and hydrogeochemistry) iteratively exchange feedback during the sequential development of model versions in order to improve and /or reinforce the characterisation of the hydrogeological system, but also to attain interdisciplinary conceptual model consistency and creditability.

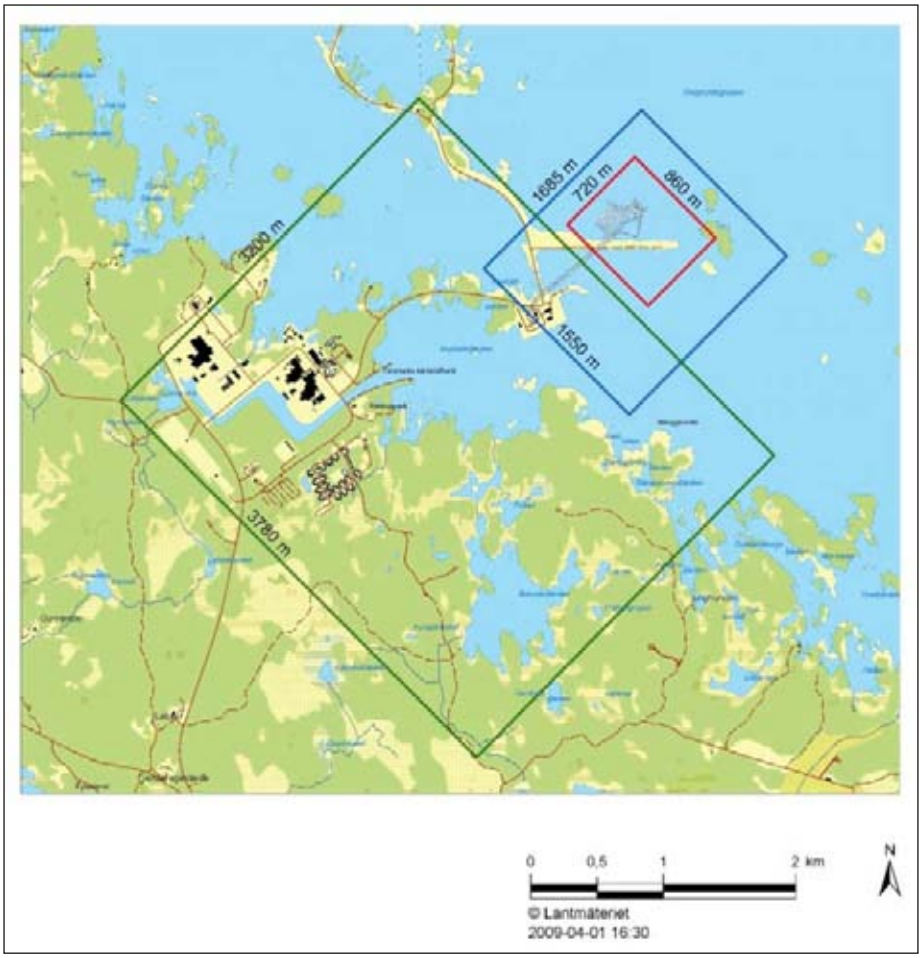

Figure 1-1. *Regional (blue) and local (red) model domains of the SFR flow model version v. 0.1, in relation to the local model area of Forsmark Site Investigation, model v. 2.2 (green).*

Four key issues have been specified for the hydrogeological modelling at SFR /SKB 2008/:

1) Hydraulic properties of interpreted low-magnetic lineaments (i.e. HCDs).
2) Hydraulic properties of the bedrock between the deformation zones within target model volume (i.e. HRD).
3) The extent and character of hydraulic connectivity within the target volume as well as the hydraulic connectivity to the surrounding bedrock.
4) Spatial extent and hydraulic properties of sheet joints and gently dipping deformation zones.

Other issues important to address in conceptual hydrogeological modelling have been raised by /Follin et al. 2007a/:

5) Is there a general observation that deformation zones are more conductive than the surrounding bedrock?
6) Is there any data support for dividing the bedrock between the deformation zones into different sub domains?
7) What is the statistical significance of a potential depth dependence in the fracture transmissivity?

These issues are crucial to the overall hydrogeological modelling at SFR. The particular scope of this work is specified in Section 1.5.

1.3 Model versions

The ongoing investigation programme at SFR involves field investigations inside the target area (Figure 1-1) as well as modelling. The hydrogeological modelling is to be developed in three model versions, 0.1, 0.2 and 1.0, that successively incorporate data from the ongoing SFR field investigations and the feedback from the other modelling disciplines. The work follows SKB's established methodology for modelling /Rhén et al. 2003/ and /Follin et al. 2007a/ and described in Chapter 2.

Flow model version v. 0.0 of SFR /Odén 2009/ was an implementation of the flow model developed by /Holmén and Stigsson 2001/ in DarcyTools v. 3.1. Hence, the objective of flow model version v.0.0 was to reproduce the modelling results from the previous state-of-the-art model of SFR using a different computer code (software) than /Holmén and Stigsson 2001/. The DarcyTools program package is comprehensively described in /Svensson et al. 2010, Svensson and Ferry 2004, Svensson 2004/.

The work reported here presents the suggested hydraulic parameterisation for flow model version v. 0.1. The associated flow modelling is reported in /Öhman 2010/. The parameterisation was carried out in two steps. First, a review of historic hydraulic data was made, i.e. hydraulic data available prior to the initiation of the current SFR investigation programme. Second, the historic data was fitted to a preliminary version of the geological model of SFR v.0.1 /Curtis et al. 2009/. In other words, flow model version v. 0.1, is based on the same hydraulic data as /Holmén and Stigsson 2001/, but uses an updated model of the geological structures. The development of SFR geologic model v.0.1 was still in progress during this study, and therefore a preliminary version, available per 2008-12-19, was used. The differences between the preliminary and the final model versions are specified in Appendix F.

The data from the ongoing hydrogeological investigations at SFR will be implemented in two forthcoming flow model versions of SFR denoted as versions v. 0.2 and v. 1.0, respectively. Flow model version v. 0.2 will primarily be based on new hydraulic data, obtained in the ongoing field investigations of the SFR extension programme. Additionally, flow model version v.0.2 will incorporate feedback and conceptual updates from the other disciplines (geology, rock mechanics, hydrogeology, and hydrogeochemistry). Flow model version 1.0 is intended to provide a foundation for the long-term safety assessment and the detailed design.

1.4 Hydraulic domains

Conceptually, the hydrogeological system is subdivided into three hydraulic units: Hydraulic Soil Domain (HSD), Hydraulic Conductor Domain (HCD), and Hydraulic Rock Domain (HRD), see Figure 1-2. Thus, the flow model requires a geometrical definition of the spatial extent and a hydraulic parameterisation (assignment of hydraulic properties) of each hydraulic domain. It is noted that each of the three hydraulic domains may be split into two or several subdomains, see the site descriptive modelling /Follin et al. 2007b/ for an example.

The parameterisation of the bedrock units (HCD and HRD) has followed a methodology developed and applied in the site investigation programme /Follin et al. 2007b/ in which the hydraulic borehole data are analysed and classified as belonging to either HCD or HRD based on the prevailing structural model. More precisely, in a first step, the recently updated structural geological model is used to classify hydraulic data as belonging to either the HCD or to the HRD, and in a second step, preliminary effective HCD and HRD parameters are calculated from the different populations (types) of hydraulic data. This methodology is explained in more detail in Chapters 3 and 4.

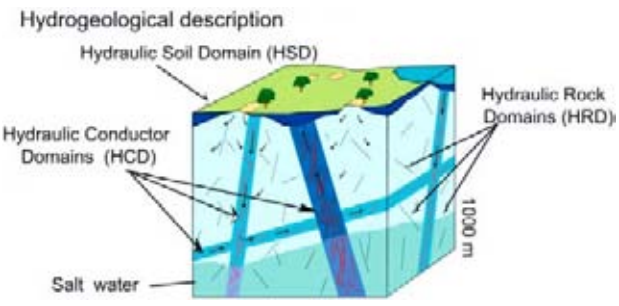

Figure 1-2. *The hydraulic subdomains of a hydrogeological model /Rhén et al. 2003/.*

1.5 Scope of model version v.0.1

As explained in sections 1.2 and 1.3 a specific aim of this study is to characterise the hydraulic domains HCD and HRD according to the geometrical definitions of the preliminary geological model SFR v.0.1[1]. The purpose is to provide a parameterisation for the SFR flow model v.0.1 /Öhman 2010/. This parameterisation constitutes a re-assessment of all relevant hydraulic data existing prior to the initiation of the SFR extension programme (i.e. prior to 2008). In other words, the review is delimited to data from the construction of SFR and the nearby Forsmark Site Investigation (see Section 1.7). The data from ongoing field investigation within the SFR extension programme are excluded from this study, but will be incorporated in the subsequent hydrogeological model SFR v.0.2.

The historic data are analysed with respect to the updated of the structural model (cf. Figure 1-3 and Figure 1-4). The structural model was still under development by the geological team during the time of this study. Therefore a preliminary version of the structural model (available per 2008-12-19) was used as the geometrical definitions for HCD and HRD. The differences between the preliminary version and the final SFR geologic model v. 0.1 are specified in Appendix F. More specifically, there are 58 updated geological structures (HCDs) which require hydraulic parameterisation (Figure 1-4) along with an effective conductivity value for the HRD.

This study also raises aspects that impose uncertainty both in the hydrogeological conceptual description and its numerical implementation and performance, such as poor data quality and data coverage in combination with spatial heterogeneity.

The HSD parameterisation is not included in this study, but the HSD has been modelled in other works, see e.g. /Bosson et al. 2008, Brydsten 2006, Hedenström et al. 2008/.

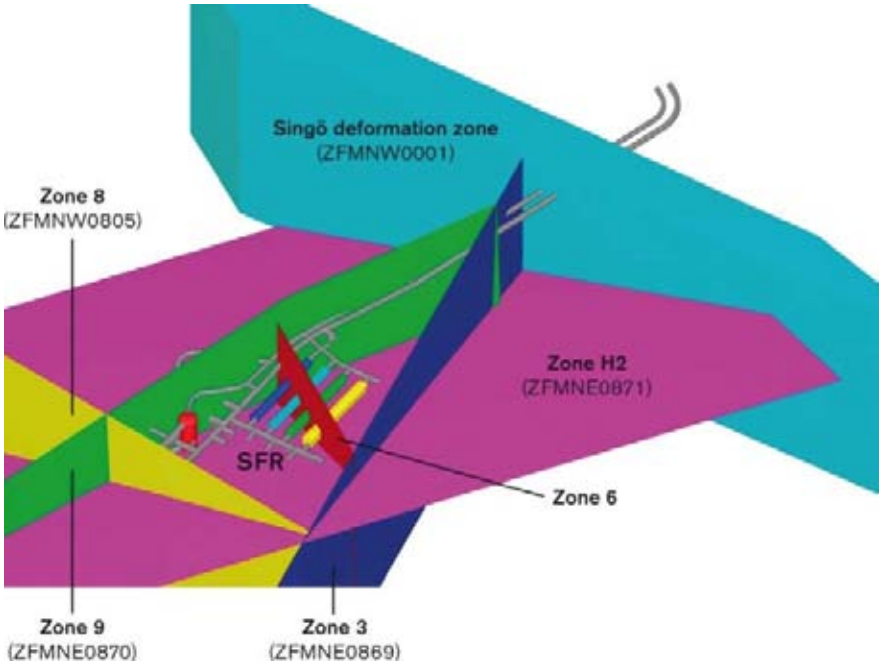

Figure 1-3. *Local structural model /Axelsson and Mærsk Hansen 1997/ used in the previous hydrogeological modelling /Holmén and Stigsson 2001, Odén 2009/. The zones are specified both according to the SFR terminology and the system established during site investigations Forsmark. Reproduced from /SKB 2004/.*

[1] 1 SKBdoc 1224847 - DZ_SFR_REG_v0.1_prelim, Version 0.1, 2010-06-08, (access might be given on request).

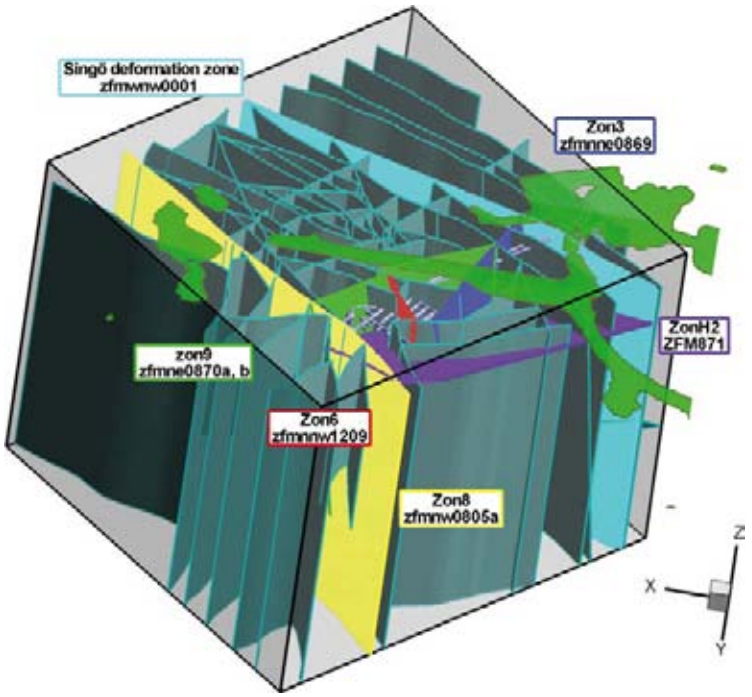

Figure 1-4. *Deformation zones of the regional SFR domain (58), as defined in the preliminary structural model SFR v. 0.1, the zones that existed in the previous structural model /Axelsson and Mærsk Hansen 1997/ are shown in similar colours as in (Figure 1-3) with both the original and the current terminology.*

1.6 Model volumes

Two different scales were used in the structural model: one regional and one local. These were originally defined in /SKB 2008/. It can be noted that the model domains are considerably smaller than the corresponding domains used in the Site Investigation programmes (e.g. Figure 1-1). In the Regional model domain, a lineament cut-off length of 1,000 m was applied, whereas shorter lineaments were included in the Local model domain. The Local model covers the existing SFR and the rock volume for the planned SFR extension. The areal extent of the two model domains are defined in Table 1-2. The Local model extends vertically from a top elevation of 100 m.a.s.l. down to 300 m.a.s.l. while the Regional model extends down to 1,100 m.a.s.l.

The difference between the regional and local model volumes is primarily a matter of characterisation-scale for deterministic geological structures /Curtis et al. 2009/, which in turn relates to the resolution scale for the modelled processes, e.g. simulated flow field and particle trajectories.

Table 1-2. Coordinates defining the model volumes for SFR. RT90 (RAK) system.

Local model volume		Regional model volume	
Easting	**Northing**	**Easting**	**Northing**
1631920.0000	6701550.0000	1632550.0000	6701880.0000
1633111.7827	6702741.1671	1633059.2484	6702388.9854
1634207.5150	6701644.8685	1633667.2031	6701780.7165
1633015.7324	6700453.7014	1633157.9547	6701271.7311

1.7 Data used

The hydrogeological model SFR v.0.1 is based on all hydraulic data inside the SFR regional domain (Table 1-2; Figure 1-1) that were available prior to the initiation of the SFR extension programme (i.e. hydraulic data measured prior to 2008). Most hydraulic data origin from the early investigation campaigns and construction phases of the existing SFR repository, measured during the 1980's, while later data come from the nearby Site Investigation Forsmark. No data from the ongoing field investigation within the SFR expansion programme are used in this model version; these latter data will be incorporated in hydrogeological model SFR v.0.2. All hydraulic data and borehole geometry data analysed in this study have been officially delivered from the primary data base (Sicada) or taken directly from a referable report (Table 1-3 and Table 2-2). The hydraulic data in KFR61–KFR67, HFR01–HFR06, and the upper half of KFM11A were delivered at a late stage of this project and were therefore not included in the general analysis (Section 5). However, the upper half of KFM11A contains particularly useful data for the definition of three HCDs (Figure B-4), and therefore calculations based on these data are reported in the summarized results (Table 6-1, Table 6-2, and Table 6-3).

The geometrical data on hydraulic conductor domains (HCDs) and their borehole intercepts are taken from the preliminary deformation zone model /Curtis et al. 2009/. For traceability, such geometrical data have been transferred from the geological modelling team via SKBdoc (Table 1-3).

Table 1-3. Summary of data.

Table /file	Description	Source
Hydraulic data		
steady_state_inj_cd	Single-hole hydraulic test, SFR	Sicada_08_199
pressure_build_up_cd	Single-hole hydraulic test, SFR	Sicada_08_199
transient_inj_cd	Single-hole hydraulic test, SFR	Sicada_08_199
falling_head_test_cd	Single-hole hydraulic test, SFR	Sicada_08_199
interference_cd	Cross-hole hydraulic test, SFR	Sicada_08_199
p_transmissivity.xls	Single-hole hydraulic test, KFM11A and HFM33–35	Sicada_09_067 Sicada_08_208
hms_press_monitoring	Point-water head, KFM11A and HFM33–35	Sicada_08_199
steady_state_inj_cd	Single-hole hydraulic test, SFR	Sicada_10_003
	Impeller flow logging data HFM33–35	/Gustavsson et al. 2006/
Geometrical data		
p_object_location	Borehole geometry (SFR boreholes, KFM11A, HFM33–35)	Sicada_08_199
object_location	Borehole geometry (HFR01–06, KFR61–67)	Sicada_10_003
Preliminary Geologic model SFR v. 0.1[2]	Deformation zone geometry (RVS) Preliminary version, available per 090212	See footnote
Extended version of ZFM871[3]	Separate, preliminary geometric definition of ZFM871 (RVS) that extends outside the Regional SFR domain	See footnote
Deformation zone properties[4]	Preliminary geometric/geologic properties of zones	See footnote
Borehole intercepts of zones[5]	Geometric borehole intercepts for zones (RVS)	See footnote
Borehole intercept envelopes[6]	Confidence envelopes for borehole intercepts with deformation zones, based on geometric uncertainty evaluation	See footnote

[2] SKBdoc 1224847 - DZ_SFR_REG_v0.1_prelim, Version 0.1, 2010-06-08, (access might be given on request).

[3] SKBdoc 1228773 - DZ_PFM_REG_v22.01-SFR_hydro_H2, Version 0.1, 2010-06-08, (access might be given on request).

[4] SKBdoc 1228775 - SFR_DZ_REG_Master-zone-report_090212, Version 0.1, 2010-06-08, (access might be given on request).

[5] SKBdoc 1228772 - BH_DZ_intercepts_jp_090119, Version 0.1, 2010-06-08, (access might be given on request).

[6] SKBdoc 1228776 - SFR_Template_RANK DZ_090130_JP_PCU_v4, Version 0.1, 2010-06-08, (access might be given on request).

1.8 This report

This report is organised as follows:

- Chapter 2 presents an overview of the available hydraulic and geometric data for this data evaluation and the parameterisation of the hydrogeologic model SFR v. 0.1. For a more comprehensible overview, these data are also visualised as a function of borehole length on a borehole-to-borehole basis in Appendix B.
- Chapter 3 discusses a number of aspects that impose uncertainty both in the hydrogeological conceptual description and its downstream model predictions. These uncertainties arise from low geometric confidence of HCDs and poor data coverage in combination with spatial variability.
- the overall approach and the different algorithms that are used in the analysis of hydraulic data are explained in Chapter 4. This analysis of hydraulic data targets the difference between the HCD and HRD, as well as signs of potential depth trends.
- the results of these analyses are shown in Chapter 5.
- the key observations are summarised in Chapter 6. This chapter also presents the recommended preliminary parameter values for HCD and HRD in the hydrogeologic model SFR v. 0.1.

2 Data overview

2.1 Hydraulic data

The hydraulic data analysed in this study can be divided into two types: a) single-hole measurements over packed-off borehole sections, which reflect the local transmissivity of the surrounding rock, and b) cross-hole measurements (interference tests), which primarily target to confirm or reject hydraulic connectivity between and /or within geological structures (see Section 3.2.3).

2.1.1 Single-hole test data

Single-hole tests are useful for evaluating the local hydraulic properties of the rock around a borehole section. A borehole section, sealed off by double packers, is exposed to a controlled hydraulic disturbance, such that the response of the hydrogeological system can be related to an interval transmissivity, an equivalent porous-media property over an assumed rock volume. In this evaluation, the imposed hydraulic disturbance is a boundary condition over the sealed borehole section, for which the hydraulic properties can be solved; the most common types of disturbances are: constant hydraulic head, constant flow rate, pulse injections (specified volume). Important aspects to consider in the evaluation of transmissivity include (see /Follin et al. 2007b/):

- detection limit (lower measurement limit),
- skin effects,
- duration time of the test (which in turn relates to test scale),
- test scale (borehole interval length),
- fracture network hydraulic diffusivity,
- fracture network connectivity and
- flow dimension.

The single-hole transmissivity data available from the construction of SFR have been measured by four different methods, Falling head (FH), pressure build-up (BU), steady state injection (PH), and transient injection (TI), see Figure 2-1. From the Site Investigation Forsmark there is also data from difference flow logging in KFM11A, down to 490 m borehole length (5 m scale) /Väisäsvaara and Pekkanen 2007/, and PSS3 injection tests down to 840 m (20 m scale) /Harrström et al. 2007/. In the percussion boreholes HFM33, HFM34, and HFM35 there is also HTHB injection tests and flow logged intervals in /Gustavsson et al. 2006/. The HTHB injection tests provide transient transmissivity evaluations and steady state approximations (Moye's formula). The flow logging is less accurate in terms of transmissivity estimates, but provides a better spatial resolution of inflow along a tested borehole.

The test durations of these tests range from a few minutes (falling head) to several hours. The lower measurement limit of interval transmissivity (i.e. detection limit) is dependent on the test duration; the detection limit for the current data set range from approximately 10^{-10} to 9×10^{-8} m^2/s. The dominating data types have detection limits in the range 5×10^{-8} to 9×10^{-8} m^2/s. In this study different data types and scales must be combined to maximise the sample size and data coverage. In these cases the highest detection limit (9×10^{-8} m^2/s) must be assigned to the joined data set. Generally, the detection limit is of lesser importance in the analysis of hydraulic data, as the focus of study is usually on high transmissivity values. However, the censoring effects of the detection limit complicate the analysis of the HRD depth trend (Section 4.2.4). The falling-head tests should be performed until 90% of the pressure pulse has been recovered (i.e. its required duration time depends on the transmissivity of the tested section). This was neglected and therefore falling head data are assigned an overall low confidence compared to other data, and in particular for low falling-head values /Carlsson et al. 1987/.

The transmissivity of a borehole section is known to be scale dependent. The interval transmissivity reflects the accumulated transmissivity of all fractures within the borehole interval, and is typically dominated by a single largest fracture transmissivity. Thus, the longer the test section, the more fractures are intersected and the higher is the probability of intersecting a highly conductive feature. The data

have been measured over intervals ranging from 1.5 m (testing individual fractures) and up to 188 m (entire borehole length). Overall, the most common test scale is 3 meters (see Figure 2-2, Figure 2-3 to Figure 2-6); it is used both in steady state tests and falling head tests. Transient injection tests were performed at either the 2 m or 10 m scale.

In the hydraulic parameterisation of SFR v.0.1, the object is to infer transmissivity variability in terms of: 1) hydraulic domains (HRD/HCD), 2) depth dependency in hydraulic domains, and 3) stochastic heterogeneity within hydraulic domains. Therefore, caution must be taken so as to filter out variability that relates to test methodology (section length, test method, errors, etc.). For example: there are hardly any steady state injection tests below –150 m.a.s.l. while this is the dominating test type above –50 m.a.s.l. (Figure 2-7). Thus, a systematic difference between steady state injection and other test types could be erroneously inferred as depth dependency in transmissivity. At the same time data are scarce and it is therefore preferable to exclude as little data as possible (see Section on depth trend analysis 4.2.4).

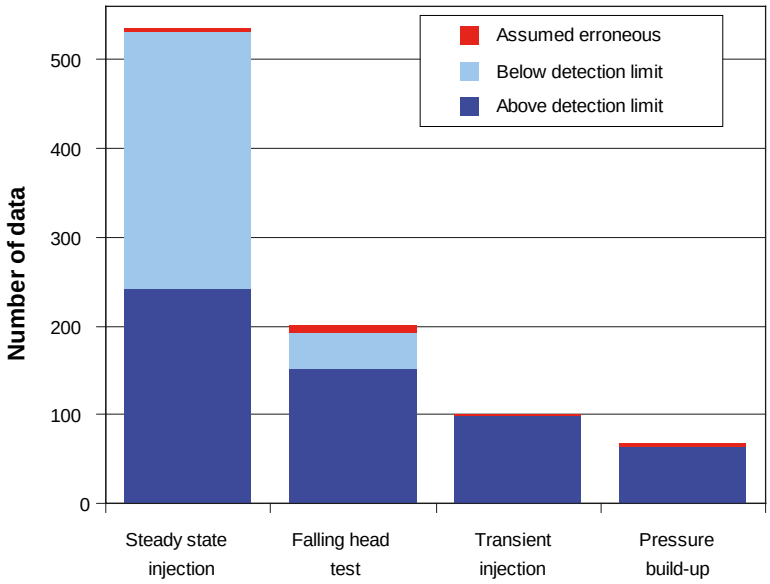

Figure 2-1. *Single-hole hydraulic test types (data from Site Investigation Forsmark excluded).*

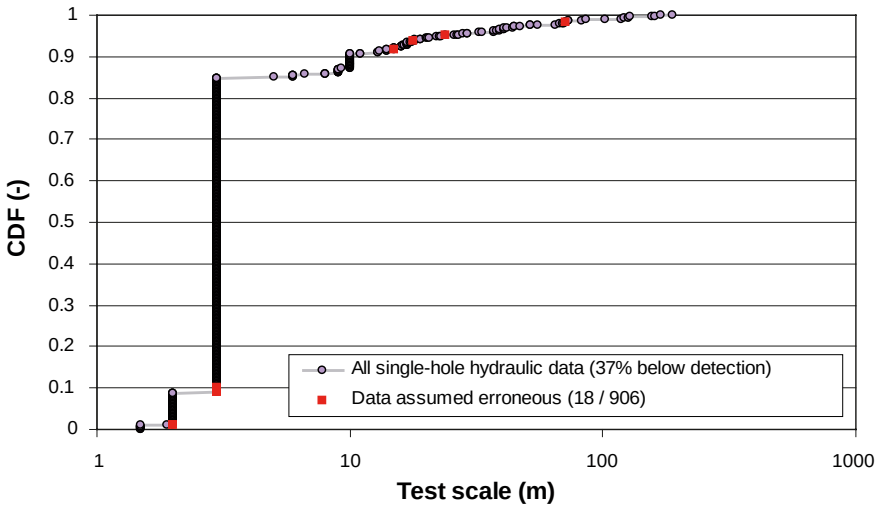

Figure 2-2. *Test-scale distribution of all single-hole hydraulic tests (data from Site Investigation Forsmark excluded).*

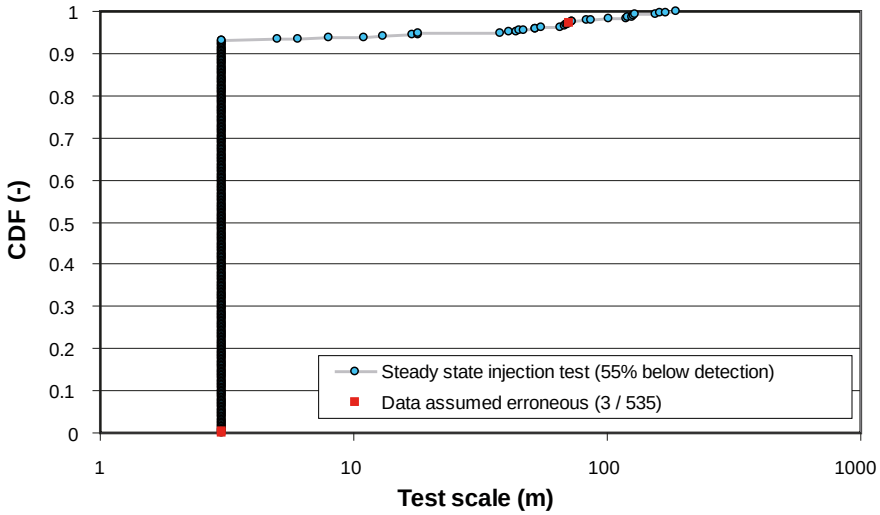

Figure 2-3. *Test-scale distribution of steady-state injection test data.*

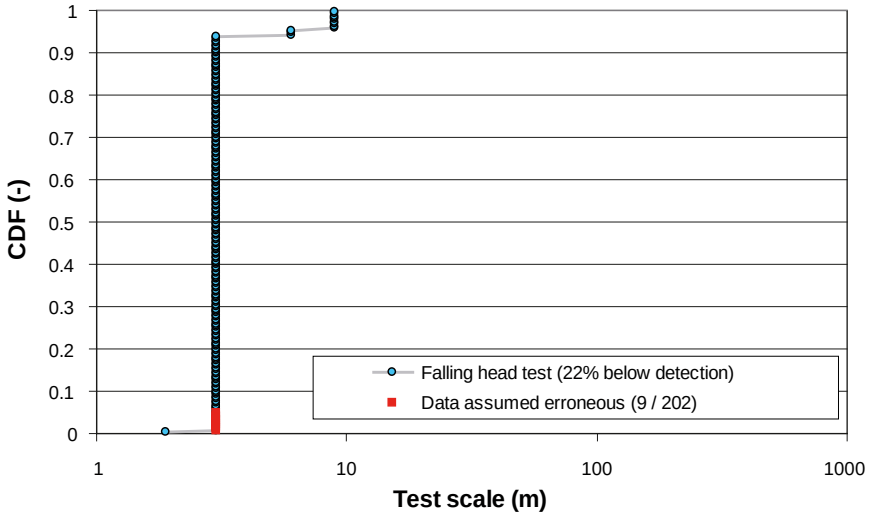

Figure 2-4. *Test-scale distribution of falling head data.*

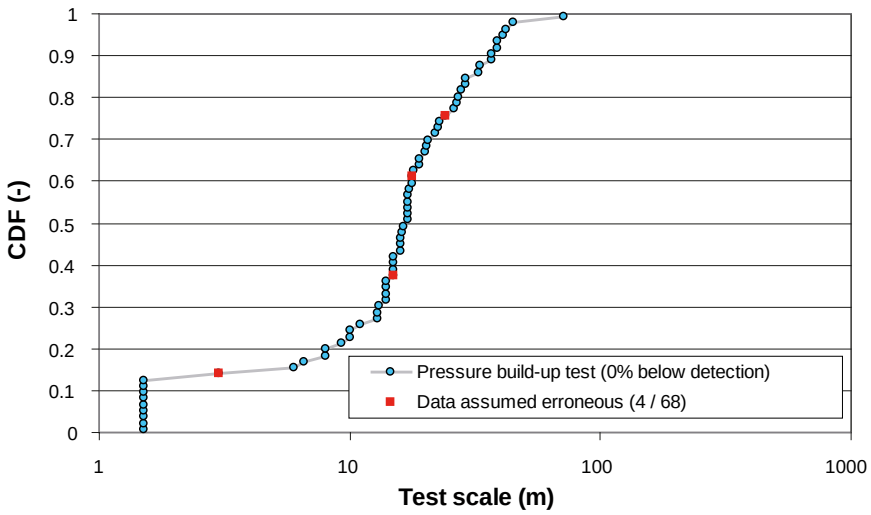

Figure 2-5. *Test-scale distribution of pressure build-up data.*

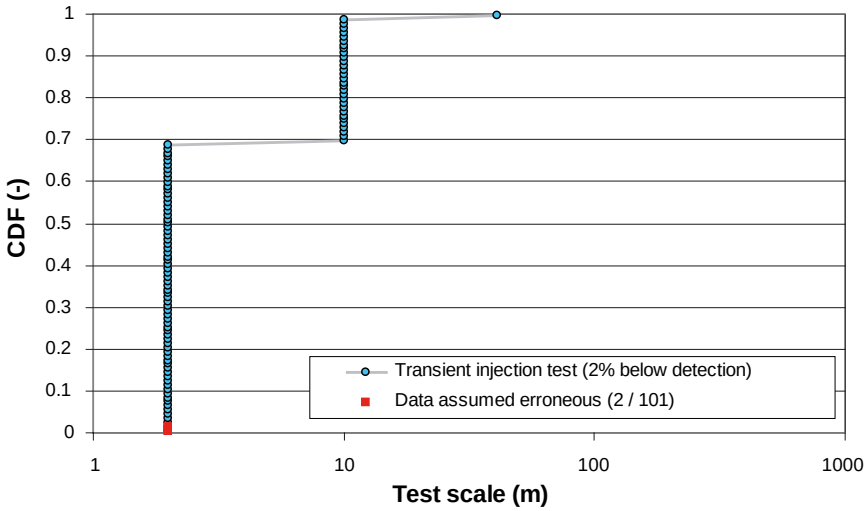

Figure 2-6. *Test-scale distribution of transient injection data.*

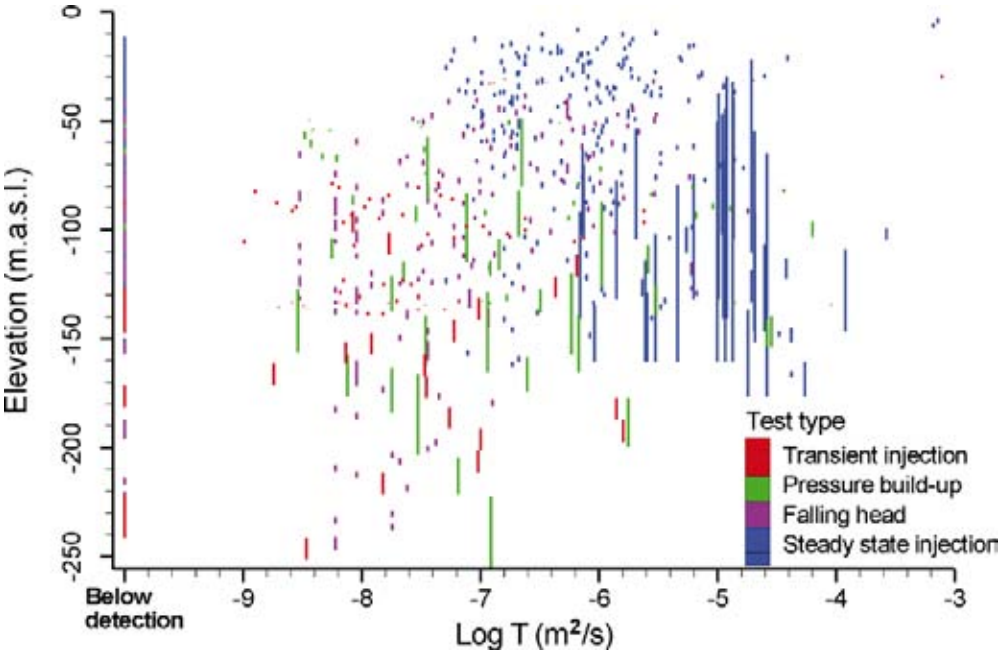

Figure 2-7. *Interval transmissivity with depth. The data set contains different test methods, a range of test scales and reflects both HCD and HRD. Data below detection limit or less than 10^{-9} m^2/s are shown next to y-axis.*

2.1.2 Interference tests

The purpose of interference tests was primarily to test the hydraulic connectivity within and between geologically identified structures for the early SFR geological model /Carlsson et al. 1987/. They were also used to estimate the hydraulic properties of hydraulic cross-hole paths. The interference test is a controlled disturbance over a borehole section which is presumed to intersect the zone of interest. Meanwhile, the response (point water head drawdown) is monitored in surrounding borehole sections. Observed drawdown in surrounding borehole sections can be inferred as direct, or indirect, hydraulic connections between the pumped and the observed borehole sections. In order to avoid disturbances caused by the tunnel construction work, the interference tests were performed during periods of longer work interruptions, such as vacations and weekends /Carlsson et al. 1987/.

The interference tests included in this study were performed 1985 to 1986 /Arnefors and Carlsson 1985, Andersson et al. 1986/. The original interpretations, both responses and hydraulic connections between borehole sections /Carlsson et al. 1987/, were later re-interpreted during an update of the structural model /Axelsson and Mærsk Hansen 1997/. The study of /Axelsson and Mærsk Hansen 1997/ also reports two technical incidents: the excavation through ZFM871 (zonH2) during construction of the NBT tunnel and a leaking packer in KFR7C (December 1987 to April 1988), which acted as strong hydraulic disturbances, and thus can be treated as interference tests (although "unintentional"; see Table 2-1).

The experimental setups of the tests (Table 2-1) were targeted to evaluate early hypotheses on the geologic structures of SFR. The interpretations resulted in the structural model of /Carlsson et al. 1987/. However, in this analysis all hydraulic data are analysed in context of the recently updated geological model /Curtis et al. 2009/. Thus, a tested borehole section, initially presumed to cover a specific zone /Carlsson et al. 1987/, may have been re-classified as HRD or even to cover another zone according to the current geological model (see Table 2-1).

For a given disturbance (flow rate, time, and distance), the drawdown in an observation section can be related to effective hydraulic properties of a hydraulic path (Figure 2-8). This was done by means of type-curve matching techniques under assumptions of idealised continuum concepts /Arnefors and Carlsson 1985, Andersson et al. 1986/, see also Appendix G. It can be noted that the effective conductivity values are generally larger than both the single-hole records (both for the test section and the observation section; Figure 2-8). Although the hydraulic connections are expected to be highly conductive, as flow is known to follow paths of least resistance, it is difficult to explain how higher conductive values can be evaluated between measuring points with more than one order of magnitude lesser conductivity. It is very difficult to assess the confidence in such values, and therefore it was decided to only use single-hole data for the calculation of HCD transmissivity. At this early modelling stage, the interference test data are only inspected to qualitatively examine the agreement between inferred hydraulic connections and structures defined in the geological model /Curtis et al. 2009/. However, these interference data may provide important calibration criteria for the final SFR hydrogeologic model v. 1.0.

Table 2-1. Summary of interference test interpretations (non-responding sections excluded).

					Number of sections with responses [3]								
Tested section	Original interpretation[1]	Updated structural interpretation[2]	Current geological model SFR v.0.1[3]	Envelope coverage [4]	HRD	ZFM871	ZFMne0870a	ZFMne0870b	ZFMnne0869	ZFMnnw0999	ZFMnw0805a	ZFMnw0805b	ZFMwnw0001
KFR04 (28–43 m)	zon9	zon9	zon9	30%	4	1	3	4					
KFR55 (22–39 m)	zon9	zon9	zon9	53%	2	2		8					
KFR55 (40–48 m)	zon9	zon9	HRD	0%	2	1		3					
KFR7B (8–21 m) [5)]	zonH2	zonH2	zonH2	53%	2	7		2		1	4	2	
KFR13 (54–77 m)	zonH2	zonH2	zonH2	72%	2	5		4		1	1		
KFR80 (1.5–20 m)[2)]	–	zonH2	zonH2	100%	6	6	2	13					2
KFR7C (3–34 m) [2)]	–	zonH2	zonH2	100%	3	9		6			2	2	
KFR09 (43–62 m)	zon3	zon3	zon3	27%	1	3			5				
KFR10 (87–107 m)	zon3	–	zon3 /H2	38%									
KFR83 (5–20 m)	zon3	zon3	zonH2	100%	1	3			6				
KFR08 (63–104 m)	zon8	zon8	zon8 [6]	100%		2					2	1	

Terminology key: ZFMnw0805a = zon8, ZFMnne0869 = zon3, ZFMne0870b = zon9, ZFM871 = zonH2.

[1] as summarized by /Carlsson et al. 1987/

[2] /Axelsson and Mærsk Hansen 1997/

[3] Current geological model SFR v.0.1 /Curtis et al. 2009/

[4] Fraction of HCD hydraulic envelope covered by the tested borehole section (see section 3.2).

[5] Due to instrumental failure in the first test (1985-12-26), it was repeated 1986-03-27, with additional monitoring sections.

[6] According to the geological model, the tested interval intersects two zones: ZFMnnw0999 and ZFMnw0805a.

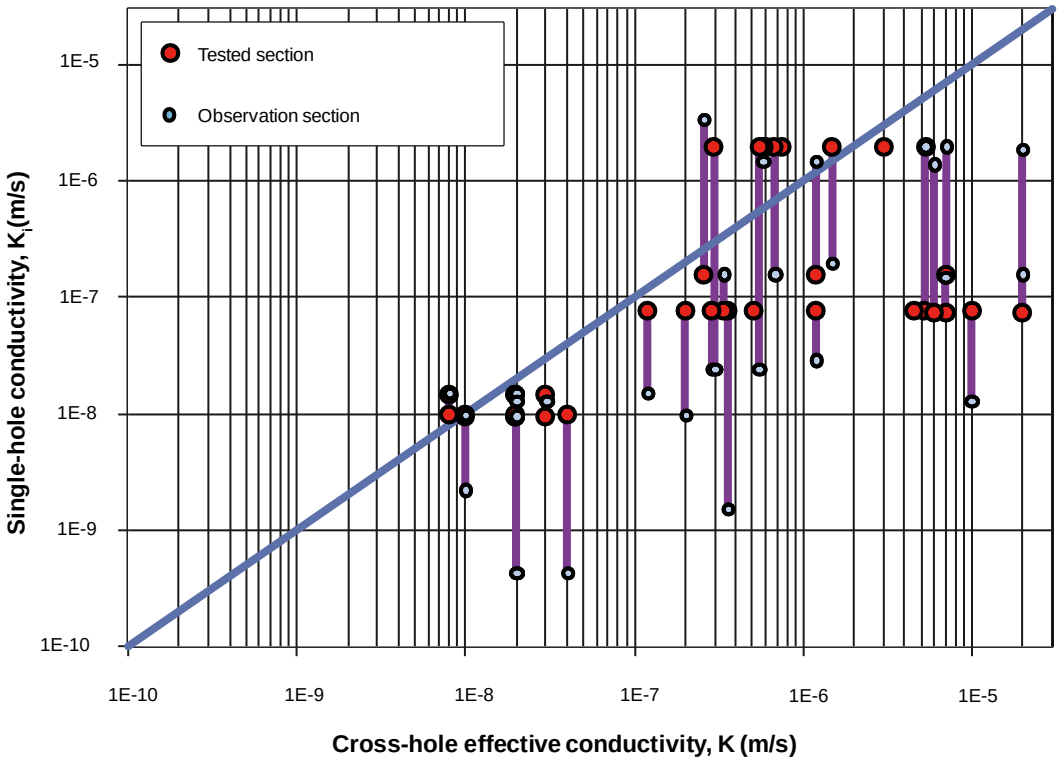

Figure 2-8. *Relation between single- and cross-hole conductivity values. The single-hole conductivities (tested, respectively, monitored sections) calculated by interval transmissivity divided by section length from pressure build-up tests, while the effective conductivity of hydraulic paths are calculated by type-curve matching techniques (see Appendix G).*

2.2 Geometric data

Altogether, there are 42 available boreholes with single-hole hydraulic data, out of totally 60 documented inside the SFR regional domain (Figure 2-9, Table 2-2). In the development of the geological model SFR v.0.1 /Curtis et al. 2009/, 11 of these boreholes (green, Figure 2-9) were selected for geological re-interpretation, based on their expected intercepts with deformation zones according to the previous structural model /Axelsson and Mærsk Hansen 1997/. The HCD intercepts in these 11 boreholes are referred to as "target HCD intercepts", and since these intercepts have been determined by means of geological support, they are assigned a relatively high confidence (Table 2-3). The HCD intercepts in the remaining boreholes are referred to as "geometrical HCD intercepts" and assigned a much lower confidence (see more detailed explanation in Section 3.2.1). The low confidence in geometrical intercepts is represented by "hydraulic HCD envelopes" (Table 2-3), which are the estimated confidence bounds for the hydraulic influence of HCDs (Section 3.2.1).

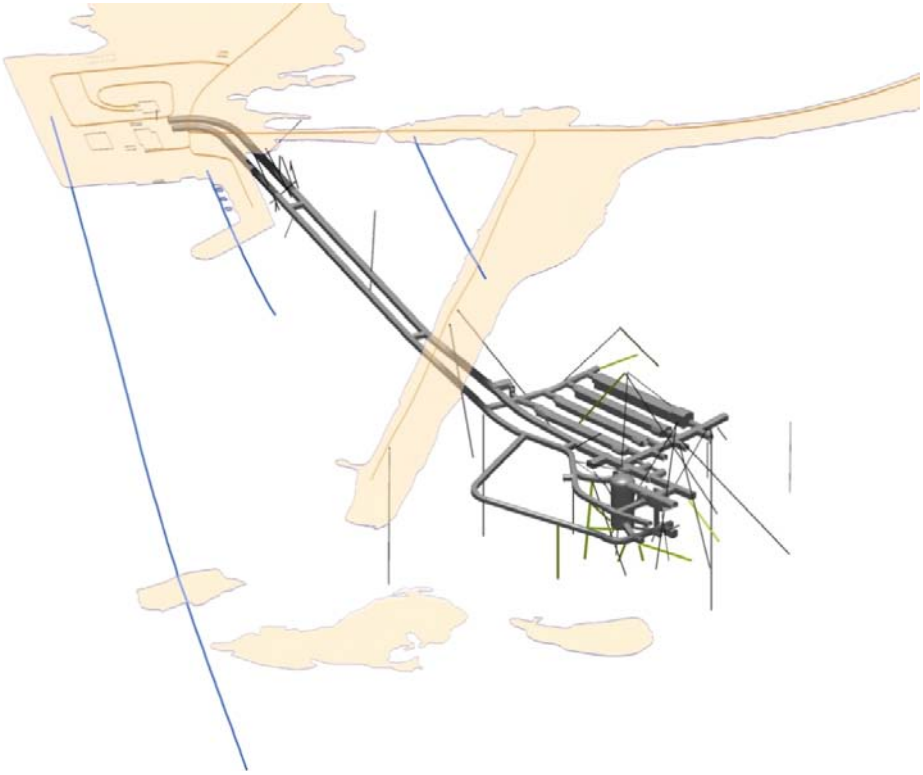

Figure 2-9. *Boreholes inside the regional model volume SFR v. 0.1; geologically reinterpreted boreholes from the construction of SFR (green), boreholes from the construction of SFR with geological intercepts only (black), and from the site investigation Forsmark (blue; reproduced from /Curtis et al. 2009/).*

Table 2-2. Summary of borehole geometry and hydraulic data populations.

Borehole	Old name	Length	Orientation (°)		Elevation (m.a.s.l.)		Single-hole hydraulic data
		(m)	Inclination	Bearing	Sec_up	Sec_low	(No. records)
HFM33	NONE (PLU)	140.2	–54	229	2.62	–110.36	3
HFM34	NONE (PLU)	200.8	–53	30	2.45	–161.28	7
HFM35	NONE (PLU)	200.8	–52	33	1.9	–150.42	9
KFM11A	NONE (PLU)	851.2	–56	42	2.95	–713.24	38
KFR01	HK1	62.3	–60	231	–47.98	–101.93	2
KFR02	HK2	170.3	–90	0	–85.43	–255.76	20
KFR03	HK3	101.6	–90	0	–82.37	–183.97	4
KFR04	HK4	100.5	–75	98	–77.19	–174.26	4
KFR05	HK5	131.4	–70	9	–77.16	–200.64	18
KFR06	HK6	39	–63	316	–76.29	–111.04	32
KFR08	HK8	104.4	–5	56	–86.02	–95.12	3
KFR09	HK9	80.2	–5	300	–77.44	–84.43	4
KFR10	HK10	107.28	–45	302.5	–78.3	–154.16	4
KFR11	HK11	98.1	–10	73	–86.5	–103.53	4
KFR12	HK12	50.3	–90	0	–87.12	–137.38	2
KFR13	HK13	76.6	–90	0	–123.34	–199.94	10
KFR14	HK14	29.1	–45	135	–89.67	–110.25	No data
KFR19	KB19	110.2	14	38	–80.82	–54.54	4
KFR20	KB20	109.7	10	56	–81.18	–61.3	4
KFR21	KB1	250.8	–90	231	0	–250.8	67
KFR22	KB2	160.1	–60	213	0	–138.65	47
KFR23	KB3	160.2	–60	257	0	–138.74	44
KFR24	KB4	159.2	–57	52	0	–133.52	45
KFR25	KB5	196.5	–46	0	0	–141.35	61
KFR27	KB7	148.5	–89	196	2.87	–145.63	No data
KFR31	KB11	242.1	–43	82	5	–160.73	70
KFR32	KB12	209.7	–47	25	5	–147.11	50
KFR33	KB13	167	–44	303	5.1	–110.49	48
KFR34	KB14	142	–49	198	5	–102.17	24
KFR35	KB15	140.2	–52	208	5.1	–104.62	28
KFR36	KB16	123.9	–46	292	5	–84.13	32
KFR37	KB17	204.9	–63	189	4.4	–177.35	59
KFR38	KB18	185.4	–58	92	4.5	–152.04	55
KFR51	KB21	46.9	35	359	–85	–58.13	No data
KFR52	KB22	30	10	231	–76	–70.8	No data
KFR53	KB23	40.6	–27	313	–81.3	–99.98	3
KFR54	KB24	53.3	–48	310	–81.65	–121.07	3
KFR55	KB25	61.9	–11	329	–125.58	–137.38	20
KFR56	KB26	81.7	26	88	–84.55	–48.72	11
KFR57	KB27	25.4	–90	231	–87.6	–112.98	No data
KFR61	DS1	70.9	–44	38	1.4	–47.85	No data
KFR62	DS2	82.8	–45	43	0.6	–57.95	No data
KFR63	DS3	15.1	–90	231	0.8	–14.28	No data
KFR64	DS4	41.4	–60	34	0.3	–35.54	No data
KFR65	DS5	29	–90	231	0	–28.95	No data
KFR66	DS6	14.2	–90	231	0	–14.18	No data
KFR67	DS7	35.2	–65	35	0	–31.91	No data
KFR68	DS8	116.7	–45	82	0	–82.52	36
KFR69	DS9	201.2	–45	15	2.4	–140.86	40
KFR70	DS10	172.5	–51	62	2.5	–132.12	30
KFR71	DS101	120.9	2	284	–33.3	–29.08	8
KFR7A	HK7A	74.7	–2	21	–132.29	–134.89	3
KFR7B	HK7B	21.1	–75	12	–133.25	–153.63	2
KFR7C	HK7C	34	–70	196	–133.4	–165.35	1
KFR80	INJ	20	–70	196	–136	–154.79	No data
KFR83	SH3	20	–35	33	–87.2	–98.67	1
KFR84	BT 5/241	29.5	25	309	–42	–29.53	No data
KFR85	BT 5/247 1	12.2	–5	115	–43	–44.06	No data
KFR86	BT 5/247 2	14.7	–90	231	–45	–59.7	No data
KFR87	NBT 1	15.1	–5	213	–135.13	–136.45	No data
KFR88	NBT 2	30	20	339	–133.76	–123.5	No data

Table 2-3. Borehole intercepts with HCDs in the preliminary Geologic model[7] SFR v.0.1; target intercepts, based on geological re-interpretation, and geometric intercepts, based on RVS modelling. Missing bounds indicated as "top of hole" (toh) or "end of hole" (eoh).

Target intercepts Deformation zone		Borehole	Thickness RVS (m)	Zone intersection From (m)	To (m)	Alpha (°)	Length (m)	Thickness Borehole (m)
ZFM871	zonH2	KFR04	20	86.65	eoh	60.6	> 13.9	> 12.1
ZFM871	zonH2	KFR13	20	49.83	70.99	70.6	21.2	20
ZFM871	zonH2	KFR7A	20	24.05	eoh	16.2	> 50.7	> 14.1
ZFM871	zonH2	KFR7B	20	6.92	eoh	80.1	> 14.2	> 14
ZFM871	zonH2	KFR7C	20	14.12	eoh	53	> 19.9	> 15.9
ZFMNE0870b	zon9b	KFR04	1	21.08	23.94	32.4	2.9	1.5
ZFMNE0870b	zon9b	KFR54	1	37.32	39.83	44.5	2.5	1.8
ZFMNE0870b	zon9b	KFR55	1	47.4	48.58	61	1.2	1
ZFMnne0869	zon3	KFR09	50	41.42	eoh	71.9	> 38.8	> 36.9
ZFMnne0869	zon3	KFR36	50	83.82	eoh	33.7	> 40.1	> 22.2
ZFMnnw0999	–	KFR08	20	67.12	90.06	60.3	22.9	19.9
ZFMnnw1209	zon6	KFR35	20	30.67	72.35	30.1	41.7	20.9
ZFMnw0805a	zon8	KFR08	20	52.1	73.36	67.3	21.3	19.6
ZFMnw0805a	zon8	KFR7A	20	68.46	eoh	74.5	> 6.2	> 6
ZFMnw0805b	–	KFR08	10	39.05	49.31	76.8	10.3	10
ZFMnw0805b	–	KFR7A	10	50.32	61.2	66.5	10.9	10

[7] SKBdoc 1228772 - BH_DZ_intercepts_jp_090119, Version 0.1, 2010-06-08, (access might be given on request).

Geometrical intercepts			HCD modelled in RVS			HCD hydraulic envelope		
			Thickness	Intercept		Thick-ness	Intercept	
Deformation zone		Borehole	(m)	From (m)	To (m)	(m)	From (m)	To (m)
ZFM871	zonH2	KFR02	20	108.58	129.73	30	103.29	135.02
ZFM871	zonH2	KFR03	20	79.87	101.02	30	74.58	eoh
ZFM871	zonH2	KFR05	20	76.86	97.15	30	71.79	102.23
ZFM871	zonH2	KFR10	20	70.56	94.03	30	64.69	99.9
ZFM871	zonH2	KFR12	20	15.37	36.52	30	10.08	41.81
ZFM871	zonH2	KFR21	20	107.36	128.52	30	102.07	133.81
ZFM871	zonH2	KFR22	20	142.55	eoh	30	135.61	eoh
ZFM871	zonH2	KFR23	20	81.9	105.72	30	75.94	111.68
ZFM871	zonH2	KFR31	20	223.64	eoh	30	215.25	eoh
ZFM871	zonH2	KFR32	20	159.15	182.85	30	153.22	188.78
ZFM871	zonH2	KFR33	20	158.49	eoh	30	152.55	eoh
ZFM871	zonH2	KFR37	20	167.51	195.82	30	160.44	202.89
ZFM871	zonH2	KFR38	20	163	eoh	30	156.16	eoh
ZFM871	zonH2	KFR80	20	0	18.79	30	toh	eoh
ZFM871	zonH2	KFR83	20	12.27	eoh	30	5.17	eoh
ZFMne0870a	zon9a	KFR02	1	32.89	36.88	20	toh	72.62
ZFMne0870a	zon9a	KFR70	1	63.84	68.4	20	22.14	111.67
ZFMne0870b	zon9b	KFR03	1	51.51	54.76	20	23.23	88.18
ZFMne0870b	zon9b	KFR05	1	116.56	eoh	20	toh	eoh
ZFMne0870b	zon9b	KFR31	1	222.82	224.51	20	206.79	240.54
ZFMne0870b	zon9b	KFR53	1	29.34	30.51	20	16.75	40.28
ZFMnne0869	zon3	HFM34	50	6.89	185.96	70	toh	eoh
ZFMnne0869	zon3	KFR10	50	71.48	eoh	70	53.49	eoh
ZFMnne0869	zon3	KFR68	50	27.44	96.62	70	13.61	110.45
ZFMnne2308	–	KFR71	15	67.95	85.18	30	59.33	93.69
ZFMnnw0999	–	KFR24	20	86.43	136.73	30	81.44	147.78
ZFMnnw1209	zon6	KFR33	20	42.77	106.29	30	26.96	125.26
ZFMnw0805a	zon8	KFR11	20	53.98	78.85	40	41.54	91.29
ZFMnw0805a	zon8	KFR24	20	86.43	124	40	67.64	142.79
ZFMnw0805a	zon8	KFR25	20	81.13	115.28	40	64.06	132.36
ZFMnw0805b	–	KFR11	10	29.03	40.56	20	23.27	46.32
ZFMnw0805b	–	KFR24	10	59.11	77.6	20	49.87	86.84
ZFMnw0805b	–	KFR25	10	80.66	115.28	20	68.1	118.34
ZFMnw0805b	–	KFR56	10	59.47	74.87	20	51.76	eoh
ZFMnw1035	–	KFR68	60	0	87.6	70	toh	94.42
ZFMnw1035	–	KFM11A	60	684.57	767.93	70	677.57	774.82
ZFMnw1035	–	HFM35	60	152	eoh	70	146	eoh
ZFMwnw0813	–	KFR71	10	75.66	99.53	40	35.55	eoh
ZFMwnw0813	–	KFM11A	10	336.74	354.78	40	308.59	381.68
ZFMwnw3262	–	KFR69	5	155.99	162.99	30	138.47	180.51
ZFMwnw3262	–	KFR34	5	–	–	30	129.67	eoh
ZFMwnw0001	Singö	HFM34	100	6.89	182.52	165	toh	eoh
ZFMwnw0001	Singö	HFM35	100	–	–	165	toh	10.19
ZFMwnw0001	Singö	KFM11A	100	552.15	735.52	165	487.67	792.58
ZFMwnw0804	–	HFM34	40	–	–	80	182.35	eoh
ZFMwnw0804	–	HFM35	40	toh	46.04	80	toh	78.04
ZFMwnw0804	–	KFM11A	40	738.98	806.43	80	704.72	839.69
ZFMwnw2496	–	KFM11A	10	97.69	119.22	20	86.81	129.87
ZFMwnw3259	–	KFM11A	10	408.14	427.24	40	378.5	455.14

3 Concepts and aspects

3.1 Role of the Hydraulic Conductor Domains (HCDs)

In the hydrogeological Site Descriptive Models for Forsmark and Laxemar, regional flow is expected to be controlled by Hydraulic Conductor Domains (HCDs) /Rhén et al. 2003, Follin et al. 2007a/. The HCDs are large-scale geological structures, geometrically defined in the deformation zone model /Curtis et al. 2009/, while the hydraulic rock domain (HRD) is defined as the rock between deformation zones. The HCDs are generally regarded as conductors with conductivity a few orders of magnitude larger than the surrounding HRD. The hydrological model is parameterised by data from single-hole hydraulic borehole tests. As the contrasts in hydraulic conductivity are expected to be large, the classification of data into HCD and HRD is a critical step for a realistic parameterisation of the HCDs and HRD, and in turn the overall performance of the flow model.

The treatment of anomalous high transmissivity values is of particular importance in this HRD/HCD classification process, as it divides the anomalies into one group geometrically constrained by structural geology (HCD) and the other without geometrical control, i.e. stochastic anomalies within HRD. The uncertainty in model predictions depends largely on the stochastic component of heterogeneity (i.e. flow paths may vary between different stochastic conductivity field realisations). On the other hand, deterministic heterogeneity is tied to conceptual models and constrained by geometrical definitions (e.g. depth trends and hydraulic sub-units); obviously, these models involve conceptual and geometrical uncertainty, but it does not contribute to the variability between realisations. Furthermore, if the spatial extent of deterministic anomalies can be reasonably well defined, it can be avoided during tunnel construction. In other words, from the Safety Analysis perspective it is preferred if hydraulic anomalies can be associated to deterministic geological structures, providing they are conceptually sound and geometrically well-defined. On the other hand, if anomalously high transmissivity values are incorrectly associated to HCD (i.e. data that in fact are *not* under geologic control), then the true uncertainty becomes underestimated in the hydrogeologic model. In other words, excessive association of high transmissivity to HCD is *not* conservative; but produces unrealistically high confidence in simulation results.

Furthermore, deformation zones are also expected to be highly heterogeneous and anisotropic. For example, a HCD may act as a barrier for flow across the structure (e.g. caused by layers of gouge-filled fractures), while it acts as a conductor for parallel flow. Likewise, a certain degree of heterogeneity can also be expected in the HRD, and therefore a high transmissivity value does not automatically imply the presence of a zone, and vice-versa. The HRD/HCD classification should therefore be treated cautiously.

3.2 Considerations for the parameterisation of HCDs

3.2.1 Confidence in HCD intercepts

In the hydrogeological Site Descriptive Model for Forsmark, hydraulic borehole data classification by HRD or HCD were done according to the geological Single Hole Interpretation (SHI) of borehole data, e.g. /Follin et al. 2007b, Stephens et al. 2007/. The SHI relies only upon geologic/geophysical zone indicators; the hydraulic data are purposely excluded from the interpretation of zone boundaries.

The hydrogeological model SFR v.0.1, however, is constrained to existing data prior to the initiation of the SFR extension program, i.e. largely measured during the 1980's, prior to the development of the SHI methodology. Therefore, in the geological model SFR v.0.1 /Curtis et al. 2009/, eleven boreholes were selected for an updated geological re-interpretation: KFR04, KFR08, KFR09, KFR13, KFR35, KFR36, KFR54, KFR55, KFR7A, KFR7B, and KFR7C. The deformation zone intercepts in these boreholes have been determined with relatively high confidence, and are referred to as "target intercepts" in /Curtis et al. 2009/. No updated geological interpretations were made for the remaining boreholes; instead their deformation zone intercepts were estimated by modelling the intercepts in RVS. This latter category is referred to as "geometrical intercepts"; they are unconfirmed by geology and therefore have a much lower confidence.

The uncertainty in geometrical intercepts implies uncertainty in the parameterisation of the hydrogeological model, as the HRD/HCD classification of hydraulic data may be critical to its overall confidence (Section 3.1). The geometrical intercepts are model predictions – not definite bounds confirmed by geology. Therefore the propagation of uncertainty from the inexact bounds of a HCD to the estimation of its transmissivity, was analysed by introducing "hydraulic HCD envelopes" (Figure 3-1). These envelopes are not derived by a strict mathematical formulation, but rely upon geological judgment with geometric consideration /Curtis et al. 2009/, and can be looked upon as the confidence bounds necessary to enclose all hydraulic influence by the actual HCD, i.e. its width is a representation of geometric uncertainty and potential range of hydraulic influence (Table 2-3).

3.2.2 Geometrical aspects in classification of hydraulic data

In assigning hydraulic test data to hydraulic domains (HCD/HRD), there are a number of aspects necessary to consider:

Geometric uncertainty of modelled zones. Either the modelled HCD intercept, or the envelope intercept can be used for classification of data (grey areas in Figure 3-2). The modelled HCD intercept is the best estimation of the actual HCD intercept and has the correct HCD thickness. The HCD envelope is wider than the estimated HCD thickness, and will therefore by definition also include HRD; on the other hand the envelope is more likely to actually contain the HCD.

Transmissivity resolved to borehole section scale. Interval transmissivity is the sum of all fracture transmissivities within that interval. Thus, a hydraulic test in a long borehole section that extends across a HCD and into the HRD cannot resolve the HCD transmissivity apart from that of the HRD (case 3 in Figure 3-2). For example, consider a section that covers 1 m HCD and extends 10 m into the HRD; to what extents should its transmissivity be assumed to reflect the HCD, respectively, the HRD?

Incomplete data coverage of HCD intercepts (case 2 in Figure 3-2). Cases where hydraulic data only covers part of the HCD intercept induce uncertainty in the interpretation of the full HCD transmissivity. Furthermore, given the geometric uncertainty of the actual position of the HCD, incomplete data coverage implies that the HCD is not necessarily represented in the data (i.e. the data may for instance only cover HRD).

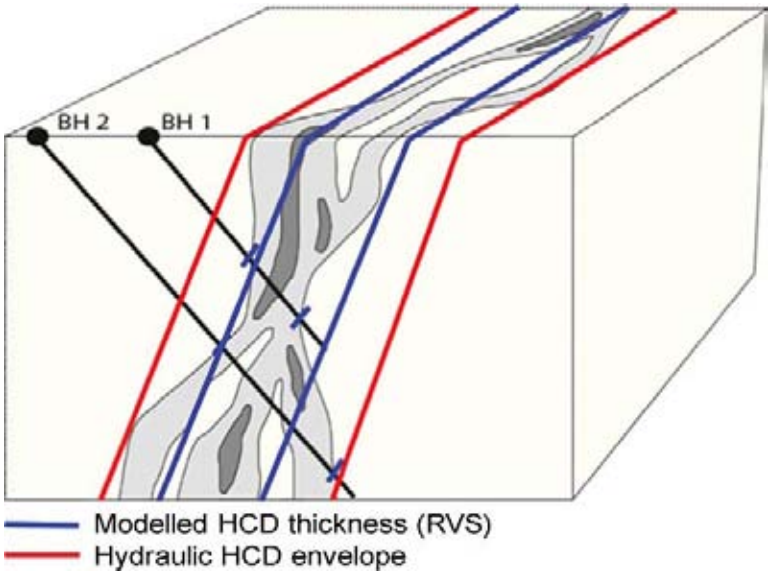

Figure 3-1. *Conceptual figure demonstrating the difference between modelled HCD thickness in RVS based on borehole intercepts and the hydraulic envelope of a HCD, i.e. extended confidence bounds for the classification of hydraulic data; modified from /Caine et al. 1996/.*

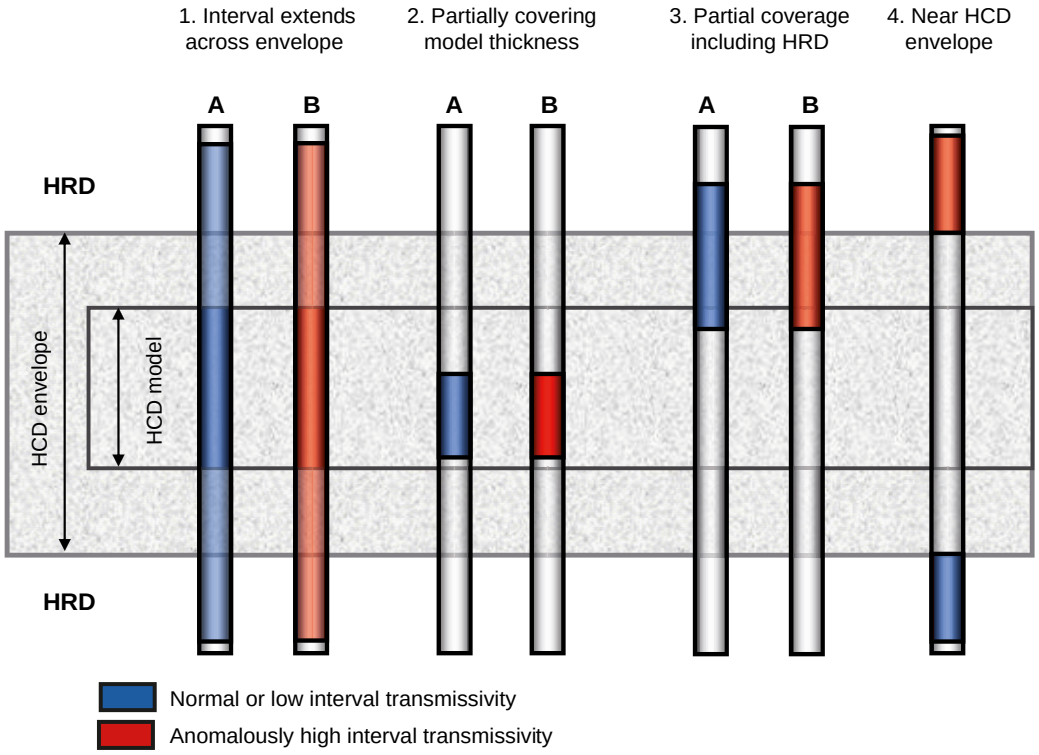

Figure 3-2. *Conceptual figure demonstrating geometrical configurations to consider in the assignment of hydraulic data to HCD/HRD.*

One possible approach could be some type of optimisation methods (e.g. Bayesian inference) based on transmissivity contrast between the data sets. In such an approach, a transmissivity-weighted probability function for discriminating between HRD and HCD would initially be estimated from data. The data would then be re-classified according to the weighted function, and the updated statistics would be used to re-define the weighing function. This procedure would be repeated until convergence. However, it is not trivial to define a statistical discriminating function that can handle variable test-scales and the various geometric configurations (Figure 3-2). As discussed in section 3.1, there is a clear risk in relying on a statistical approach based on a-priori expectations.

Instead the effects of geometrical uncertainty were examined by means of a sensitivity analysis (Section 4.2). Aspects 2) and 3) can be dealt with using two different approaches:

The continuum principle: under the assumption that transmissivity is uniformly distributed over the tested borehole sections, data can easily be rescaled to conform to HCD domain boundaries. The method is simple and circumvents relying on a priori assumption on the relation between HRD and HCD. Furthermore, it can universally be applied to all configurations (Figure 3-2) and therefore provides a large data set of T_{HCD}, which is preferable for the estimation of the effective HCD transmissivity (see discussion in Section 3.2.3). Although this approach is practical and convenient, it is well known that its underlying assumption is inappropriate for fractured rock.

The discrete principle: an alternative approach to honour the heterogeneity in fractured rock. Instead of re-scaling data, data are divided into HCD/HRD populations in a binary manner, based on a set of defined rules. The criterion for classifying data is based on fraction of interval length inside the HCD bounds. The drawback of this strategy is that the terms modelled HCD thickness and HCD domain cannot strictly be used without relying on some a priori assumption, such as HRD transmissivity is insignificant in comparison to HCD.

The methodology used is described further in Section 4.2.

3.2.3 HCD heterogeneity, spatial resolution and depth trend

Another difficulty in the characterisation of a HCD is the interpretation of its within-plane heterogeneity. Unless deterministic relations can be inferred, e.g. depth trend, geological interpretation, orientation versus stress field, etc. this heterogeneity must be interpreted as purely stochastic. The available information on spatial heterogeneity in HCDs is limited to the available hydraulic test data at borehole intercepts, which typically means one or two intercept transmissivity values. Thus, in addition to the uncertainties in the determination of intercept transmissivities (see discussion above), the few borehole intercepts available provides a poor spatial resolution to characterise complex within-plane HCD heterogeneity, which makes the characterisation of HCDs highly uncertain. Particularly when considering that the determined effective HCD values are intended to represent the hydraulic properties of kilometre-sized geological structures.

To demonstrate these difficulties, let us consider two hypothetical HCDs, one vertical and one horizontal (Figure 3-3a). The hydraulic pathways inside the HCD are highly heterogeneous and canalized (illustrated as orange/red paths in Figure 3-3a). Patched sheets of clay-filled fractures form local barriers for perpendicular flow (illustrated as brown sheets in Figure 3-3a). A depth trend has been superimposed to HCD transmissivity. These HCDs are to be parameterised hydraulically based on a given number of borehole intercepts with hydraulic tests. The effective HCD transmissivities will be determined from single-hole hydraulic test data, e.g. double-packer short time injection tests, available from 8 borehole intercepts labelled clock-wise A-H. The hydraulic connectivity, within HCDs and between HCDs, will then be evaluated from a cross-hole interference test.

High-transmissive intercepts reflect larger amount of tested rock (i.e. HCD area), while no-flow tests provide little spatial information (i.e. no tested rock volume if no flow occurs). For example, if the flow dimension of tests equals 2 (cylindrical flow regime), and test duration time and borehole interval lengths are kept constant, the “radius of influence” of tests (i.e. its radial-symmetric spatial extent) can be said to be proportional to the square root of transmissivity (Figure 3-3b). Thus, Figure 3-3b) illustrates a possible interpretation of the within-plane heterogeneity inside the HCDs, based on the information obtained from single-hole hydraulic tests at intercepts A-H. The uncertainty in this interpretation related to amount of data and its spatial resolution becomes obvious, if for example the hydraulic data from intercept A were unavailable. Based on hydraulic data from the borehole intercepts, it is hardly possible to confirm or reject the depth trend in HCD transmissivity (Figure 3-3b). Furthermore, these short-time injection tests do not reveal if hydraulic data are connected or compartmentalized.

Based on the results of single-hole data, a cross-hole interference test is therefore performed in the most conductive borehole interval (intercept A), and monitored in other sections (intercepts B-H). The purpose is to explore the hydraulic connectivity within the vertical zone and its hydraulic connection to the horizontal zone. This interference test only confirms hydraulic connections between intercepts A, D, and F. The high transmissivities at intercepts B and G can be interpreted as either compartmentalized, or that, the draw-down from intercept A is masked by some positive flow boundary.

A pragmatic method to transfer the parameterisation from well-characterised HCDs to poorly characterised HCDs is to use pooled statistics, which are defined by means of simple geometric or geological parameters. The method is to identify statistically “homogeneous” HCD subgroups based on simple geometry measures or geological character (such as orientation versus stress field, length, or type) which share common traits. This way hydraulic properties can be determined for each subgroup and extrapolated within that subgroup with a higher confidence to all HCDs with few, or no, borehole intercepts. The approach taken during the Site Investigations, e.g. /Follin et al. 2007b/, was to group HCDs by orientation. The methodology used to infer depth dependency from HCD intercept transmissivity is described further in Section 4.2.2.

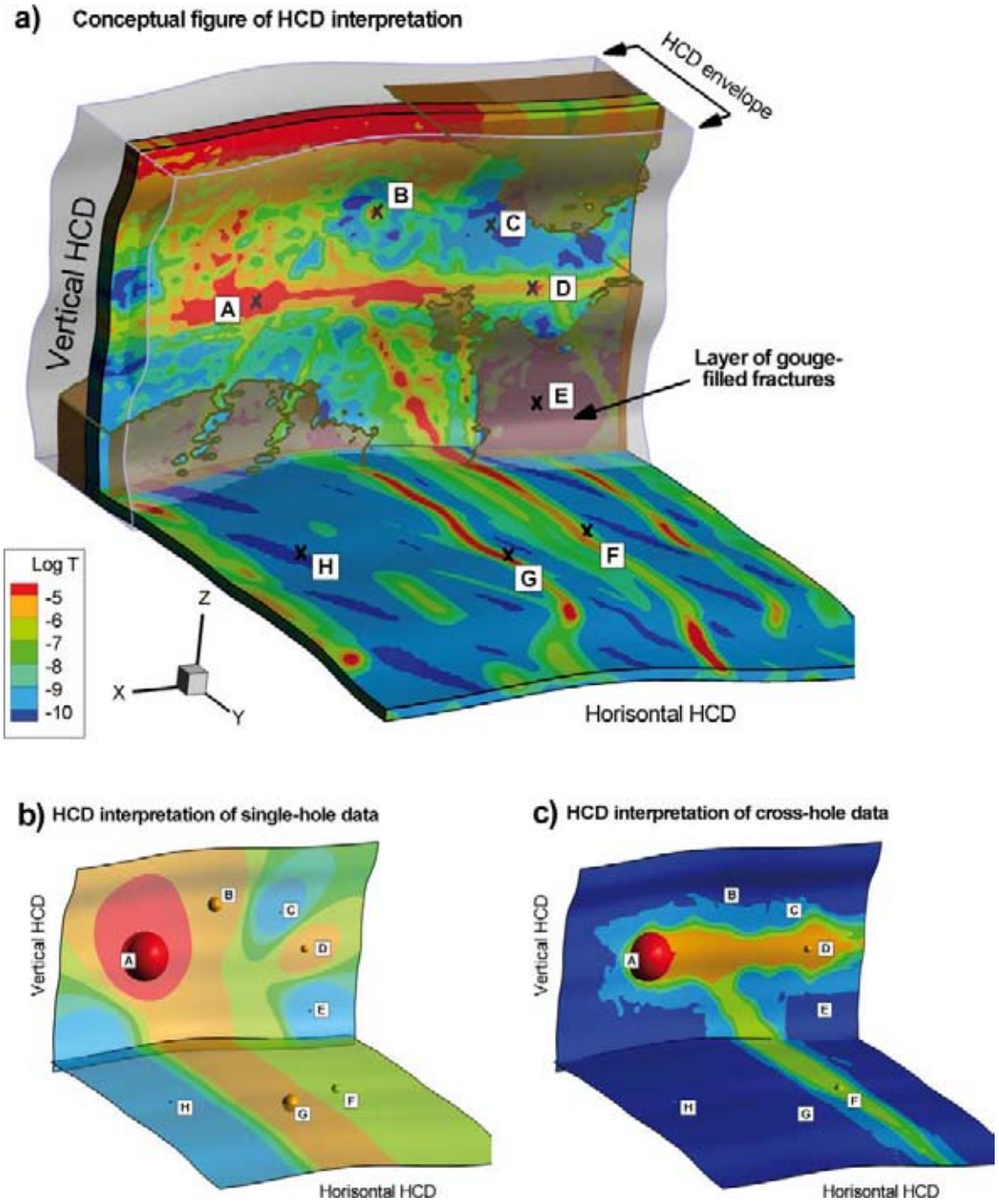

Figure 3-3. *Conceptual figure of the interpretation of HCD transmissivity, given a limited amount of borehole intercepts; trends and within-plane heterogeneity and channelling.*

4 Methodology

4.1 Preparation of data prior to the parameterisation of HCDs

4.1.1 Screening of data

The hydraulic data have been measured with different techniques, at different time periods, and at different scales. Furthermore, several borehole sections have been subject to more than one test. Consequently, such borehole sections have overlapping hydraulic data, which in many cases exhibit inconsistencies. In order to avoid "double-counting" transmissivity for sections with overlapping hydraulic data, a screening procedure was undertaken to establish an unambiguous transmissivity definition. The aim is to exclude erroneous, inconsistent, and redundant data, while keeping the loss of valid data and its spatial resolution to a minimum. It is difficult to formulate general criteria for strict application in this screening process; rather the screening must rely on judgement which allows some flexibility from case to case. The screening is a simple and pragmatic method to reduce the data set in such a way that, according to personal judgement and understanding, it is still a realistic representation of the hydraulic properties of the rock. In general:

- Obvious errors and data inconsistencies were excluded. In case of internal inconsistencies, it is often unclear which of the data that is correct and should be retained. To determine which data should be retained, the reliability of different measurements is weighed against each other. For example, a long test section has a higher confidence in the estimation of total transmissivity compared to the sum of many short test sections, i.e. due to the risk of short-circuiting into the borehole, non-radial flow regime, etc. The reliability in data is based on comments available in Sicada, consistency with observations made in other boreholes, and – not the least – expert judgement. In the end, expert judgement is used to retain data which are considered to form a realistic hydraulic representation of the rock.
- In order to maintain maximal resolution of hydraulic heterogeneity near HCD/HRD boundaries, borehole data from short sections were retained in preference of longer sections. Particularly, the 3 m test scale was given priority. However, in case of inconsistencies, short-scale measurements are given lower confidence (as discussed above).
- Falling head measurements were excluded in preference of other test methods, as low-transmissive falling head measurements have lower confidence /Carlsson et al. 1987/.
- Exclusion of hydraulic data was done so as to minimize loss of total borehole data coverage. Where data partially overlap at different scales, the combination with maximum borehole cover is retained, if not contradicted by criteria above.
- For transient injection data, three transmissivity values are available (for the three phases: injection, steady-state and fall-off). One of these three values is recommended in the Sicada table. This recommended T-value was always used.
- Boreholes in the vicinity of the Silo, KFR05, KFR06, and KFR55 were measured before and after its construction, and the "virgin" data were retained.
- If none of the criteria above are applicable, it was considered conservative to retain the highest transmissivity value.

The raw data and the corresponding screened data are shown in Figures 6-1 to 6-61.

4.1.2 Review of HCD envelopes based on hydraulic anomalies.

In this review, anomalous hydraulic data are examined near the HCD intercept envelopes (case 4 in Figure 3-2) to assess how well the hydraulic data conform to the geological model. In this analysis, it must be kept in mind that hydraulic data are heterogeneous in general and that therefore high transmissivity data does not necessarily imply the presence of a zone. Vice versa, non-flowing borehole sections cannot reject a modelled zone. On the other hand, the geometrical intercepts (Table 2-3) are unconfirmed by borehole data. Instead these are model results with some inherent degree of uncertainty, being based on extrapolations of assumingly planar structures from known intercepts. This uncertainty is represented

by HCD intercept envelopes. However, envelopes are uncertainty estimates - not definite bounds for a zone. An even more important role for HCD intercept envelopes is to classify whether hydraulic anomalies belong to HCD or HRD. In other words, hydraulic anomalies outside envelopes must be treated as a random occurrence outside the geometrical control of structural geology. This HCD envelope review is to ensure that envelopes agree reasonably well with observed patterns of hydraulic data, to avoid relying on geological model predictions alone.

The deformation zone model is based on geological and geophysical data alone /Curtis et al. 2009/. Hydraulic data were excluded from the geological modelling. The deformation zone model is conditioned to lineament data at the surface and at the subsurface, to tunnel observations and single hole interpretations of the selected 11 boreholes (Table 2-3). Thus, the geometrical uncertainty of modelled zones grows with extrapolated distance from their conditioning points. Furthermore, this uncertainty is accentuated for geometrical borehole intercepts (Table 2-3) if the alpha-angle, i.e. the solid angle between the zone and the borehole, is low.

The purpose of HCD envelopes is to discriminate between the hydraulic data that can be inferred as deterministic, and those that must be perceived as stochastic. Anomalous high transmissivity data inferred as deterministic are strictly linked to the presence of zones: either directly, reflecting the hydraulic properties of the zone (HCD) itself, or indirectly, a local hydraulic connection to a nearby HCD. Thereby, deterministic anomalies are geometrically constrained by deformation zones, and can be avoided in tunnel construction. Stochastic anomalies lack a structure-geological interpretation and geometrical control and must therefore be modelled as randomly distributed. From a modelling perspective, anomalous hydraulic data that cannot be associated to HCD increases the HRD heterogeneity, an in turn, the range of possible outcomes in model predictions (Section 3.1). It is important to keep in mind that the role of HCD envelopes is not only to parameterise the HCDs, but more importantly to differentiate between deterministic and stochastic hydraulic anomalies.

The hydraulic data set is an independent source of information for the geometrically extrapolated deformation zones, a potent tool to confirm geometric intercepts or motivate a revision of HCD boundaries. However, it must be emphasized that the purpose is not to make geometrical adjustments to deformation zones, but only to their envelopes, i.e. the bound enclosing the volume of rock that is considered possibly under influence from the zone (Figure 3-1).

4.2 Algorithms

4.2.1 Parameterisation of HCDs

Geometrical HCD intercepts have low confidence and in many cases it is unclear to what extent a borehole interval transmissivity reflects the HCD or the HRD (Section 3.2.2). In order to examine the sensitivity of these geometrical uncertainties, the HRD/HCD classification of hydraulic data was not done by judgement, but instead by means of processing algorithms. In these algorithms the uncertainties identified in section 3.2.2 were represented by a set of parameters (Table 4-1), which were allowed to vary. In this way HCD intercept transmissivity, T_{HCD}, could be calculated for any combination of definition bounds, data inclusion criteria, calculation methods and acceptance criteria (see Table 4-1).

One exception in this analysis is that HCD intercepts in boreholes HFM34, HFM35, and KFR56 are considered to have complete data coverage, irrespectively of data inclusion criterion. The reason for this is that the hydraulic data in these boreholes come from short sections overlapped by longer test sections. The long section data were removed during the screening process (Section 5.1.1), but the retained data from the short, non-covering, sections indicate a similar total transmissivity (Figure B-2, Figure B-3, Figure B-39). This was taken as evidence for negligible transmissivity outside the HCD bounds (even though the long test section data were removed).

In the calculation of T_{HCD}, there are two ways to treat tested borehole sections which fall below detection limit; they can be assigned zero transmissivity (its minimum value), or they can be assigned the detection-limit transmissivity (its maximum value). Preliminary tests (not shown here) demonstrate that the detection limit is low enough in comparison to T_{HCD} to be considered negligible in the calculation of HCD intercept transmissivity. The hydraulic data falling below detection limit are assumed to take on its maximum value possible and set equal to the detection limit.

Table 4-1. Parameters in HCD/HRD classification of hydraulic data.

Definition bounds	Modelled HCD thickness	Actual HCD thickness (RVS)
	Hydraulic HCD envelope	Enclosing HCD hydraulic influence
Data inclusion criterion	Fraction of borehole interval required inside bounds (i.e. only borehole data with sections at least XX% inside bounds are used to calculate T_{HCD})	> 0 (i.e. any data "touching" bounds) 0.25 0.5 0.75 1 (i.e. only data *strictly* inside bounds)
Calculation of T_{HCD}	Discrete principle, a binary sum of interval transmissivity	$T_{HCD} = \Sigma T_i - (\Sigma L_i * K_{HRD})$
	Continuum principle, rescale borehole intervals to HCD modelled thickness	$T_{HCD} = \Sigma T_i / \Sigma L_i * L_{HCD} - (L_{HCD} * K_{HRD})$
Acceptance criterion	data coverage > 75% (75% of the HCD bounds must be covered by borehole data), or $T_{HCD} > 10^{-6}$	

The total length of tested borehole intervals is included in the calculation of T_{HCD} In most cases, this is considerably longer than the modelled thickness of the zone. There are three reasons: 1) the hydraulic envelope is by definition larger than the modelled zone thickness, 2) non-perpendicular borehole orientations versus the HCD plane (i.e. $\alpha < 90°$) and 3) hydraulic test data partly outside the HCD bounds are included. This may lead to an overestimation of HCD transmissivity.

The inclusion of excessive borehole data outside the HCD bounds is expected to have a lesser impact on the calculation of HCD transmissivity, as a transmissivity sum is generally dominated by the single highest value (owing to the general skewness in transmissivity distributions); it is reasonable to assume that this highest value occurs within the HCD bounds.. This potential overestimation is analysed by subtraction of excessive borehole length multiplied by K_{HRD} (set to 10^{-8} m/s). It is a well-know phenomenon that, over a given borehole interval, the sum of several independently tested sections tends to exceed the interval transmissivity as calculated from a single test. One of the reasons for this is that the flow-dimension varies with test scale, which leads to some degree of "double-counting" transmissivity, when summed over several short-scale tests. This effect is expected to be small if the borehole intercept is perpendicular to the HCD, as it appears reasonable to assume a cylindrical flow regime, parallel to the zone. It is not obvious that the same should hold for low alpha-angle intercepts. T_{HCD} was therefore also analysed as a function of alpha-angle (Section 5.3.2).

This analysis of hydraulic data is done strictly according to the geometric definitions available in the geological model SFR v.0.1. The geological model SFR v.0.1 did not include sheet joints, e.g. /Follin et al. 2008/ or SHI interpretations of deformation zones in HFM34, HFM35, and KFM11A /Carlsten et al. 2007/. Consequently, neither sheet joints, nor SHI definitions from Site Investigation Forsmark are considered in the HCD/HRD classification of hydraulic data. This may lead to an overestimation in transmissivity of vertical structures south of the Singö deformation zone, as high transmissivity data observed in HFM34, HFM35, and KFM11A is limited to association with vertical deformation zones, overlooking the potential link to sheet joints.

4.2.2 Depth trend analysis, HCD

An analysis of depth dependency in hydraulic data requires abundant data that cover the entire depth range for which the model is intended to apply. However, the SFR repository is shallow (approximately –100 m), in comparison to e.g. the investigated domain for the future deep repository of nuclear waste. Consequently, the current data set is concentrated to the upper 150 m of the bedrock, while in the Site investigations most hydraulic data are available below –100 or –200 m elevation and extending down to –1,000 m. Thus, the overlap between the SFR and the Site investigation data sets is small, and moreover, the SFR data set may be subject to processes which are specific for shallow bedrock, e.g. excessive fracturing due to glacial rebound, weathering, and stress relief. In other words, it may be unsuitable to extrapolate the hydraulic properties in the SFR data set down to a model depth of –1,100 m. Therefore, it was decided to rely on experience, methods, and conclusions drawn from the Site Investigation program.

The method to account for depth dependency in HCD transmissivity follow a concept developed in the Site Investigation (e.g. /Follin et al. 2007b and Follin et al. 2008/). Although it is conceptually more appealing to express the trends in terms of depth below ground, it is more practical to use elevation, z. The topography within the model domain is shallow (ranging from 7 to 16 m RHB70), so the difference should be small. Based on observations made in maximum HCD transmissivity as a function of depth, the depth dependency in HCD transmissivity is assumed to follow an exponential model:

$$T(z) = T(0)10^{z/k} \quad (4\text{-}1)$$

where $T(z)$ is transmissivity at elevation z (RHB70), $T(0)$ is the expected transmissivity at zero elevation, and k is the depth interval over which transmissivity decreases one order of magnitude. The value of $T(0)$ can be calculated by inserting a measured value $T(z')$ at its reference elevation z'.

$$T(0) = T(z')10^{-z'/k} \quad (4\text{-}2)$$

An effective value for HCD transmissivity at reference elevation 0 m.a.s.l. $T_{eff}(0)$, is then defined for each zone. In case HCD transmissivity is available at several intercepts of the same zone, $T_{eff}(0)$ is calculated by an average of the intercepts. The arithmetic mean provides the highest estimate, and corresponds to parallel flow in heterogeneous channels within the HCD. The most commonly used estimate for stochastic heterogeneity within a 2D plane is the geometric mean, which provides a lower value. In this study, the geometric mean was used, as it was also used in the Site Investigation Forsmark /Follin et al. 2007b/.

Thus, the depth interval constant k has two important functions: 1) to weigh different HCD intercept transmissivity values taken from different depths in the calculation of $T_{eff}(0)$, and 2) to extrapolate mean HCD transmissivity to depths lacking borehole intercept data.

4.2.3 Depth trend analysis, Hydraulic Rock Domain (HRD)

Two issues raised in /Follin et al. 2007a/ are: 1) if there is any data support for dividing HRDs into different sub domains, and 2) the statistical significance of potential depth dependence. However, the SFR hydraulic data set v.0.1 is only available for the shallow bedrock, primarily above –150 m, which makes it difficult to draw any general conclusions on depth dependency, without taking observations from the Site Investigation Forsmark into account. In the Forsmark Site Investigation, the HRD conductivity was divided into three different elevation bins: < –200 m, –200 to –400 m, and –400 to 1,200 m.a.s.l. /Follin et al. 2007c/.

For the analysis of HRD depth dependency, it is preferred to use a large homogeneous data set that has been measured over a wide range of depths. In the current data set, several difficulties can be identified:

- The data amount below –150 m is small,
- measurements have been targeted to measure HCDs, not HRD,
- a range of test scales have been used (Figure 2-2 and Figure 2-7),
- different test metods have been used,
  - which have different detection limits, and a large subset of the data population fall below the highest detection limtit, and
  - are concentrated to different depths and boreholes, which may possibly induce articficial trends.

In order to simplify the analysis of a depth trend in HRD transmissivity, a refined data set is used where the influence of depth has been isolated from the influence of other factors, as far as possible. The following steps were taken to refine the data set:

- Only data ratained in the screening process are used (Section 5.1.1).
- Only data with fraction inside HCD envelope less than 50% are retained.
- Only data with a test scale less than or equal to 3 m are retained.
- Minimum tranmissivity value set to the highest detection limit (9×10^{-8} m^2/s), independently of test method.
- Exclusion of falling head data is explored.

Depth dependency in transmissivity can be tested by means of inference tests. For the case of transmissivity data, which are heavily censored by the detection limit, non-parametric tests are suitable. These tests were performed on a subset of the available hydraulic data, from which all HCD data and variation in test scale are excluded, in order to isolate the potential HRD depth dependency in transmissivity. It was also explored if the exclusion of test type, falling head, improves the significance of tests. It was decided to use the two-sample Kolmogorov-Smirnov Test, which tests if two data sets come from the same underlying distribution. The data are divided into tentative elevation bins and their cumulative density functions are compared to determine the absolute maximum difference in cumulative probability, D_{12}, between the experimental CDFs of two data samples F_1 and F_2. The two-sample Kolmogorov-Smirnov Test rejects the null-hypothesis that two one-dimensional data sets belong to a common distribution, at significance α, if the absolute maximum difference, D_{12}, is larger than the critical K-S test statistics:

$$D_{12} = \max \left| F_1^e(x) - F_2^e(x) \right| \geq c(\alpha) \sqrt{\frac{n_1 + n_2}{n_1\, n_2}}, \quad c(0.01) = 1.63, \tag{4-3}$$

where n_1 and n_2 are sample sizes of the two data sets compared. The Kolmogorov-Smirnov test is known to be a weaker test if the maximum difference occurs far from the median of the two data samples.

4.2.4 Depth trend model, HRD

In case a statistical significance can be identified for hydraulic data with depth, it is also of interest to analyse whether the depth dependency should be modelled by a continuous model (for example, eqs. (41), (44), and (45)), or as a step function (i.e. different expectation values for different elevation bins, as was done for the Forsmark Site Investigation /Follin et al. 2007b/). A simple HRD conductivity model was suggested by /Carlsson et al. 1986/,

$$K(z) = K_0(-z)^{-\beta} \tag{4-4}$$

where the conductivity at 1 m depth $K_0 = 5.65 \times 10^{-6}$ m/s, z is elevation coordinate (m, RHB70), and $\beta = 1.3$. This equation was criticised by /Axelsson 1986/, as it tends to infinity at ground level, and instead the following model was suggested:

$$K(z) = K_0 \left(1 - \frac{z}{\eta} \right)^{-\beta} \tag{4-5}$$

where the ground level conductivity is $K_0 = 2.1 \times 10^{-7}$ m/s, z is elevation coordinate (m, RHB70), $\eta = 50$ m, and $\beta = 2.54$. These different depth dependency models are compared in Figure 6-1.

One method to analyse trends in heterogeneous data is to visualise data with depth using some type of moving average. As hydraulic data often are lognormally distributed, the appropriate choice would be a moving geometric mean, or median with depth. However, for the current data set this is complicated by the censoring effects of the detection limit, and the fact that the fraction of censored data increases with depth, which in itself is an evidence for a depth trend. A method was used to extrapolate the transmissivity median with depth, by assuming that the shape of the transmissivity distribution changes less with depth than its location (median; Figure 4-1). The proportion of data below detection limit for a rolling data set (hereafter referred to as the detection-limit percentile) can be studied as a continuous function with depth (Figure 5-30). This rolling data sample size should be chosen small enough to capture as much as possible of the depth range, and yet large enough to hamper the noise of heterogeneity. The rolling data sample sizes tested were 50 and 100. The next step is to, somehow, relate the depth trend in detection-limit percentile to a depth trend in transmissivity.

If it can be assumed that the shape of the transmissivity distribution (i.e. variance and higher statistical moments) changes negligibly with depth in comparison to its location (median), then the detection-limit percentile can be related to a logarithmic translation in transmissivity with depth. The translation in distribution between two data sets can then be calculated as the numerical shift between their cumulative distributions, i.e. the distributions are expected to differ by an approximately constant transmissivity at any given percentile. For a given data sample of size n, with mean elevation z, a detection-limit percentile can be calculated, $T_{\%}(z)$. Next, an order-of-magnitude ratio (i.e. shift in logarithmic transmissivity)

can be evaluated between this $T_{\%}(z)$ and its corresponding percentile value in the distribution at some other reference level, $T_{\%}(z_0)$. Finally, this order-of-magnitude ratio between elevations z and z_0 , which has been calculated for some percentile %, is assumed to apply also for the medians, $T_{0.5}(z)$

$$\hat{T}_{0.5}(z) = T_{0.5}(z_0)\frac{T_{\%}(z)}{T_{\%}(z_0)} = T_{0.5}(z_0)\frac{9\times10^{-8}}{T_{\%}(z_0)} \qquad (4\text{-}6)$$

An example is shown in Figure 4-1: a reference data set is formed by the highest 50 contiguous data values of the present data set, spanning from –10 to –23 m.a.s.l. with z_0 = –17.8 m.a.s.l. and a median transmissivity of $T_{0.5}(z_0) = 2.25\times10^{-7}$ m²/s. A second deeper set of 50 contiguous data spans from –50 to –66 m.a.s.l. and has a mean elevation z = –58 m.a.s.l. and its detection limit occurs at percentile 0.67. Thus, the 67th percentile is $T_{0.67}(z) = 9\times10^{-8}$ m²/s in the lower data set, while $T_{0.67}(z_0) = 6.6\times10^{-7}$ m²/s in the reference data set, which means that the transmissivity in the lower data set is a factor 7.3 less compared to the reference data set, at least at the 67th percentile. If the two data sets have similar distribution shapes, the median of the lower data set can be estimated to be $2.25\times10^{-7}/7.3 = 2.9\times10^{-8}$ m²/s (see Section 5.4.2).

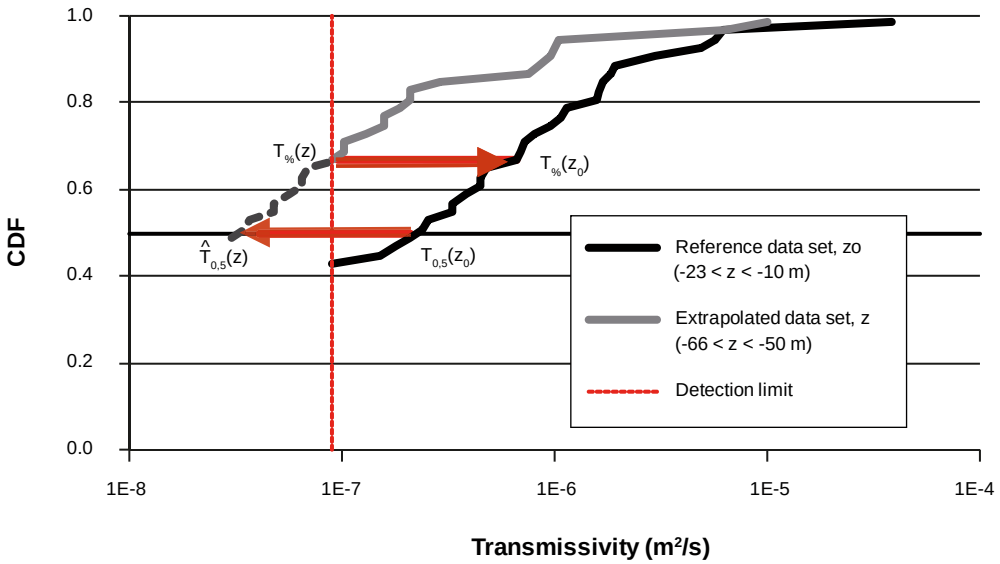

Figure 4-1. *An example of extrapolating the transmissivity distribution below the detection limit. The reference data set, z_0 (–23 < z < –10 m) is used to extrapolate an estimated median of a deeper data set, z (–66 < z < –50 m), which is censored by the detection limit 9×10^{-8} m²/s.*

5 Results

5.1 Preparation of data

5.1.1 Screening of data

The data excluded in the screening process are listed in Appendix A, Table A-1. One objective of the screening was to retain a high spatial resolution of the transmissivity data: short section data are preferred over long test sections. In terms of number of data, more than 80% of the hydraulic data are available at the 2- or 3-m test scale (blue line, Figure 5-1), but in terms of total borehole length tested these 2- or 3-m scale hydraulic data only comprise 25% of the rock volume tested (red line, Figure 5-1). In other words, long test sections are perhaps few in terms of number of data, but nevertheless important as they represent a large proportion of the total rock volume tested. The impact of preferably retaining short test scale data in the screening process can be observed in the test-scale distribution of transmissivity data (c.f. Figure 5-1 and Figure 5-2), where the fraction of borehole coverage by test scales exceeding the 3 m-scale drops from 75% to 50% (although the change appears insignificant if expressed in terms of cumulative number of data).

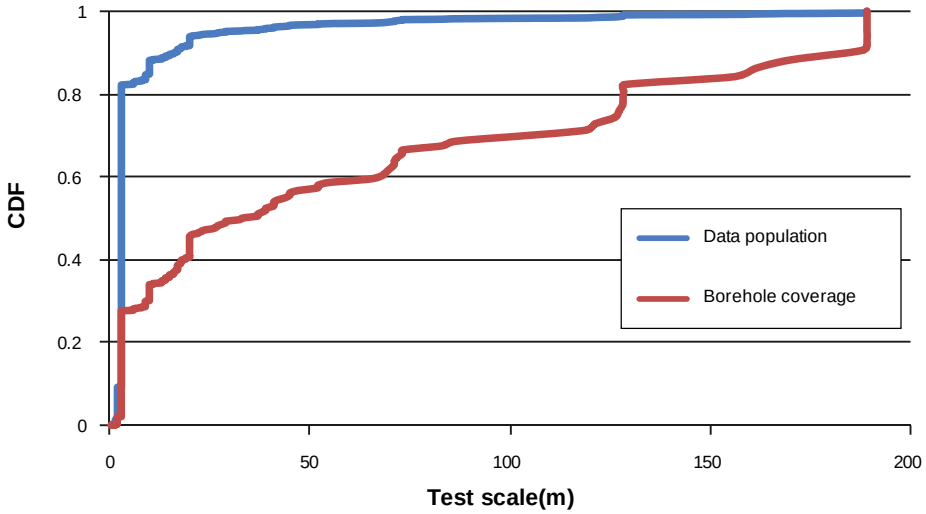

Figure 5-1. *Distribution of test scales for hydraulic data prior to screening. The distribution is shown in terms of cumulative number of data with test scale (blue line) and in terms of cumulative tested borehole length (red line).*

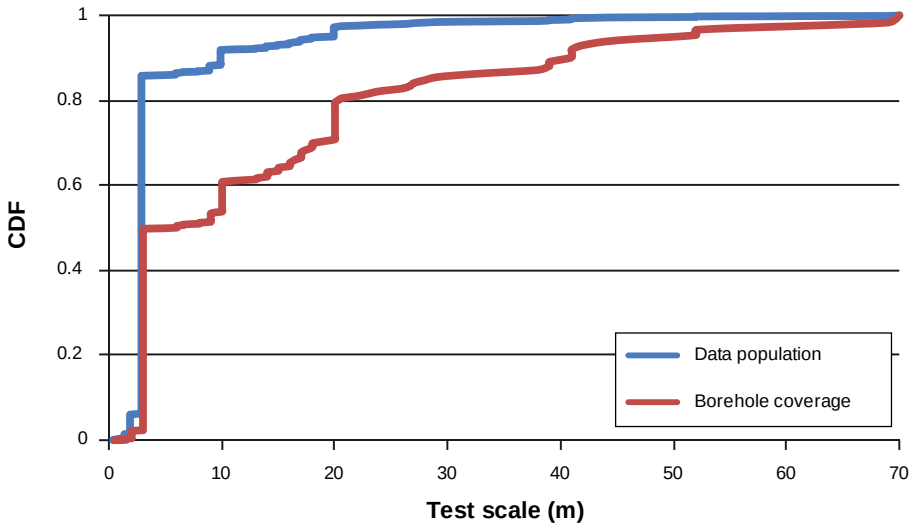

Figure 5-2. *Distribution of hydraulic data test scales after screening.*

5.1.2 Review of HCD envelopes based on hydraulic anomalies

On the basis of anomalous hydraulic data located near the HCD envelope (case 4 in Figure 3-2), it was decided to extend the HCD envelopes for five out of 67 HCD intercepts (Table 6-1). These modifications are fairly small, ranging from 5 to 15 m in terms of borehole length. Also, the entire intercept of ZFMwnw0813 in KFM11A was moved 50 m upwards (Table 6-1; Figure B-4). Additionally, four unusually high transmissivity data are found at –130 m.a.s.l. in boreholes KFR25 and KFR37 (Figure 5-3). In KFR37, these borehole sections are only 10 m outside the hydraulic envelope of ZFM871, and the same would be true for the sections in KFR25 if ZFM871 continues through ZFMNW0805a; see Figure 5-3). It was decided not to expand the hydraulic envelope of ZFM871 to include these four borehole sections. In KFR37 there is no definite break between HCD/HRD in hydraulic data to support modifying the envelope boundaries (Figure B-32), and for KFR25, according to the modelled termination of ZFM871 against ZFMNW0805a in the current geological model, its potential hydraulic influence in KFR25 appears unlikely (Figure B-24). These four borehole sections are discussed further in the depth trend analysis, Section 5.4.2.

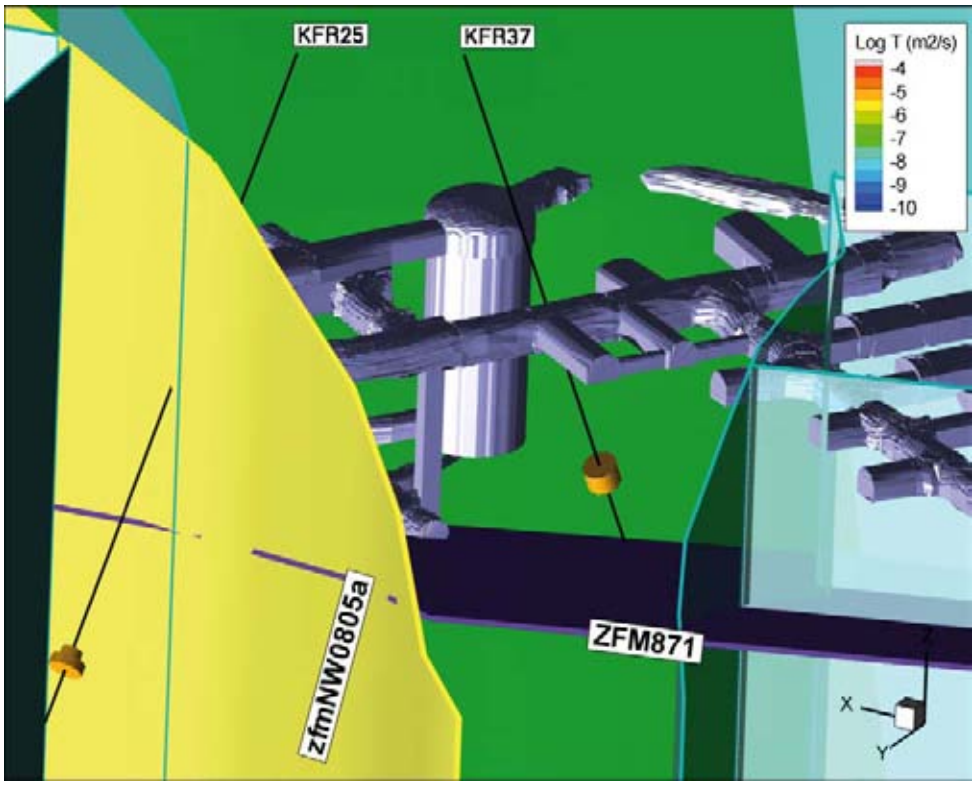

Figure 5-3. *Four unusually transmissive 3 m sections in HRD at –130 m.a.s.l. The sections are within 10 m from the envelope of ZFM871 (providing a continuation of ZFM871 through ZFMNW0805a).*

5.2 HRD/HCD classification of hydraulic data

The screened hydraulic data fall into three groups: 1) completely inside HCD, 2) completely inside HRD, and 3) data that extend across the HCD/HRD bounds: the "undecided group". As stated above, most hydraulic tests have been conducted at the 3 m scale. Eventhough the 3 m scale domainates the data population in terms of number of data, it is less dominant in terms of borehole coverage (see Figure 5-2; Table 5-1). In particular, the undecided hydraulic data is dominated by longer test scales (i.e. 79% of the undecided data reflect scales larger than 3 m). This is the reason for analysing the sensitivity in HCD/HRD classification for the calculation of HCD intercept transmissivity (Section 5.3.1).

5.3 HCD transmissivity

HCD intercept transmissivity is calculated based on a varying "minimum fraction of hydraulic data section required inside HCD bounds" (Section 4.2; Table 4-1). The criteria for calculating intercept transmissivity were set to, either that: 1) the available hydraulic data must cover 75% of the intercept, or 2) - if the coverage is less than 75% - the calculated intercept transmissivity must be at least 10^{-6} m^2/s (Table 4-1). Thus, the number of retained intercepts decline with a stricter requirement on fraction of section inside bounds (Figure 5-4). More HCD intercepts are retained if hydraulic envelopes are used, compared to if the modelled HCD thickness is used to define HCD bounds. The use of hydraulic envelopes makes intercept transmissivity less sensitive to "minimum fraction required inside HCD bounds", and retains fewer intercepts with transmissivity on par with HRD.

5.3.1 Sensitivity to HRD/HCD classification

Interval transmissivities calculated from data strictly inside HCD (i.e. minimum fraction inside HCD = 1) are shown with light grey lines in Figure 5-5 to Figure 5-8. The darker grey lines represent the gradual inclusion of undecided data (Table 5-1), sections partially extending into the HRD. If the classification is based on modelled HCD thickness and intercept transmissivity is calculated by the continuum principle, the gradual inclusion of data partly inside HRD lowers the median transmissivity, and in general, the lower end of the distribution (Figure 5-5). However, if intercept transmissivity is calculated by discrete principle (Table 4-1), the transmissivity distribution apperars more stable (c.f. Figure 5-5 and Figure 5-6). The reason is that the gradual inclusion of data partly inside HRD results in a larger number of intercepts retained (Figure 5-4), and the transmissivity of these additional intercepts are interpreted as lower than average if the continuum principle is used, while interpreted as more similar to the data completely inside HCD (i.e. Table 5-1), if the discrete principle is used. Clearly, it is difficult to motivate a dependency between poor data coverage and HCD transmissivity. Therefore, the discrete principle appears a preferable method, at least in the case of using modelled HCD thickness as discriminating bounds for data.

Table 5-1. Relative proportions of hydraulic data per test scale class and hydraulic domain classification.

	Test scale classes			
Relative data populations (%)	**< 3 m**	**3 m**	**> 3 m**	**Grand Total (no. data)**
Completely inside HCD	6%	80%	14%	175
Completely inside HRD	5%	87%	8%	484
Undecided	9%	58%	33%	166
Grand Total (no. data)	52	656	117	825
Relative borehole coverage (%)	**< 3 m**	**3 m**	**> 3 m**	**Grand Total (m)**
Completely inside HCD	2%	50%	48%	841.28
Completely inside HRD	1%	70%	29%	1,792.9
Undecided	2%	19%	79%	1,478.97
Grand Total (m)	64.9	1,968	2,080.25	4,113.15

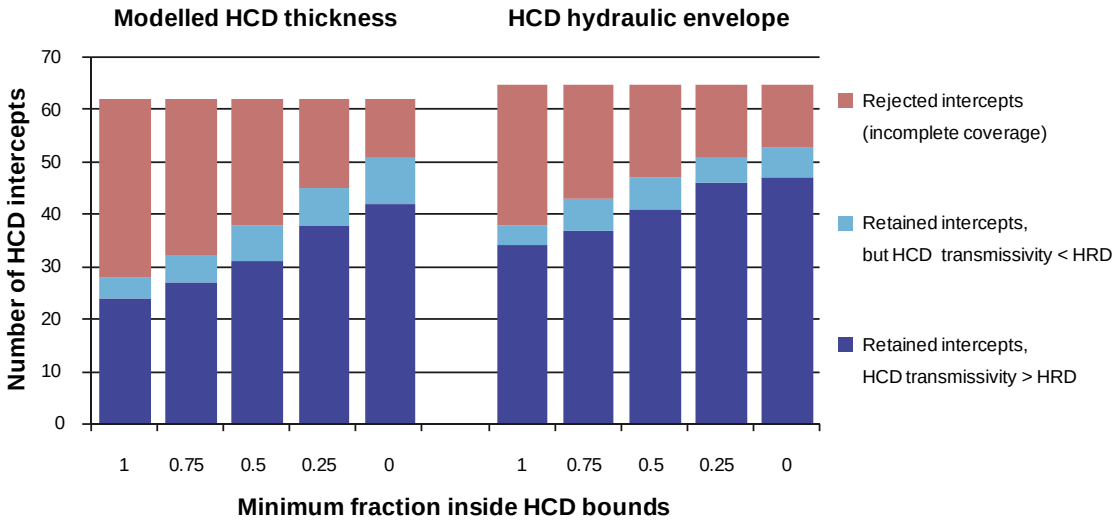

Figure 5-4. *Population of retained HCD intercepts depending on classification constraint. The HCD is assumed bounded by modelled thickness (left) and hydraulic envelope (right). Transmissivity calculated by continuum principle and HRD conductivity assumed to be 10^{-8} m^2/s.*

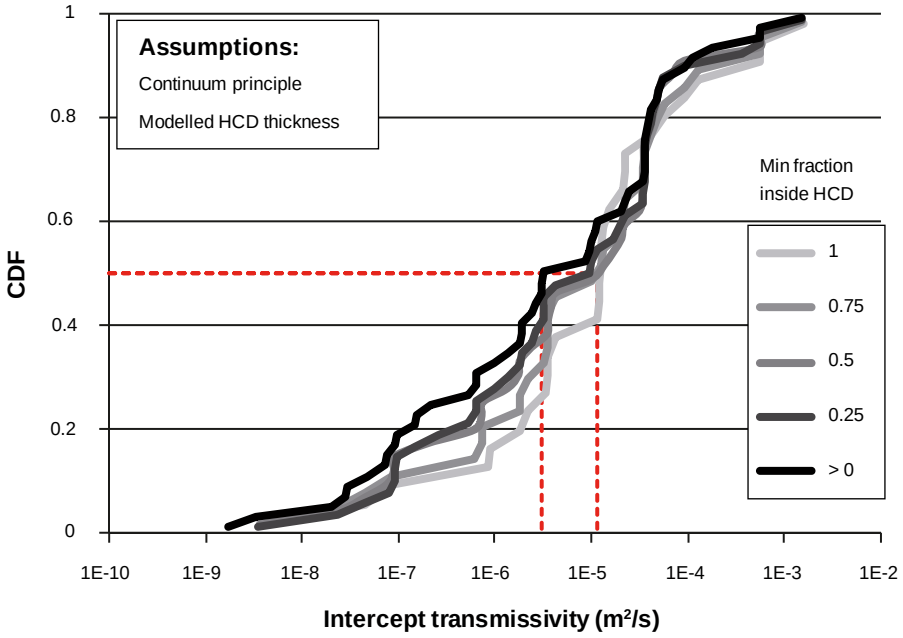

Figure 5-5. *HCD intercept transmissivity depending on data classification. The HCD is assumed bounded by modelled thickness. Transmissivity values divided between HCD/HRD by the continuum principle.*

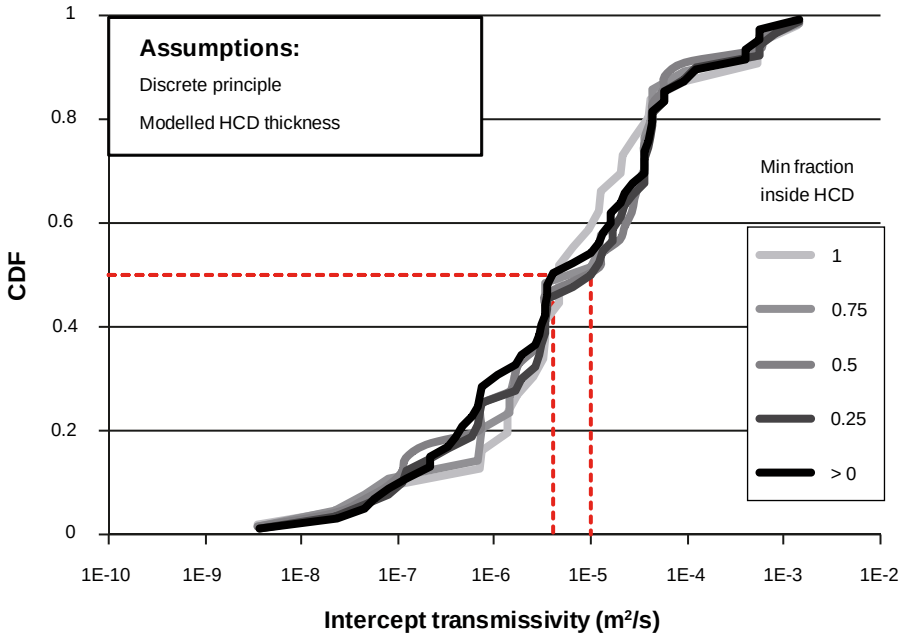

Figure 5-6. *HCD intercept transmissivity depending on data classification. The HCD is assumed bounded by modelled thickness. Transmissivity values divided between HCD/HRD by the discrete principle.*

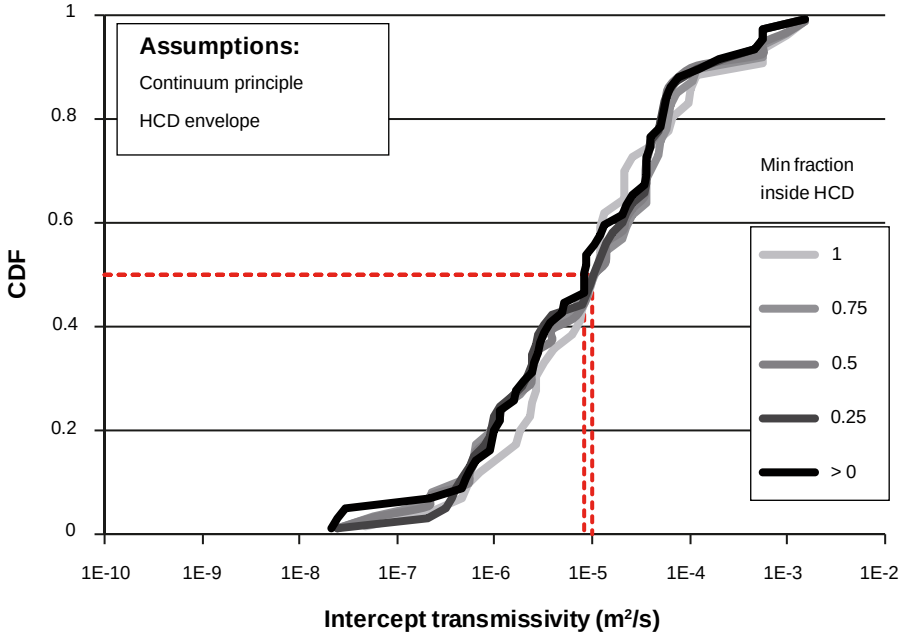

Figure 5-7. *HCD intercept transmissivity depending on data classification. The HCD is assumed bounded by hydraulic envelope. Transmissivity values divided between HCD/HRD by the continuum principle.*

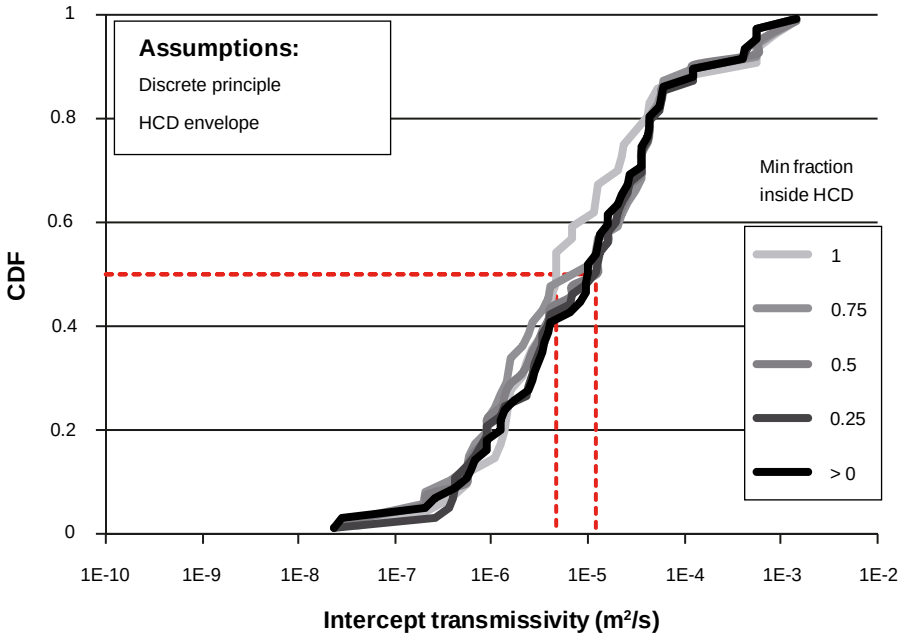

Figure 5-8. *HCD intercept transmissivity depending on data classification. The HCD is assumed bounded by hydraulic envelope. Transmissivity values divided between HCD/HRD by the discrete principle.*

If HCD envelopes are used, the gradual inclusion of undecided data has a less drastic impact on number of intercepts retained (i.e. data sample; Figure 5-4). In this case, the continuum principle provides a more stable intercept transmissivity distribution (Figure 5-7). The discrete principle gives a lower median transmissivity for the case of data strictly inside HCD (i.e. min fraction inside HCD = 1; Figure 5-8). This pattern can also be observed for the earlier case where the modelled HCD thickness was used as discriminating bounds (Figure 5-6). Irrespectively of what principle is used to divide transmissivity between HCD and HRD, the distributions grow more stable with larger data sample (i.e. more data classified as HCD). Thus, it is considered preferable to base the estimation of HCD transmissivity on a larger data set. However, in doing so, the risk of including systematic errors must be considered (Section 5.3.2).

The effective HCD transmissivity, calculated by the continuum principle with a minimum fraction inside HCD = 0.5, is presented for individual HCDs (Table 6-2) and for HCDs grouped by orientation (Table 6-3).

5.3.2 Analysis of conceptual/systematic errors

The uncertainty in bounds of HCD intercepts is represented by hydraulic HCD envelopes and the gradual inclusion of data partly extending outside HCD bounds. This implies that the calculations of HCD intercept transmissivity to varying degrees include hydraulic data which actually belong to HRD. To examine the significance of excessive inclusion of HRD data, an approximate background HRD transmissivity was subtracted from the HCD intercept transmissivity (i.e. the results of Section 5.3.1). In this analysis, the HRD conductivity was assumed to be 10^{-8} m/s, which appears realistic (Section 5.4). The transmissivity of each HCD intercept was then subtracted by its HRD transmissivity, calculated as HRD conductivity multiplied by the borehole length of the data used in the calculation of the intercept (Section 4.2; Table 5-3). For example, with a 5 m HCD intercept, the subtracted HRD transmissivity is 5×10^{-8} m²/s, which is higher than the lower tail of the calculated HCD transmissivities (e.g. Figure 5-5).

Independently of discriminating bounds used or principle of HCD transmissivity calculation, this subtraction of HRD transmissivity only affects the lower part of the transmissivity distribution (Figure 5-9 to Figure 5-12). The relative contribution of HRD transmissivity to the estimation of median transmissivity of HCD intercepts is small. This indicates that, excessive inclusion of HRD data probably has little impact on the estimation of median HCD transmissivity. The effects are expected to be larger at the lower tail of distributions, where the calculated HCD transmissivity

values are of similar magnitude as the background HRD value (Figure 5-13). The HCD has lower transmissivity than HRD for 20% of the intercepts, if modelled thickness is used as discriminating bounds (Figure 5-9 and Figure 5-10), while only 10% is lower than HRD, if hydraulic envelopes are used (Figure 5-11 and Figure 5-12). This is considered to be of lesser importance, as the parameterisation of HCDs primarily targets the upper tail of transmissivity.

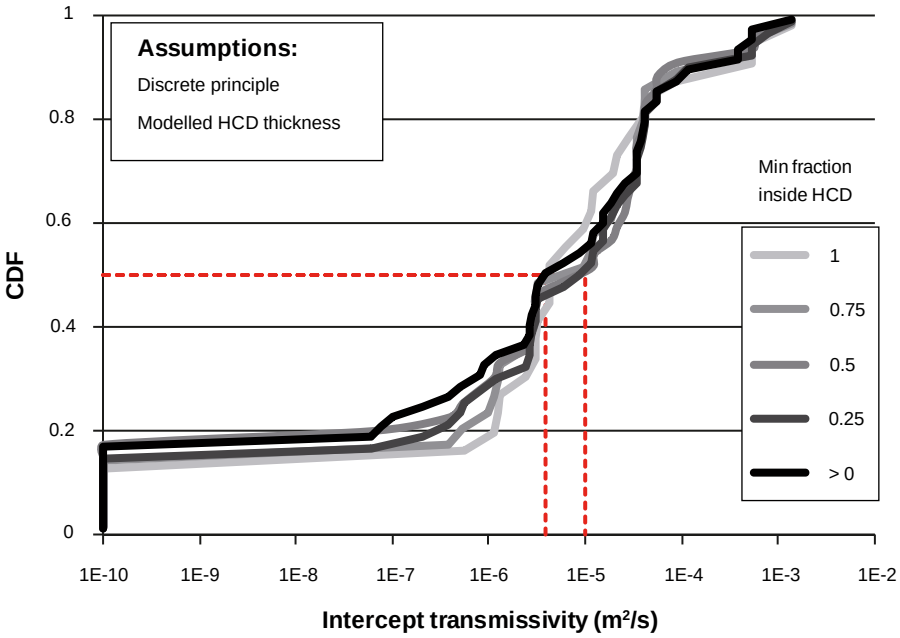

Figure 5-9. *HCD intercept transmissivity depending on data classification; HRD transmissivity subtracted. Modelled HCD thickness used as discriminating bounds, and transmissivity calculated by the continuum principle (cf Figure 5-5).*

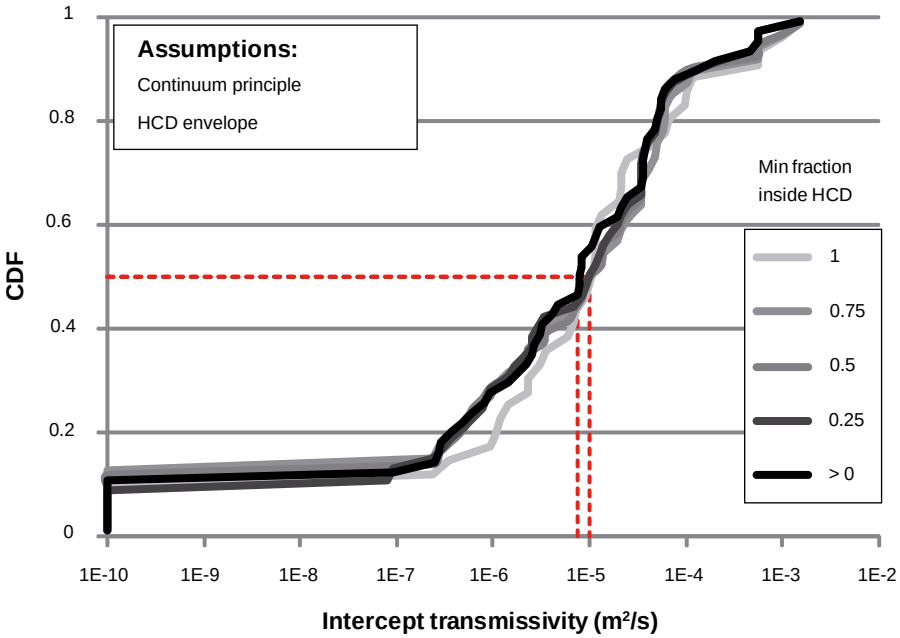

Figure 5-10. *HCD intercept transmissivity depending on data classification; HRD transmissivity subtracted. Modelled HCD thickness used as discriminating bounds, and transmissivity calculated by the discrete principle (cf Figure 5-6).*

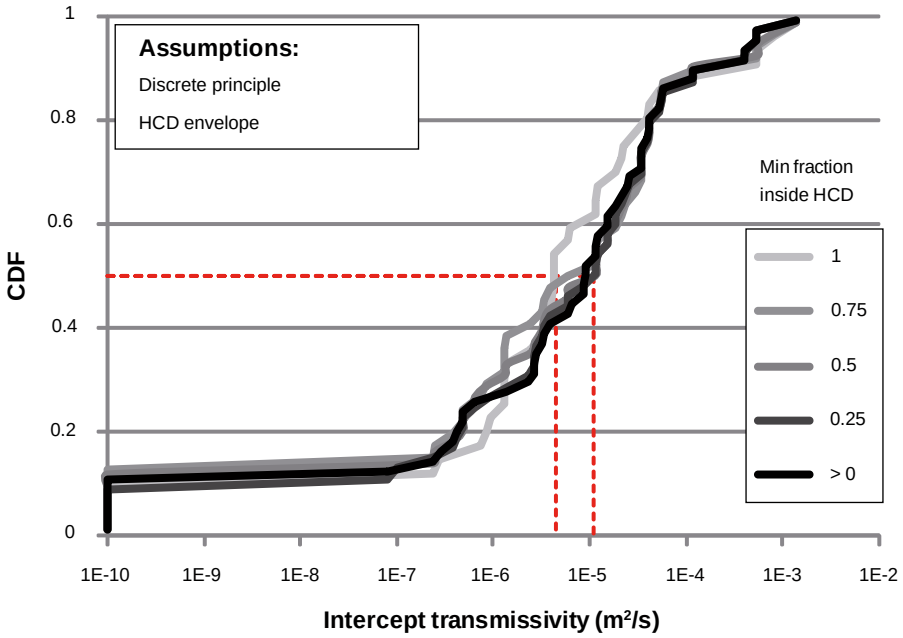

Figure 5-11. *HCD intercept transmissivity depending on data classification; HRD transmissivity subtracted. HCD hydraulic envelope used as discriminating bounds, and transmissivity calculated by the continuum principle (cf Figure 5-7).*

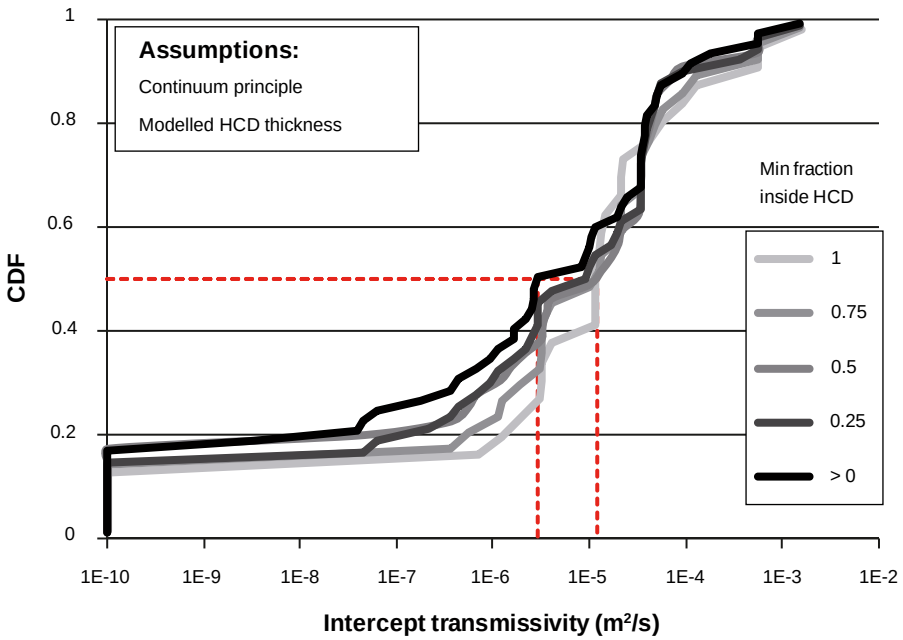

Figure 5-12. *HCD intercept transmissivity depending on data classification; HRD transmissivity subtracted. HCD hydraulic envelope used as discriminating bounds, and transmissivity calculated by the discrete principle (cf Figure 5-8).*

HCD intercept transmissivity is an integrated property across the width of a HCD. Ideally, this property should therefore be calculated along an axis perpendicular to the plane of the HCD. However, in Section 5.3.1, all borehole data inside or partly inside discriminating bounds are used in the calculation of HCD transmissivity, and the relation between borehole length inside a HCD and its true thickness depend on the alpha angle between the borehole and the zone. Thus, the calculation of intercept transmissivity may potentially be subject to geometric sampling bias. A borehole subparallel to a HCD plane (low alpha in Figure 5-13) covers a longer interval of the HCD than a perpendicular borehole would have done. Now, if this longer HCD interval contains several packer-sections, each with a transmissivity that is fairly representative for the HCD, then the sum of all tested intervals will overestimate the HCD transmissivity.

This geometric factor may exaggerate intercept transmissivity for low alpha angles. For example, the three highest intercept transmissivity values are all calculated for borehole intercepts with alpha angles less than 40° (assuming continuum principle, hydraulic envelope and minimum fraction inside = 0.5; Figure 5-13). However, there does not seem to be a clear trend between alpha and transmissivity with respect to the natural variation (and the uncertainties in data and the HCD parameterisation). Therefore, it was decided not to compensate for geometrical sampling bias.

5.3.3 HCD heterogeneity and depth trend

The HCD heterogeneity and its potential depth trend must be analysed simultaneously, as otherwise the depth dependency can be mistaken for random heterogeneity. The intercept transmissivities are plotted as a function of depth for all HCDs and compared to the depth trend of Site Investigation Forsmark (Figure 5-14). Below –250 m elevation, there are only 3 retained HCD intercepts. These values are calculated from KFM11A data of the Forsmark Site Investigation, which come from Singö and South of Singö, and are therefore less representative of the SFR regional domain. The data above –200 m.a.s.l. exhibit strong heterogeneity. The combination of a narrow elevation range (200 m) and highly heterogeneous data makes the identification and fitting of a depth trend highly uncertain. Furthermore, there is little support for studying all HCDs as a single homogeneous group: the hydraulic properties of HCDs are known to depend on other factors as well, like size, type of zone, orientation versus stress field, etc /Follin et al. 2007b/. The major principal direction of stress at SFR is NW (with a trend of 330°), while closer to the Singö-zone it becomes sub-parallel to the Singö-zone /Carlsson et al. 1987/. As an average of 10 stress measurements in KFR27, KFR51, and KFR52 (within the elevation range –40 to –140 m RHB70), the horizontal stress anisotropy is 2.5 and the vertical component generally being the minimum principal component. KFR27 is below the

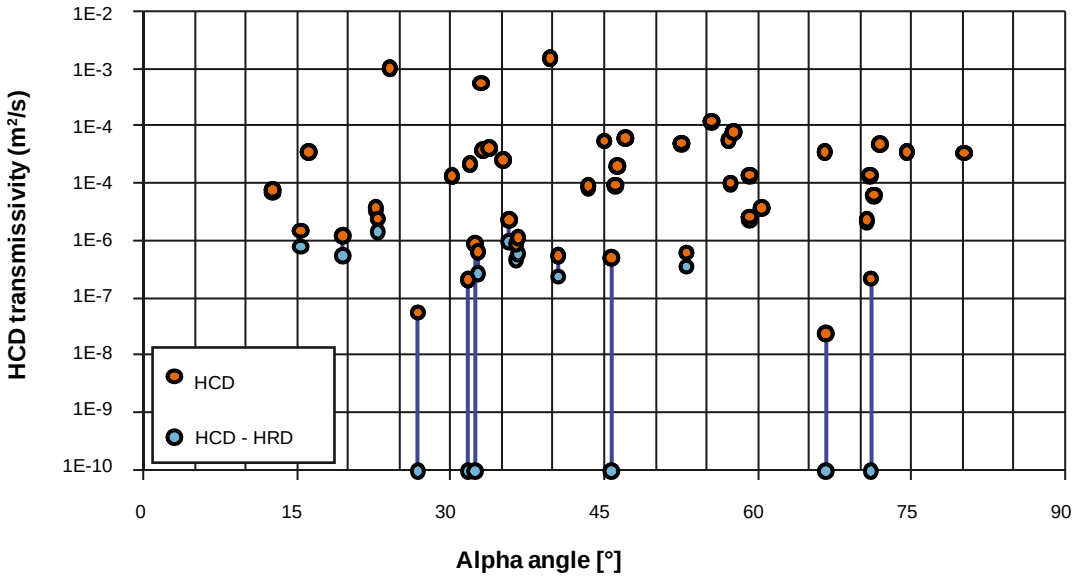

Figure 5-13. *Intercept transmissivity and alpha angle; assuming continuum principle, hydraulic envelope and minimum fraction inside = 0.5.*

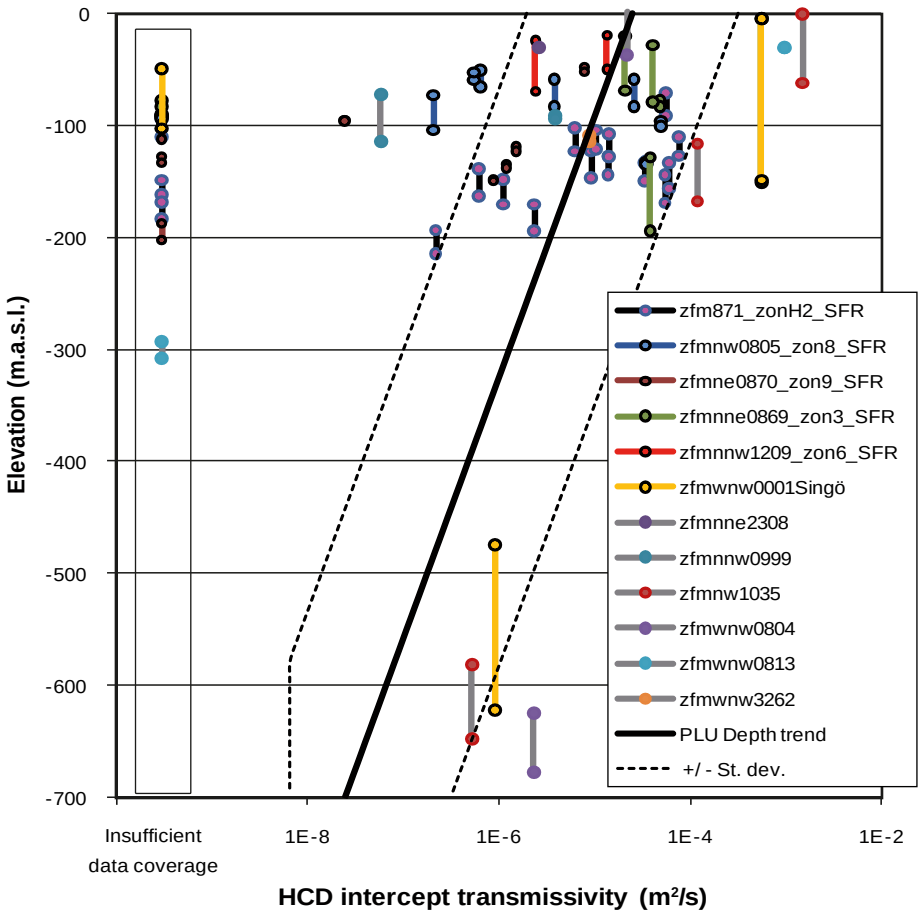

Figure 5-14. *HCD transmissivity as function of depth, shown with a depth trend. k = 232 m, eq. (41), according to /Follin et al. 2007b/. No HCD transmissivity calculated for intercepts with insufficient data coverage (shown next to y-axis). Data points show modelled elevation interval of HCDs.*

pier, KFR51 is close to BTF1, and KFR52 is close to the Silo. The average magnitudes of the principal components are approximately 12 MPa, 5 MPa, respectively, 2 MPa. Based on the stress regime, the hydraulic anisotropy in zones and fractures can be expected to be predominantly horizontal and NW-striking. This will be further investigated in subsequent hydrogeological model versions.

Nevertheless, the data do exhibit erratic indications of transmissivity depth dependency. For example the deepest intercept of ZFM871 has the lowest transmissivity, while its shallowest intercept has one of the highest transmissivities (Figure 5-15). In ZFMne0870 there are five retained intercepts; the transmissivity of four of these fall remarkably well onto a fitted exponential trend, while the fifth intercept has a lower transmissivity (Figure 5-16). The generality and the applicability range of these fitted trends are highly uncertain.

The tentative depth trend shown in Figure 5-14 is based on principles and findings developed during from the Site Investigation Forsmark /Follin et al. 2007b/, and has been calculated according to eq. (4-1) (See Section 4.2.2). It is difficult to state how well the HCD data conform to this depth trend, and it must also be considered that the Forsmark and the SFR domains are different geological units, separated by the regional deformation zone Singö /Stephens et al. 2007/. Nevertheless, it is unrealistic to assume a HCD transmissivity that is constant with depth down to bottom of the model domain (1,100 m). In lack of contradictive evidence, it was considered pragmatic to apply the Site-Investigation-Forsmark trend in the calculation of effective ground-level T_0, as calculated by eq. (4-2). The effective HCD transmissivity is summarized in Section 6.1, for individual HCDs (Table 6-2) and for HCDs grouped by orientation (Table 6-3).

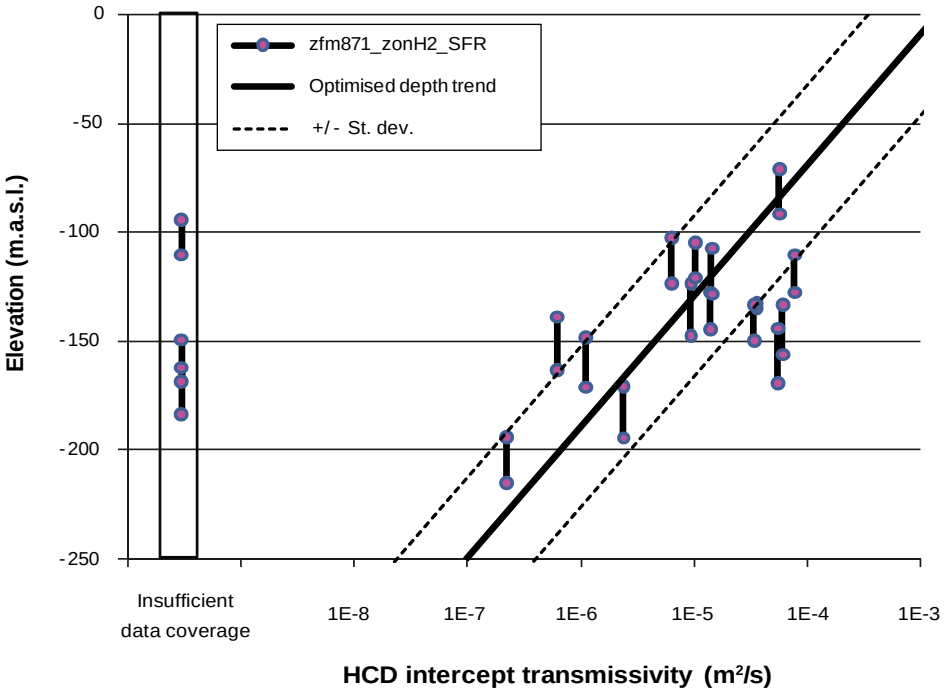

Figure 5-15. *Transmissivity in ZFM871 as function of depth shown with a fitted depth trend. k = 60 m, eq. (41).*

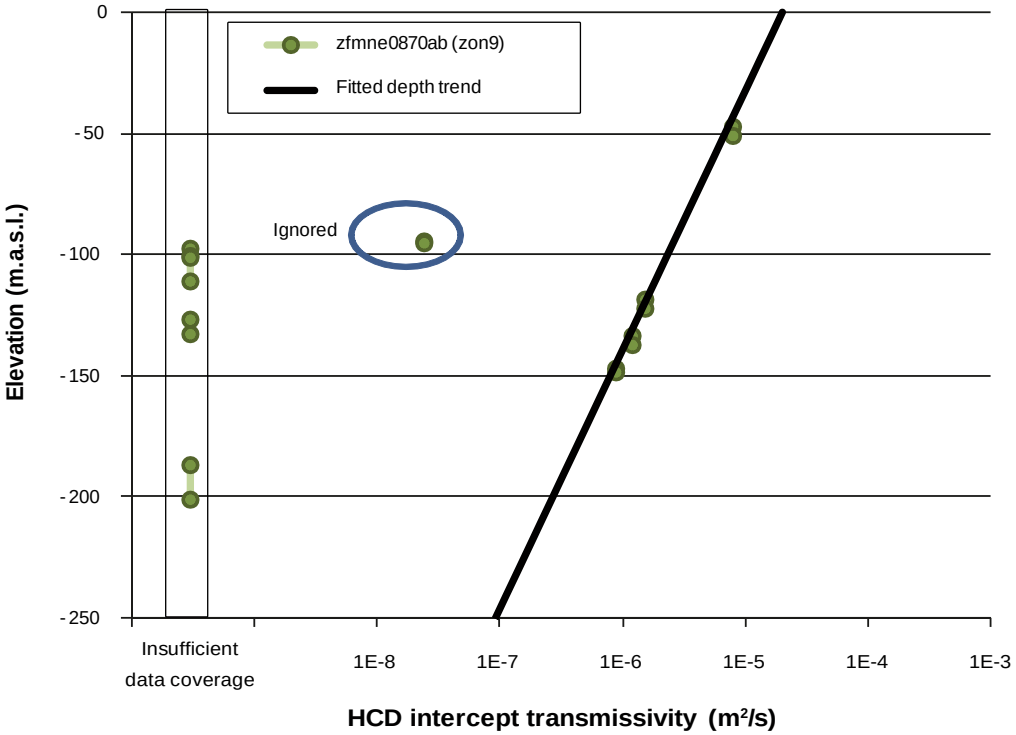

Figure 5-16. *Transmissivity in ZFMne0870 as function of depth shown with a depth trend. k = 107 m, eq. (41), fitted to four different intercepts (KFR02, KFR03, KFR31, and KFR70).*

During the Site Investigations e.g. /Follin et al. 2007b/ a pragmatic method was developed to transfer the parameterisation from well-characterised HCDs to poorly characterised HCDs. The method was to find a method to identify statistically "homogeneous" HCD subgroups with similar properties, such that these properties can be assigned to all HCDs within that group (i.e. a method to extrapolate hydraulic properties to HCDs without intercepts). In the SFR data set, the logarithmic transmissivity of all HCD intercepts, log T_0, have a standard deviation of 1.0; meaning that 95% of the variability in transmissivity is generally within four orders of magnitude. If the HCDs are grouped by orientation (Table 6-3), the standard deviations within subgroups is smaller for the only gently dipping HCD (ZFM871), and the NE to NNE-oriented HCDs. The fact that heterogeneity is smaller within these HCD subgroups supports the validity in grouping of HCDs by orientation. The perpendicular HCD groups, WNW- to NNW-oriented HCDs have higher internal heterogeneity.

The within-plane heterogeneity in ZFM871 is shown in relation to its modelled HCD depth trend (k = 232 m; Figure 5-17 and Figure 5-18).

5.3.4 HCD heterogeneity length scale

In the site investigation programme for Forsmark, the characteristic length scale of hydraulic heterogeneity in HCDs was determined to be approximately 100 m /Follin et al. 2007b/. This value was based on the separation distance between the two closest HCD intercepts, which nevertheless display large differences in transmissivity. The scale of heterogeneity was analyzed in ZFM871, as it is the single HCD with largest number of intercepts (i.e. the maximum number of data pairs for separation distances). The difference in logarithmic depth trend-compensated transmissivity, T_0 for all intercepts located less than 50 m apart in ZFM871 are shown in Table 5-2. Two values, with separation distances of 30 m and 45 m, have exceptionally high difference in logarithmic T_0, in comparison to the standard deviation of T_0 in ZFM871, $\sigma_{\log T_0} = 0.71$, and the average difference between all intercepts, $\Delta \log T_0 = 0.83$. This indicates that a scale of heterogeneity is less than 50 m. On the other hand, four out of the six data pairs closer than 50 m have exceptionally low difference in logarithmic T_0. The heterogeneity scale can be assumed to be 20 m, based on the two shortest separation distances (Table 5-2; or alternatively 40 m, if the large difference at separation distance 30 m is neglected). This length scale, 20 to 40 m, is comparable to the size of fractures with reason-

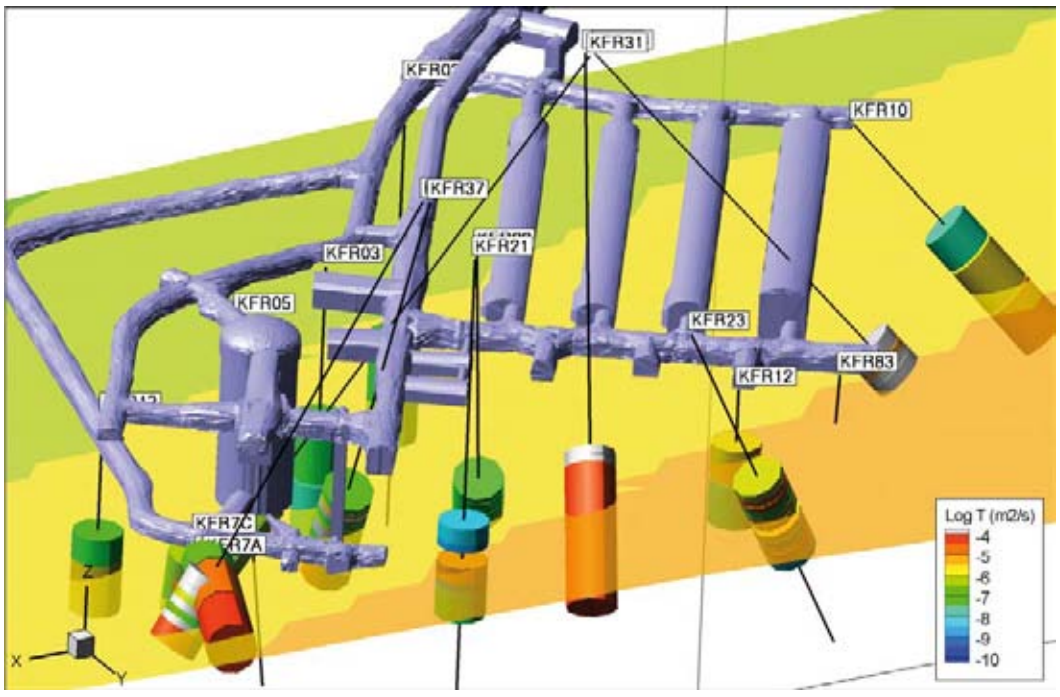

Figure 5-17. *Hydraulic data used to calculate intercept transmissivity in ZFM871 (ZonH2); assuming hydraulic envelope and minimum fraction inside = 0.5. The modelled centre plane of ZFM871 is contoured by its transmissivity depth trend, k = 232 m. Data below detection limit are shaded grey.*

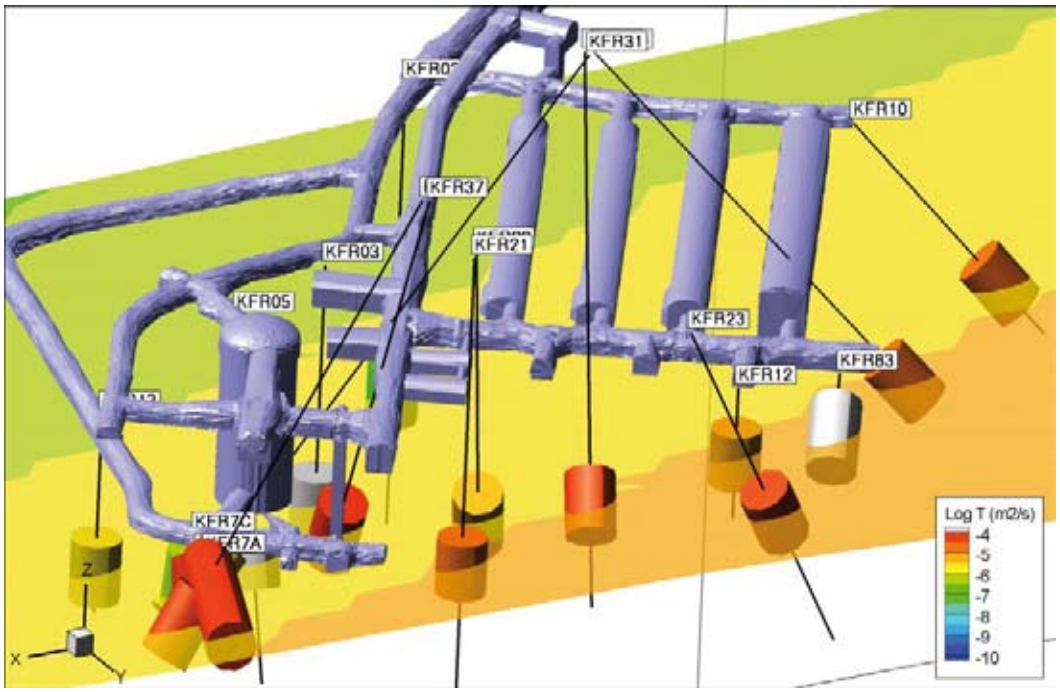

Figure 5-18. *Calculated intercept transmissivity in ZFM871 (ZonH2): heterogeneity and modelled depth trend. Continuum principle assumed, rejected intercepts KFR03, KFR05, KFR83 shaded grey. Cylinder length equal to modelled HCD thickness.*

Table 5-2. Transmissivity differences in ZFM871 between intercepts closer than 50 m.

Borehole intercepts		Separation distance, h (m)	$\Delta\log T_0$
KFR7C	KFR31	15.8	0.29
KFR7A	KFR38	18.4	0.23
KFR7C	KFR7B	30.6	1.71
KFR7B	KFR38	32.4	0.25
KFR7B	KFR7A	39.3	0.02
KFR31	KFR7B	45.4	1.42

ably high transmissivity. A few scope calculations: applying the correlated transmissivity relations for a 20 m radius fracture in the upper 200 m HRD in Site Investigation Forsmark, renders an approximate transmissivity of 5×10^{-7} m^2/s (FFM01 or FFM02) /Follin et al. 2007b/. At SFR depth, ZFM871 (Figure 5-15).

The spatial dependency of hydraulic heterogeneity of ZFM871 was also examined by means of experimental semi variograms, with separation distances binned by 100 m (Figure 5-19) and by 50 m (Figure 5-20). The purpose is to identify the lag distance where a sill is reached in the semi variogram (which can be taken as the scale of HCD heterogeneity). Unfortunately, the semi variograms provide little information on the scale of HCD heterogeneity. Apart from an unexpected peak hydraulic heterogeneity at 75 m separation distance, little else than nugget appearance can be observed in the semi variograms. Note that the semi variogram has been set to zero at separation distance equal to zero by definition. This makes it impossible to determine the lag distance for the sill, i.e. it appears to be reached already in the first bin. Thus, even in ZFM871, which has the highest number of borehole intercepts, the data are too sparse and separated too far apart to determine the lag distance of the sill. It is reassuring to observe that the spatial heterogeneity in depth-trend compensated T_0 appears more constant at large separation distances in comparison to the actual intercept transmissivity values. This indicates that the T_0 values are more stationary than the original intercept transmissivity values (and in turn that the depth trend has been successfully delineated).

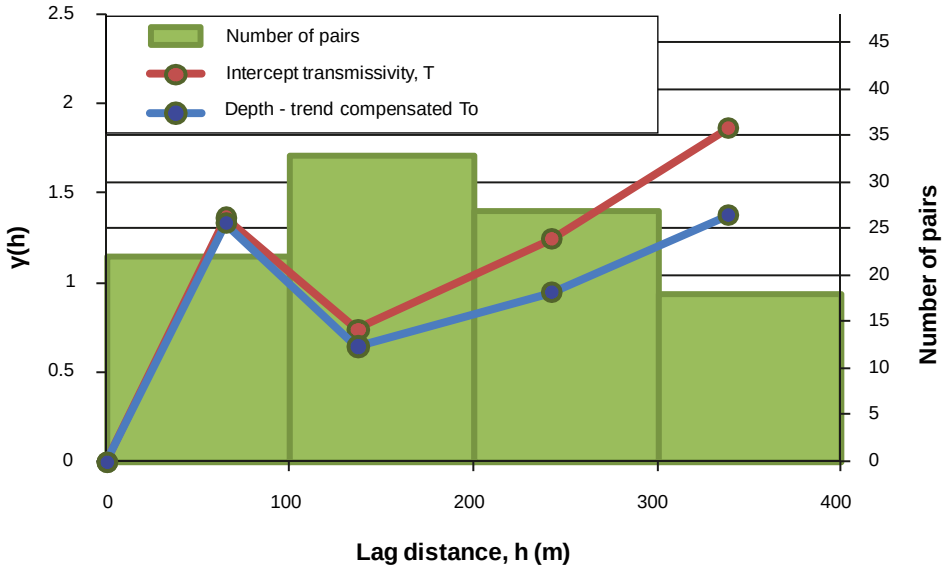

Figure 5-19. *Experimental semi-variogram of logarithmic intercept transmissivity in ZFM871 (ZonH2), calculated transmissivity and depth-trend compensated T_0, with distance binned by 100 m.*

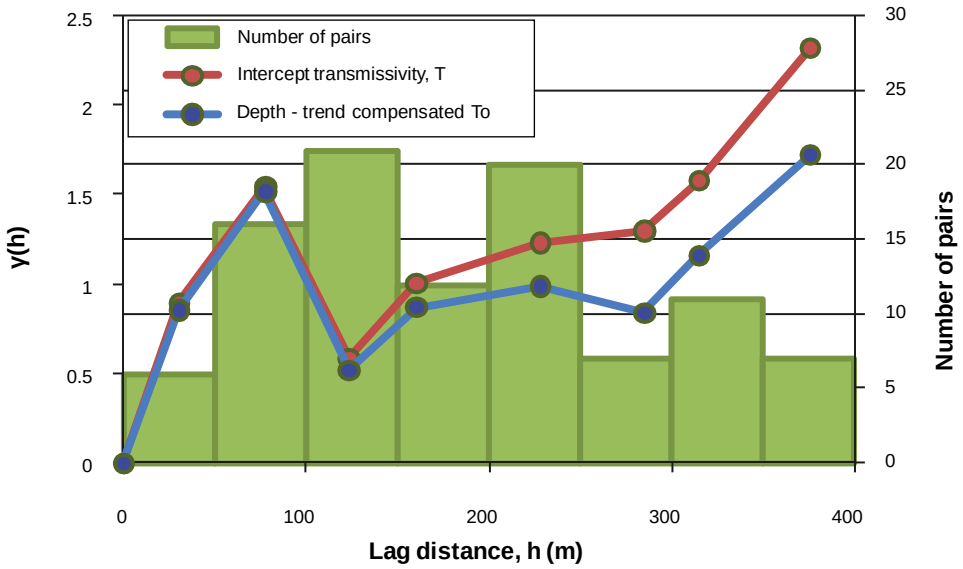

Figure 5-20. *Experimental semi-variogram of logarithmic intercept transmissivity in ZFM871 (ZonH2), calculated transmissivity and depth-trend compensated T0, with distance binned by 50 m.*

5.4 HRD transmissivity

5.4.1 Sensitivity to HRD/HCD classification

The HRD is the complement to the HCD. Thus, the HRD includes both data classified as completely inside HRD (Table 5-1), but also the leftovers from the undecided data in the HRD/HCD classification. Two different aspects were considered in the HRD/HCD classification of hydraulic data (Section 4.2): 1) the discriminating bounds and 2) the principle of treating data that extend across these bounds. The two alternative discriminating bounds are geometric definition of the deformation zone model, and the hydraulic envelope of a zone. The impact of the uncertainty in HCD bounds is analysed by comparing the results of gradual classification criteria “minimum fraction inside HCD” (Table 4-1). A minimum fraction inside HRD > 0 only requires tested sections to partially extend outside HCD bounds for a HRD classification, while fraction inside HRD = 1 requires that the enitre borehole section is inside HRD (i.e. strictly outside the HCD bounds).

Apart from the gradual criteria for classification of borehole sections, this sensitivity study also examines how the transmissivity values can be split between HRD and HCD, either according to the continuum principle (by proportionality), or by the discrete principle (binary; see Section 4.2). The HRD conductivity is evaluated in terms of arithmetic conductivity, K_A (sum of transmissivity divided by total tested borehole length), and in terms of geometric mean conductivity, K_G (and its logarithmic standard deviation $\sigma_{\log KG}$), at the 3 m scale. The 3 m scale was choosen, as most hydraulic data have a support scale of 3 m (Table 5-1). However, among the uncdecided data larger test scales are more frequent, particularily in terms of borehole length coverage. In order to resolve the hydraulic data at the 3 m scale distributions, longer test sections were subdivided into "artificial 3 m sections". For sections classified as completely inside HRD (Table 5-1), the transmissivity of such a subdivided section is assigned to one of the artificial 3 m sections, while all other artificial 3 m sections are assigned "below detection limit" transmissivity. For sections classified as "undecided" (Table 5-1), the artificial 3 m bins are assigned transmissivity, either according to the continuum principle (equally among bins), or to the discrete principle (only to bins inside HCD). Sections classified as completely inside HCD (Table 5-1) are excluded form this study.

The distribution of 3 m transmissivity, classified as strictly inside HRD (i.e. minimum fraction inside HRD = 1) are shown with light grey lines in Figure 5-21 to Figure 5-24. These distributions are independent of principle to divide transmissivity, but depends only on discriminating bounds, either modelled HCD thickness, or HCD envelopes. Darker grey lines represent the gradual inclusion of sections extending further into the HCD. The continuum principle increases mean conductivity (as more high transmissivity values are transferred from the HCD to the HRD), while the discrete principle decreases mean conductivity (as only sections below detection limit are transferred from the HCD to the HRD). Lognormal distributions are fitted to the transmissivity distributions, and a geometrical mean conductivity, K_G, is calculated from the transmissivity median and dividing by the 3 m section length.

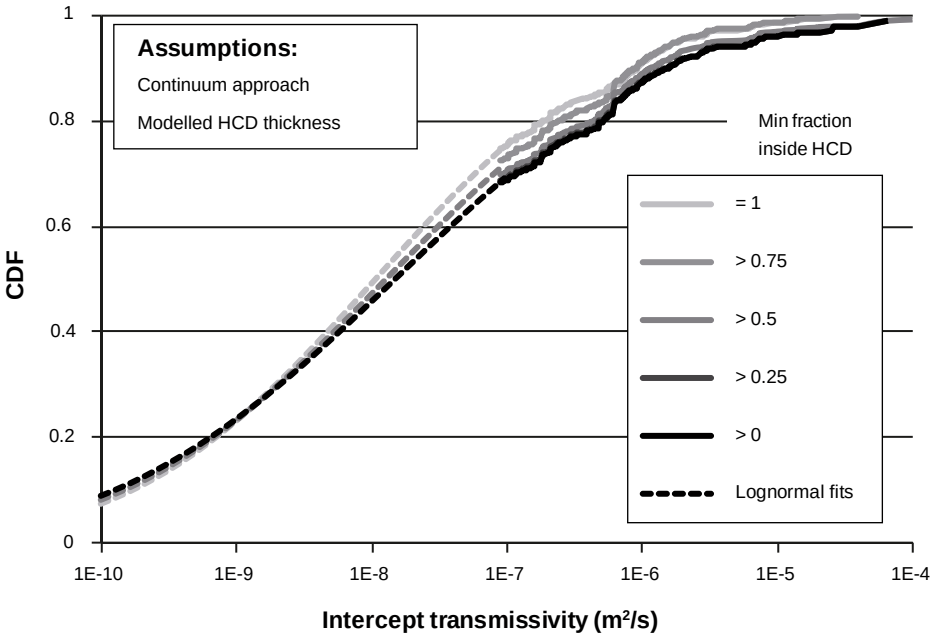

Figure 5-21. *HRD transmissivity distribution depending on constraint for excluding HCD. Borehole sections classified based on modelled HCD thickness. Transmissivity values divided between HCD/HRD by the continuum principle. Lognormal fit presented in Table 5-3.*

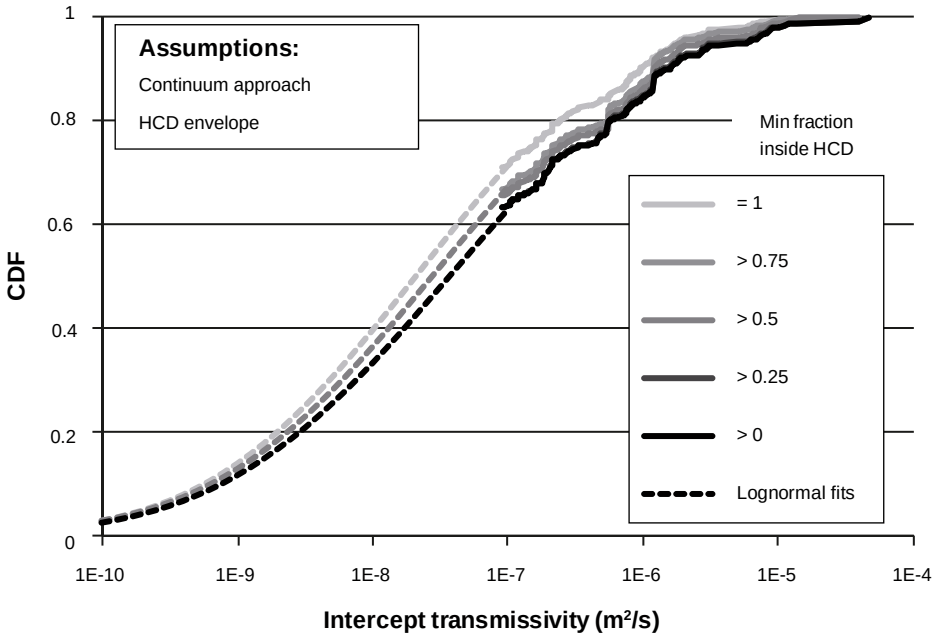

Figure 5-22. *HRD transmissivity distribution depending on constraint for excluding HCD. Borehole sections classified based on HCD envelopes. Transmissivity values divided between HCD/HRD by the continuum principle. Lognormal fit presented in Table 5-3.*

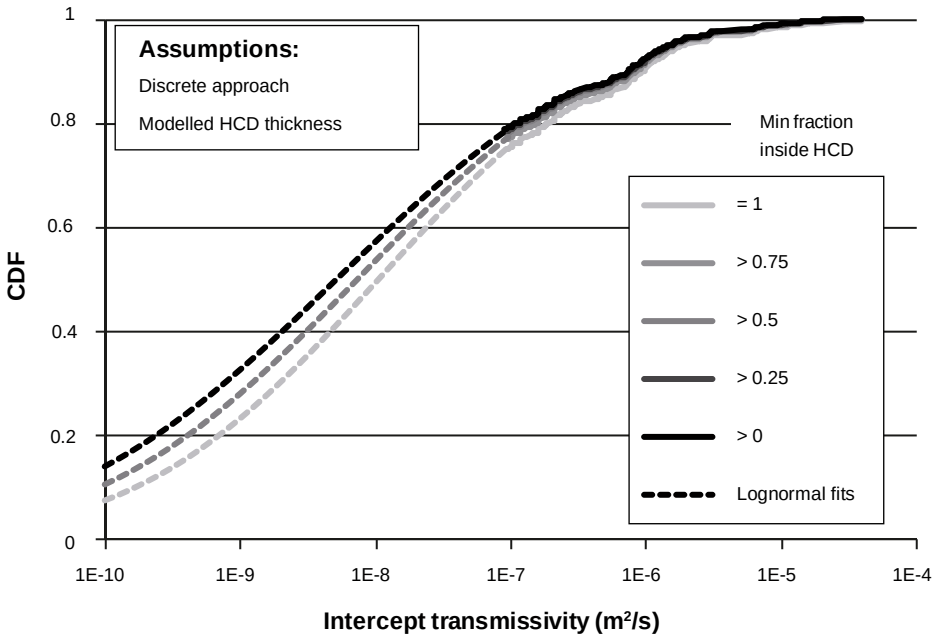

Figure 5-23. *HRD transmissivity distribution depending on constraint for excluding HCD. Borehole sections classified based on modelled HCD thickness. Transmissivity values divided between HCD/HRD by the discrete principle. Lognormal fit presented in Table 5-3.*

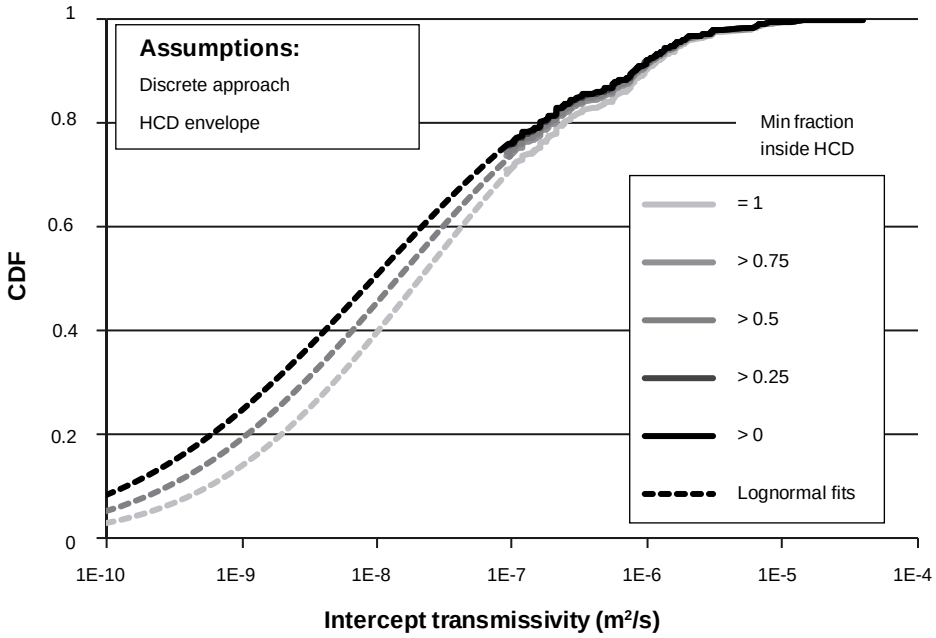

Figure 5-24. *HRD transmissivity distribution depending on constraint for excluding HCD. Borehole sections classified based on HCD envelopes. Transmissivity values divided between HCD/HRD by the discrete principle. Lognormal fit presented in Table 5-3.*

Table 5-3. Estimated HRD conductivity, depending on constraint for excluding HCD.

Discriminating bounds	Modelled zone thickness					Hydraulic envelope				
Min fraction inside HRD	= 1	0.75	0.5	0.25	> 0	= 1	0.75	0.5	0.25	> 0
Averaging borehole length (m)	2,468	2,672	2,800	2,869	2,890	1,819	1,999	2,070	2,165	2,188
Continuum method										
Arithmetic mean, K_A (10^{-8} m/s)	16.7	15.7	32.5	34.1	34.1	14.2	13.5	14.1	16.2	16.9
Log K_A	–6.8	–6.8	–6.5	–6.5	–6.5	–6.8	–6.9	–6.9	–6.8	–6.8
Geometric mean, K_G (10^{-8} m/s)	0.4		0.4		0.5	0.7		0.9		1.2
Log K_G	–8.5		–8.4		–8.3	–8.2		–8.0		–7.9
$\sigma_{log\ K}$	1.40		1.51		1.63	1.21		1.26		1.31
Discrete method										
Arithmetic mean, K_A (10^{-8} m/s)	16.7	15.5	14.8	14.4	14.3	14.2	12.9	12.5	11.9	11.8
Log K_A	–6.8	–6.8	–6.8	–6.8	–6.8	–6.8	–6.9	–6.9	–6.9	–6.9
Geometric mean, K_G (10^{-8} m/s)	0.4		0.2		0.2	0.7		0.5		0.3
Log K_G	–8.5		–8.6		–8.3	–8.2		–8.3		–8.5
$\sigma_{log\ K}$	1.40		1.48		1.57	1.21		1.31		1.41

5.4.2 HRD Depth trend

In order to simplify the analysis of depth trend in HRD transmissivity, a refined data set is used where the influence of depth has been isolated from the influence of other factors, as far as possible (Section 4.2.3). The remaining data population is shown in *Table 5-4*. Note that all pressure-build up tests have test intervals larger than 3 m, and are therefore excluded. The data amount of this refined data set is fairly constant with depth in the range –10 m to –140 m (*Figure 5-25*), scarce between –140 m and –250 m, and unavailable below –250 m.a.s.l. The data in the range between –140 m and –250 m is composed of 20 records of falling head data from KFR21, with only one value (1.2×10^{-7} m^2/s) barely above the detection threshold (9×10^{-8} m^2/s). It was decided to exclude these data from the analysis below, not because the data are contradictive, but in order to avoid drawing false conclusions. This large depth range is only represented by data from a single borehole, and has been measured with the lower confidence falling head method /Carlsson et al. 1987/. On the contrary, this excluded deep data conform well to the trend observed in the more shallower data.

As a first attempt, the HRD depth trend was analysed similarily as to how the HCD depth trend was fitted in the Forsmark Site investigation /Follin et al. 2007b/. The data were plotted as a function of depth, and by visual inspection, an exponential function is fitted from ground surface to the maximum transmissivity value at each depth level (Figure 5-26). This estimation is fixed to two data points, one at –20 m and a pair of data at –130 m. The depth interval that gives an order of magnitude decrease in transmissivity is 140 m. At the –130 m level, there are four data with transmissivity higher than 10^{-6} m^2/s. These come from sections only 10 m outside the envelope of ZFM871 (Figure 5-3). If these four data are excluded due to possible influence of ZFM871, the depth interval for a magnitude decrease in transmissivity is halved to 70 m (Figure 5-27). Thus, this method of fitting a depth trend is sensitive to the classification of HRD/HCD. Therefore it was explored if some more robust alternative could be used.

Table 5-4. Data population used in analysis for HRD depth trend.

	2 m scale	3 m scale	Total
Steady state tests		330	330
Transient injection	24		24
Falling head	1	98	99
Total	25	428	453

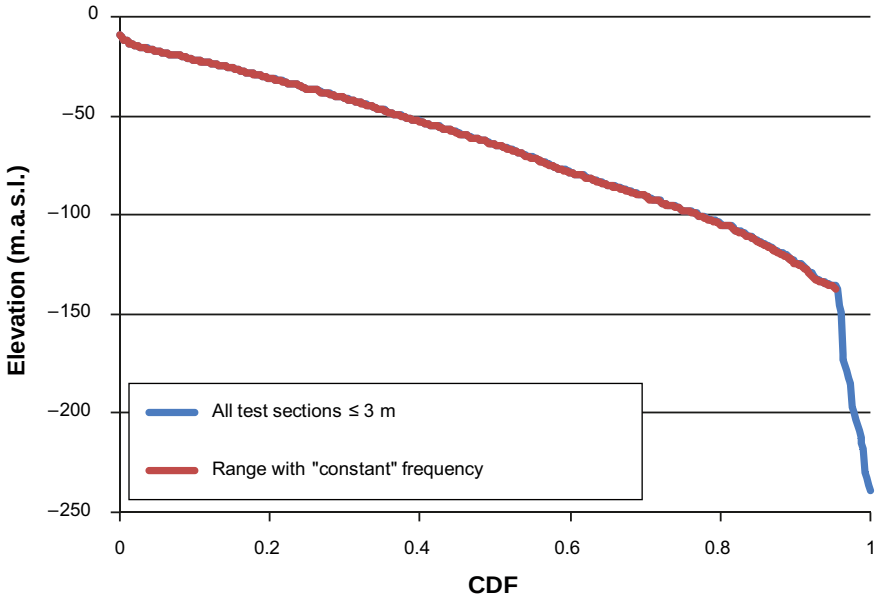

Figure 5-25. *Distribution of 3 m scale data with depth.*

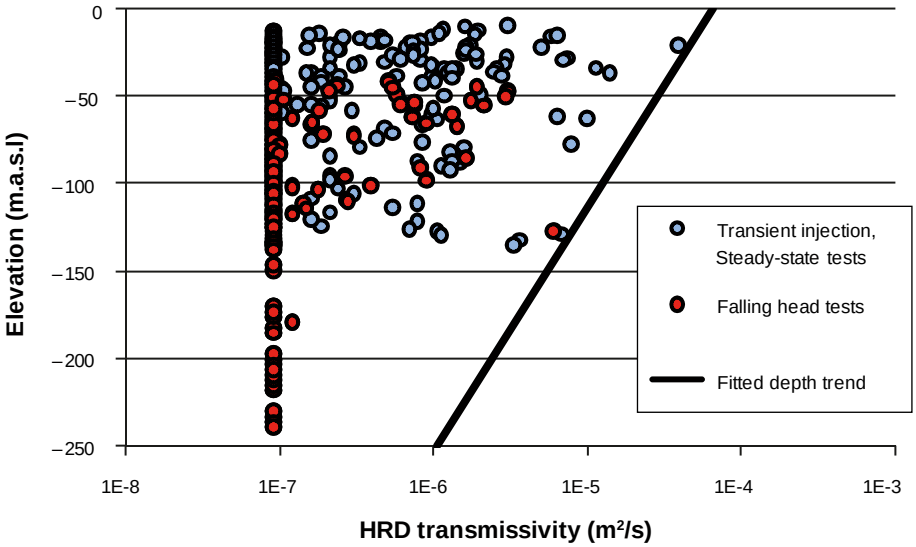

Figure 5-26. *HRD transmissivity at the 3 m-scale and a depth trend fitted to maximum values, k = 140 m, eq. (41). Note that falling-head data dominate at greater depths, while transient and steady state injection tests dominate at shallower depths.*

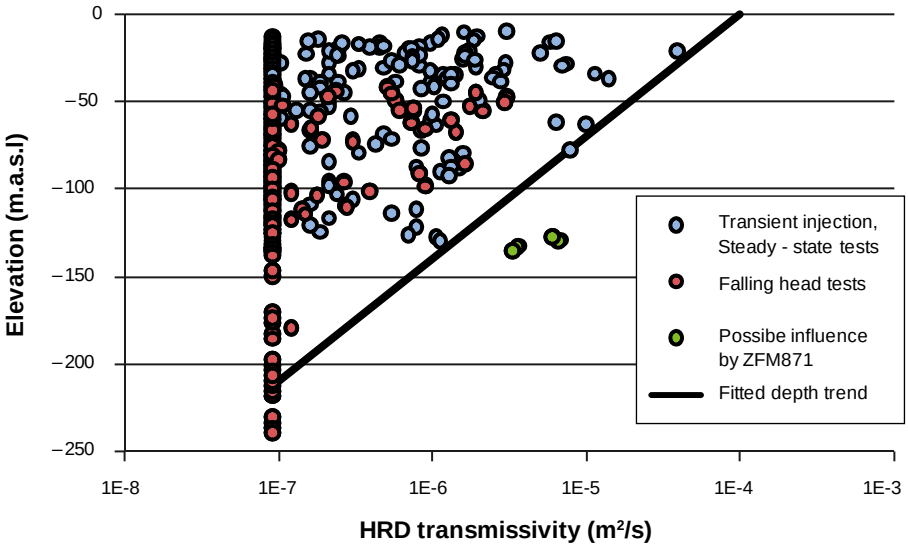

Figure 5-27. *HRD transmissivity at the 3 m-scale as function of depth excluding four sections possibly affected by ZFM871 (see Section 5.1.2; Figure 5-3). A depth trend with k = 70 m, eq. (41), is fitted to maximum values.*

If the data are divided into three tentative elevation bins and compared in terms of cumulative density functions, the decrease in transmissivity with depth is evident (Figure 5-28). The three bins are numbered from the top with the test statistics: $n_1 = n_2 = 172$, $n_3 = 78$, $D_{12} = 0.23$, $D_{13} = 0.30$, and $D_{23} = 0.10$, eq. (43). The two-sample Kolmogorov-Smirnov test rejects the null-hypothesis, that the data sets 1 and 2, respectively, 1 and 3 come from the same underlying distribution, at significance $\alpha = 0.01$ (note that it does not specify what type this common distribution is). The null-hypothesis cannot be rejected for data sets 2 and 3, that is: the difference between data sets 2 and 3 is not statistically significant. Perhaps a significant difference could have been identified between the middle and the lower group, had the groups been more representatively divided and the distributions would be less masked by the detection limit. The two-sample Kolmogorov-Smirnov test is known to be weaker for percentiles further away from the median.

A second case was tested, where falling head data were excluded from the examined 3 m-scale data, and the population was divided into an upper data set $z > -56$ m.a.s.l. and a lower data set $z < -56$ m.a.s.l. (Figure 5-29). The test statistics are $n_1 = n_2 = 177$ and $D_{12} = 0.25$, eq. (43), and the two-sample Kolmogorov-Smirnov test rejects the null-hypothesis at significance $\alpha = 0.01$.

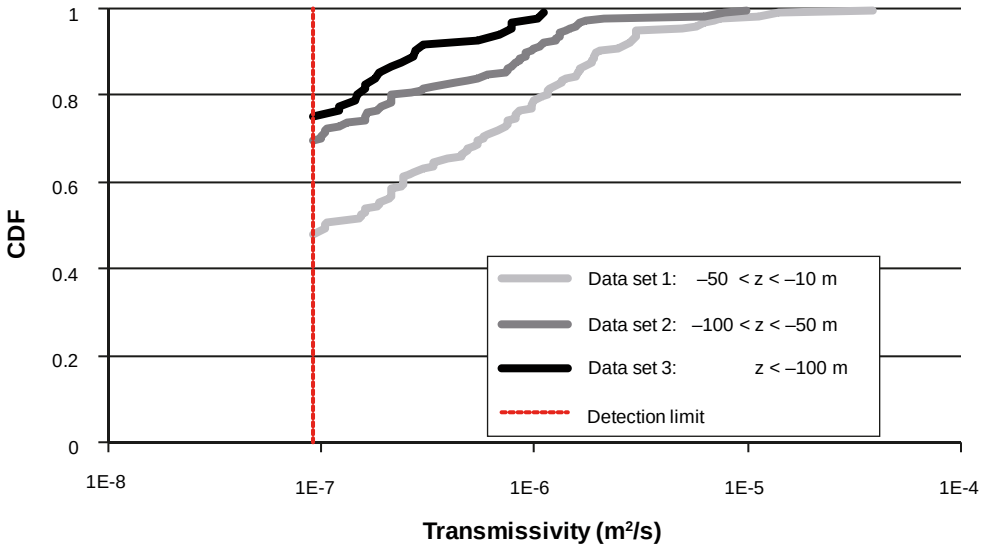

Figure 5-28. *Transmissivity distributions of 3 m test scale data binned by elevation, z. Note that neither of the cumulative density functions overlap (at least for the range above detection limit).*

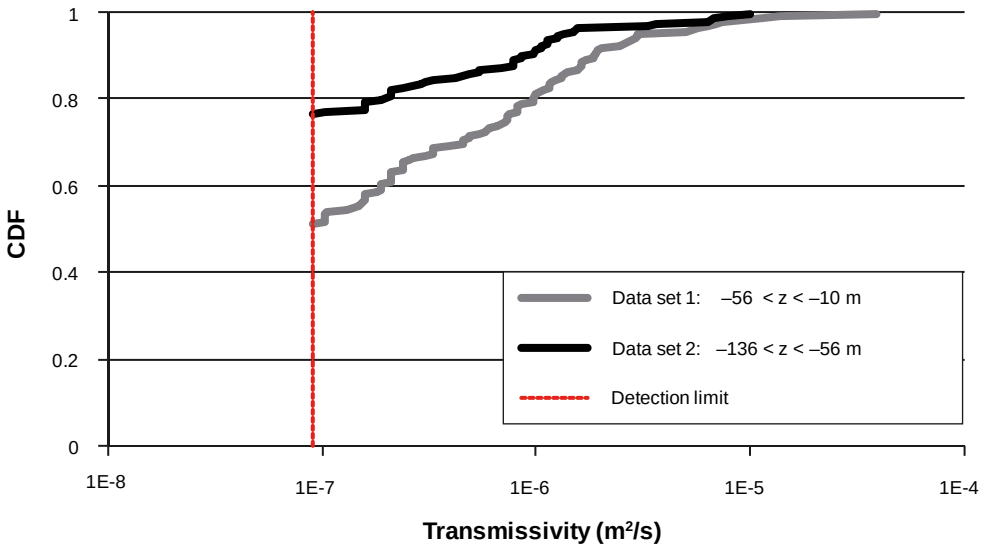

Figure 5-29. *Transmissivity distributions of 3 m test scale data, excluding the falling-head data, divided into two data sets by elevation, z.*

Having established a statistically significant difference between the shallower and deeper hydraulic data subsets, the next step is to investigate how the depth dependency should be modelled (see Section 4.2.3). This is done by studying the logarithmic translation in transmissivity distribution with depth (see Figure 4-1). Under the assumption that the shape of the transmissivity distribution remains relatively constant with depth, the detection-limit percentile was related to an estimated median as a function of depth (see Section 4.2.4). The percentile of the detection limit (i.e. the proportion of data below 9×10^{-8} m^2/s) can be studied as a continuous function of depth (Figure 5-30) for a rolling data set of given size. The anomaly at –120 m relates to the four data possibly under influence of ZFM871 (Figure 5-27). Note also, that the excluded data subset in the range –140 m to –250 m (Figure 5-25) has a detection limit percentile of 0.95, which would support a continuation of the depth trend below –140 m, although this data is considered less reliable. The median is only at, or above, detection limit in the range –20 to –50 m.

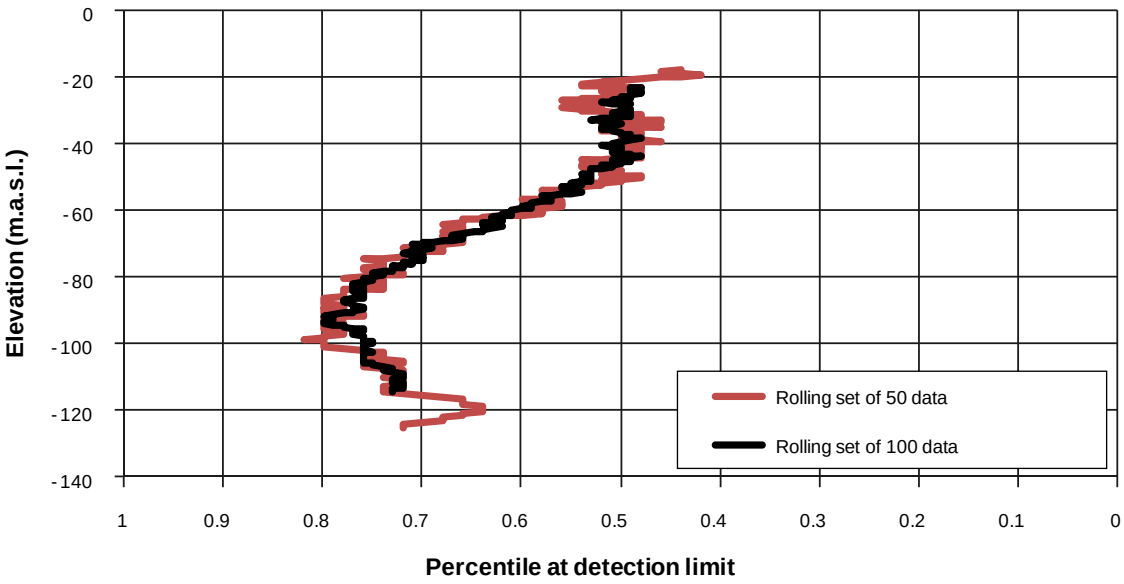

Figure 5-30. *Fraction of data below detection limit increasing with depth for rolling data sets; a 50 data window compared to a 100 data window. Note that the x-axis is plotted in reverse in order to facilitate comparison to Figures below.*

Given the fraction below detection limit (Figure 5-30), the median can also be estimated as a function of depth (Figure 4-1). For a given data sample of size n, with mean elevation z, the percentile at detection limit, $T_{\%}$, can be calculated for elevation, z (Figure 5-30). If the shape of the transmissivity distribution (i.e. variance and higher statistical moments) can be assumed to change insignificantly with depth, relative to its location (median), the logarithmic translation in transmissivity can be evaluated as a function of depth. The translation in distribution between two data sets can then be calculated as the numerical shift between their cumulative distributions, i.e. the distributions are expected to differ by an approximately constant transmissivity at any given percentile. The detection limit percentile, $T_{\%}$, at some mean elevation z (Figure 5-30) can be related to an estimated median transmissivity, $T_{0.5}(z)$, eq. (46).

The estimated trend in median can either be interpreted as a continous trend, with a depth interval for a magnitude decrease in transmissivity of 65–70 m, or a step function with transmissivity in the upper 50 to 60 meter barely an order of magnitude higher than the lower rock. The influence of the unusually high values at –130 m (Figure 5-27) can also be observed in Figure 5-31–Figure 5-34. Even if the trend is fitted to match the estimated median at –120 m.a.s.l. the depth interval for a magnitude decrease in transmissivity is less than 100 m (c.f. Figure 5-26). Exclusion of all low confidence falling head data (see Table 5-4) only increases the indications of depth trend (c.f. Figure 5-31 and Figure 5-32 to Figure 5-33 and Figure 5-34).

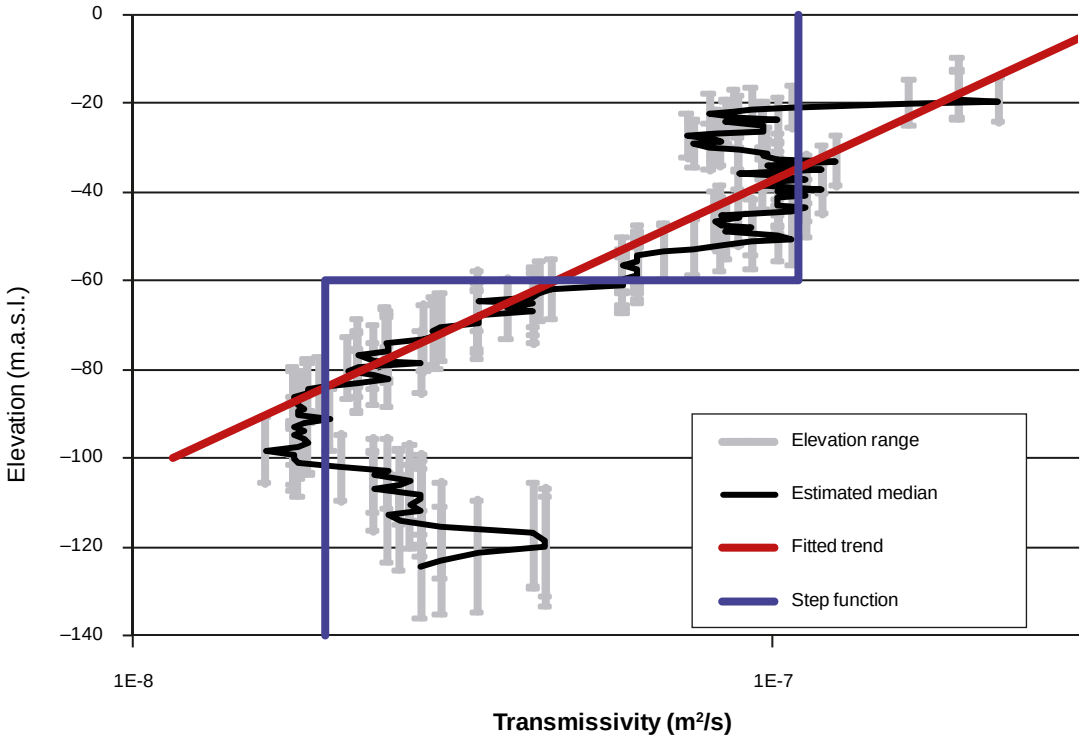

Figure 5-31. *Estimated median transmissivity depth trend with a rolling set for 50 data, k = 67 m, eq. (41).*

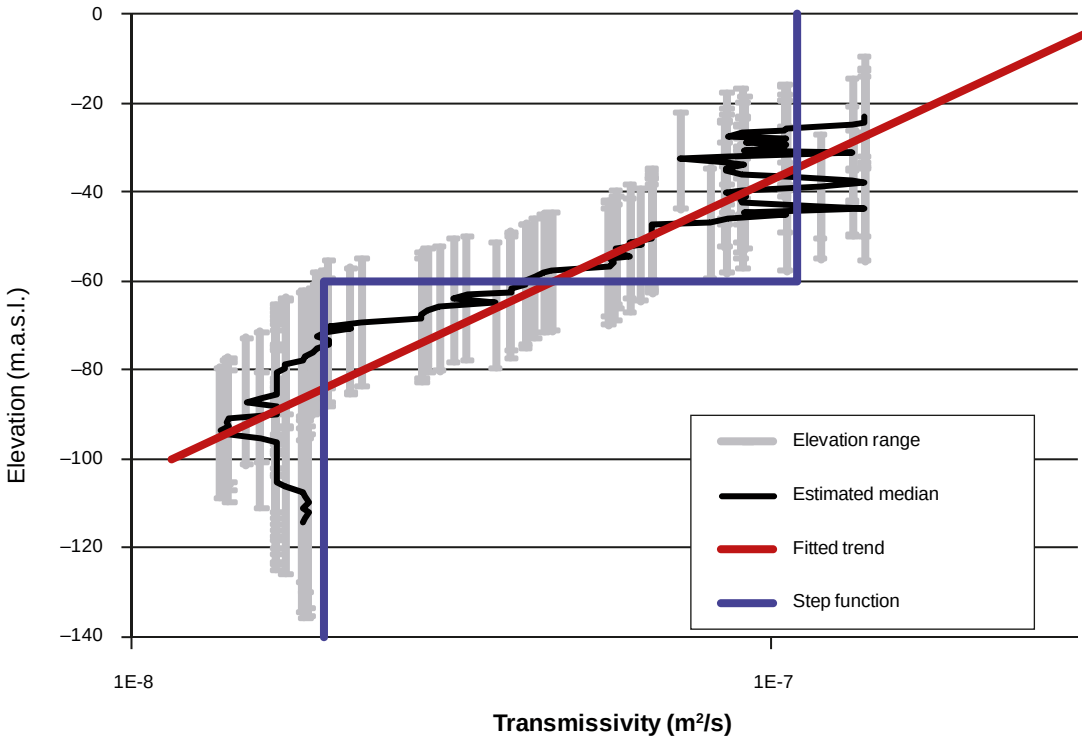

Figure 5-32. *Estimated median transmissivity depth trend for a rolling set of 100 data, k = 67 m, eq. (41).*

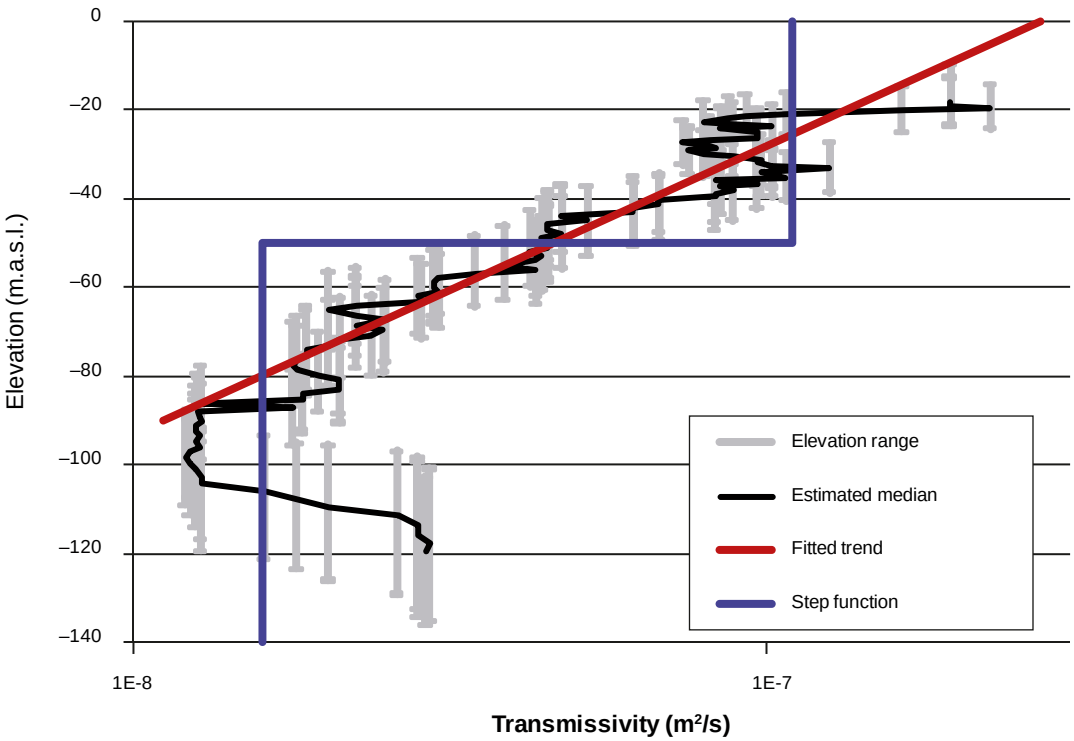

Figure 5-33. *Estimated median transmissivity depth trend for a rolling set of 50 data, excluding all falling-head data, k = 65 m, eq. (41) (Table 5-4).*

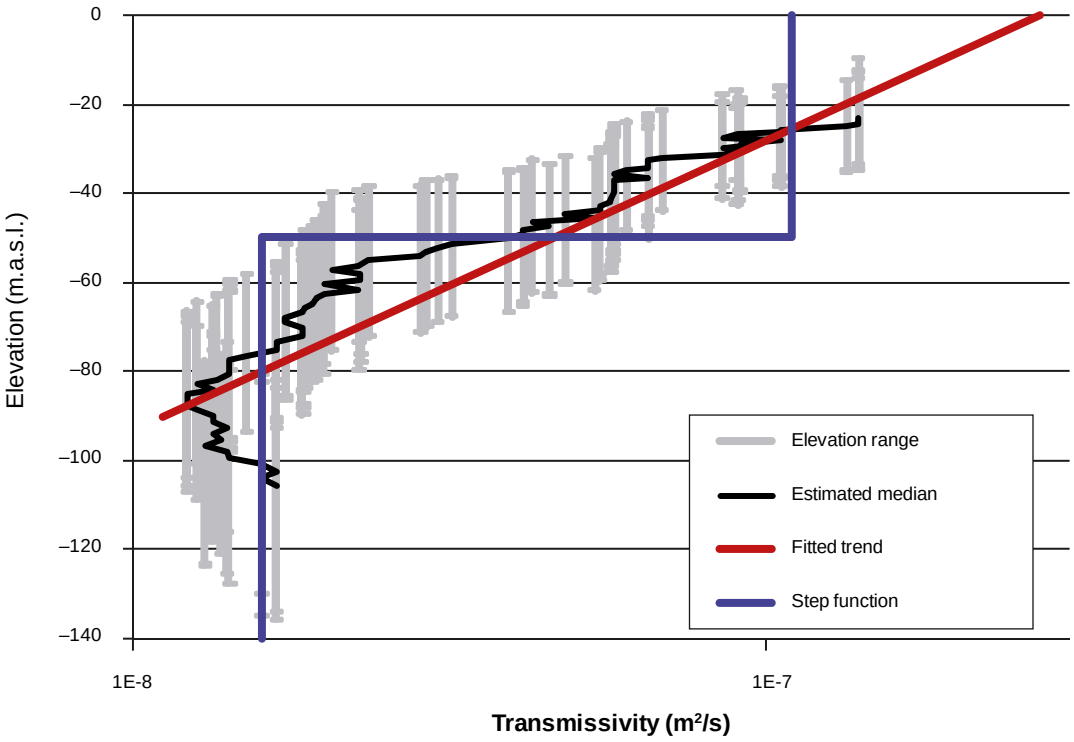

Figure 5-34. *Estimated median transmissivity depth trend for a rolling set of 100 data, excluding all falling-head data, k = 65 m, eq. (41) (Table 5-4).*

6 Conclusions and recommendations

6.1 Summary

The primary objective of the ongoing hydrogeological investigations at SFR is to develop a description of the hydrogeological system inside the SFR regional domain. This descriptive model should provide parameter values to a *groundwater flow model*, which will be used by Safety Assessment and Design for predictions. This report presents a re-evaluation of the existing hydrogeological information in the context of the recently updated geologic structural model /Curtis et al. 2009/. This study is delimited to hydraulic data available prior to the current investigations at SFR (i.e. from the constructions of the Forsmark nuclear power plant, the existing SFR, and the nearby site investigations for a deep repository for high level spent nuclear fuel). The resulting hydrogeological description, referred to as hydrogeological model SFR v. 0.1, provides preliminary parameter values for the groundwater flow modelling (see Sections 6.3 and 6.4).

A second objective is to provide feedback to the other modelling disciplines and the overall SFR field investigation programme. In the analysis of hydraulic data, the modelled geometrical HCD intercepts were reviewed in the context of hydraulic anomalies (Sections 3.2.1 and 4.1.2). Based on this review, it was judged reasonable to reconsider the borehole intercepts for six HCDs in order to match hydraulic anomalies (Section 6.2).

Four key issues have been raised specifically for the hydrogeological modelling of SFR /SKB 2008/ and additionally three generic modelling issues have been raised by /Follin et al. 2007a/ (these issues have been numbered from 1 through 7, see Section 1.2). This report has primarily targeted the first two key issues: the hydraulic parameterisation of: 1) interpreted low-magnetic lineaments (i.e. HCDs, as defined by /Curtis et al. 2009/) and, 2) the bedrock between the deformation zones within target model volume (i.e. HRD). The recommended parameter values are summarized in (Sections 6.3, respectively, 6.4).

The third key issue concerns hydraulic connectivity within/across the model domains and has only been studied briefly in this report. The hydraulic connectivity between/within HCDs has been analysed in terms of an overview compilation of the interference test data in the context of the updated structural model (see Appendix C). However, the hydraulic connectivity within the HRD has not been addressed in this report. The reason for this is that the data available provides little information for inferring the level of connectivity or compartmentalisation of the fracture network in a tested borehole section (see discussion on hydraulic test methods, e.g. in Section 4.3, /Follin et al. 2007b/). The pressure build-up test is the only data type studied here, which exclusively detects the transmissivity of continuously flowing fractures. Unfortunately, this data type comprises a relatively small portion of the data set (Figure 2-1) and its test scale is generally on the order 10–50 m (Figure 2-5), which provides a poor resolution of hydraulic connectivity. However, the next version of the hydrogeologic model, v. 0.2, will include data from the ongoing site investigations at SFR. This data set contains fracture transmissivity measurements from the Posiva Flow Log (PFL) pumping tests, which provides a high level detail of the hydraulic connectivity. Potentially, this new data set will also provide means for a rigorous hydraulic connectivity analysis by means of discrete fracture network (DFN) modelling.

The fourth key issue, which concerns the spatial extent and hydraulic properties of sheet joints and gently dipping deformation zones, has only been addressed in part in this report. The depth trend and the within-plane heterogeneity of the gently dipping deformation zone ZFM871 has been analysed (see Figure 5-15 and Figure 5-17 to Figure 5-20). However, the crucial question to whether the sheet joints extends across the Singö zone and into the SFR domain (see e.g. Sections 4.5.3 and 6.4.1 in /Follin et al. 2008/) has not been investigated in this report. The data from the ongoing site investigations at SFR, are expected provide more insight to this concern in model version 0.2.

The fifth issue concerns whether deformation zones are generally more conductive than the surrounding bedrock. This question is difficult to answer conclusively, primarily because the HCDs should probably not be treated as a homogeneous group. For example, ZFMne0870b (Zon9) exhibits no sign of excessive conductivity, while ZFM871 (ZonH2) is at least one order of magnitude more conductive than the HRD (cf Figure 5-15 and Figure 5-16). Furthermore, a direct comparison between HCD

intercept transmissivity and HRD borehole interval transmissivity is complicated by depth dependency in combination with heterogeneity (compare Figure 5-14 to Figure 5-16, with discussion in Section 3) and effects of measurement scale (i.e. variable HCD thicknesses and borehole interval test scales). A visual inspection of the concurrence between hydraulic anomalies and HCD bounds provides a fairly scattered picture (Appendix B). To some extent, this depends on the poor resolution of transmissivity and HCD bounds, relative to the, generally, short borehole lengths (or model scale). However, in some cases the two data types do coincide well (e.g. KFM11A, KFR10, KFR13, KFR21, KFR22, KFR31, KFR32, and KFR33).

The sixth issue concerns possible data support for dividing the HRD into sub domains. This aspect has not been investigated in the current study. This evaluation requires detailed data on fracture characteristics as well as defined geologic rock domains. Neither was available for the model version 0.1.

The last issue concerns the statistical significance of depth dependence in transmissivity. In previous modelling of SFR, the effective conductivity in the upper 25 m HRD was assigned one order of magnitude higher than the HRD below /Holmén 2005/. The current data set of HRD transmissivity extends down to approximately 200 m.a.s.l. The HRD below 56 m.a.s.l. is significantly less transmissive than the HRD above 56 m.a.s.l. (Section 5.4.2). It is inconclusive whether this should be interpreted as part of a continuous depth trend that extends deep into the bedrock (i.e. 1,000 m.a.s.l.), or if it relates to shallow geologic processes (such as glacial rebound). Note that the latter would provide evidence for subdividing the HRD by elevation, as was done by /Follin et al. 2007b/ (see paragraph above). Alternative HRD depth trend models that have been suggested by different authors in previous modelling work are compared in Section 6.4.

6.2 HCD borehole intercepts

On the basis of anomalous hydraulic data located near the HCD envelope, it is recommended that the borehole intercepts of five out of 67 HCD envelopes are extended (Table 6-1). That is, the thickness of the five HCDs could be thicker than modelled by /Curtis et al. 2009/. Also, the entire intercept of ZFMwnw0813 in KFM11A should be moved 50 m upwards to conform to hydraulic data (Table 6-1; Figure B-4). Additionally, four unusually high transmissivities have been identified at –130 m.a.s.l. in boreholes KFR25 and KFR37 (Figure 5-3), which stand out in the depth trend analysis. These anomalies were not considered as strong evidence enough to change the envelope of ZFM871 in the current model version, but it is possible that the definition ZFM871 will be modified in the next geological model SFR v.0.2, as more detailed data are included.

Table 6-1. Modifications of HCD envelopes. (eoh = “end of hole”).

HCD intercept			Original envelope		Modified envelope			
IDCODE	HCD	Alias	Secup	Seclow	Secup	Seclow	Comment	
HFM35	ZFMnw1035	–	146	eoh	141	eoh	5 m	upwards
KFM11A	ZFMwnw2496	–	74.3	129.9	86.81	129.9	12.5 m	upwards
KFM11A	ZFMwnw0813	–	258.6	331.7	308.6	381.7	50 m	upwards
KFR25	ZFMnw0805a	zon8	64.06	132.36	64.06	142	10 m	downwards
KFR31	ZFM871	zonH2	215.25	eoh	201	eoh	14 m	upwards
KFR31	ZFMne0870b	zon9	206.79	240.54	201	240.54	5 m	upwards

6.3 HCD transmissivity

In the calculation of HCD transmissivity, the HCD hydraulic envelopes proved useful for defining bounds of the geometrical intercepts; calculations based on envelopes provide more stable estimates compared to using the modelled thickness in RVS directly (Section 5.3.1). Geometrical compensation for non-perpendicular borehole intercepts was not considered necessary (Section 5.3.2). It was considered reasonable to use the continuum principle for calculation of HCD transmissivity, and to include all hydraulic data with at least half its interval length inside the hydraulic envelope (i.e. "minimum fraction required inside HCD bounds" = 0.5; Table 4-1). The effective ground-level transmissivity, T_0, calculated by eq. (42) are shown for individual HCDs (Table 6-2) and for HCDs grouped by orientation (Table 6-3). It can be noted that the groups ne and nnw have lower transmissivity (Table 6-3), which would agree with expectations based on the stress-regime (Section 5.3.3). However, ZFMnne0869 (zon3) has a high transmissivity in spite of its orientation. The evidence for HCD depth dependency is weak, owing to high lateral heterogeneity combined with hydraulic data only available within a narrow depth range. However, it is unrealistic to neglect depth dependency in transmissivity – particularity as the model domain extends down to 1,100 m.a.s.l. Depth-trend-compensation of HCD transmissivity (using k = 232.5 m) improves stationary in experimental semivariograms (Section 5.3.4), which is taken as support for depth dependency. There are examples indicating an exponential depth dependency within the top 200 m, with *k* in eq. (41) ranging from 60 to 110 m. Lacking evidence of depth dependency below –200 m.a.s.l. it is recommended that HCD transmissivity is modelled with a depth dependency of k = 232.5 m (taken from findings of the nearby Site Investigation Forsmark /Follin et al. 2007b/). There are also indications that the length scale of within-plane-heterogeneity in transmissivity of ZFM871 is about 30 m (Section 5.3.4).

Table 6-2. Individual effective ground-level HCD transmissivity.

HCD	Alias	Retained intercepts	Rejected intercepts	$\mu_{log\ To}$	$\sigma_{log\ To}$
ZFM871	H2	15	3	–4.5	0.7
ZFMnw0805	Zon8	8	3	–4.9	1.1
ZFMne0870	Zon9	5	4	–5.6	0.9
ZFMnne0869	Zon3	5	1	–4	0.5
ZFMwnw0001	Singö	2	2	–3.6	0.5
ZFMnw1035	–	3	0	–3.3	0.5
ZFMwnw0804	–	2	1	–3.8	1.2
ZFMnnw0999	–	2	0	–6	1.3
ZFMnnw1209	Zon6	2	0	–5.1	0.5
ZFMwnw0813	–	2	1	–4.4	2.1
ZFMwnw3262	–	1	1	–4.6	–
ZFMwnw2496	–	1	1	–4.2	–
ZFMwnw3259	–	1	1	–4.2	–
ZFMnne2308	–	1	0	–5.4	–
Total		50	18	–4.6	1.0

Table 6-3. Effective ground-level HCD transmissivity grouped by orientation.

HCD group	Retained intercepts	Min T_0	$\mu_{log\ To}$	Max T_0	$\sigma_{log\ To}$
Gently dipping (ZFM871)	15	–5.8	–4.5	–3.6	0.7
Subvertical (ne)	5	–7.2	–5.6	–4.9	0.9
Subvertical (nne)	6	–5.4	–4.2	–3.2	0.7
Subvertical (nnw)	4	–6.9	–5.6	–4.8	1.0
Subvertical (nw)	11	–6.4	–4.5	–2.8	1.2
Subvertical (wnw)	9	–5.9	–4.0	–2.9	1.0

6.4 HRD conductivity

It is difficult to provide a realistic estimate for effective HRD conductivity from borehole data. In principle, the entire range of the 3-m test scale data could be applied, if a stochastic continuum approach is pursued. However, strictly speaking, such an approach requires grid-cells to be of equal size to the support scale of data. A stochastic continuum approach would therefore be inappropriate for the SFR flow model v.0.1, as it will employ an unstructured grid with flexible grid size. Subsequent model versions will be based on the translation from a hydraulic fracture network to define the conductivity field (ECPM approach). At the current modelling stage, it was therefore considered sufficient to use a CPM approach (with spatially constant effective HRD conductivity).

The estimate based on 3-m test scale data is bounded by the geometric mean and the arithmetic mean conductivity, $5 \times 10^{-9} – 1.5 \times 10^{-7}$ m/s (Table 5-3). If the effective HRD conductivity is closer to its geometric or arithmetic mean depends on the connectivity of highly conductive features. In the present conceptual model (Figure 1-2), it is presumed that large connected features have been identified in the geological model and excluded from the HRD; thus a poorly connected HRD system motivates the use of geometric mean. Previous hydrogeological models have used an effective HRD conductivity of 6.5×10^{-9} m/s, which is close to the geometric mean. In /Holmén 2005/, the upper 25 m of the HRD was assigned an effective conductivity ranging from 5×10^{-9} to 5×10^{-7} m/s, while the lower HRD conductivity was one order of magnitude less.

There is a statistically significant difference between shallow and deep HRD conductivity. There are indications which support modelling the depth dependency within the top 150 m, either by an exponential model *k* in eq. (41) ranging from 65 to 140 m (Figure 6-1), or by dividing the HRD into a shallow domain above –55 m.a.s.l. and an underlying HRD domain between –150 and –55 m.a.s.l. Possible models to extrapolate HRD conductivity below 200 m depth are compared in Figure 6-1. The HRD conductivity at greater depths will be addressed in the next model version SFR v.0.2.

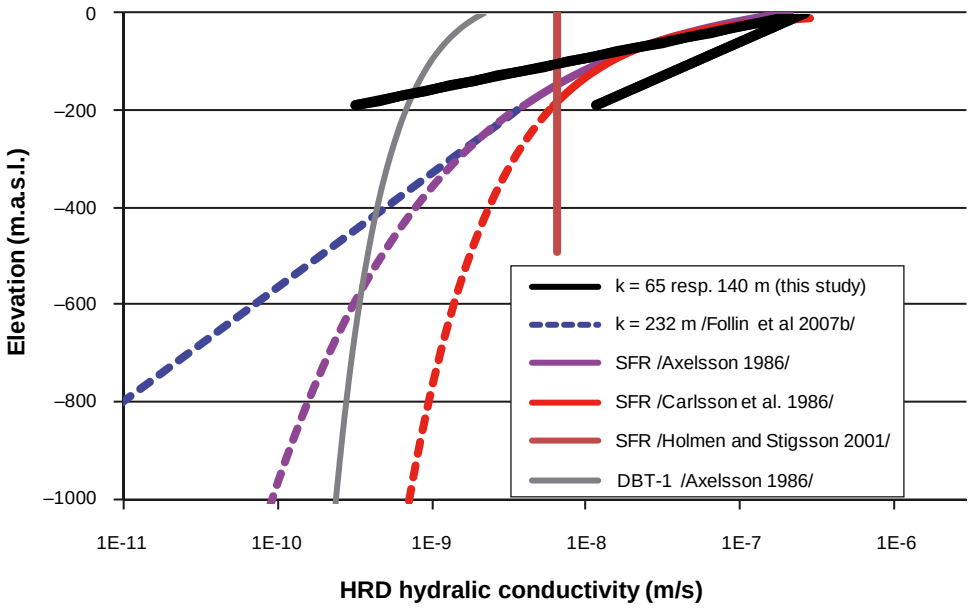

Figure 6-1. *Fitted depth trend in 3-m scale HRD conductivity within the top 150–200 m, and comparing possible models for extrapolation with depth suggested by different authors. Note that the exponential model with k = 232 m was not fitted to HRD data, but to HCD transmissivity in Forsmark.*

References

SKB's (Svensk Kärnbränslehantering AB) publications can be found at www.skb.se/publications.

Andersson J-E, Arnefors J, Carlsson L, Danielsson J, Hansson K, 1986. Tryckuppbyggnads- och mellanhålstester inom SFR. Del 2: Borrhålen HK2, HK7A, HK7B, HK7C, HK8, HK9, HK10, HK11, HK12, HK13, Kb26 och SH3. Swedish Geological Co, IRAP 86403, June 1986, Gothenburg (In Swedish).

Arnefors J, Carlsson L, 1985. Tryckuppbyggnads- och mellanhålstester inom SFR. Del 1: Borrhålen HK1, HK3, HK4, Kb19, Kb20, Kb23, Kb24 och Kb25. Swedish Geological Co, IRAP 85409, September 1985, Gothenburg (In Swedish).

Axelsson C-L, 1986. Modeling of groundwater flow with salt-water interference at the final repository for reactor waste (SFR). SSI P 311.85.

Axelsson C-L, Ekstav A, Lindblad Påsse A, 2002. SFR – Utvärdering av hydrogeologi. SKB R-02-14, Svensk Kärnbränslehantering AB.

Axelsson C-L, Mærsk Hansen L, 1997. Update of structural models at SFR nuclear waste repository, Forsmark, Sweden. SKB R-98-05, Svensk Kärnbränslehantering AB.

Bosson E, Gustafsson L-G, Sassner M, 2008. Numerical modelling of surface hydrology and near-surface hydrogeology at Forsmark. Site descriptive modelling, SDM-Site Forsmark. SKB R-08-09, Svensk Kärnbränslehantering AB.

Brydsten L, 2006. A model for landscape development in terms of shoreline displacement, sediment dynamics, lake formation, and choke-up processes, SKB TR-06-40, Svensk Kärnbränslehantering AB.

Caine J S, Evans J P, Forster C B, 1996. Fault zone architecture and permeability structure. Geology 24, 1025–1028.

Carlsson L, Winberg A, Arnefors J, 1986. Hydraulic Modeling of the Final Repository for Reactor Waste (SFR). Compilation and Conceptualization of Geological and Available Hydrogeological Data. SKB Progress Report SFR 86-03, Svensk Kärnbränslehantering AB. Quality assurance SKBdoc 1258697.

Carlsson L, Grundfelt B, Winberg A, 1987. Hydraulic Modeling of the Final Repository for Reactor Waste (SFR). Evaluation of the groundwater flow situation at SFR. SKB Progress Report SFR 86-07, Svensk Kärnbränslehantering AB. Quality assurance SKBdoc 1258697.

Carlsten S, Döse C, Samuelsson E, Gustafsson J, Petersson J, Stephens M, Thunehed H, 2007. Forsmark site investigation. Geological single-hole interpretation of KFM11A, HFM33, HFM34 and HFM35. SKB P-07-109, Svensk Kärnbränslehantering AB.

Curtis P, Petersson J, Triumf C-A, 2009. Site investigation SFR. Deformation zone modelling. Model version 0.1. SKB P-09-48, Svensk Kärnbränslehantering AB.

Follin S, Johansson P-O, Levén J, Hartley L, Holton D, McCarthy R, Roberts D, 2007a. Updated strategy and test of new concepts for groundwater flow modelling in Forsmark in preparation of site descriptive stage 2.2. SKB R-07-20, Svensk Kärnbränslehantering AB.

Follin S, Levén J, Hartley L, Jackson P, Joyce S, Roberts D, Swift B, 2007b. Hydrogeological characterisation and modelling of deformation zones and fracture domains, Forsmark modelling stage 2.2. SKB R-07-48, Svensk Kärnbränslehantering AB.

Follin S, Johansson P-O, Hartley L, Jackson P, Roberts D, Marsic N, 2007c. Hydrogeological conceptual model development and numerical modelling using CONNECTFLOW, Forsmark modelling stage 2.2. SKB R-07-49, Svensk Kärnbränslehantering AB.

Follin S, Hartley L, Jackson P, Roberts D, Marsic N, 2008. Hydrogeological conceptual model development and numerical modelling using CONNECTFLOW, Forsmark modelling stage 2.3. SKB R-08-23, Svensk Kärnbränslehantering AB.

Harrström J, Svensson T, Ludvigson J-E, 2007. Forsmark site investigation. Single-hole hydraulic tests in borehole KFM11A. SKB P-07-177, Svensk Kärnbränslehantering AB.

Hedenström A, Sohlenius G, Strömgren M, Brydsten L, Nyman H, 2008. Depth and stratigraphy of regolith at Forsmark. Site descriptive modelling, SDM-Site Forsmark. SKB R-08-07, Svensk Kärnbränslehantering AB.

Gustavsson E, Jönsson S, Ludvigson J-E, 2006. Forsmark site investigation. Pumping tests and flow logging. Boreholes HFM33, HFM34 and HFM35. SKB P-06-193, Svensk Kärnbränslehantering AB.

Holmén J G, Stigsson M, 2001. Modelling of future hydrogeological conditions at SFR. SKB R-01-02, Svensk Kärnbränslehantering AB.

Holmén J G, 2005. SFR-1, Inverse modelling of inflow to tunnels and propagation of estimated uncertainties to predictive stages. SKB-R-05-74, Svensk Kärnbränslehantering AB.

Odén M, 2009. Site investigation SFR, Hydrogeological modelling at SFR using DarcyTools, Site description SFR version 0.0, SKB P-08-94, Svensk Kärnbränslehantering AB.

Öhman J, 2010. Site investigation SFR, Hydrogeologic modelling of SFR v 0.1, Influence of the ridge on the flow fields for different target volumes. SKB R-09-43, Svensk Kärnbränslehantering AB.

Rhén I, Follin S, Hermanson J, 2003. Hydrogeological Site Descriptive Model – a strategy for its development during Site Investigations. SKB-R-03-08, Svensk Kärnbränslehantering AB.

SKB, 2004. Preliminary site description Forsmark area – version 1.1. SKB R-04-15, Svensk Kärnbränslehantering AB.

SKB, 2008. Geovetenskapligt undersökningsprogram för utbyggnad av SFR. SKB-R-08-67, Svensk Kärnbränslehantering AB.

Stephens M B, Fox A, La Pointe P, Simeonov A, Isaksson H, Hermanson J, Öhman J, 2007. Geology Forsmark. Site descriptive modelling Forsmark stage 2.2. SKB R-07-45, Svensk Kärnbränslehantering AB.

Svensson U, 2004. DarcyTools, Version 2.1. Verification and validation. SKB R-04-21, Svensk Kärnbränslehantering AB.

Svensson U, Ferry M, 2004. DarcyTools, Version 2.1. User's guide. SKB R-04-20, Svensk Kärnbränslehantering AB.

Svensson U, Kuylenstierna, H-O, Ferry M, 2010. DarcyTools, Version 3.4. Concepts, methods, equations and demo simulations. SKB R-07-38, Svensk Kärnbränslehantering AB.

Väisäsvaara J, Pekkanen J, 2007. Forsmark site investigation. Difference flow logging in borehole KFM11A. SKB P-07-85, Svensk Kärnbränslehantering AB.

Appendix A

Data excluded in screening

Table A-1. Data excluded in screening.

Borehole	From borehole length (m)	To borehole length (m)	Section length (m)	Type	Transmissivity (m^2/s)	Comment
KFR01	44.50	62.30	17.80	BU	1.4E-6	Suspected error
KFR02	16.00	26.00	10.00	TI	1.7E-8	Suspected error
KFR02	81.00	118.00	37.00	BU	2.2E-8	Overlapping data, shorter intervals used instead
KFR02	119.00	136.00	17.00	BU	6.5E-8	Overlapping data, shorter intervals used instead
KFR02	137.00	170.30	33.30	BU	1.2E-7	Overlapping data, shorter intervals used instead
KFR02	43.00	80.00	37.00	BU	1.2E-7	Overlapping data, shorter intervals used instead
KFR05	60.10	62.10	2.00	TI	4.6E-10	Values prior to Silo construction used instead
KFR05	62.10	64.10	2.00	TI	–1.0E-10	Values prior to Silo construction used instead
KFR05	64.10	66.10	2.00	TI	1.1E-8	Values prior to Silo construction used instead
KFR05	48.10	50.10	2.00	TI	2.2E-8	Values prior to Silo construction used instead
KFR05	50.10	52.10	2.00	TI	2.6E-8	Values prior to Silo construction used instead
KFR05	52.10	54.10	2.00	TI	5.4E-10	Values prior to Silo construction used instead
KFR05	54.10	56.10	2.00	TI	4.6E-10	Values prior to Silo construction used instead
KFR05	56.10	58.10	2.00	TI	9.6E-9	Values prior to Silo construction used instead
KFR05	58.10	60.10	2.00	TI	2.0E-8	Values prior to Silo construction used instead
KFR06	2.00	4.00	2.00	TI	2.2E-8	Values prior to Silo construction used instead
KFR06	4.00	6.00	2.00	TI	1.5E-8	Values prior to Silo construction used instead
KFR06	6.00	8.00	2.00	TI	6.3E-10	Values prior to Silo construction used instead
KFR06	8.00	10.00	2.00	TI	8.4E-9	Values prior to Silo construction used instead
KFR06	10.00	12.00	2.00	TI	5.8E-9	Values prior to Silo construction used instead
KFR06	12.00	14.00	2.00	TI	2.9E-10	Values prior to Silo construction used instead
KFR06	14.00	16.00	2.00	TI	1.4E-9	Values prior to Silo construction used instead
KFR06	16.00	18.00	2.00	TI	1.2E-6	Values prior to Silo construction used instead
KFR06	18.00	20.00	2.00	TI	1.1E-8	Values prior to Silo construction used instead
KFR06	20.00	22.00	2.00	TI	1.2E-7	Values prior to Silo construction used instead
KFR06	22.00	24.00	2.00	TI	1.2E-6	Values prior to Silo construction used instead
KFR06	24.00	26.00	2.00	TI	5.3E-8	Values prior to Silo construction used instead
KFR06	26.00	28.00	2.00	TI	1.2E-7	Values prior to Silo construction used instead
KFR06	28.00	30.00	2.00	TI	8.4E-8	Values prior to Silo construction used instead
KFR06	30.00	32.00	2.00	TI	3.7E-7	Values prior to Silo construction used instead
KFR06	32.00	34.00	2.00	TI	3.1E-7	Values prior to Silo construction used instead
KFR06	34.00	36.00	2.00	TI	1.6E-8	Values prior to Silo construction used instead
KFR13	4.00	33.00	29.00	BU	2.9E-9	Overlapping data, shorter intervals used instead
KFR13	34.00	53.00	19.00	BU	7.6E-9	Overlapping data, shorter intervals used instead
KFR13	54.00	76.60	22.60	BU	1.8E-6	Overlapping data, shorter intervals used instead
KFR19	66.00	76.00	10.00	BU	5.0E-10	Suspected error
KFR21	154.00	157.00	3.00	FH	–1.0E-10	Highest T retained
KFR21	43.00	46.00	3.00	FH	1.4E-7	Highest T retained
KFR21	151.00	154.00	3.00	FH	–1.0E-10	Highest T retained
KFR21	46.00	49.00	3.00	FH	3.9E-8	Highest T retained
KFR21	139.00	142.00	3.00	FH	–1.0E-10	Highest T retained
KFR21	136.00	139.00	3.00	FH	6.0E-9	Highest T retained
KFR22	67.00	70.00	3.00	FH	1.4E-8	Suspected error
KFR22	79.00	82.00	3.00	FH	2.6E-6	Suspected error
KFR23	122.00	125.00	3.00	FH	6.0E-9	Suspected error

KFR23	146.00	149.00	3.00	FH	6.0E-9	overlapping data
KFR24	54.00	57.00	3.00	FH	3.0E-8	Suspected error
KFR24	141.00	144.00	3.00	FH	–1.0E-10	Intervals chosen to maximize borehole coverage
KFR24	48.00	51.00	3.00	FH	–1.0E-10	Missing value
KFR25	133.00	136.00	3.00	FH	6.6E-8	Suspected error
KFR25	157.00	160.00	3.00	FH	–1.0E-10	Suspected error
KFR25	169.00	172.00	3.00	FH	–1.0E-10	Missing value
KFR31	156.00	242.00	86.00	PH	3.0E-6	overlapping data
KFR31	174.00	242.00	68.00	PH	2.5E-6	Overlapping data, shorter intervals used instead
KFR31	81.00	242.00	161.00	PH	9.9E-6	Overlapping data, shorter intervals used instead
KFR31	123.00	242.00	119.00	PH	4.6E-6	Overlapping data, shorter intervals used instead
KFR31	54.00	242.00	188.00	PH	1.3E-5	Overlapping data, shorter intervals used instead
KFR31	72.00	242.00	170.00	PH	1.2E-5	Overlapping data, shorter intervals used instead
KFR31	204.00	207.00	3.00	PH	–5.1E-8	Intervals chosen to maximize borehole coverage
KFR31	207.00	210.00	3.00	PH	–5.1E-8	Intervals chosen to maximize borehole coverage
KFR31	210.00	213.00	3.00	PH	–5.1E-8	Intervals chosen to maximize borehole coverage
KFR31	213.00	216.00	3.00	PH	–5.1E-8	Intervals chosen to maximize borehole coverage
KFR31	195.00	242.00	47.00	PH	2.5E-6	Overlapping data, shorter intervals used instead
KFR32	157.00	160.00	3.00	PH	–5.1E-8	Intervals chosen to maximize borehole coverage
KFR32	176.00	187.00	11.00	PH	2.3E-6	Intervals chosen to maximize borehole coverage
KFR32	163.00	176.00	13.00	PH	3.8E-5	Intervals chosen to maximize borehole coverage
KFR32	154.00	209.00	55.00	PH	2.5E-5	Inconsistency, highest T retained
KFR32	82.00	209.00	127.00	PH	2.1E-5	Overlapping data, shorter intervals used instead
KFR33	150.00	167.00	17.00	PH	5.4E-6	Overlapping data, shorter intervals used instead
KFR33	96.00	167.00	71.00	PH	–1.0E-10	Inconsistency, highest T retained
KFR33	39.00	167.00	128.00	PH	1.9E-5	Overlapping data, shorter intervals used instead
KFR34	90.00	93.00	3.00	PH	–5.1E-8	Intervals chosen to maximize borehole coverage
KFR34	69.00	142.00	73.00	PH	1.1E-5	Overlapping data, shorter intervals used instead
KFR35	99.00	102.00	3.00	PH	–5.1E-8	Intervals chosen to maximize resolution
KFR35	96.00	140.00	44.00	PH	7.4E-7	Intervals chosen to maximize resolution
KFR35	75.00	140.00	65.00	PH	2.1E-6	Intervals chosen to maximize resolution
KFR35	57.00	140.00	83.00	PH	1.4E-5	Intervals chosen to maximize resolution
KFR36	117.00	120.00	3.00	PH	6.6E-7	Intervals chosen to maximize resolution
KFR37	117.00	120.00	3.00	PH	2.6E-4	Suspected error, contradicts the 78–204m test
KFR37	120.00	123.00	3.00	PH	2.6E-4	Suspected error, contradicts the 78–204m test
KFR37	186.00	189.00	3.00	PH	1.9E-7	Intervals chosen to maximize resolution
KFR37	191.00	194.00	3.00	PH	4.2E-5	Intervals chosen to maximize resolution
KFR37	159.00	204.00	45.00	PH	1.8E-5	Overlapping data, shorter intervals used instead
KFR37	78.00	204.00	126.00	PH	2.6E-5	Overlapping data, shorter intervals used instead
KFR38	177.00	180.00	3.00	PH	–5.1E-8	Intervals chosen to maximize resolution
KFR38	179.00	182.00	3.00	PH	3.3E-5	Intervals chosen to maximize resolution
KFR38	114.00	185.00	71.00	PH	2.1E-5	Intervals chosen to maximize resolution
KFR54	30.00	43.00	13.00	BU	5.6E-8	Suspected error
KFR55	40.00	42.00	2.00	TI	2.6E-9	Values prior to Silo construction used instead
KFR55	42.00	44.00	2.00	TI	5.8E-10	Values prior to Silo construction used instead
KFR55	44.00	46.00	2.00	TI	5.2E-10	Values prior to Silo construction used instead
KFR55	46.00	48.00	2.00	TI	3.8E-10	Values prior to Silo construction used instead
KFR55	48.00	50.00	2.00	TI	3.0E-10	Values prior to Silo construction used instead
KFR55	50.00	52.00	2.00	TI	9.0E-10	Values prior to Silo construction used instead
KFR55	52.00	54.00	2.00	TI	6.0E-10	Values prior to Silo construction used instead
KFR55	54.00	56.00	2.00	TI	8.0E-9	Values prior to Silo construction used instead
KFR55	56.00	58.00	2.00	TI	5.0E-8	Values prior to Silo construction used instead
KFR55	40.00	48.00	8.00	BU	1.2E-7	overlapping data
KFR56	10.00	81.70	71.70	BU	2.2E-7	Shorter intervals used to improve resolution, T < value for 76–77.5 m section, thus negligible T assumed over 10 m–65 m
KFR56	73.00	74.50	1.50	BU	–1.0E-10	Overlapping data, shorter intervals used instead
KFR56	74.50	80.50	6.00	BU	1.7E-7	Intervals chosen to maximize resolution

KFR69	132.00	135.00	3.00	PH	–5.7E-8	overlapping data
KFR69	99.00	201.00	102.00	PH	1.1E-5	Intervals chosen to maximize resolution, replaced by single value 126–129 m
KFR69	45.00	201.00	156.00	PH	1.2E-5	Intervals chosen to maximize resolution, replaced by single value 126–129 m
KFR70	102.00	105.00	3.00	PH	–6.0E-8	Intervals chosen to maximize resolution
KFR70	99.00	172.00	73.00	PH	6.3E-6	Intervals chosen to maximize resolution
KFR70	51.00	172.00	121.00	PH	1.0E-5	Intervals chosen to maximize resolution
KFR7B	4.00	7.00	3.00	BU	3.9E-7	Suspected error
KFR83	5.00	20.00	15.00	BU	1.1E-7	Suspected error
HFM33	12	140.2	128.20	TM	5.1E-4	T assumed small outside flow-logged interval
HFM33	12	140.2	128.20	TT	4.7E-4	T assumed small outside flow-logged interval
HFM34	12	200.8	188.80	TM	3.0E-3	T assumed small outside flow-logged intervals
HFM34	12	200.8	188.80	TT	1.1E-3	T assumed small outside flow-logged intervals
HFM35	12	200.8	188.80	TM	1.4E-4	T assumed small outside flow-logged intervals
HFM35	12	200.8	188.80	TT	1.6E-4	T assumed small outside flow-logged intervals
HFM35	12	21	9.00	TT	2.2E-5	Overlapping data, shorter intervals used instead
KFM11A	514.50	534.50	20.00	TM	2.5E-10	overlapping data
KFM11A	820.00	840.00	20.00	TM	4.7E-7	overlapping data
KFM11A	470.00	490.00	20.00	TT	3.6E-8	overlapping data, TM used instead
KFM11A	488.50	508.50	20.00	TT	1.5E-8	overlapping data, TM used instead
KFM11A	530.00	550.00	20.00	TT	4.1E-10	overlapping data, TM used instead
KFM11A	550.00	570.00	20.00	TT	1.3E-10	overlapping data, TM used instead
KFM11A	570.00	590.00	20.00	TT	1.8E-9	overlapping data, TM used instead
KFM11A	590.00	610.00	20.00	TT	7.1E-8	overlapping data, TM used instead
KFM11A	610.00	630.00	20.00	TT	1.4E-8	overlapping data, TM used instead
KFM11A	630.00	650.00	20.00	TT	2.7E-9	overlapping data, TM used instead
KFM11A	650.00	670.00	20.00	TT	3.8E-10	overlapping data, TM used instead
KFM11A	670.00	690.00	20.00	TT	1.0E-7	overlapping data, TM used instead
KFM11A	690.00	710.00	20.00	TT	7.6E-7	overlapping data, TM used instead
KFM11A	710.00	730.00	20.00	TT	2.7E-9	overlapping data, TM used instead
KFM11A	730.00	750.00	20.00	TT	6.2E-9	overlapping data, TM used instead
KFM11A	750.00	770.00	20.00	TT	9.8E-9	overlapping data, TM used instead
KFM11A	770.00	790.00	20.00	TT	3.0E-7	overlapping data, TM used instead
KFM11A	790.00	810.00	20.00	TT	1.2E-6	overlapping data, TM used instead
KFM11A	810.00	830.00	20.00	TT	5.6E-7	overlapping data, TM used instead
KFM11A	820.00	840.00	20.00	TT	3.5E-7	overlapping data, TM used instead

Appendix B

Presentation of hydraulic data, screening, and HRD/HCD classification

The available hydraulic data is presented on borehole basis in this appendix. The data screening and HRD/HCD classification of data are also shown.

Data below detection limit are shown at the detection limit, but indicated by a pale colour.

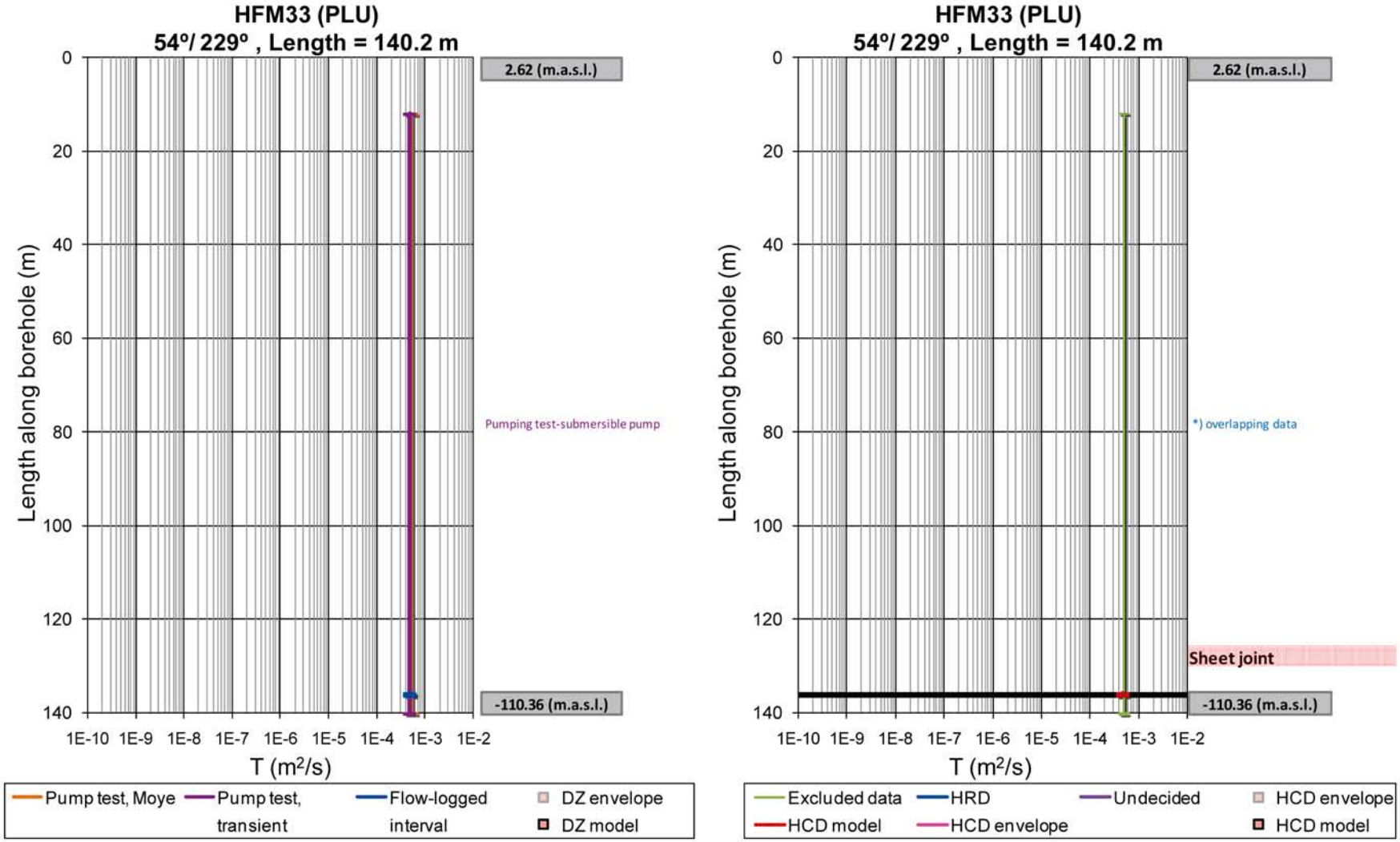

Figure B-1. *HFM33 raw data (left) and interpretation (right). Flow anomaly assumed to coincide with sheet joint , as no possible deformation zone according to SHI /Carlsten et al. 2007/.*

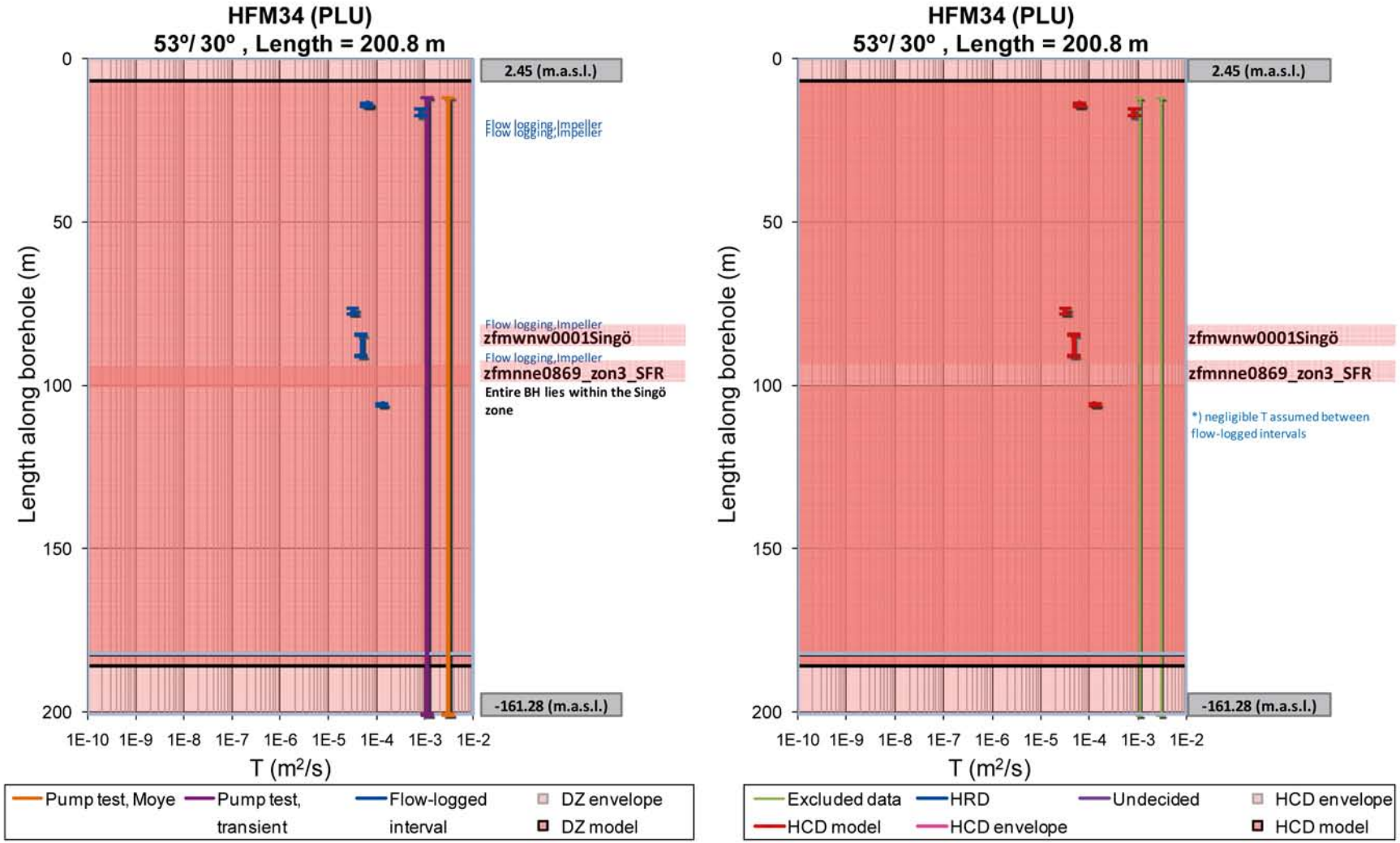

Figure B-2. *HFM34 raw data (left) and interpretation (right). Transmissivity between flow anomalies assumed negligible. Transmissivity assigned to HCDs, despite possible sheet joints. Possible deformation zone according to SHI at 37–133 m, 180–184 m, and 188–192 m /Carlsten et al. 2007/.*

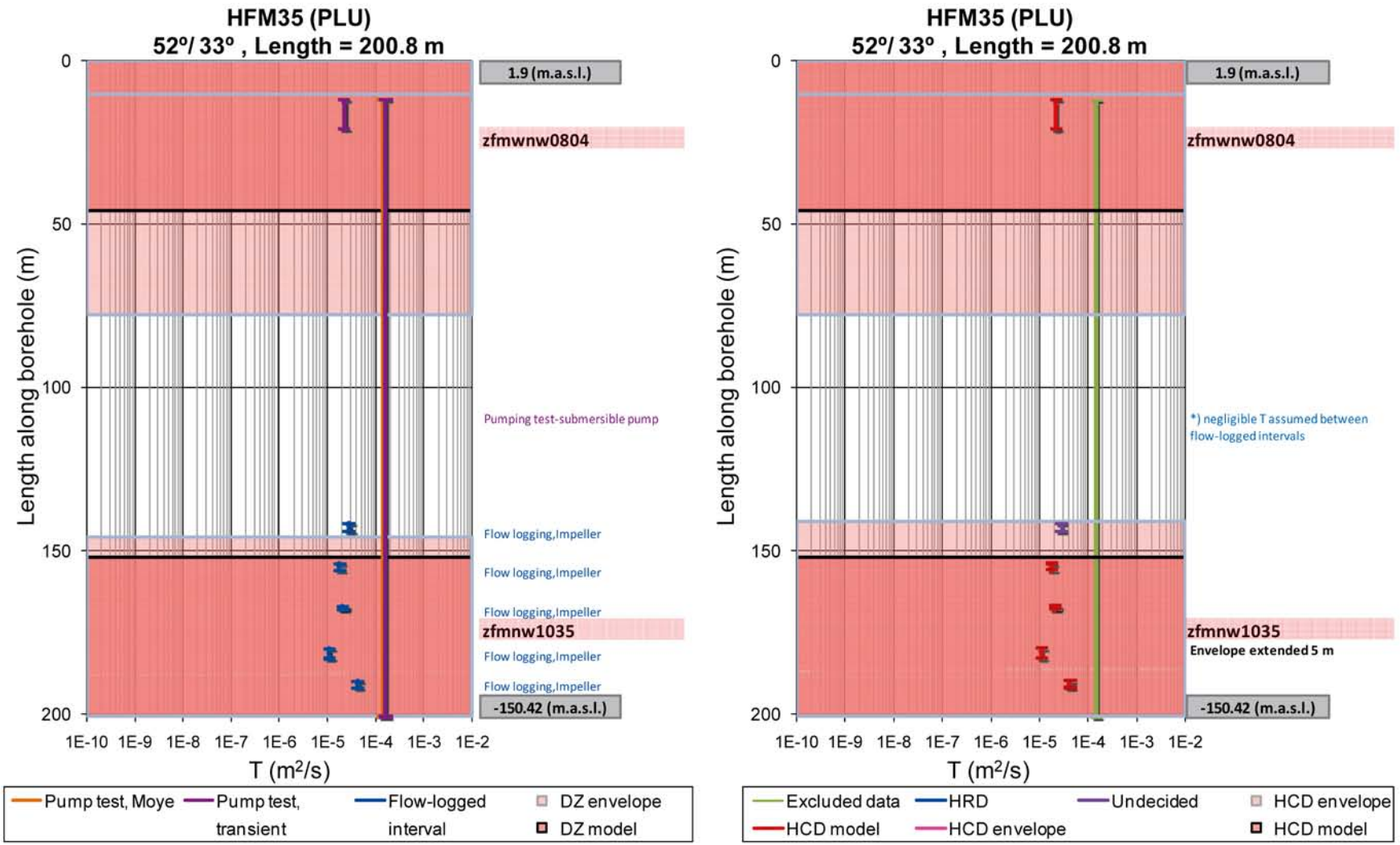

Figure B-3. *HFM35 raw data (left) and interpretation (right). Transmissivity outside flow-logged anomalies negliglected. Transmissivity assigned only to HCDs, despite possible sheet joints. Possible deformation zone according to SHI at 24–33 m, 47.2–52.5 m, and 104–200 m /Carlsten et al. 2007/.*

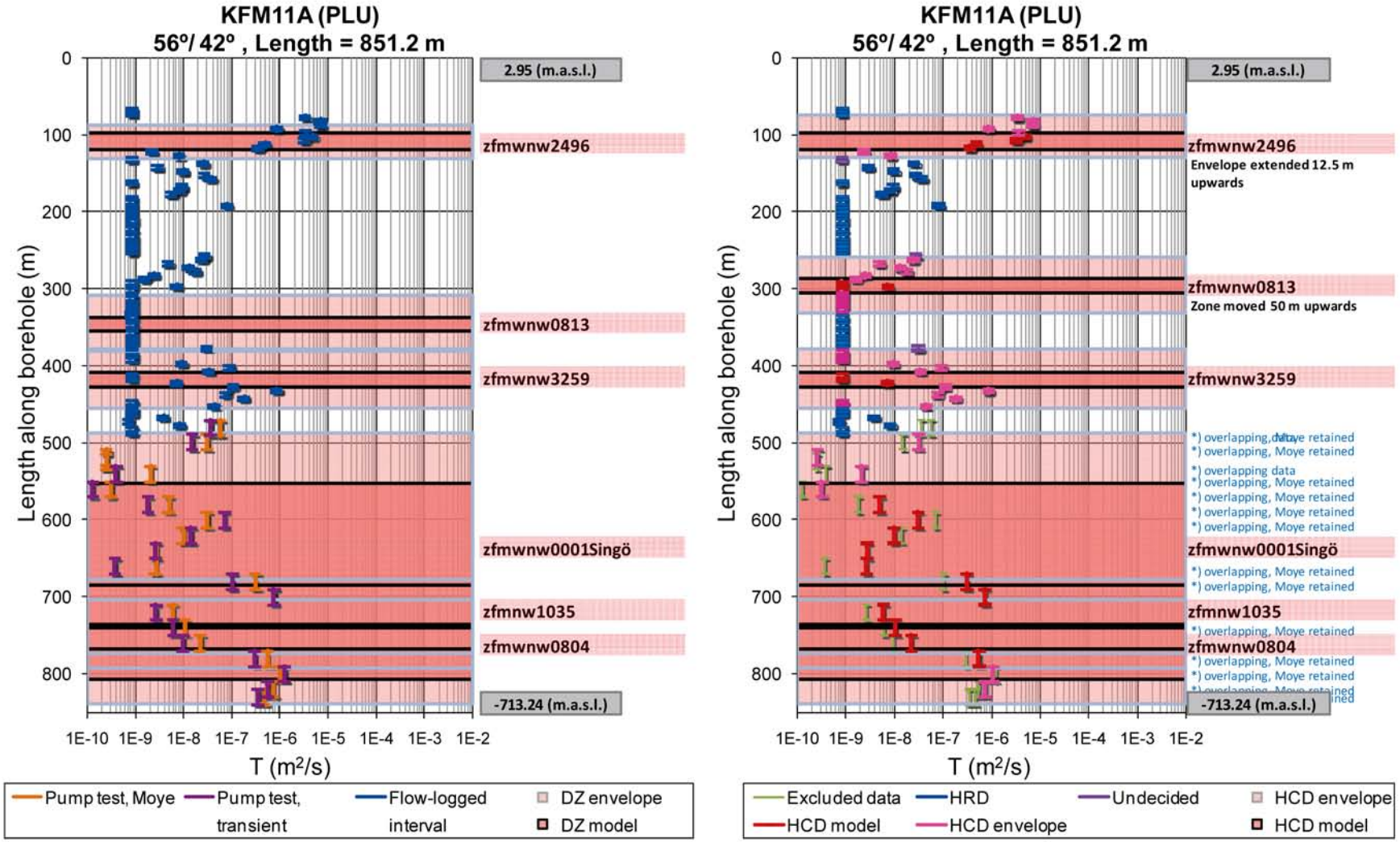

Figure B-4. *KFM11A raw data (left) and interpretation (right). Note that the hydraulic envelope of zfmwnw2496 was expanded upwards and that zfmwnw0813 was moved 50 m (borehole length) upwards. Possible deformation zone 245–824 m, according to SHI /Carlsten et al. 2007/.*

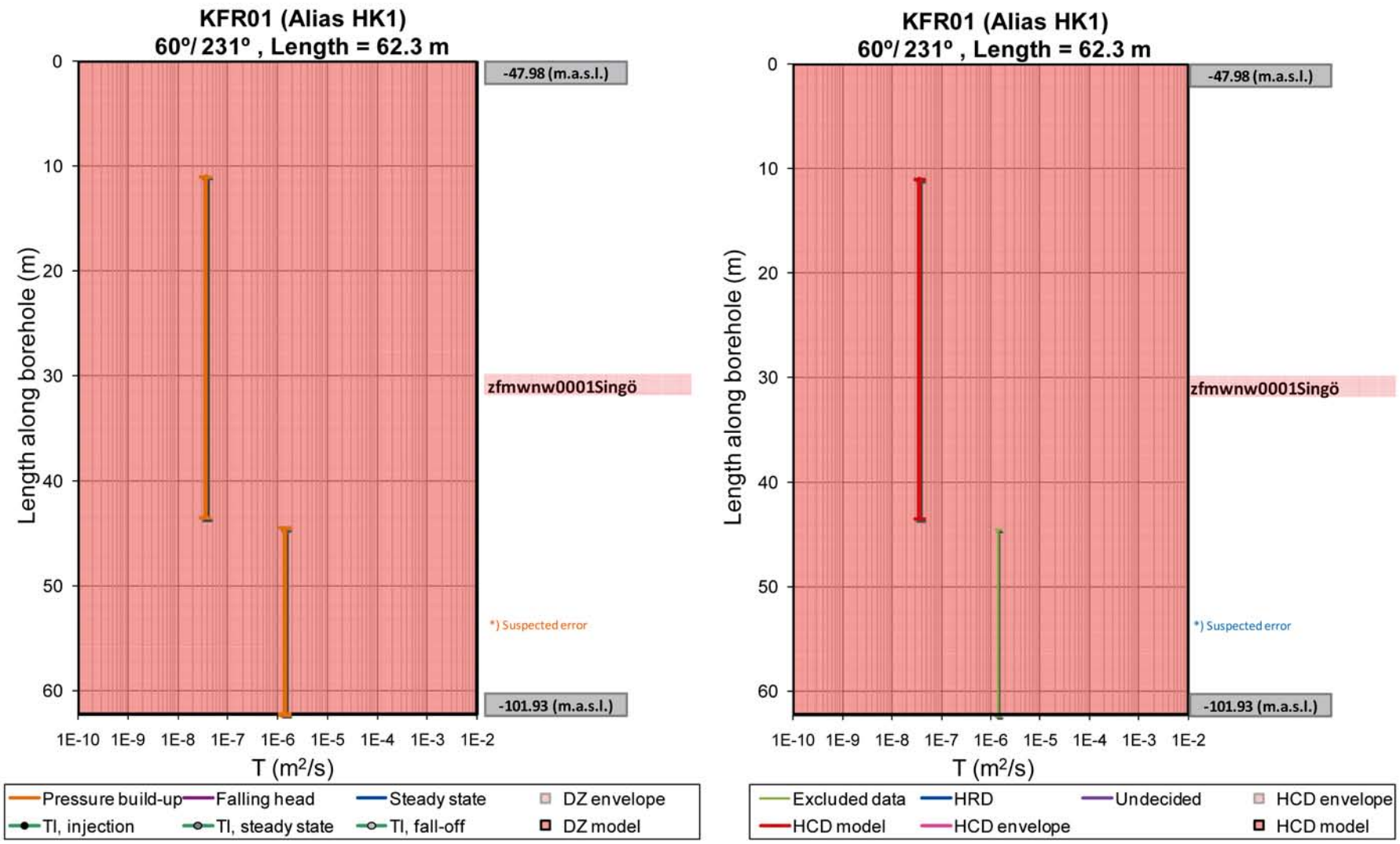

Figure B-5. *KFR01 raw data (left) and interpretation (right).*

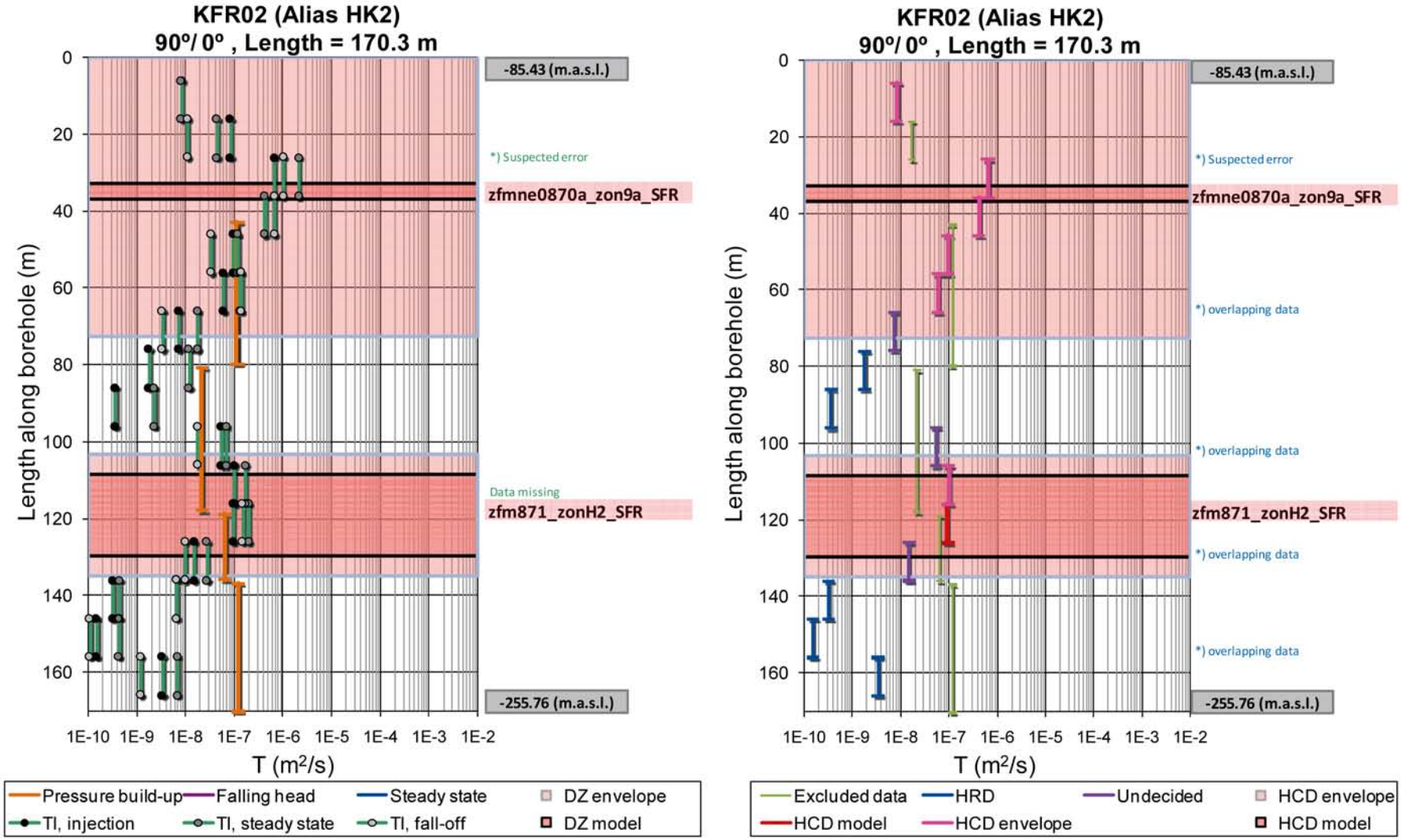

Figure B-6. *KFR02 raw data (left) and interpretation (right).*

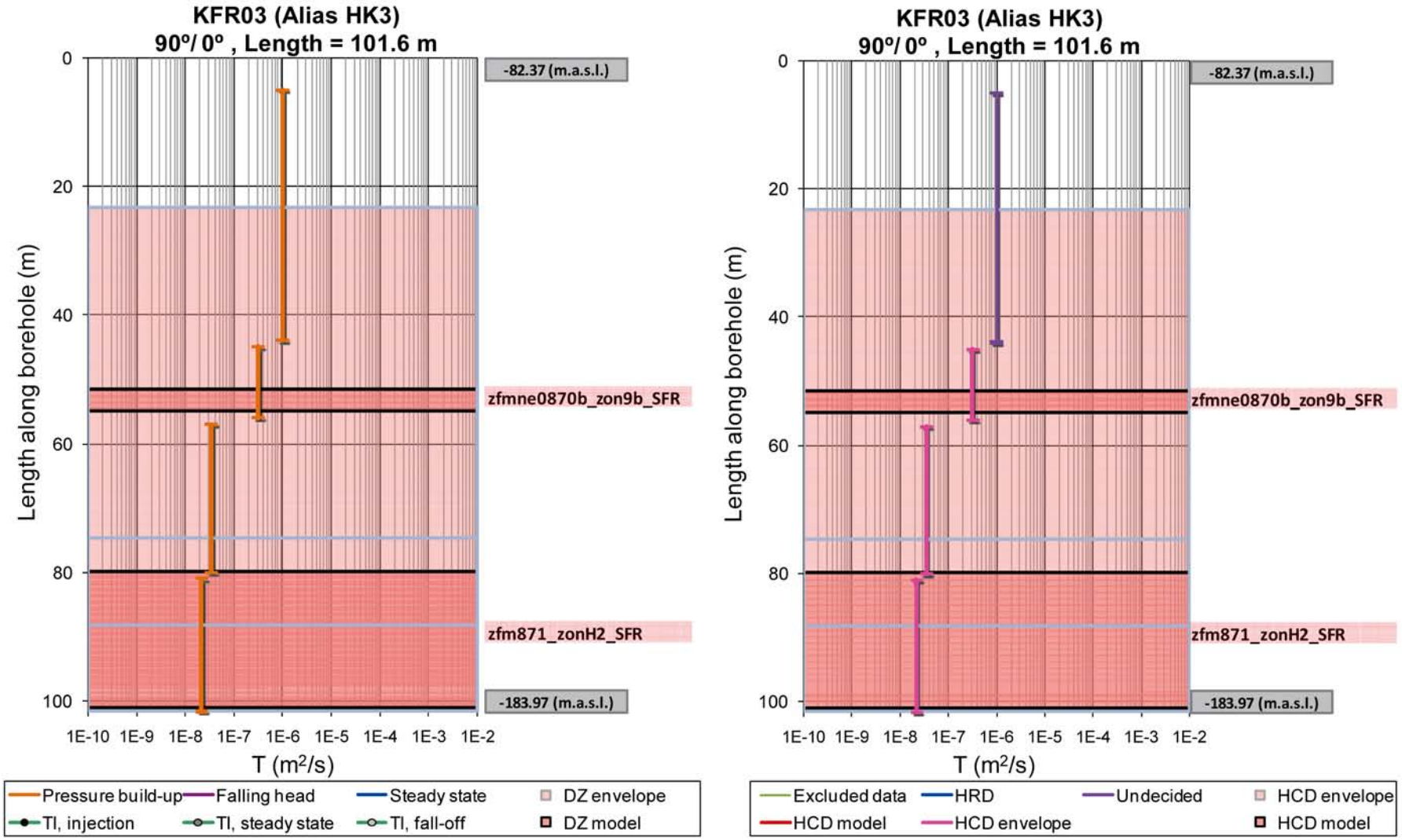

Figure B-7. *KFR03 raw data (left) and interpretation (right).*

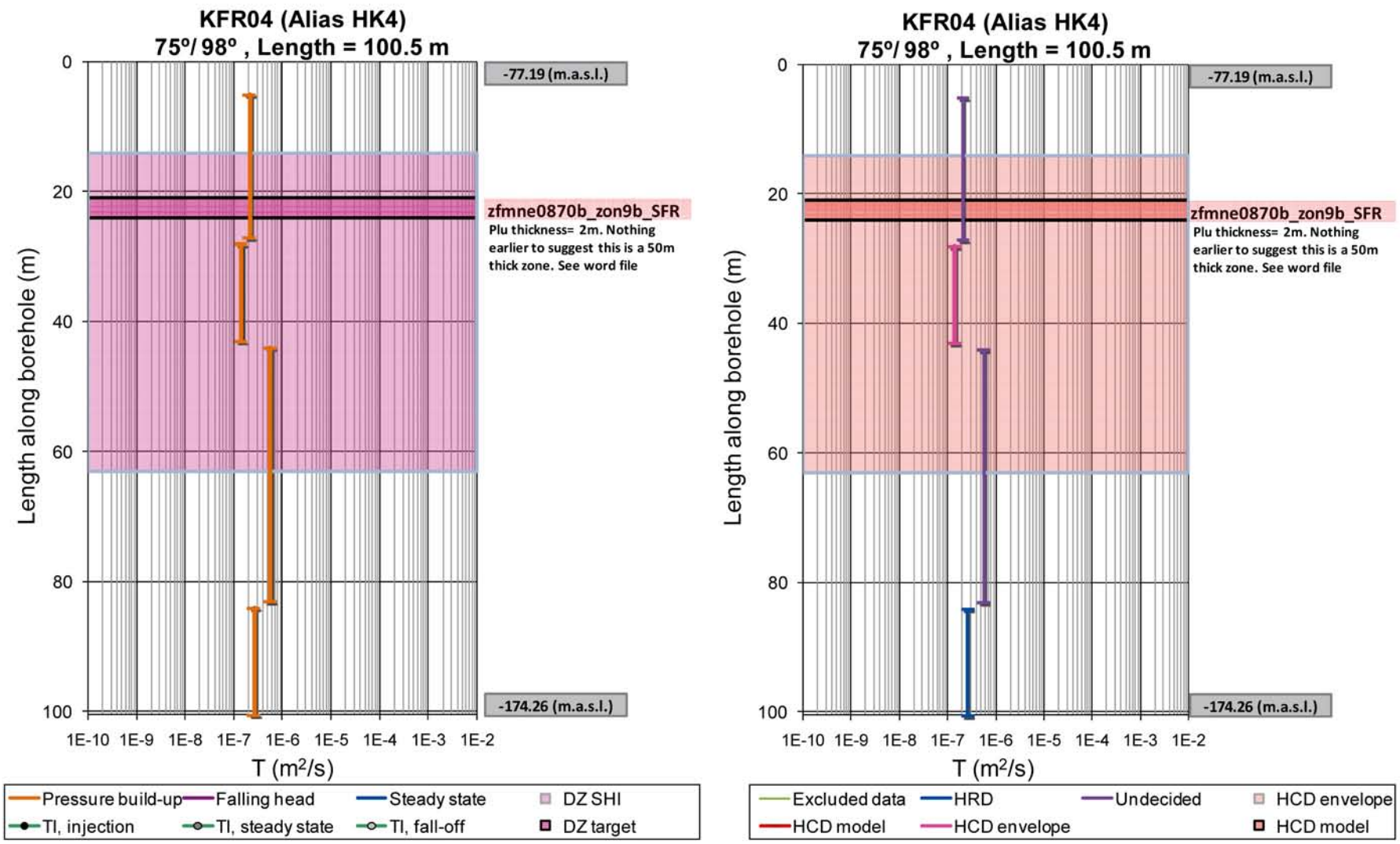

Figure B-8. *KFR04 raw data (left) and interpretation (right). An interference test performed (28–43 m) to examine zfmne0870; this section is outside the modeled zone, but inside the possible zone according to SHI.*

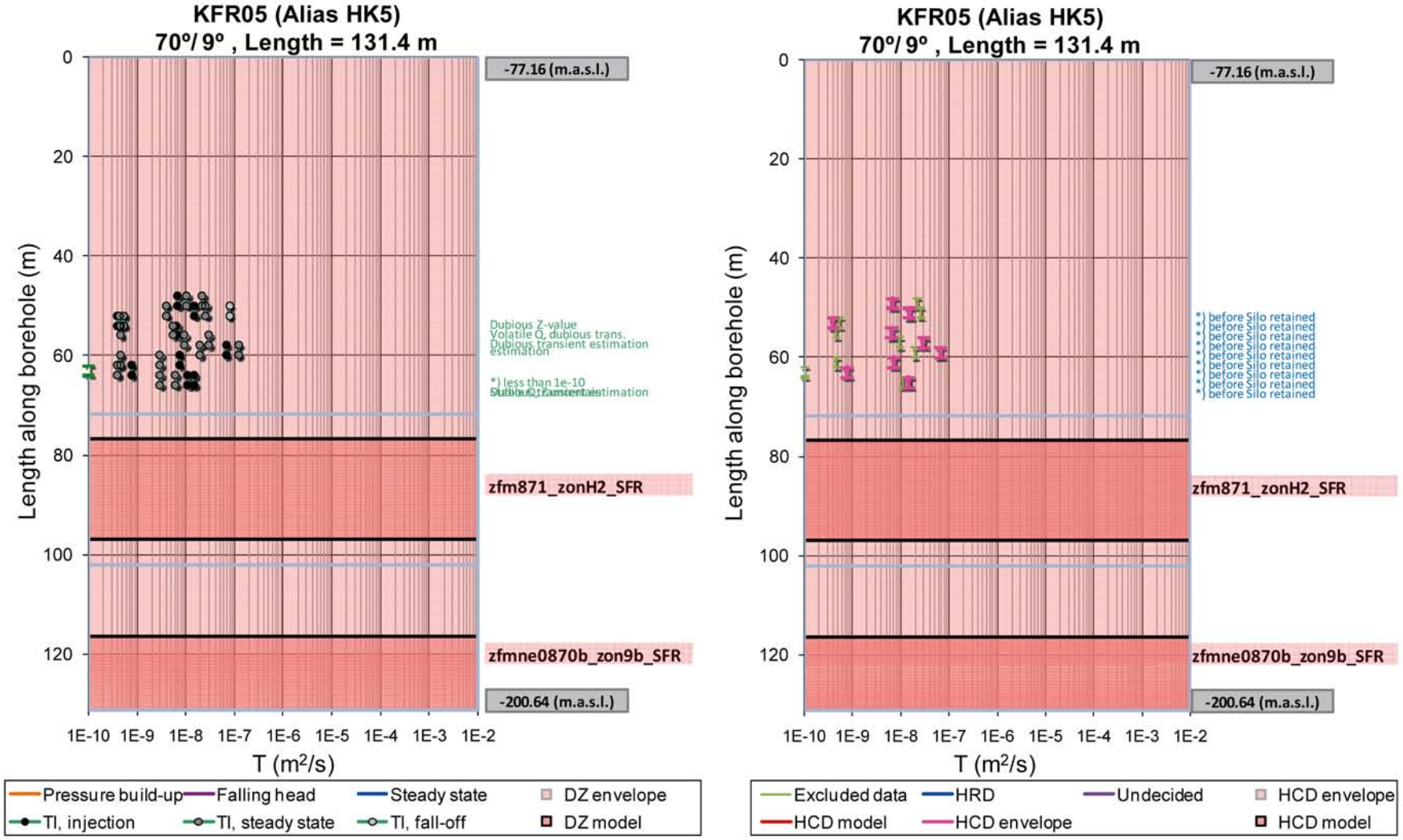

Figure B-9. *KFR05 raw data (left) and interpretation (right). Data measured after construction of the Silo are excluded.*

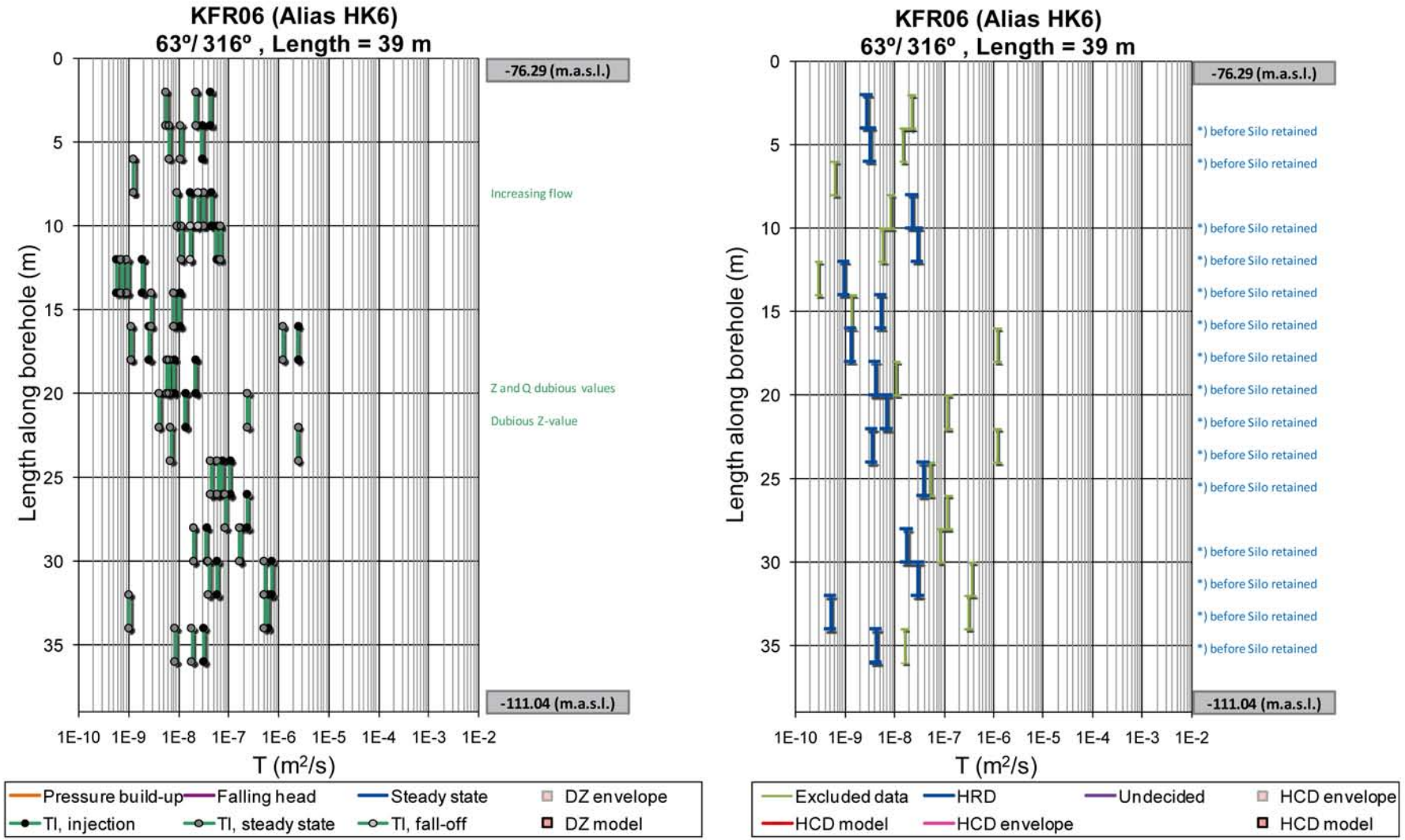

Figure B-10. *KFR06 raw data (left) and interpretation (right). Data measured after construction of the Silo are excluded.*

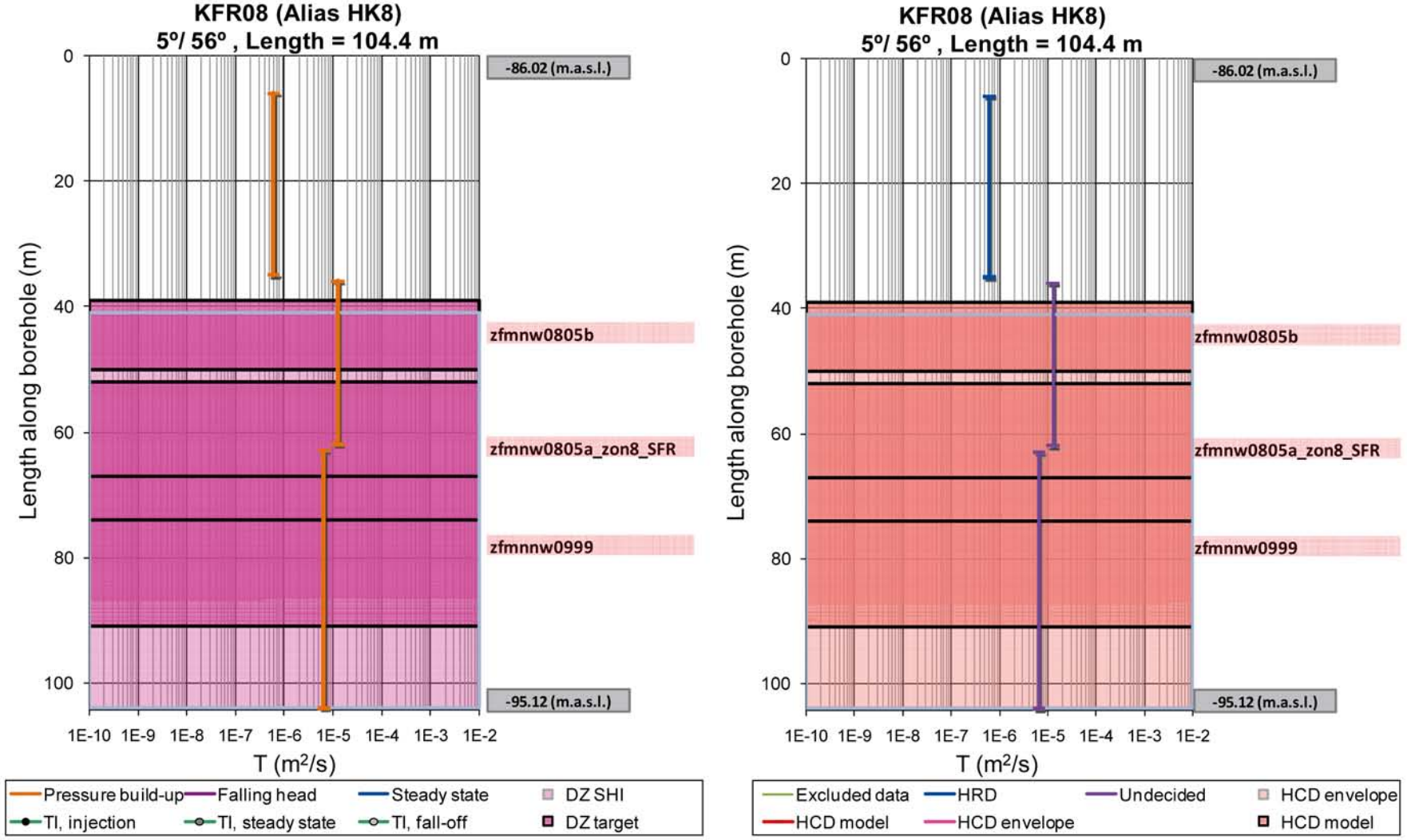

Figure B-11. *KFR08 raw data (left) and interpretation (right). An interference test performed (63–104 m) to examine zfmnw0805.*

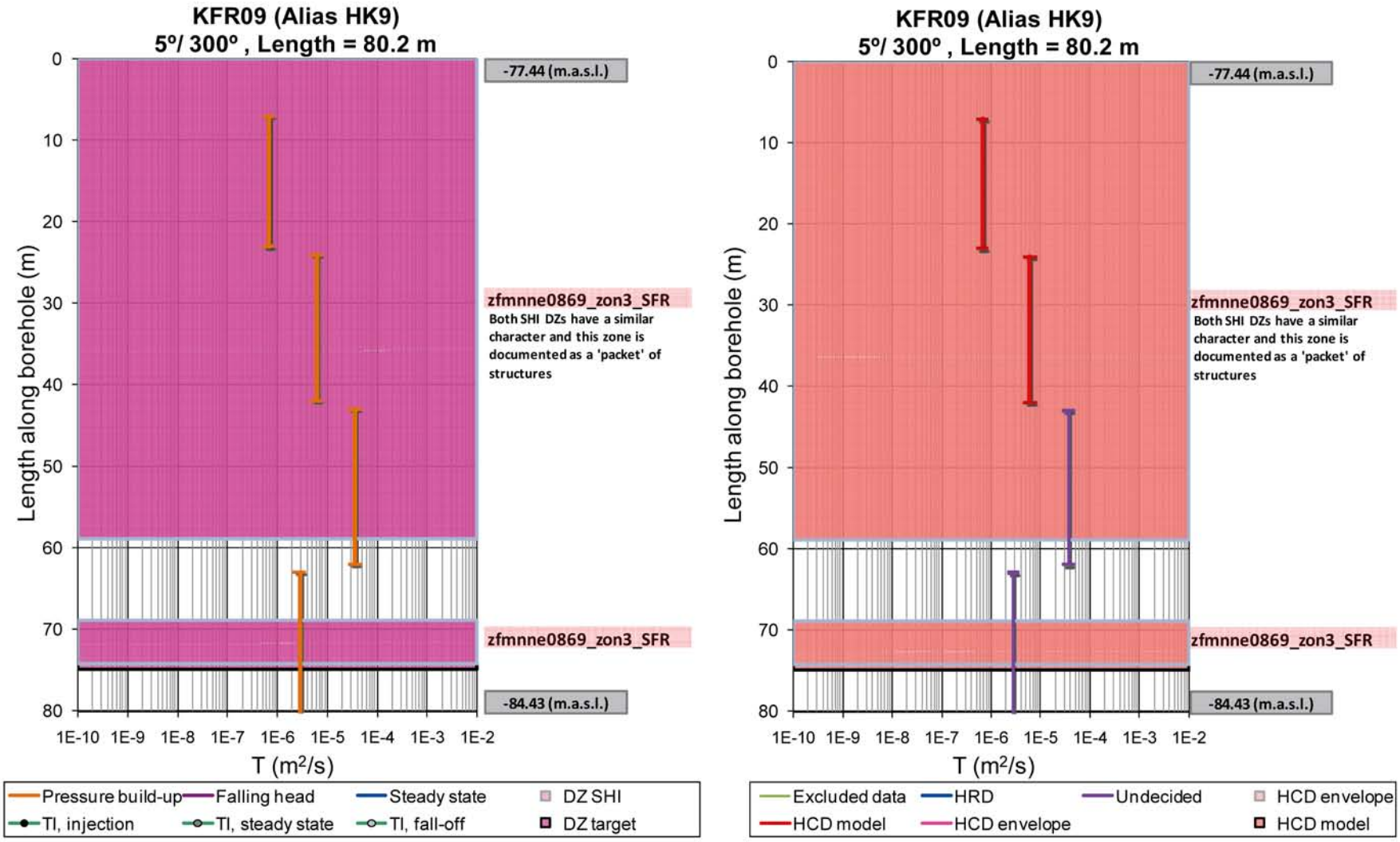

Figure B-12. *KFR09 raw data (left) and interpretation (right). An interference test performed (43–62 m) to examine zfmne0869; direct responses in all monitored sections of both KFR09 (except 7–23 m) and KFR10. Note that: the corresponding test in KFR10 (87–107.28 m) provided no responses.*

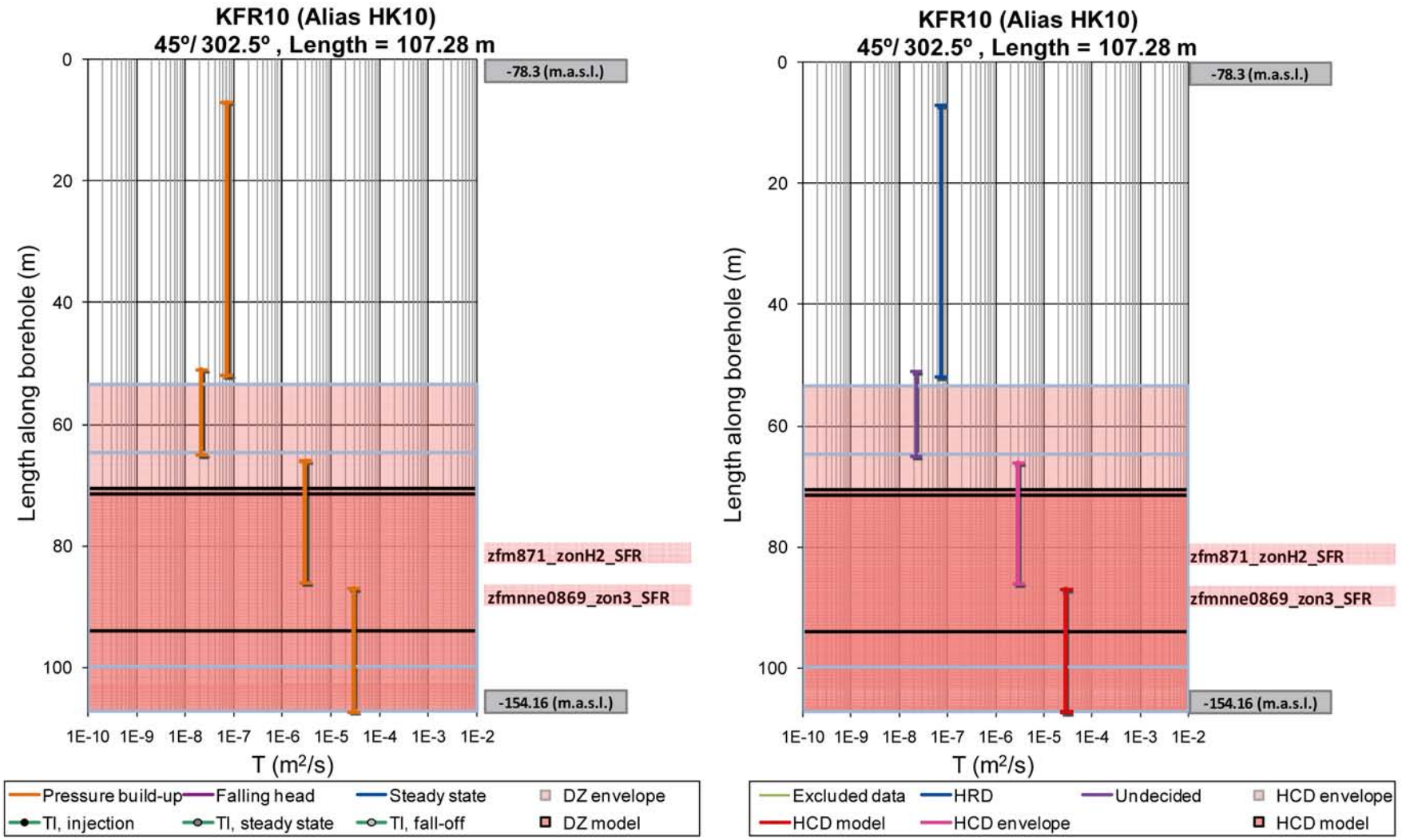

Figure B-13. *KFR10 raw data (left) and interpretation (right). An interference test performed (87–107.28 m) to examine zfmne0869 (note that the section also contains zfm871); no responses confirmed – possibly due to ongoing disturbances from construction work.*

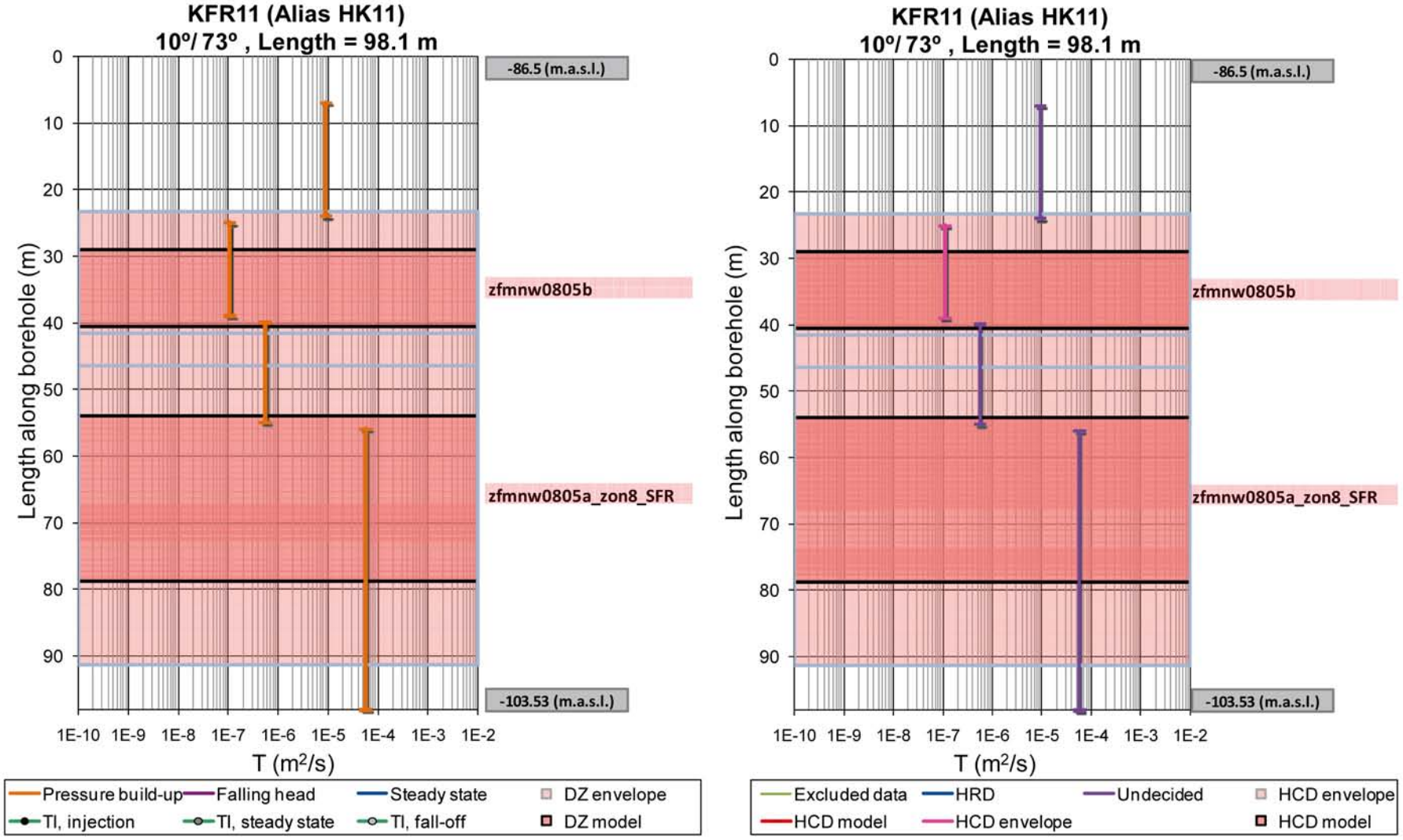

Figure B-14. *KFR11 raw data (left) and interpretation (right).*

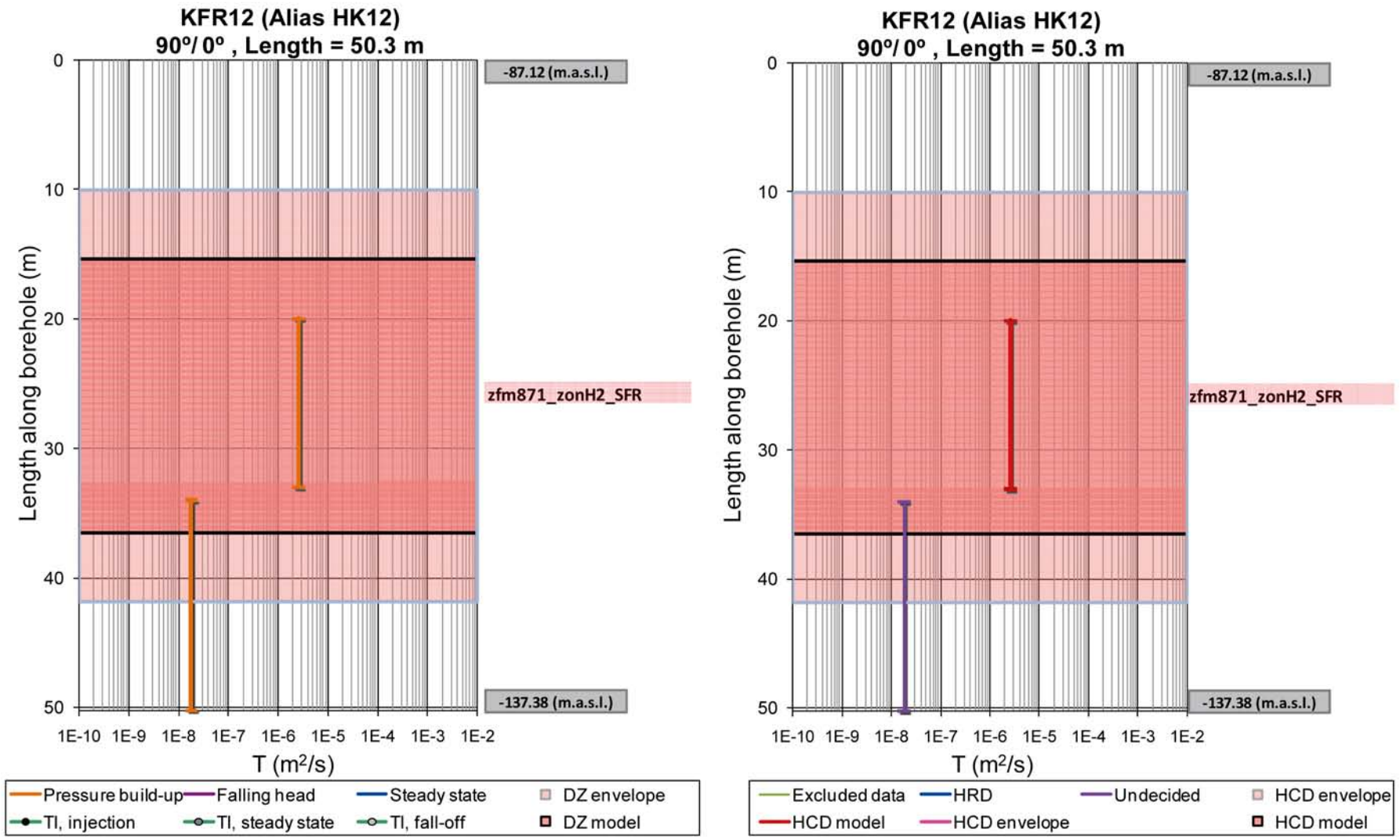

Figure B-15. *KFR12 raw data (left) and interpretation (right).*

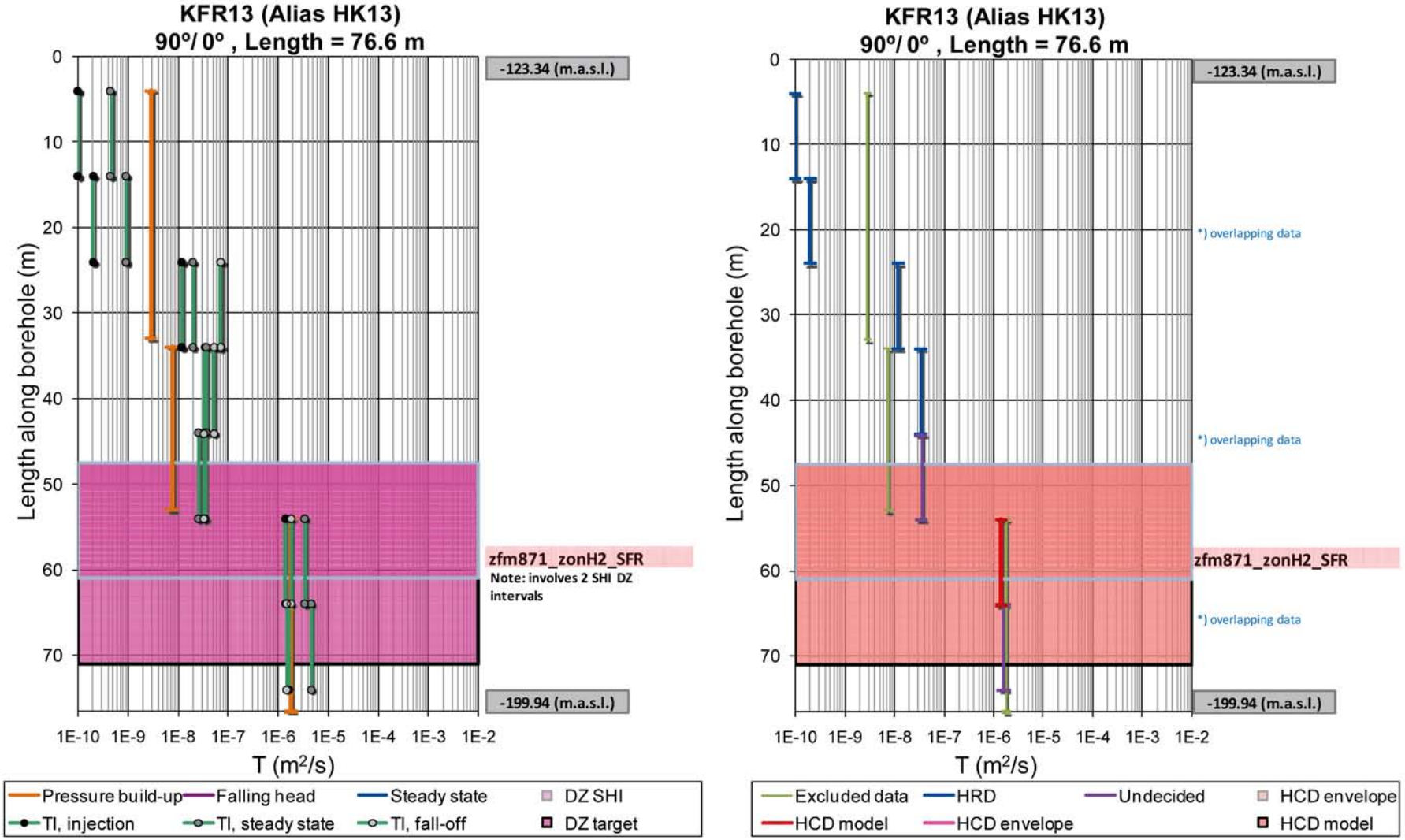

Figure B-16. *KFR13 raw data (left) and interpretation (right). An interference test performed in a single packer section to test zfm871, from 54 m borehole length to the end of borehole.*

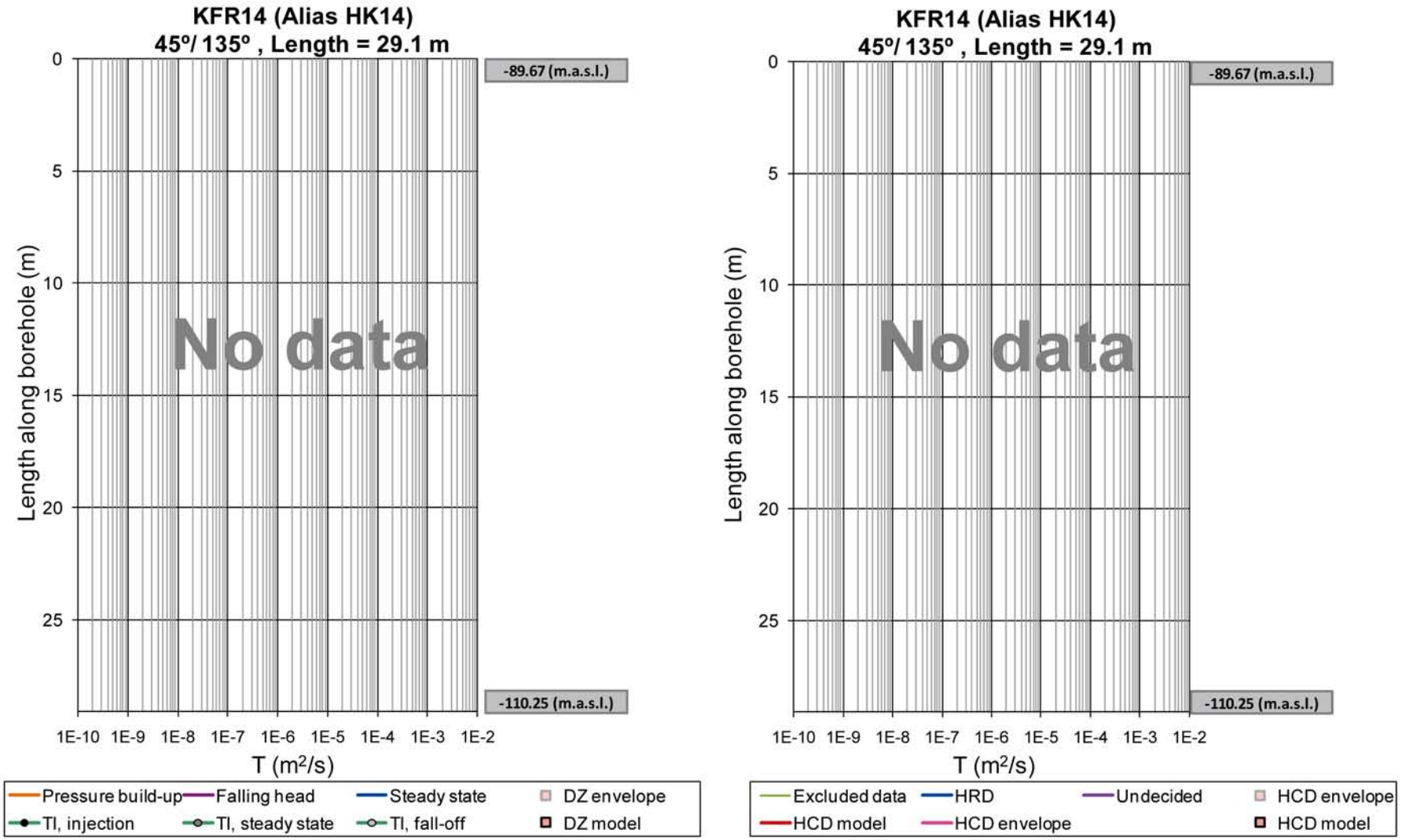

Figure B-17. *No hydraulic data available in KFR14.*

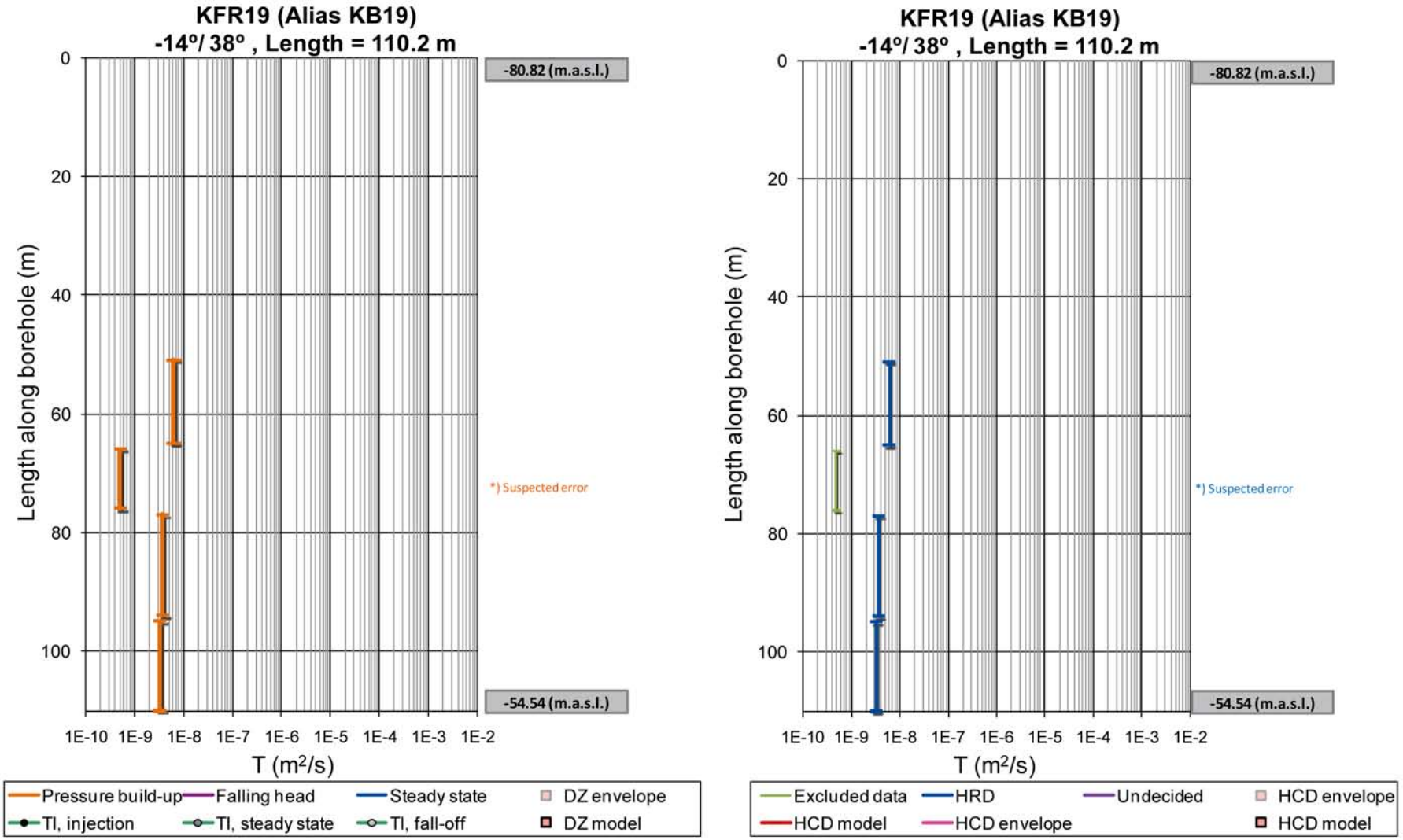

Figure B-18. *KFR19 raw data (left) and interpretation (right).*

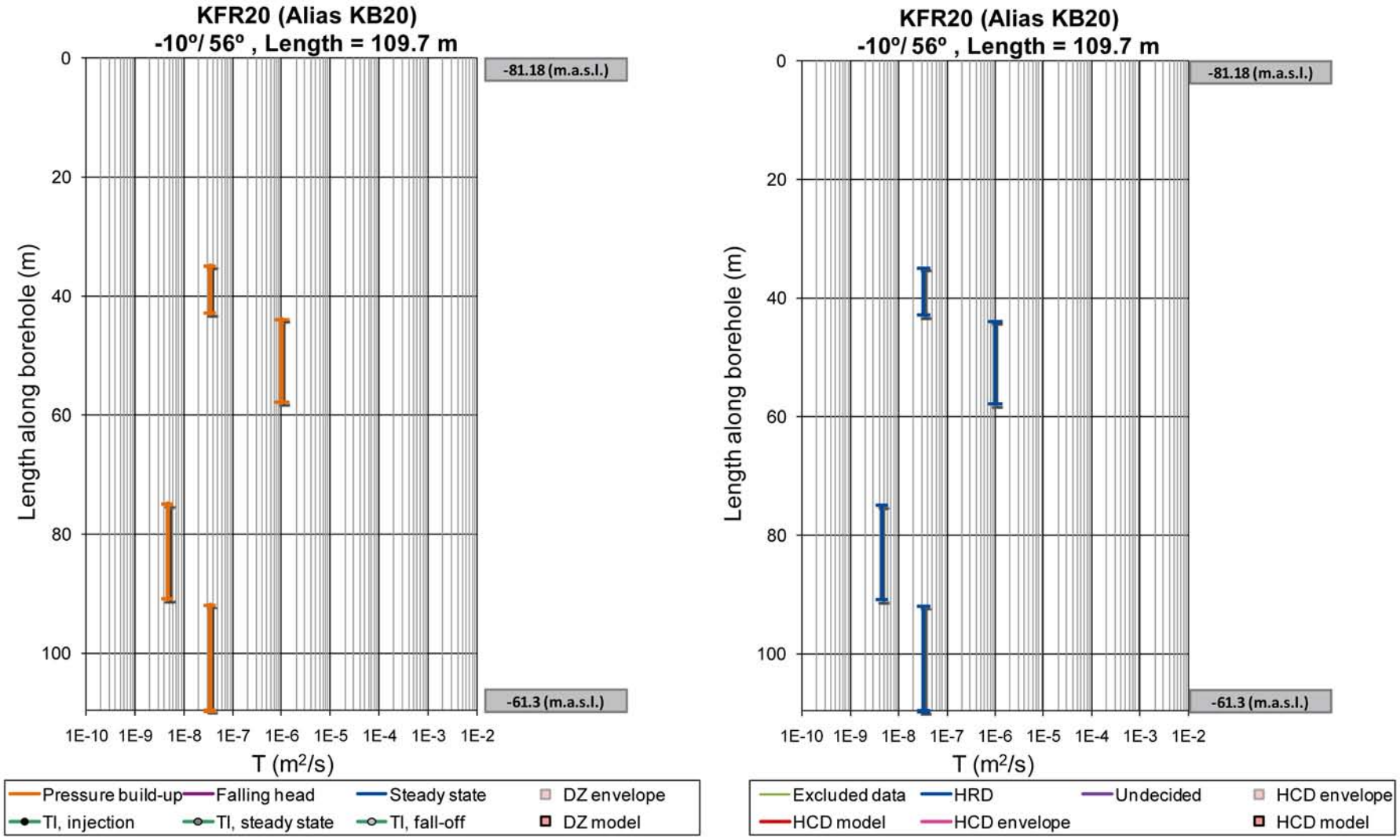

Figure B-19. *KFR20 raw data (left) and interpretation (right).*

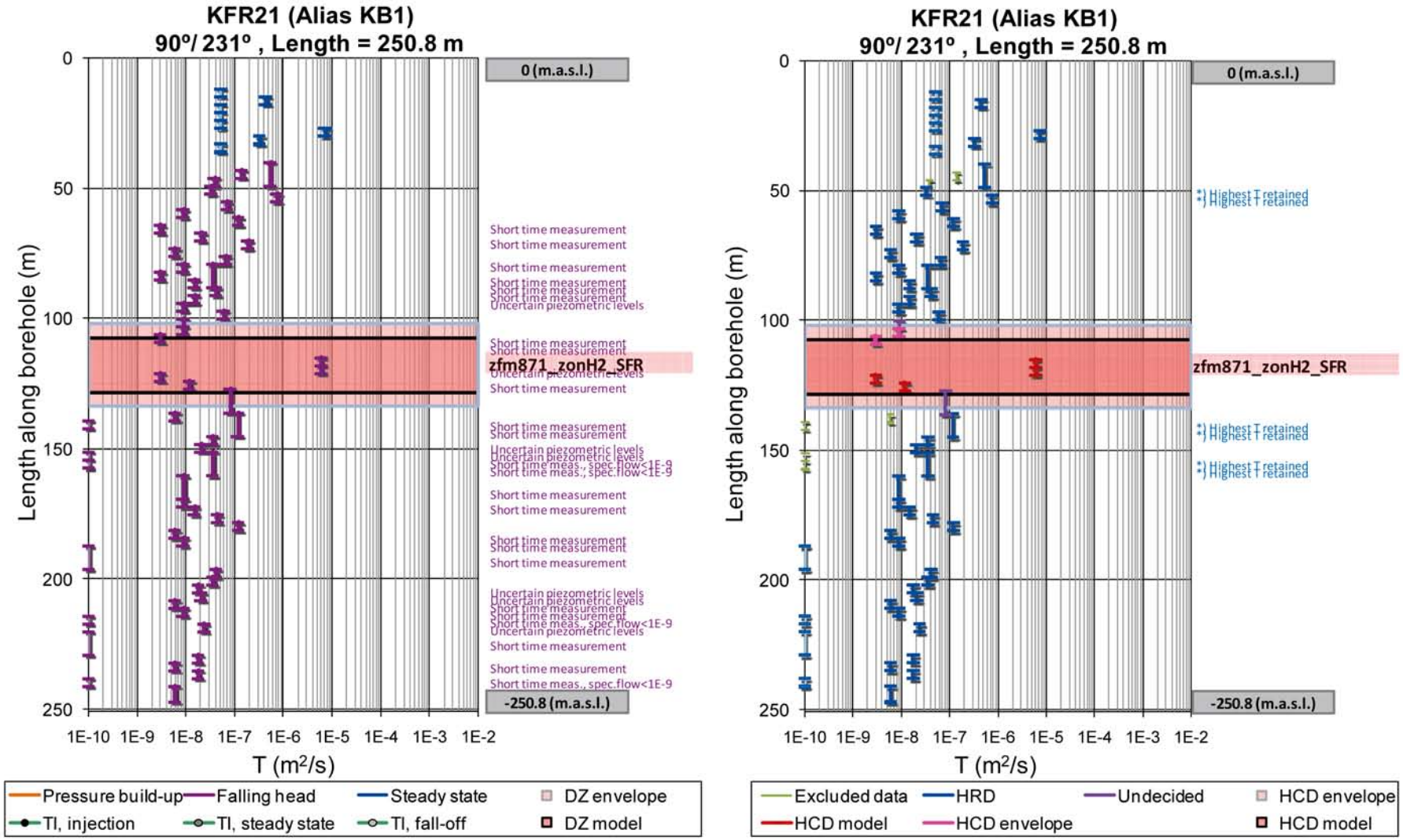

Figure B-20. *KFR21 raw data (left) and interpretation (right).*

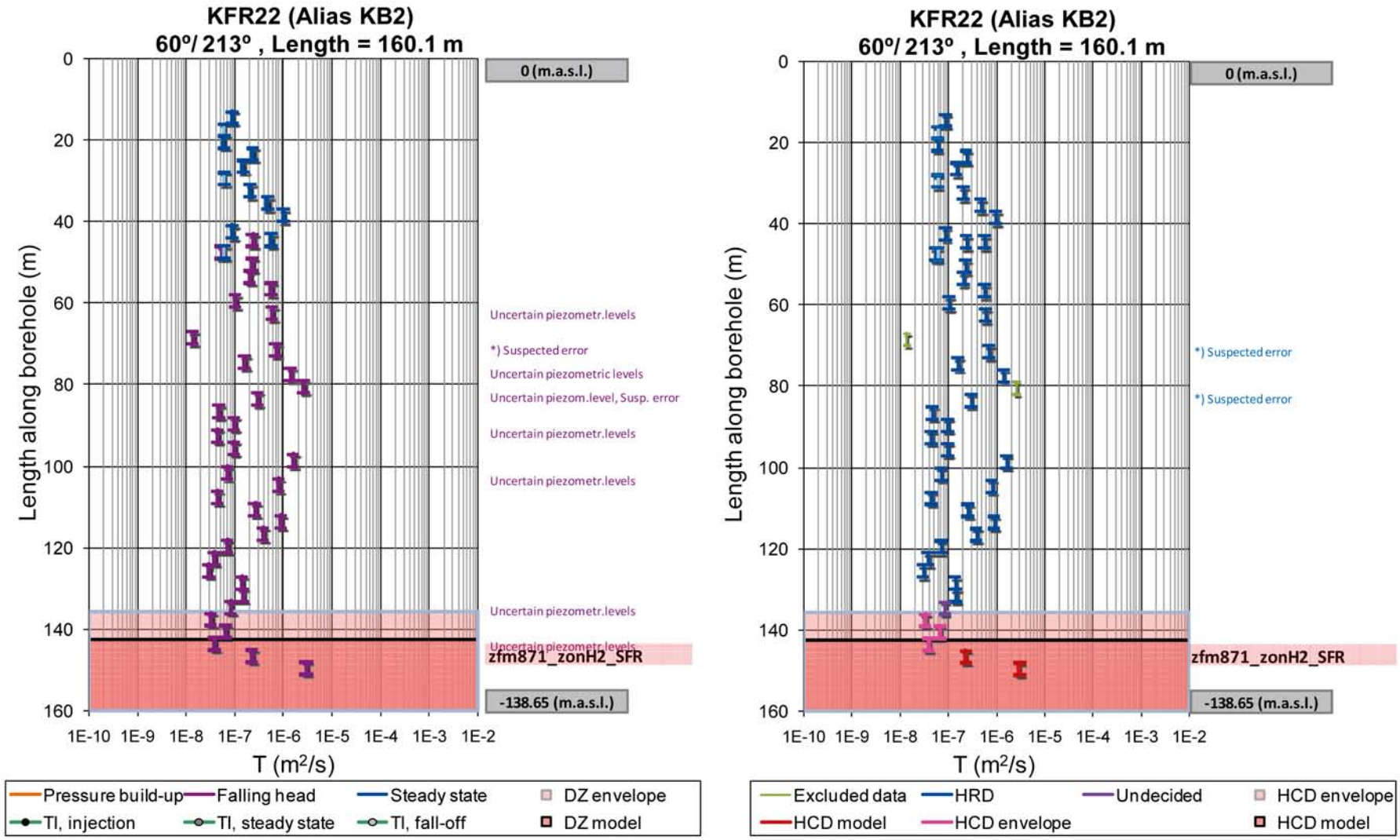

Figure B-21. *KFR22 raw data (left) and interpretation (right).*

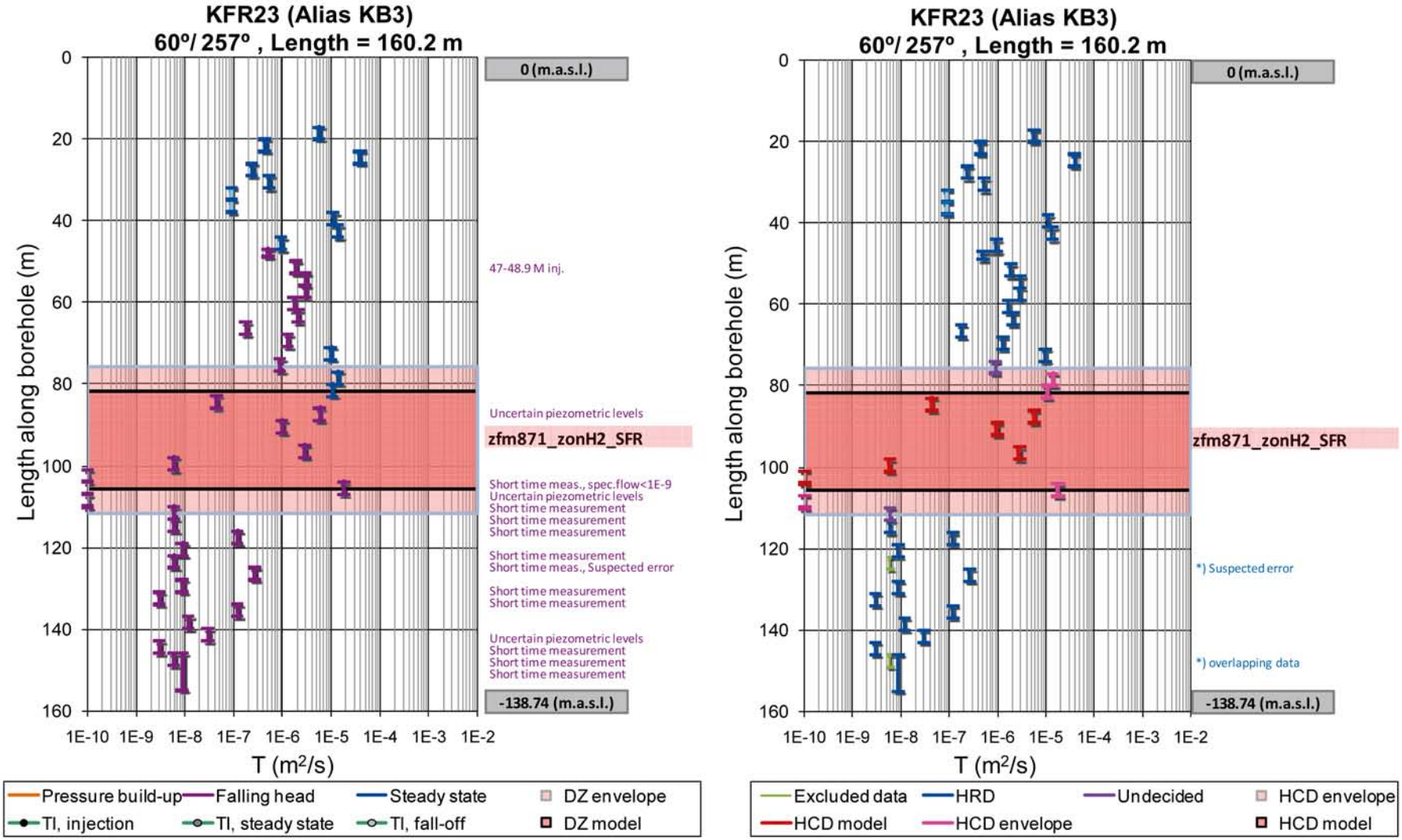

Figure B-22. *KFR23 raw data (left) and interpretation (right).*

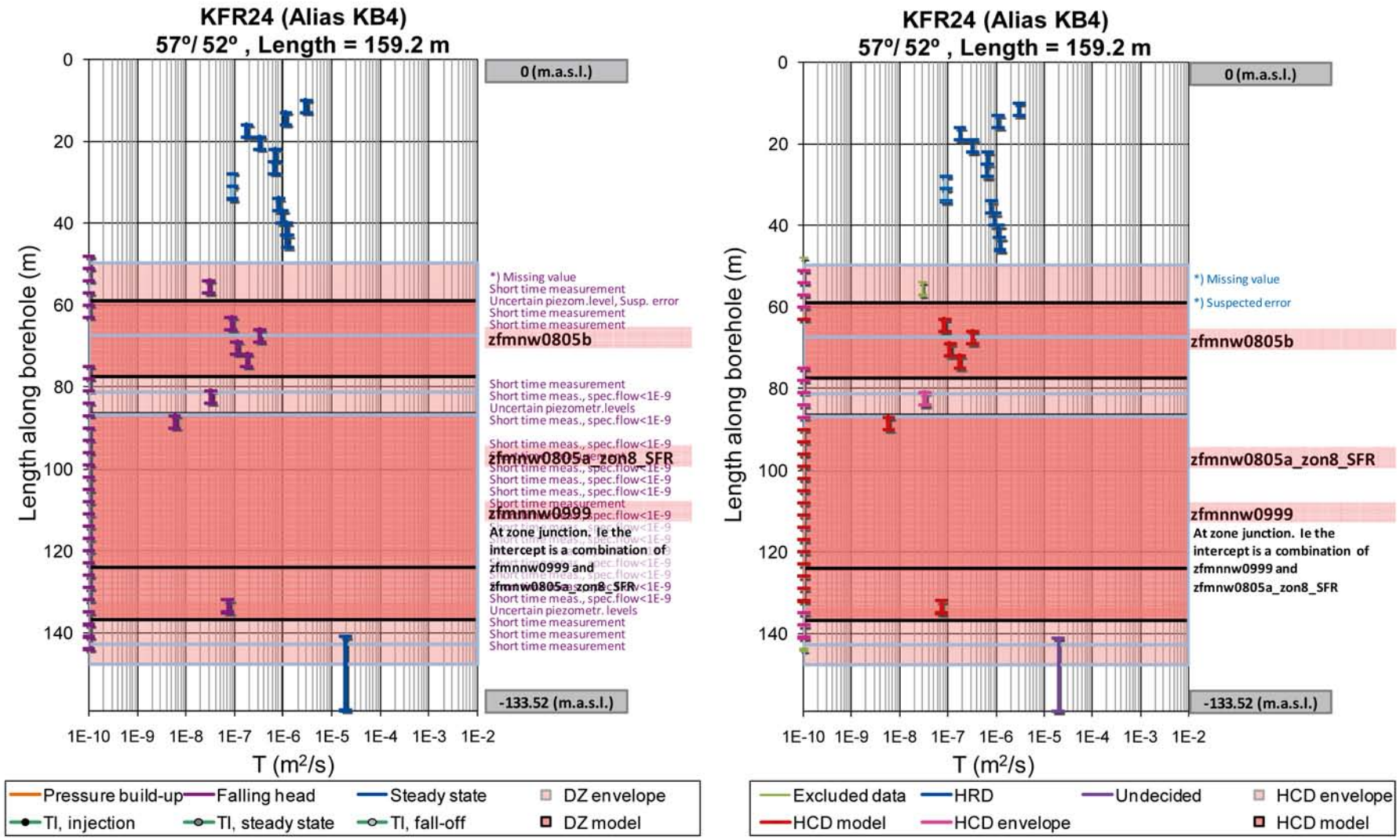

Figure B-23. *KFR24 raw data (left) and interpretation (right).*

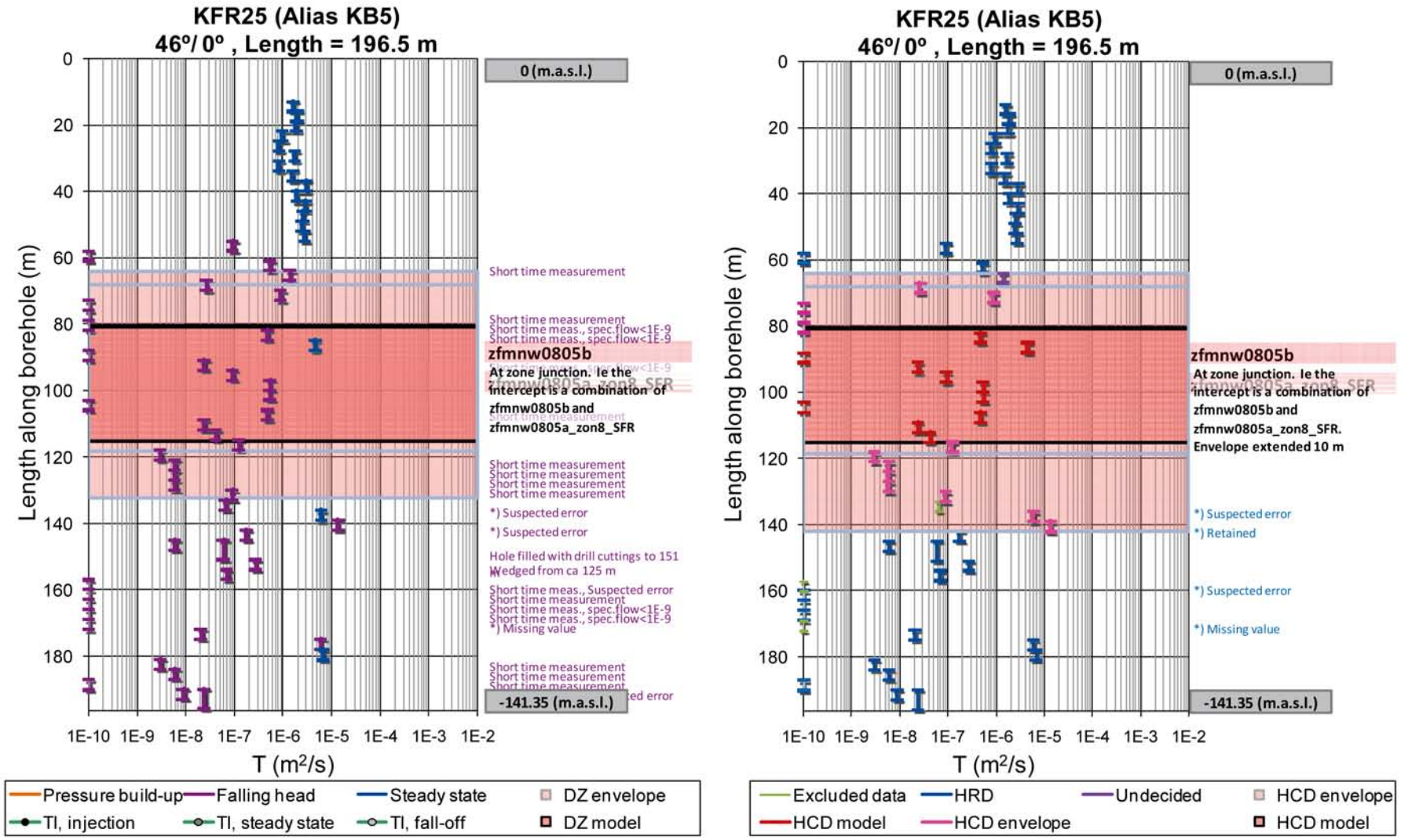

Figure B-24. *KFR25 raw data (left) and interpretation (right).*

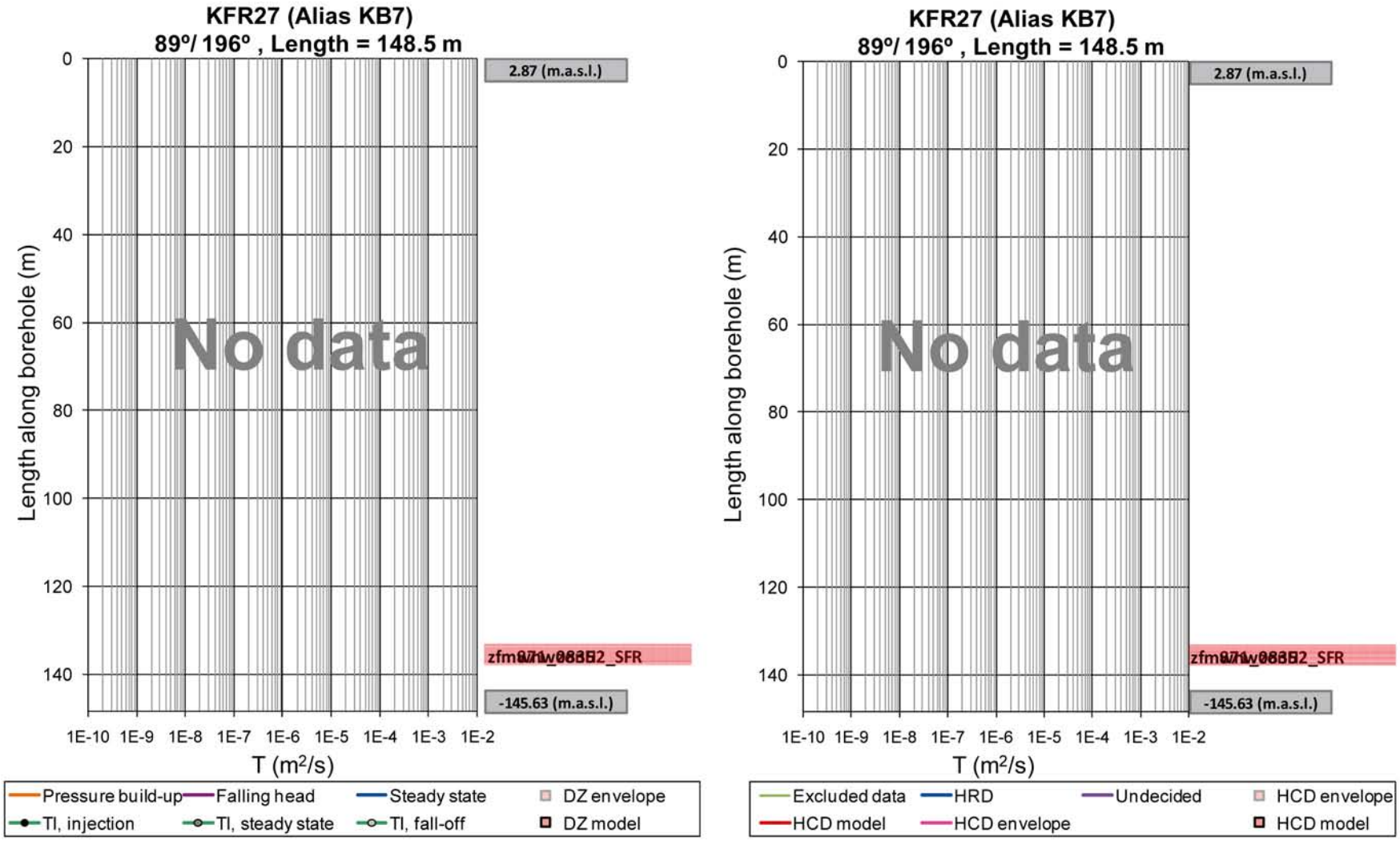

Figure B-25. *No hydraulic data currently available for the SFR v.0.1 model in KFR27. The borehole has been extended in the ongoing field investigations and is expected to intersect zfm871 at 250 to 270 m length, and zfmwnw0835 at 380 to 425 m borehole length.*

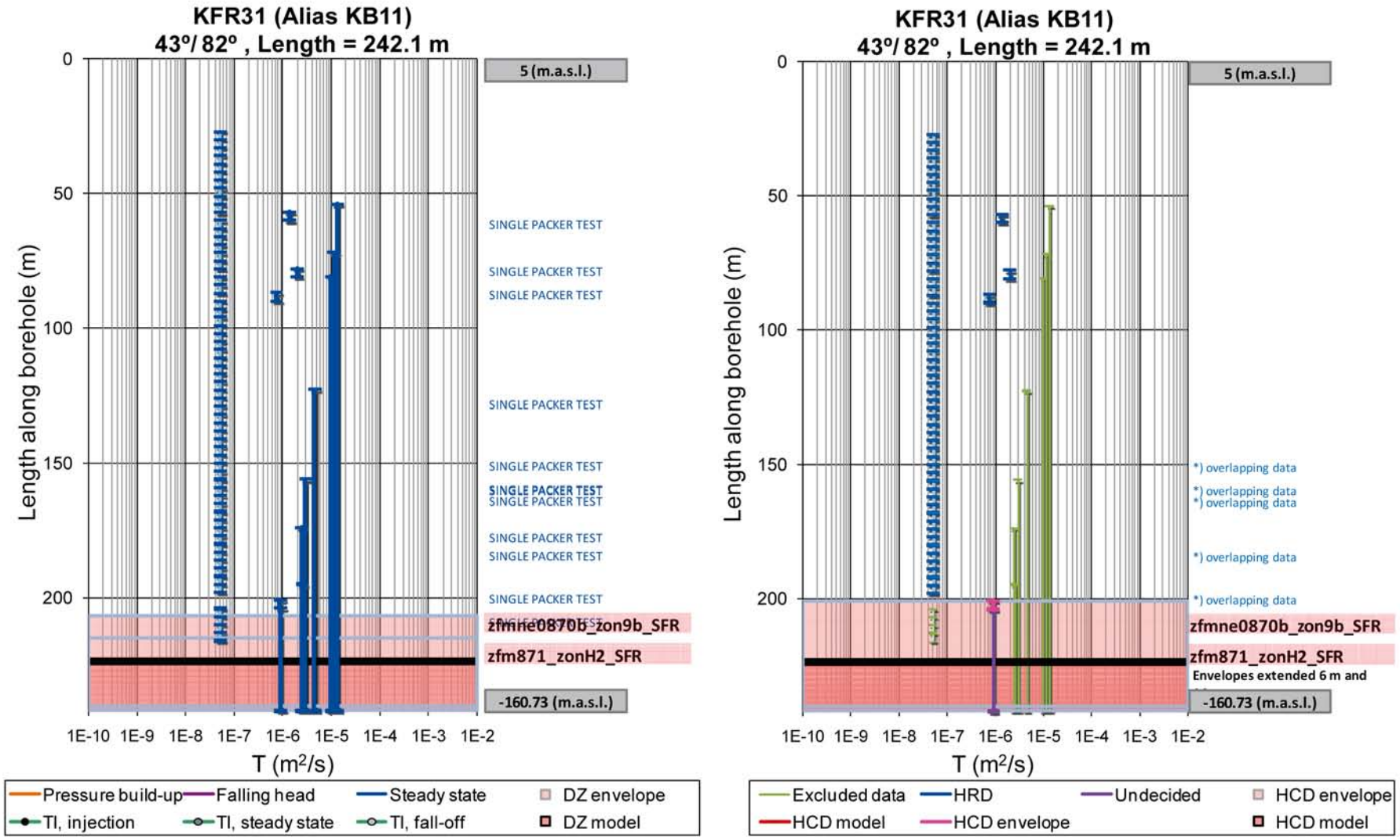

Figure B-26. *KFR31 raw data (left) and interpretation (right).*

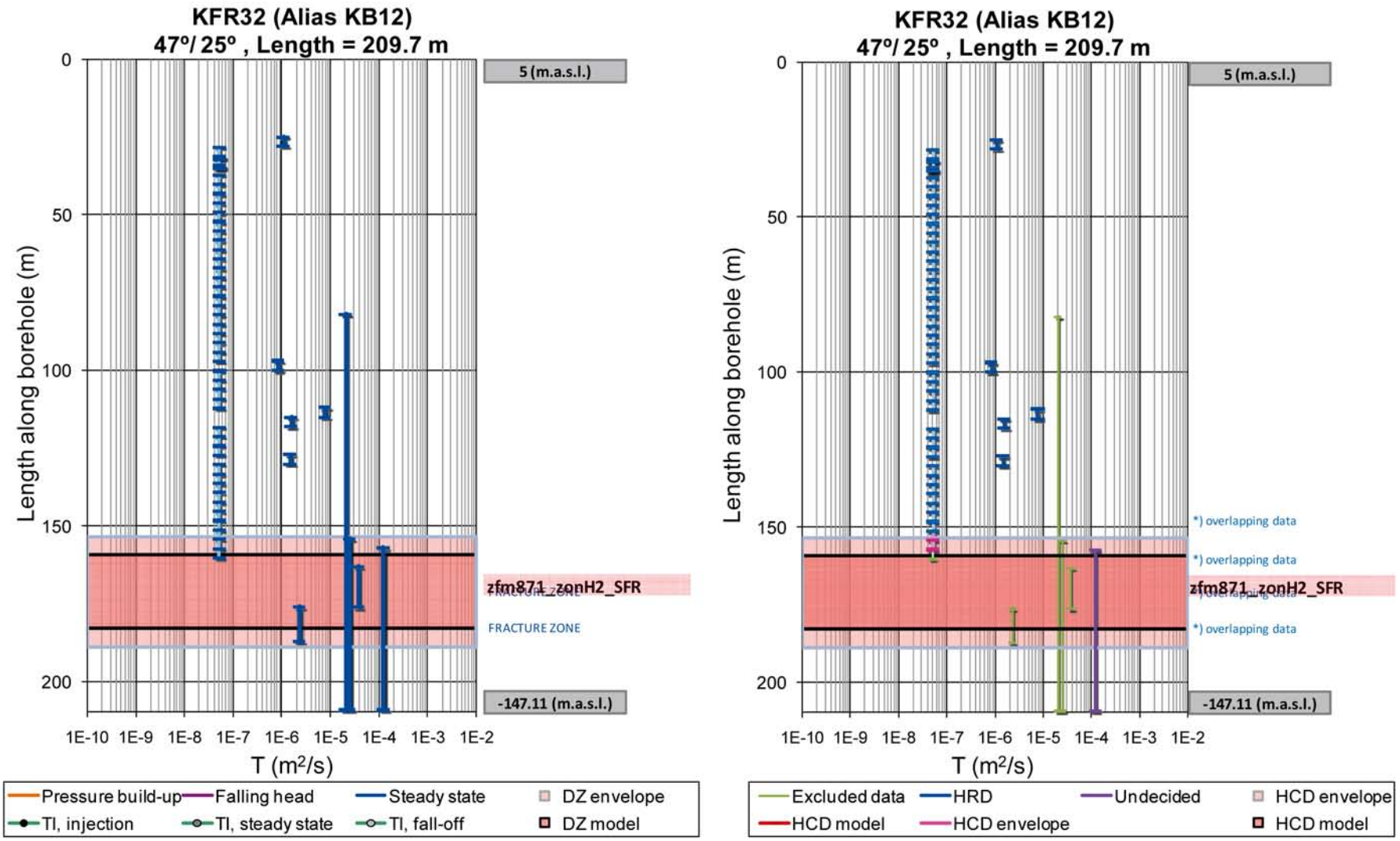

Figure B-27. *KFR32 raw data (left) and interpretation (right).*

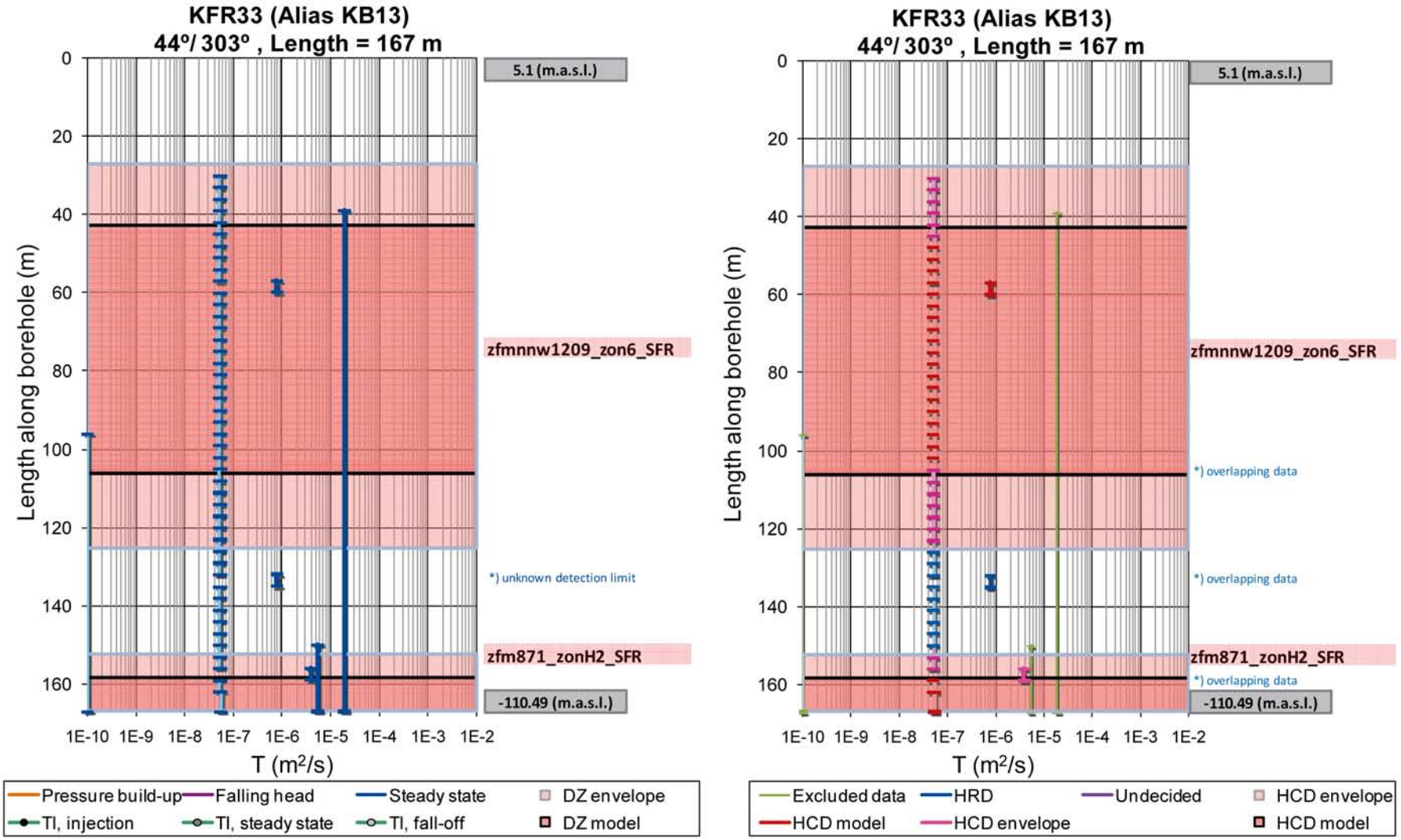

Figure B-28. *KFR33 raw data (left) and interpretation (right).*

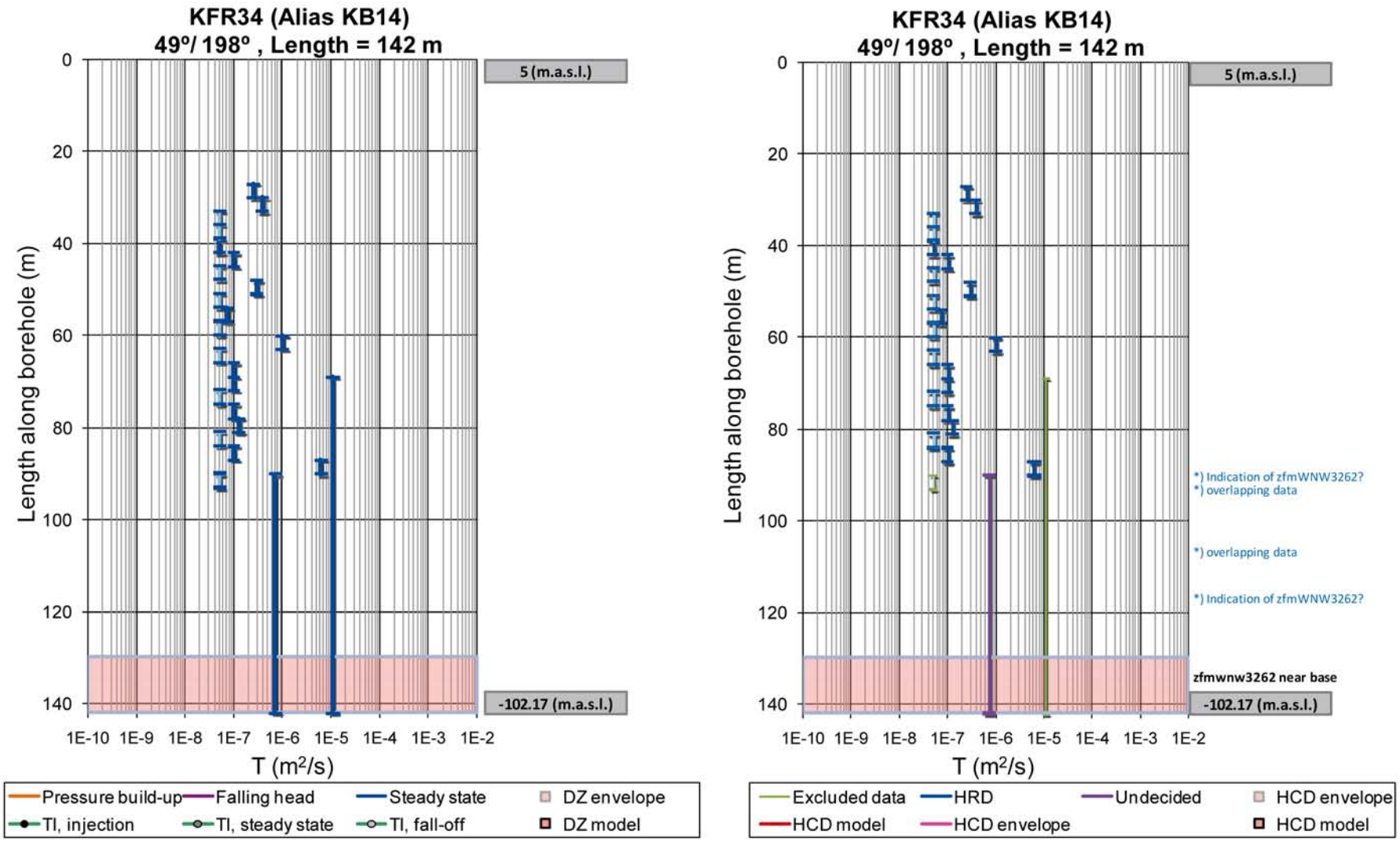

Figure B-29. *KFR34 raw data (left) and interpretation (right).*

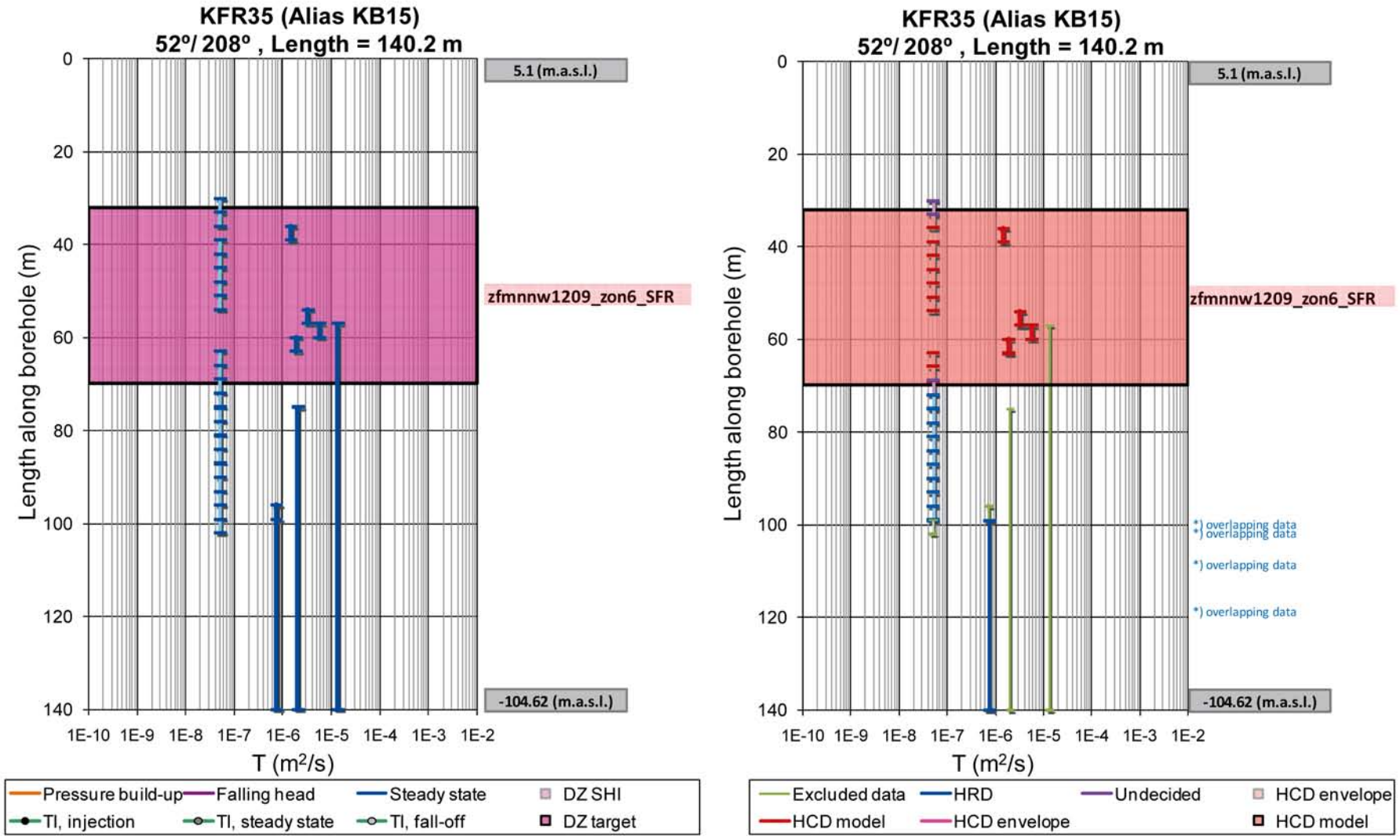

Figure B-30. *KFR35 raw data (left) and interpretation (right).*

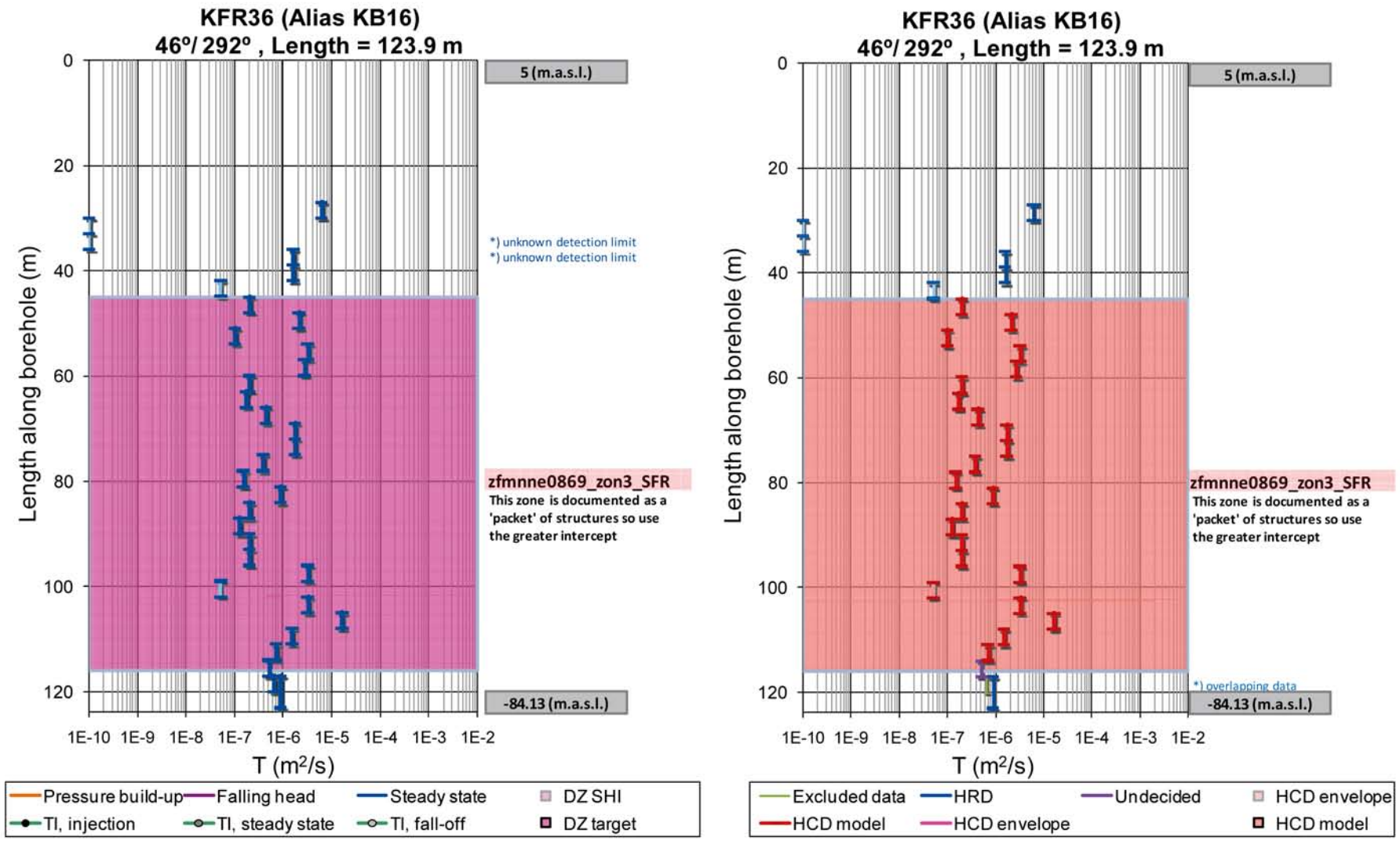

Figure B-31. *KFR36 raw data (left) and interpretation (right).*

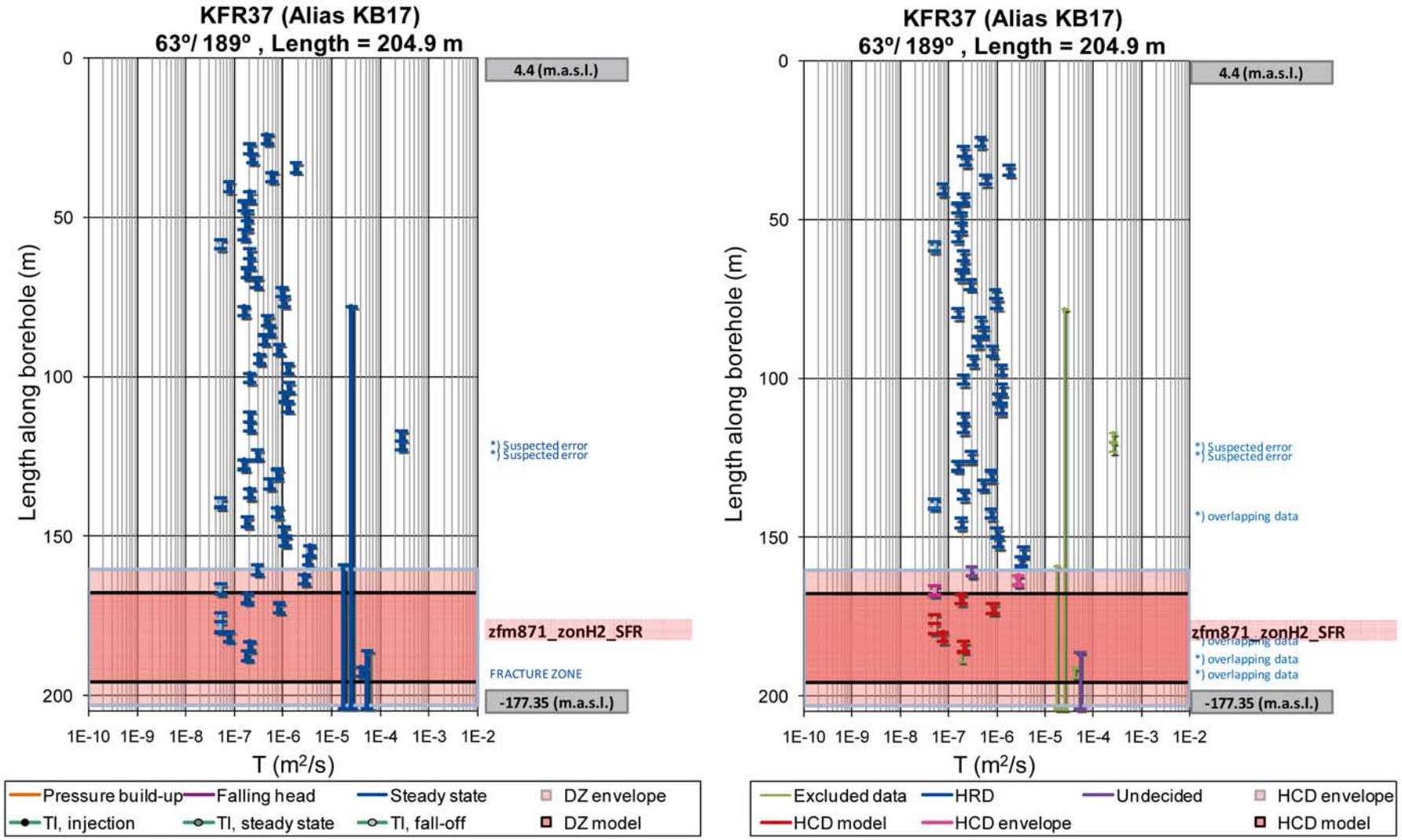

Figure B-32. *KFR37 raw data (left) and interpretation (right).*

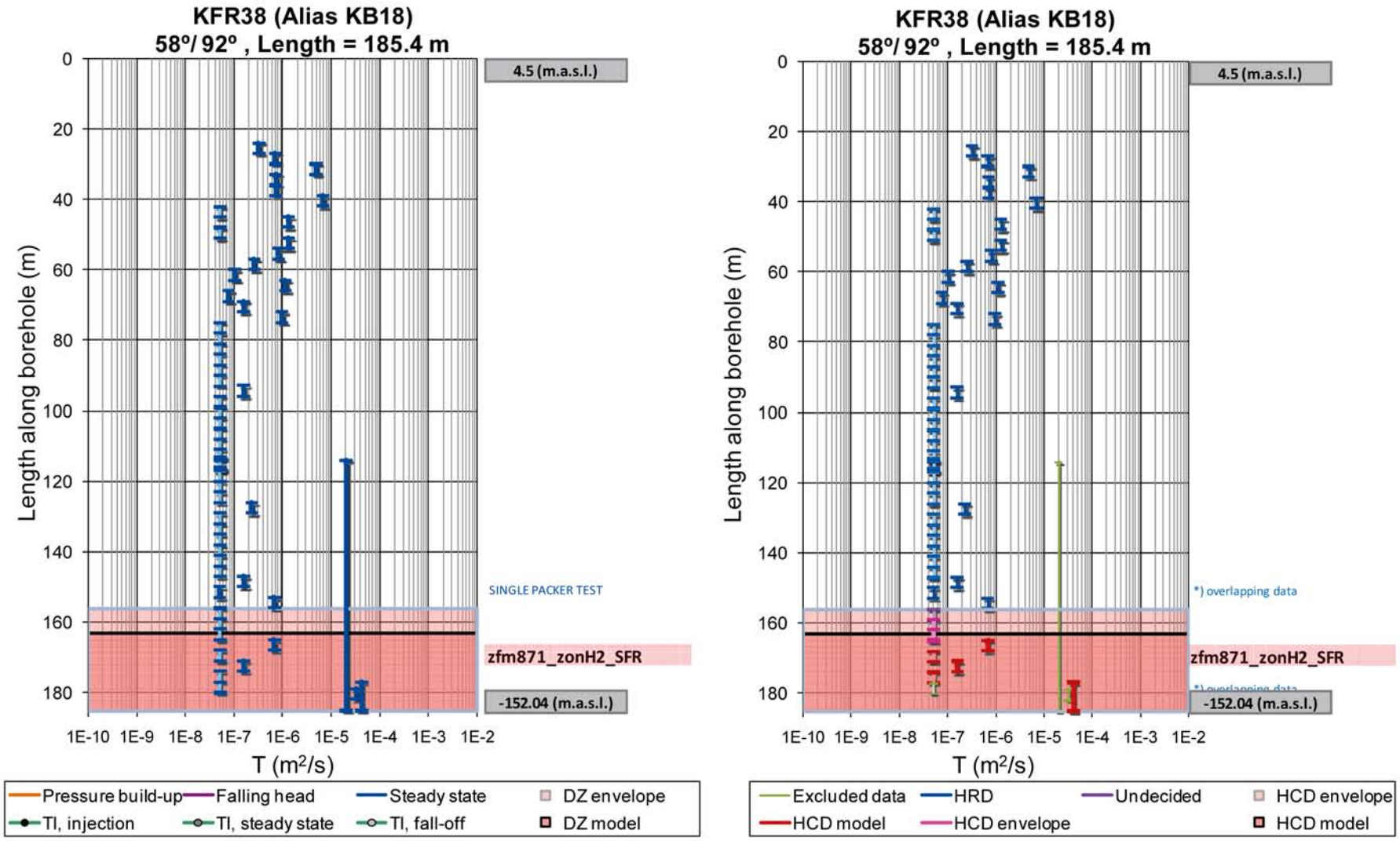

Figure B-33. *KFR38 raw data (left) and interpretation (right).*

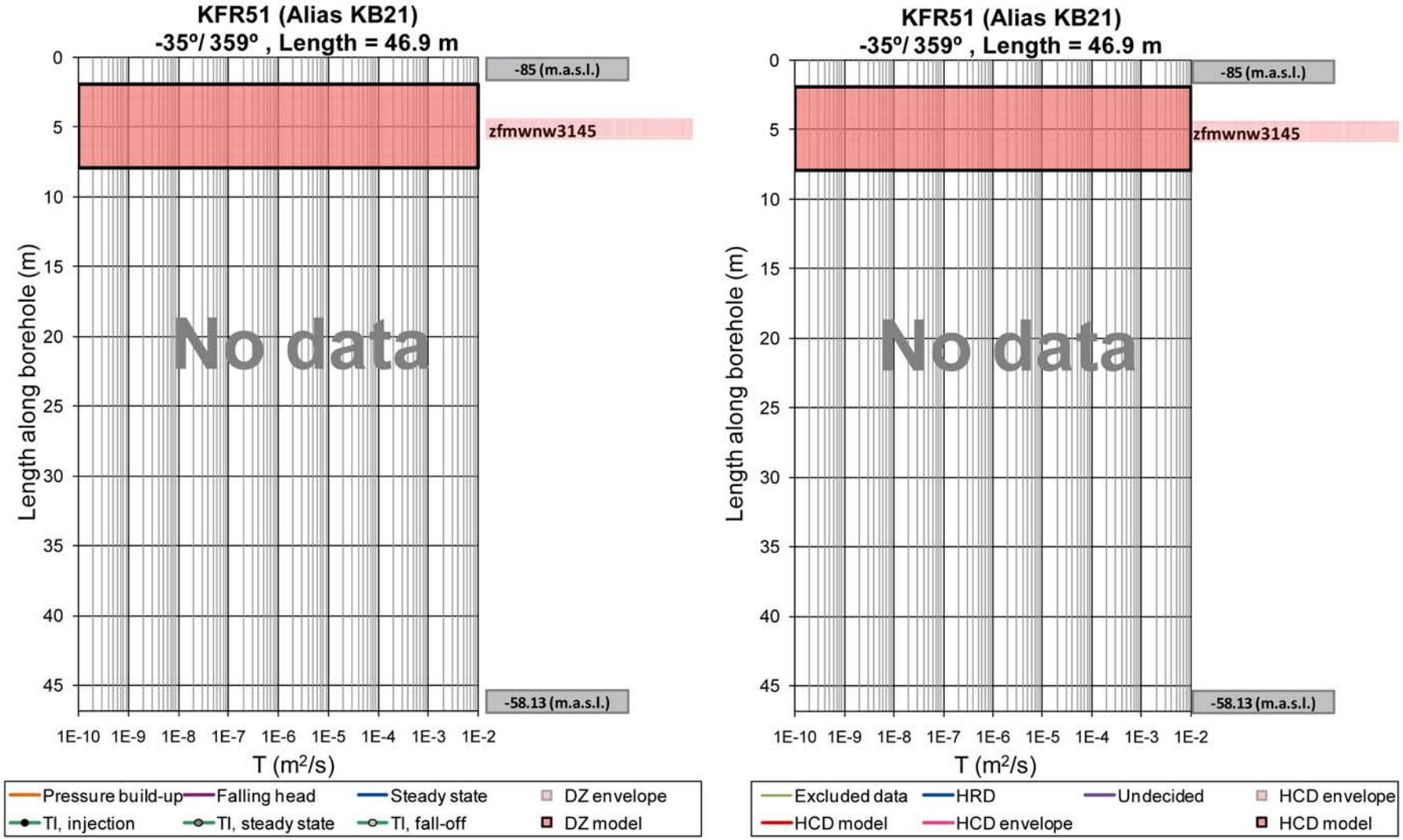

Figure B-34. *No data available in KFR51.*

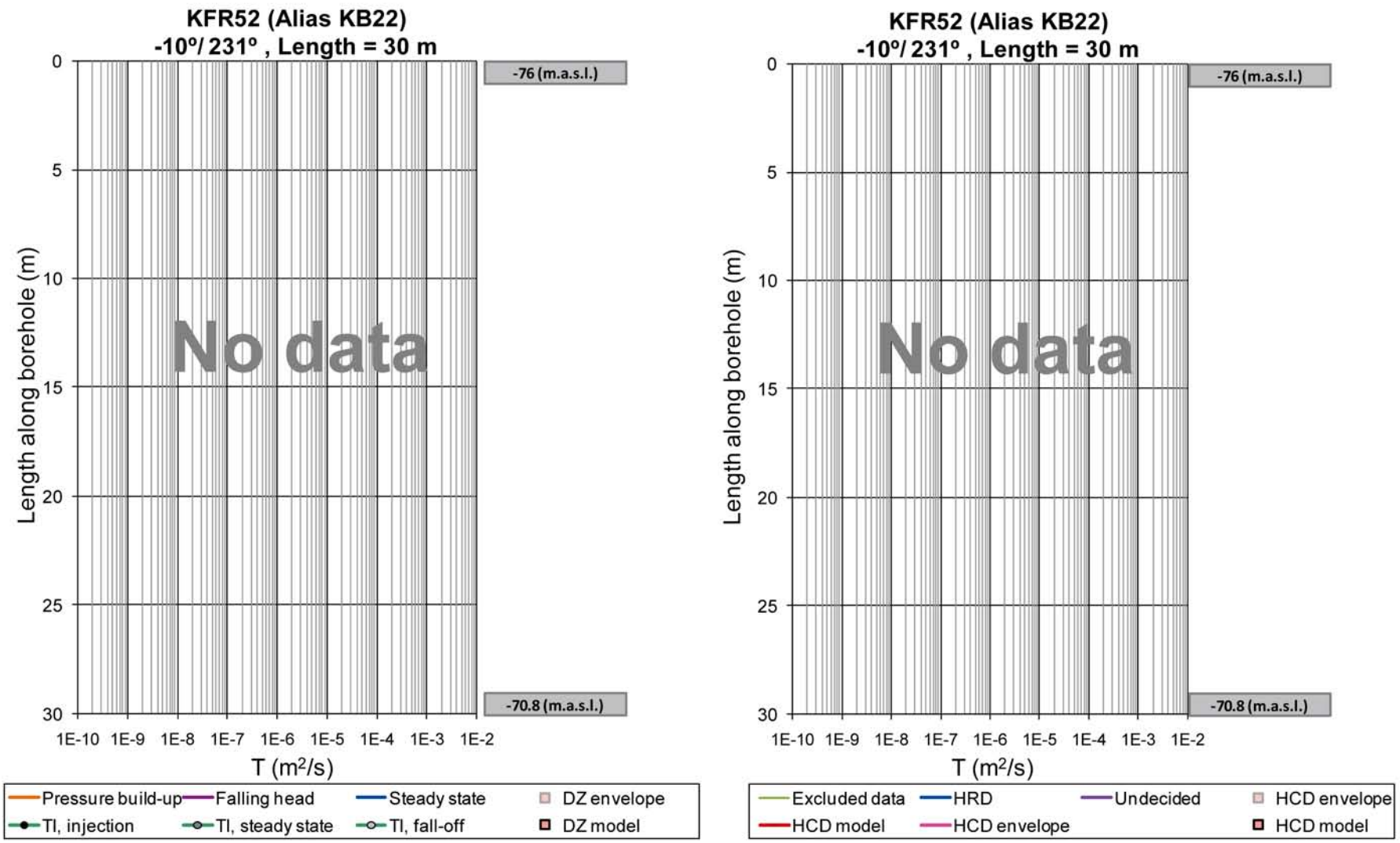

Figure B-35. *No data available in KFR52.*

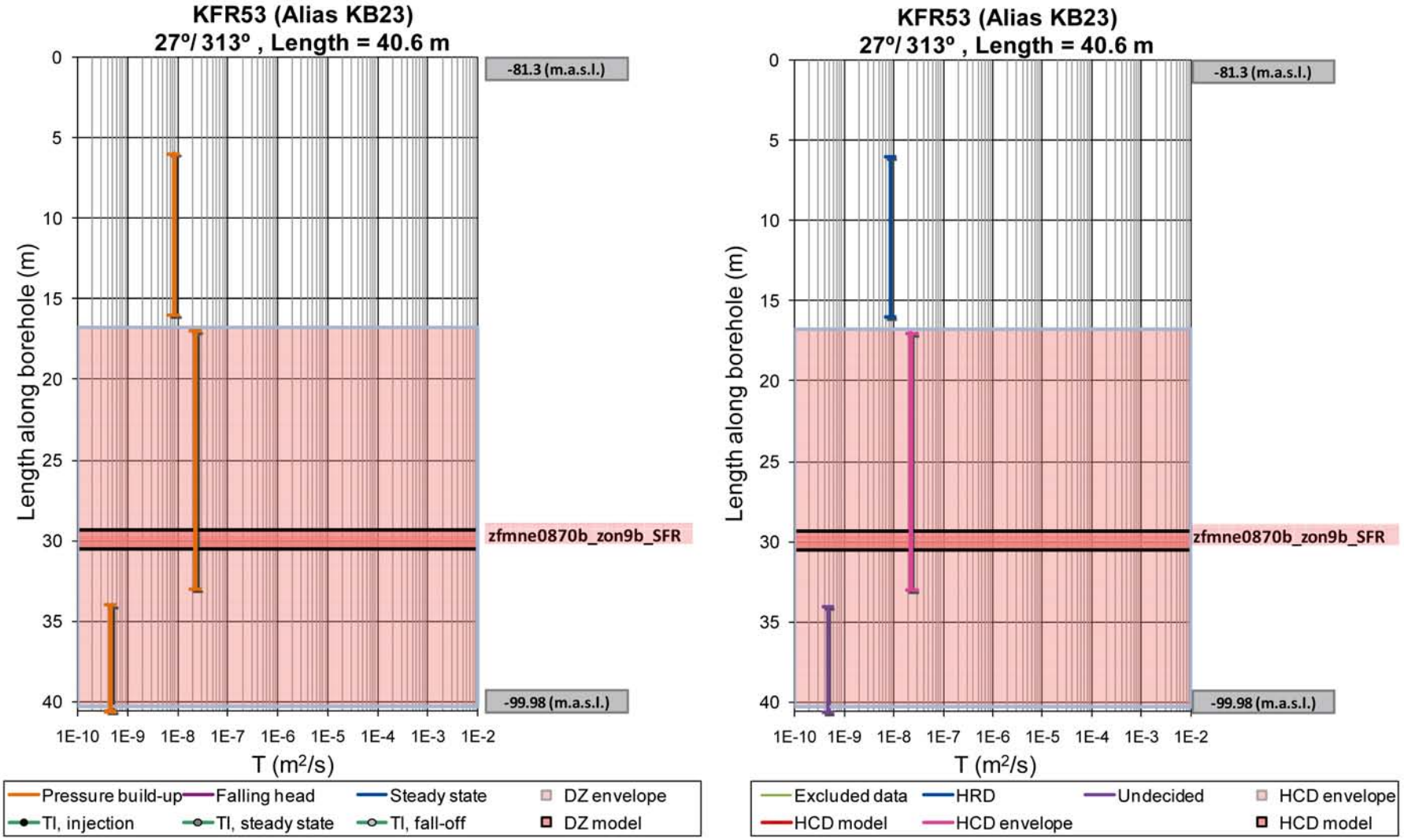

Figure B-36. *KFR53 raw data (left) and interpretation (right).*

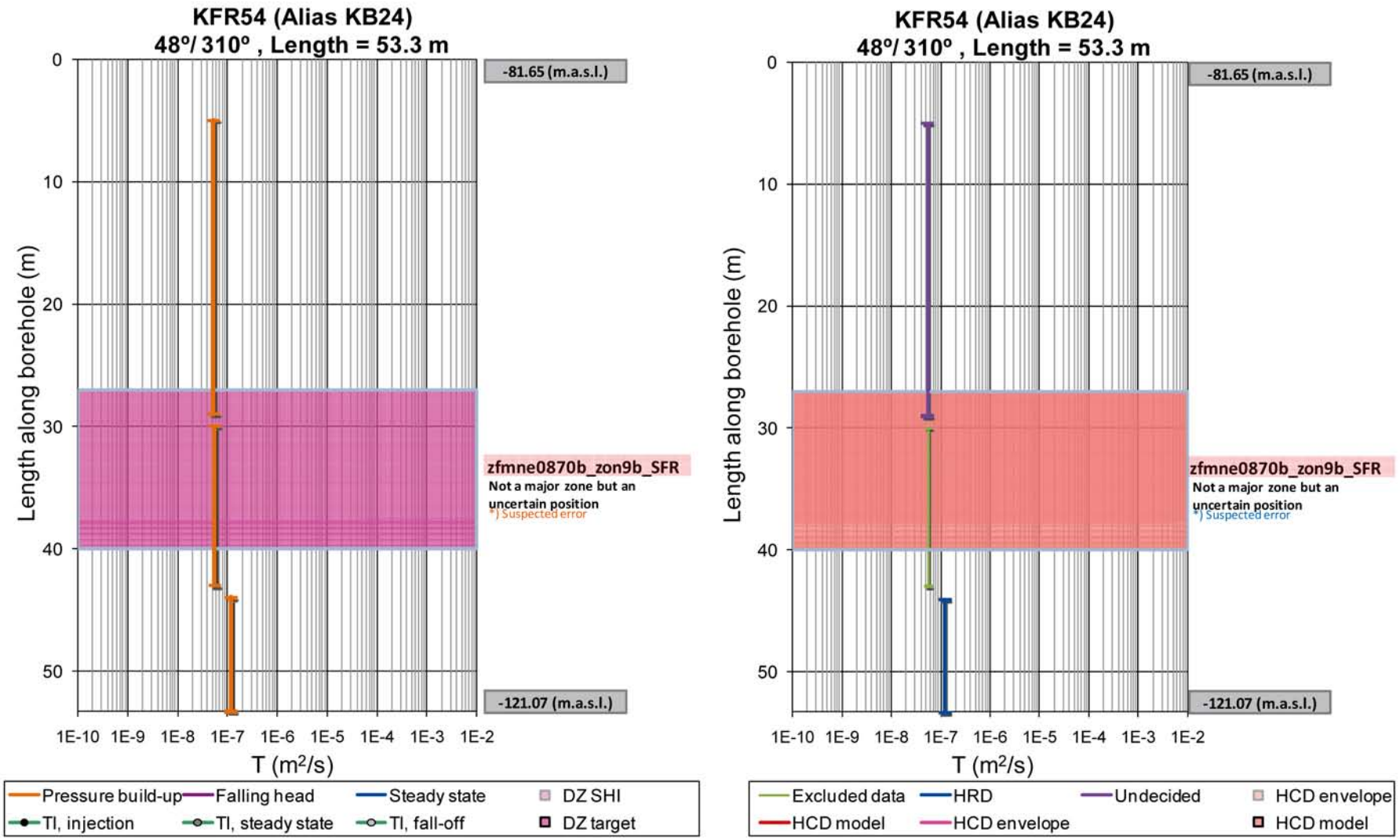

Figure B-37. *KFR54 raw data (left) and interpretation (right).*

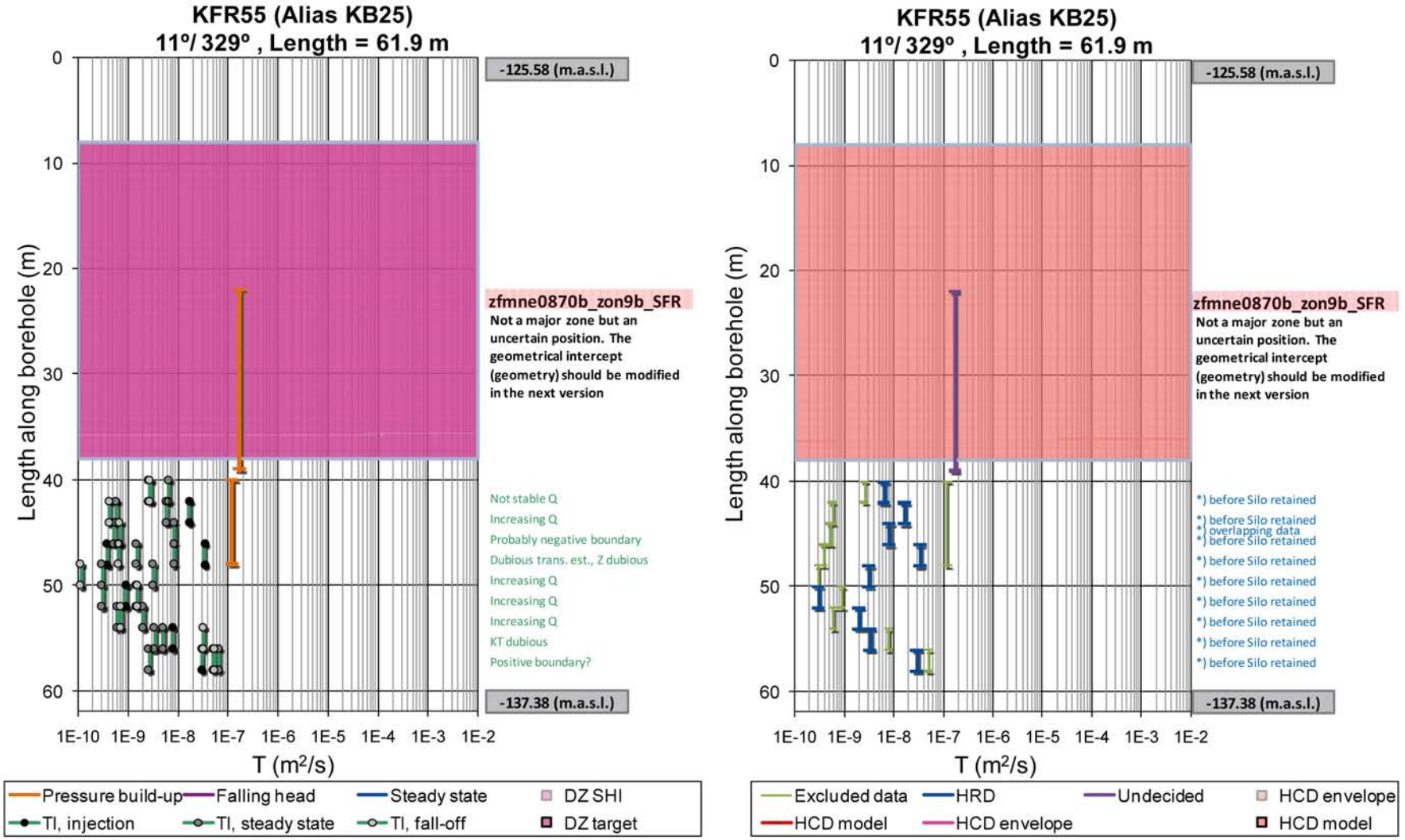

Figure B-38. *KFR55 raw data (left) and interpretation (right). Two interference tests were performed in this borehole (22–39 m) and (40–48 m) to examine zfmne0870. Data measured after construction of the Silo are excluded.*

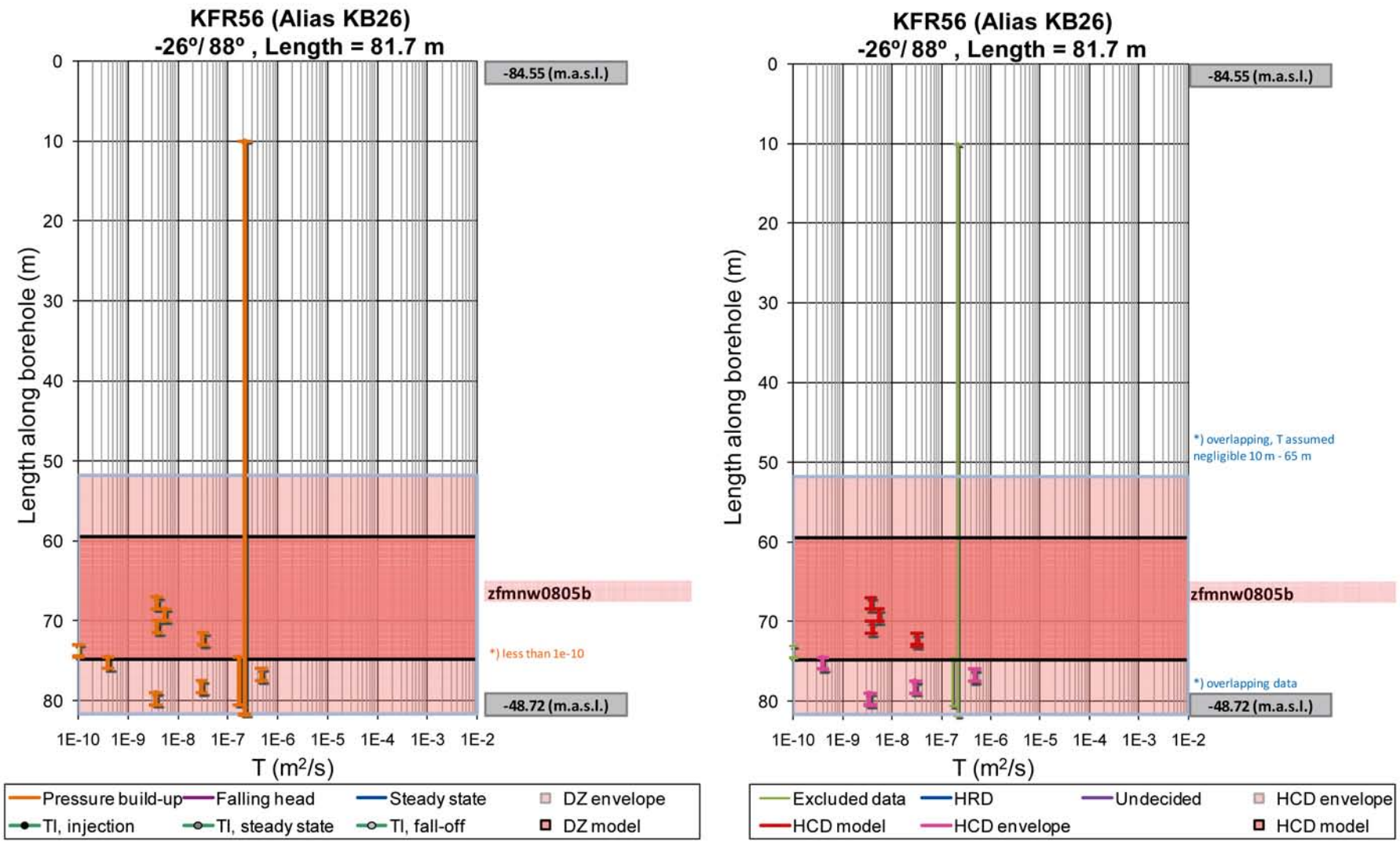

Figure B-39. *KFR56 raw data (left) and interpretation (right).*

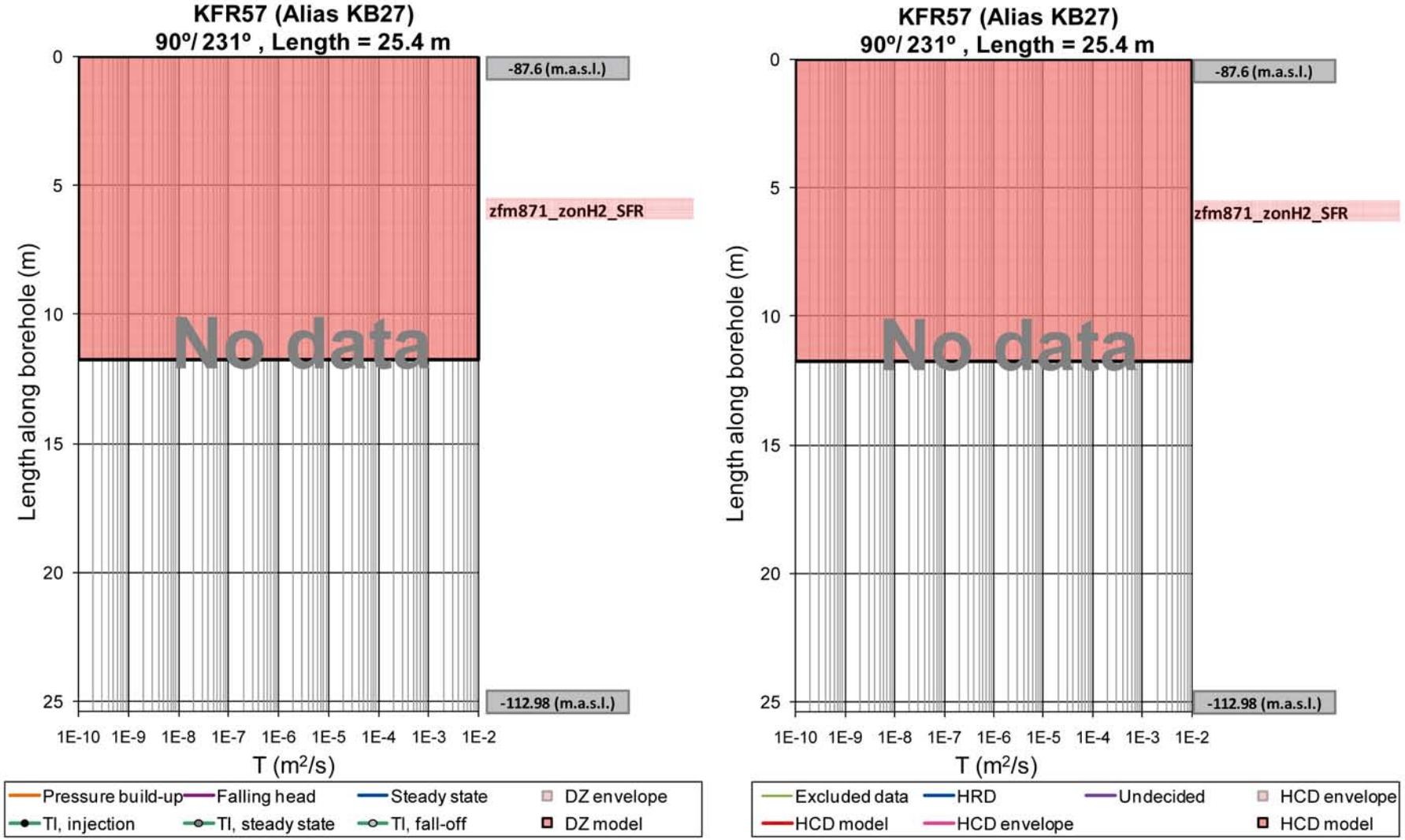

Figure B-40. *No hydraulic data available for KFR57.*

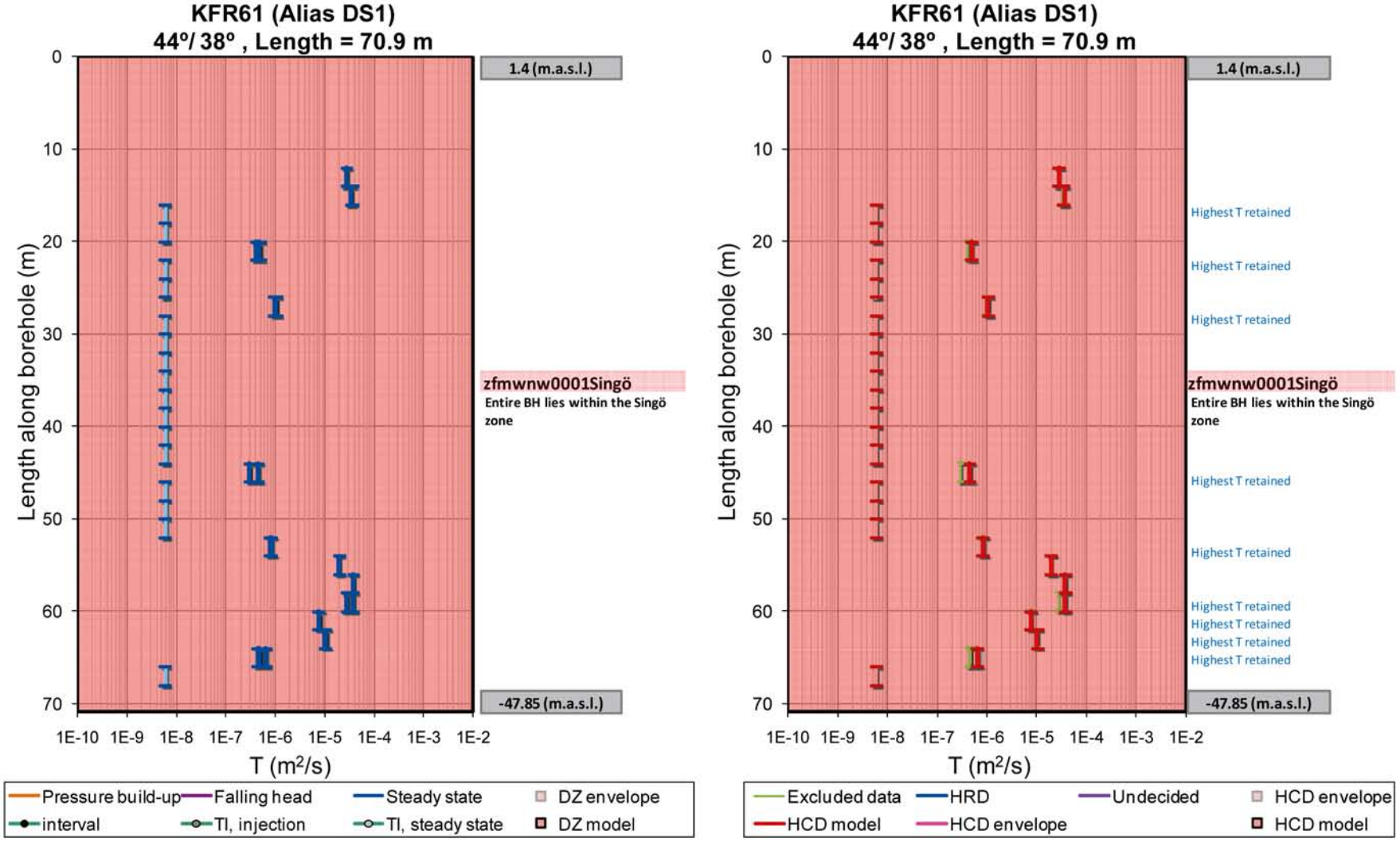

Figure B-41. *KFR61 raw data (left) and interpretation (right).*

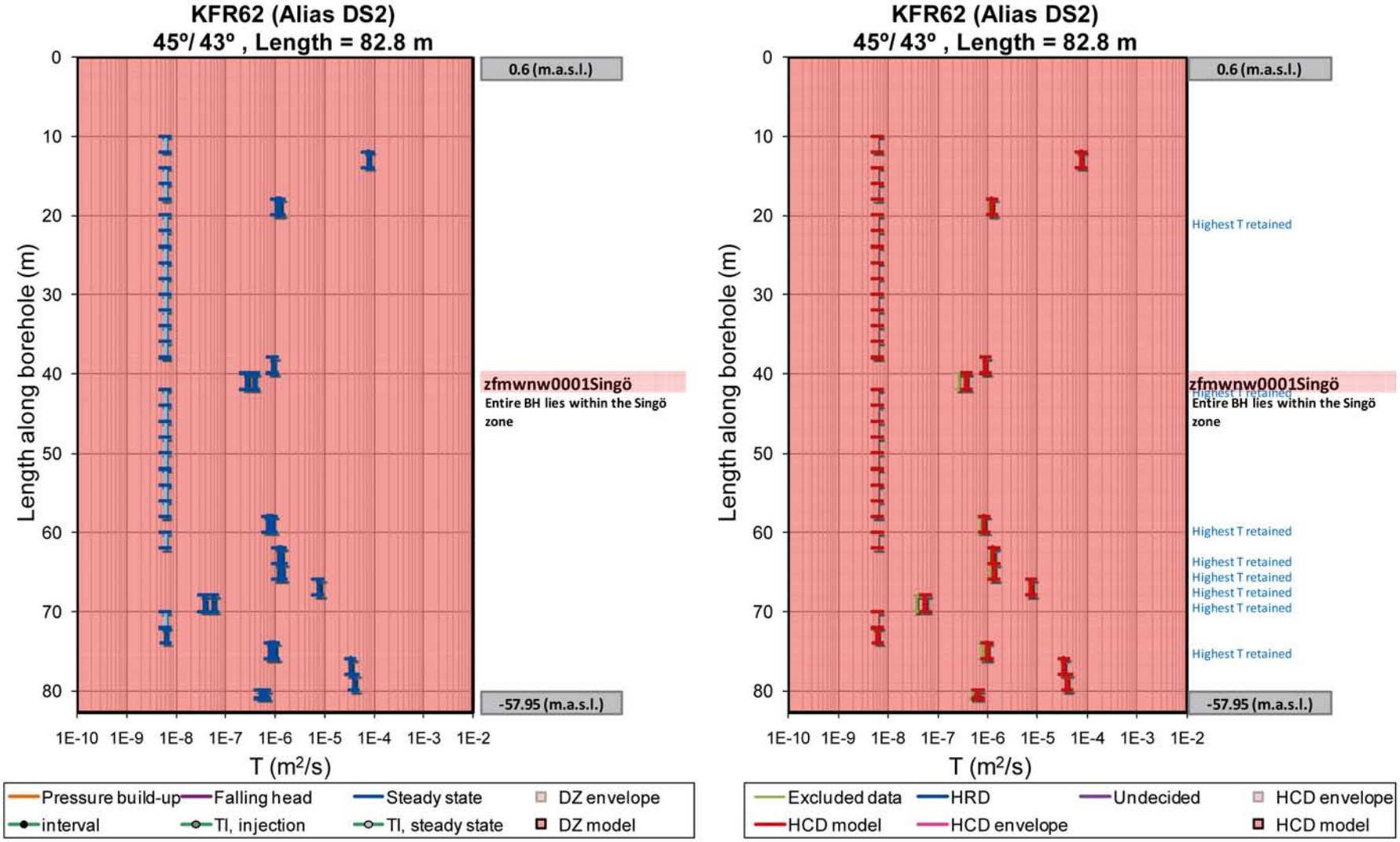

Figure B-42. *KFR62 raw data (left) and interpretation (right).*

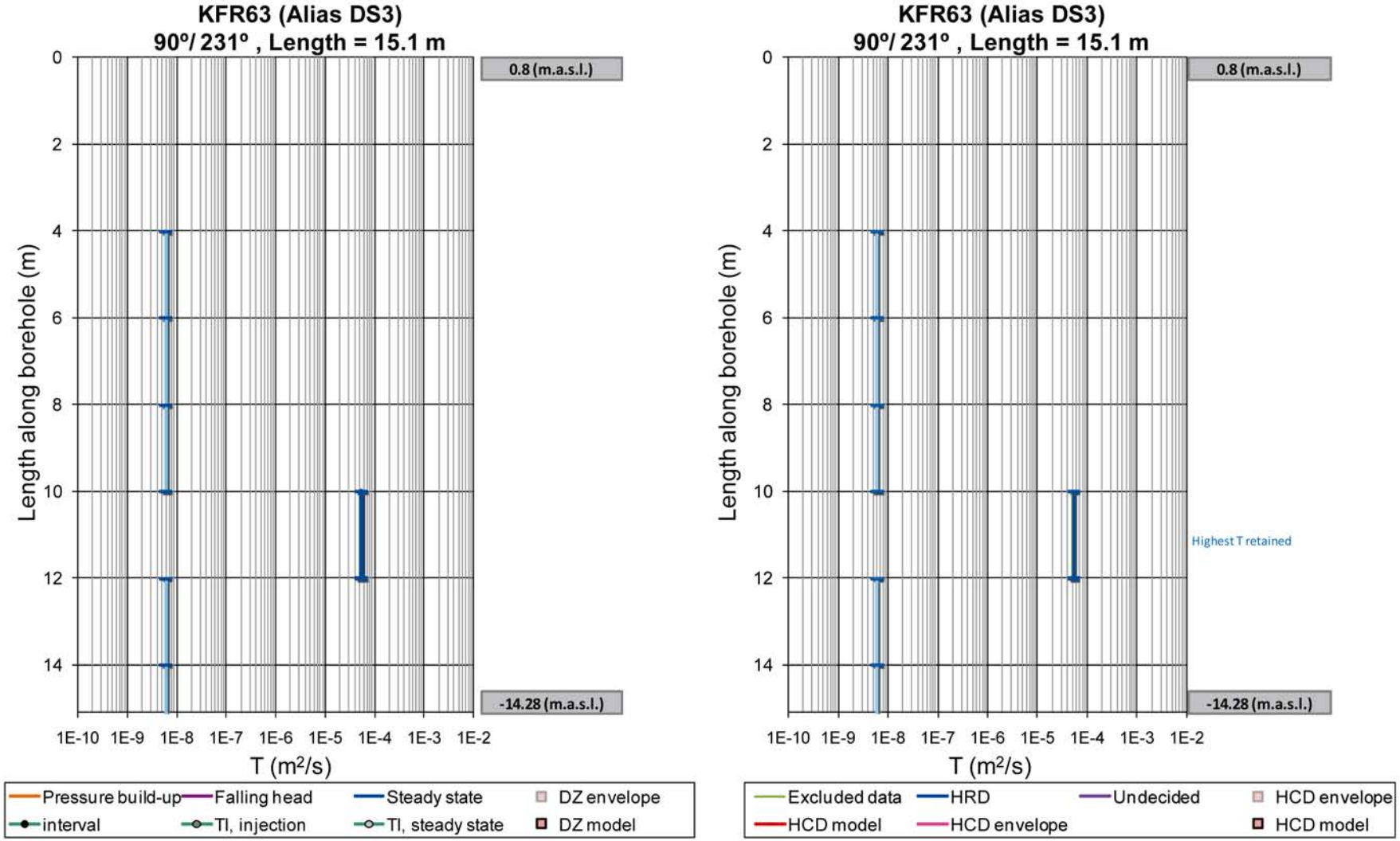

Figure B-43. *KFR63 raw data (left) and interpretation (right).*

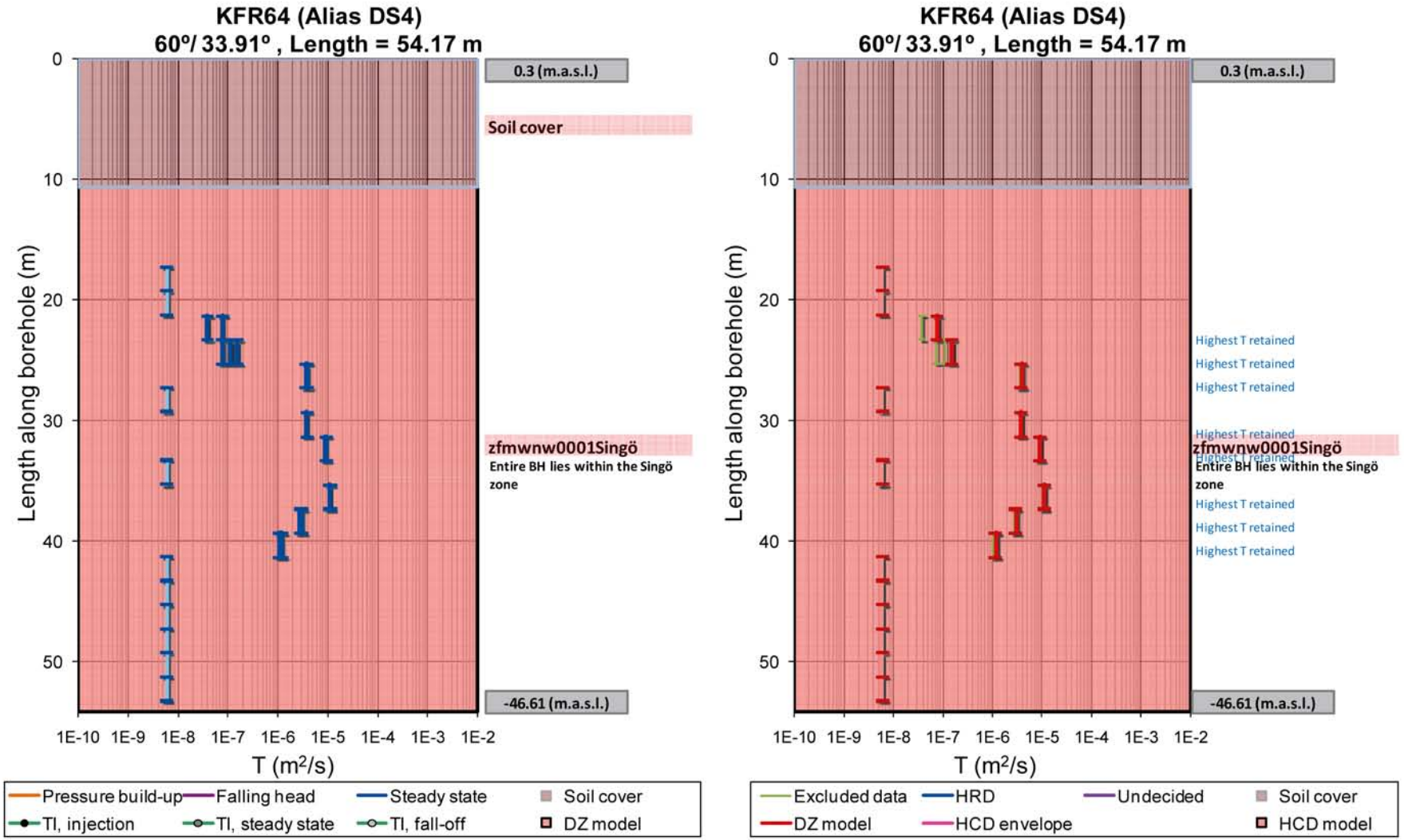

Figure B-44. *KFR64 raw data (left) and interpretation (right).*

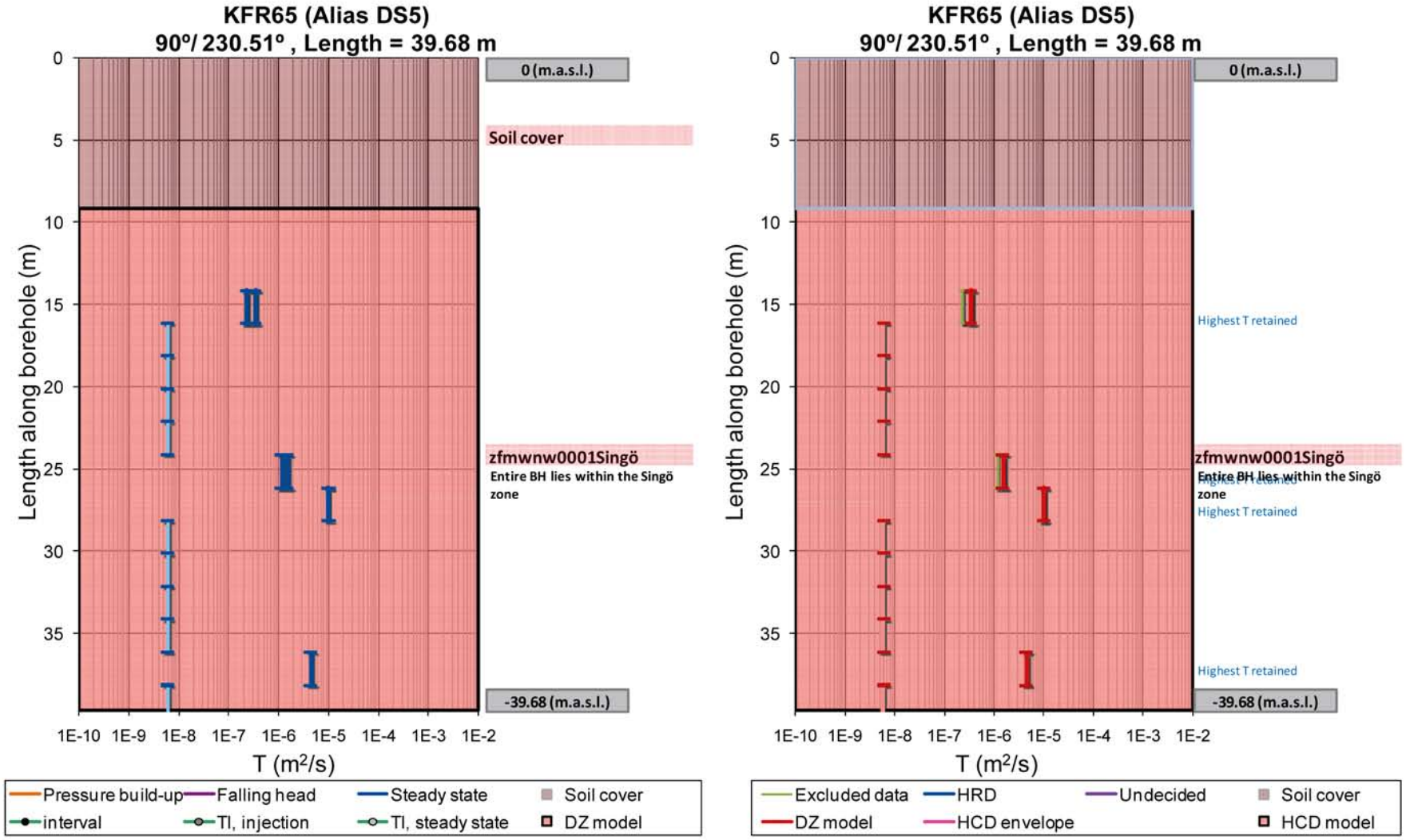

Figure B-45. *KFR65 raw data (left) and interpretation (right).*

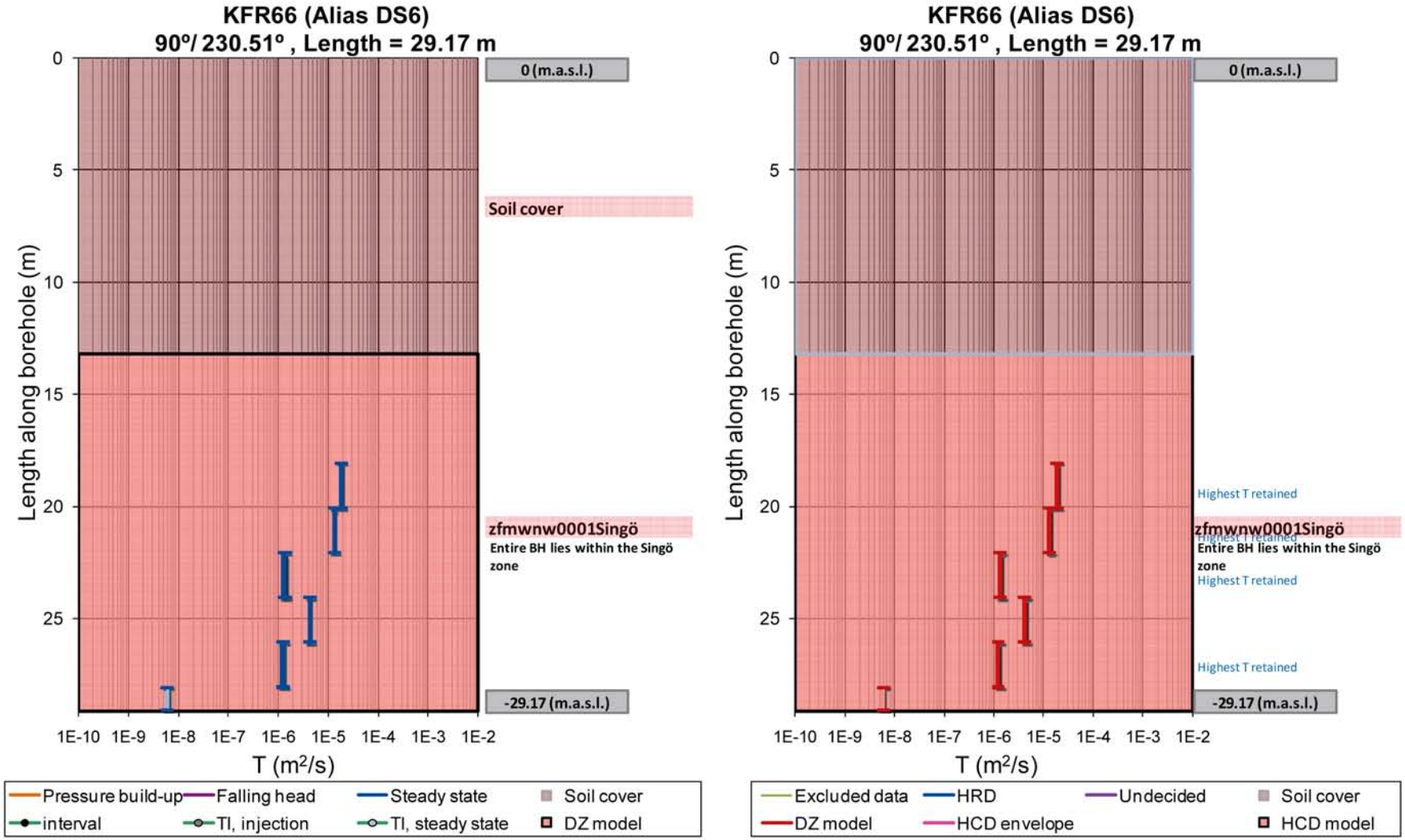

Figure B-46. *KFR66 raw data (left) and interpretation (right).*

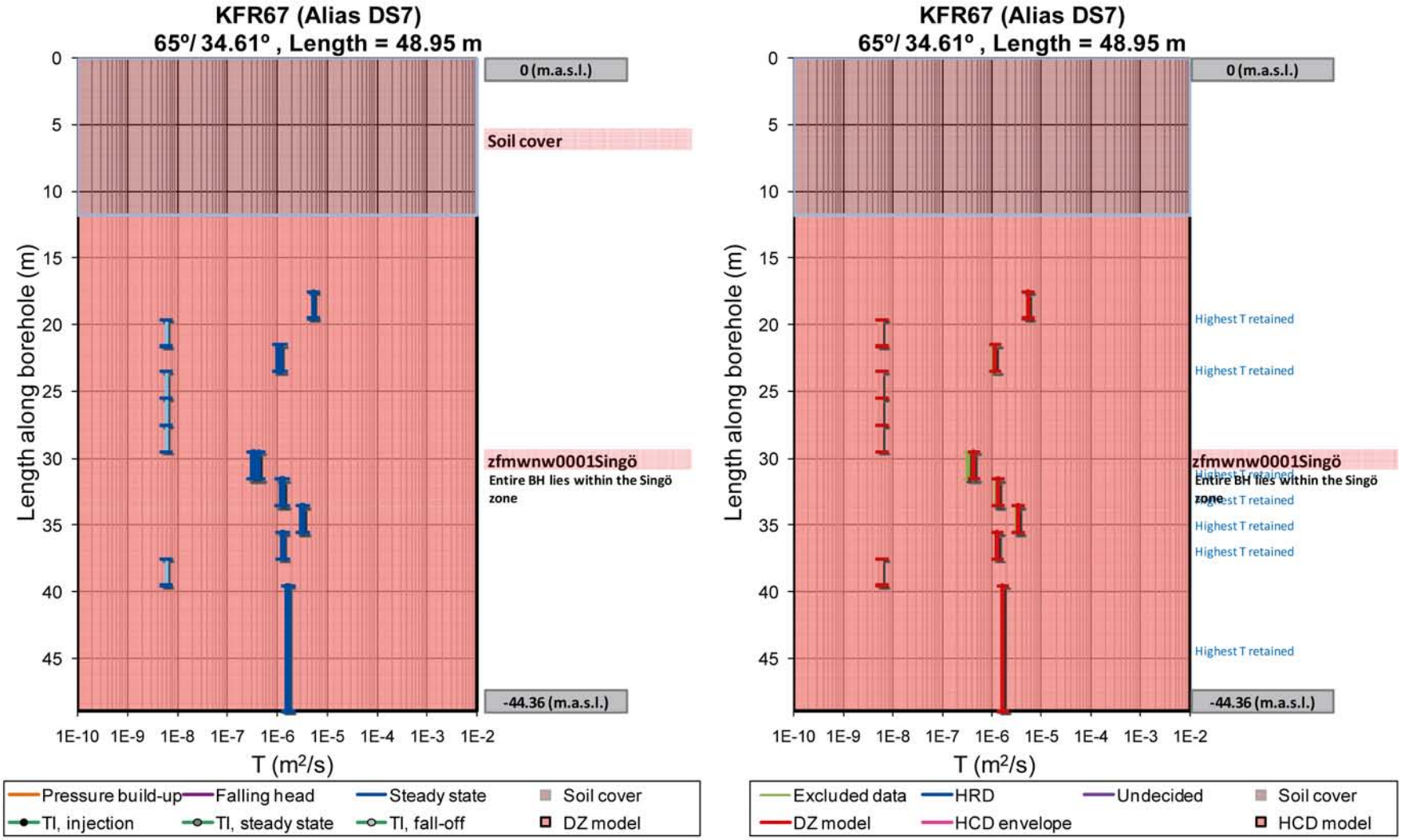

Figure B-47. *KFR67 raw data (left) and interpretation (right).*

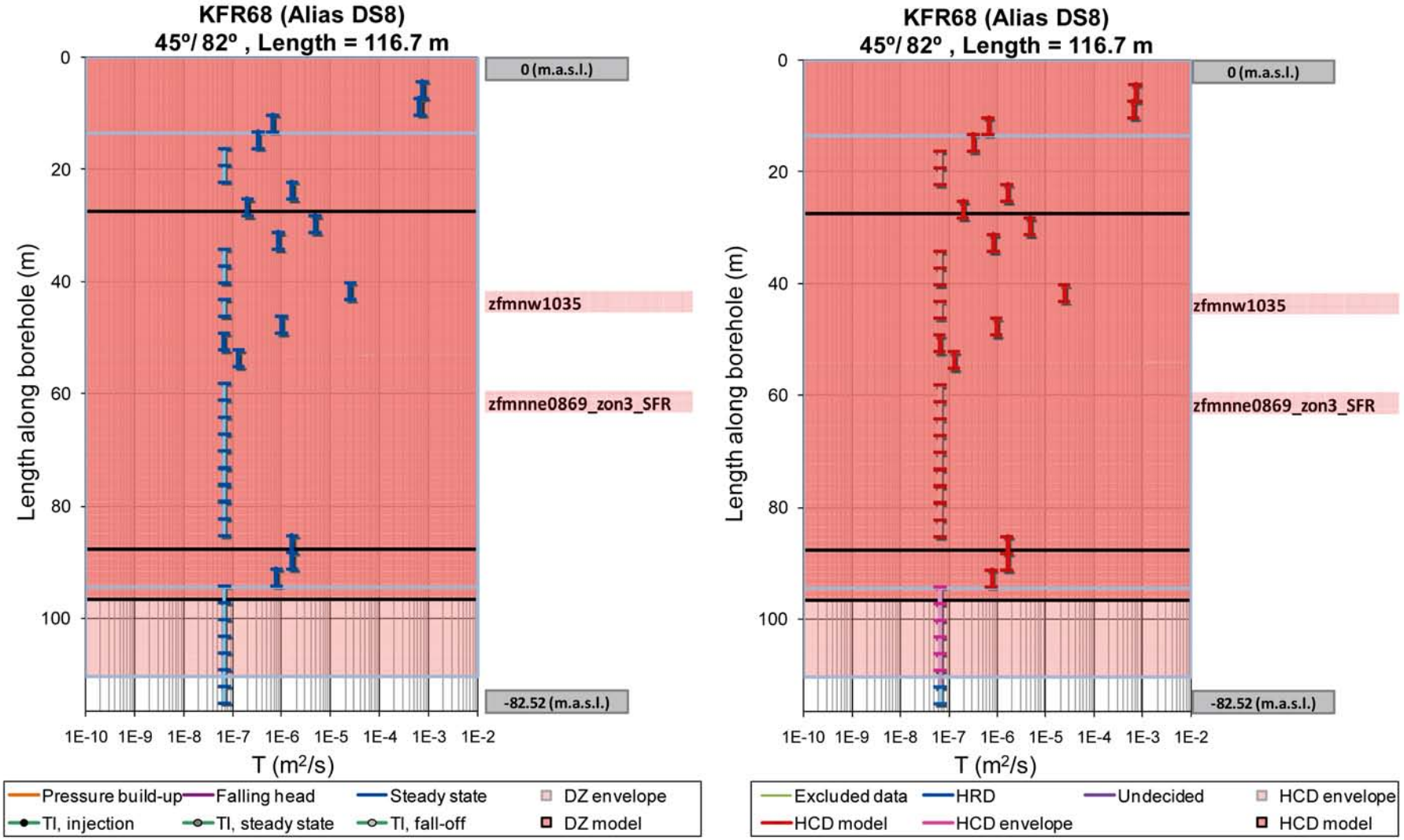

Figure B-48. *KFR68 raw data (left) and interpretation (right).*

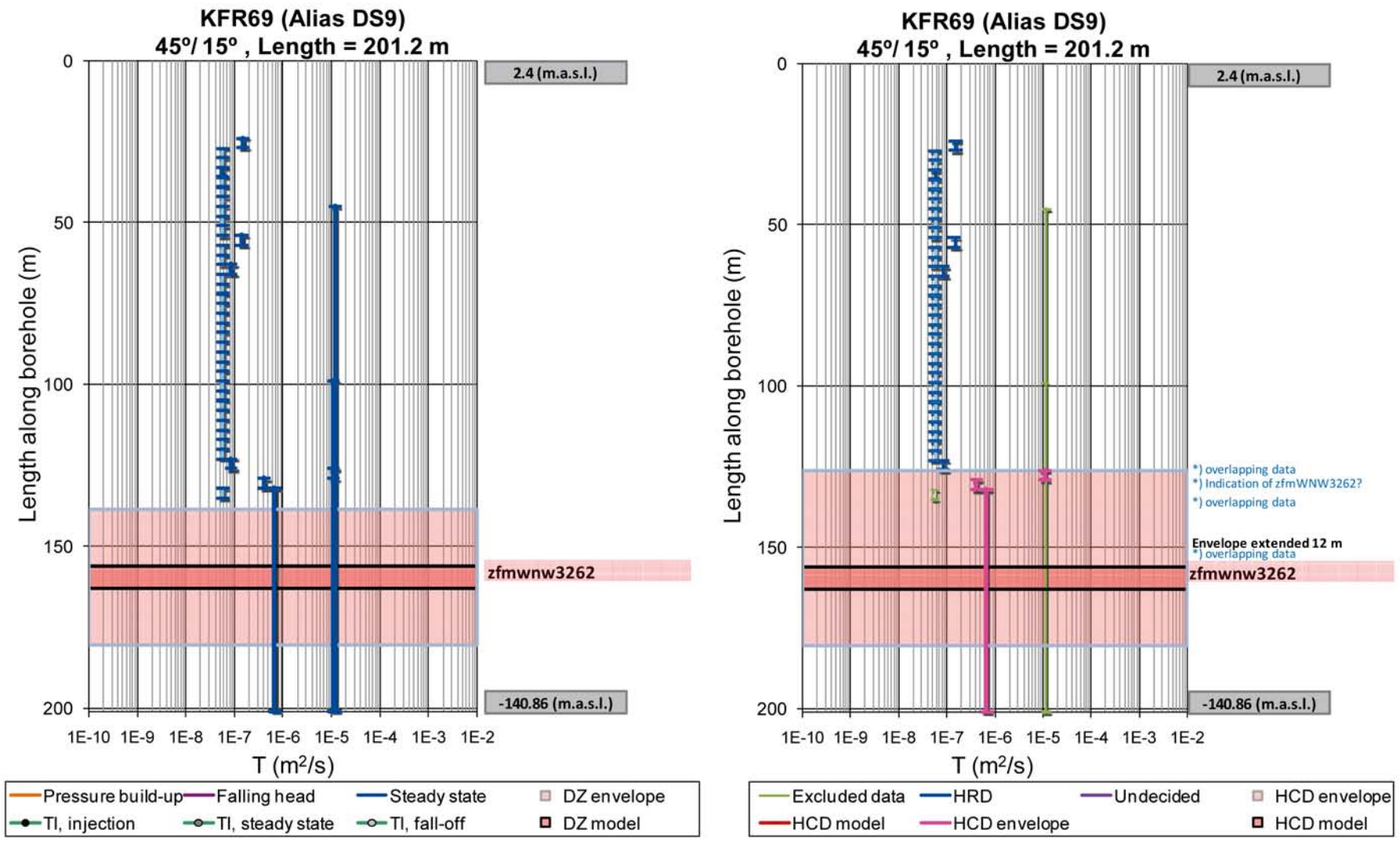

Figure B-49. *KFR69 raw data (left) and interpretation (right).*

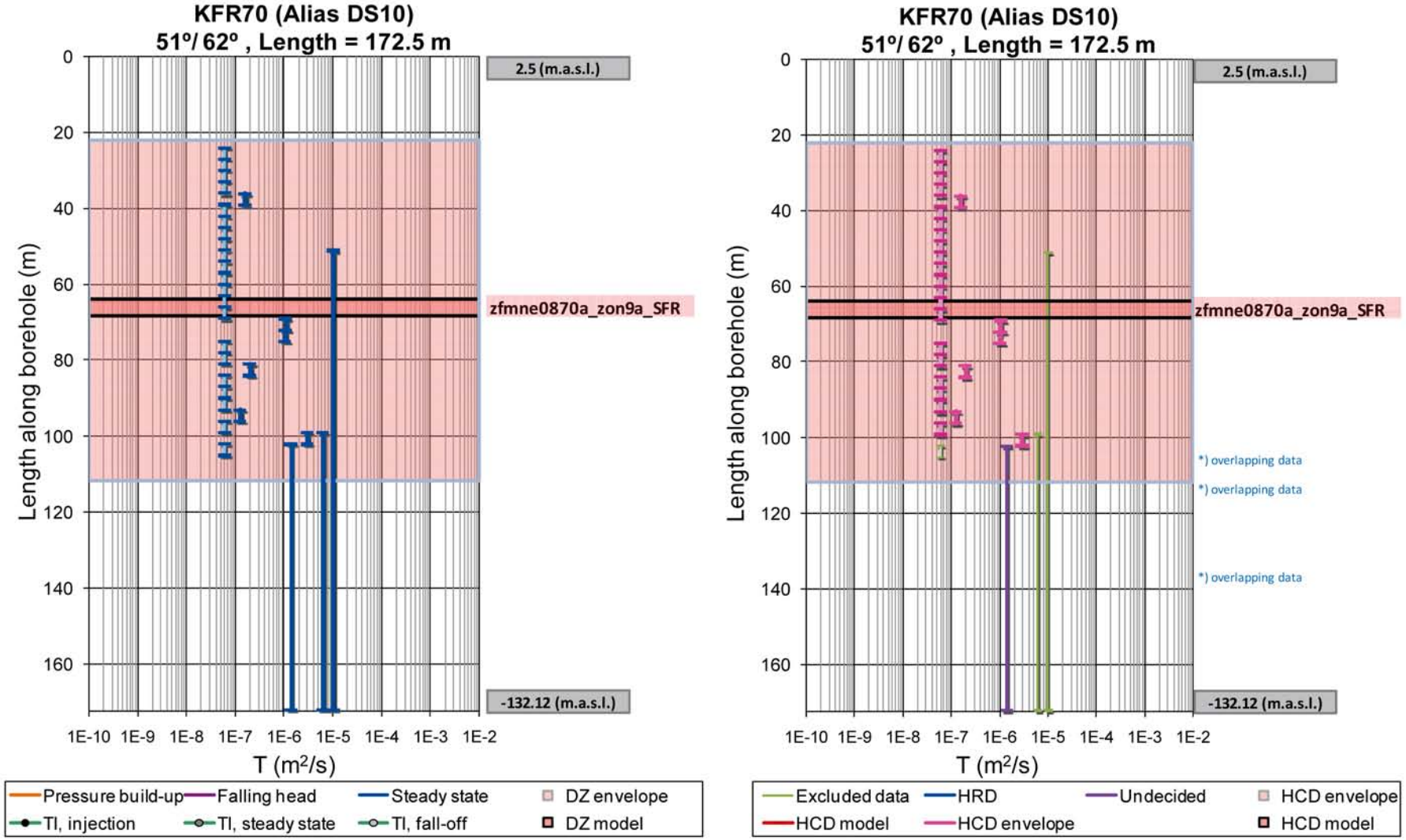

Figure B-50. *KFR70 raw data (left) and interpretation (right).*

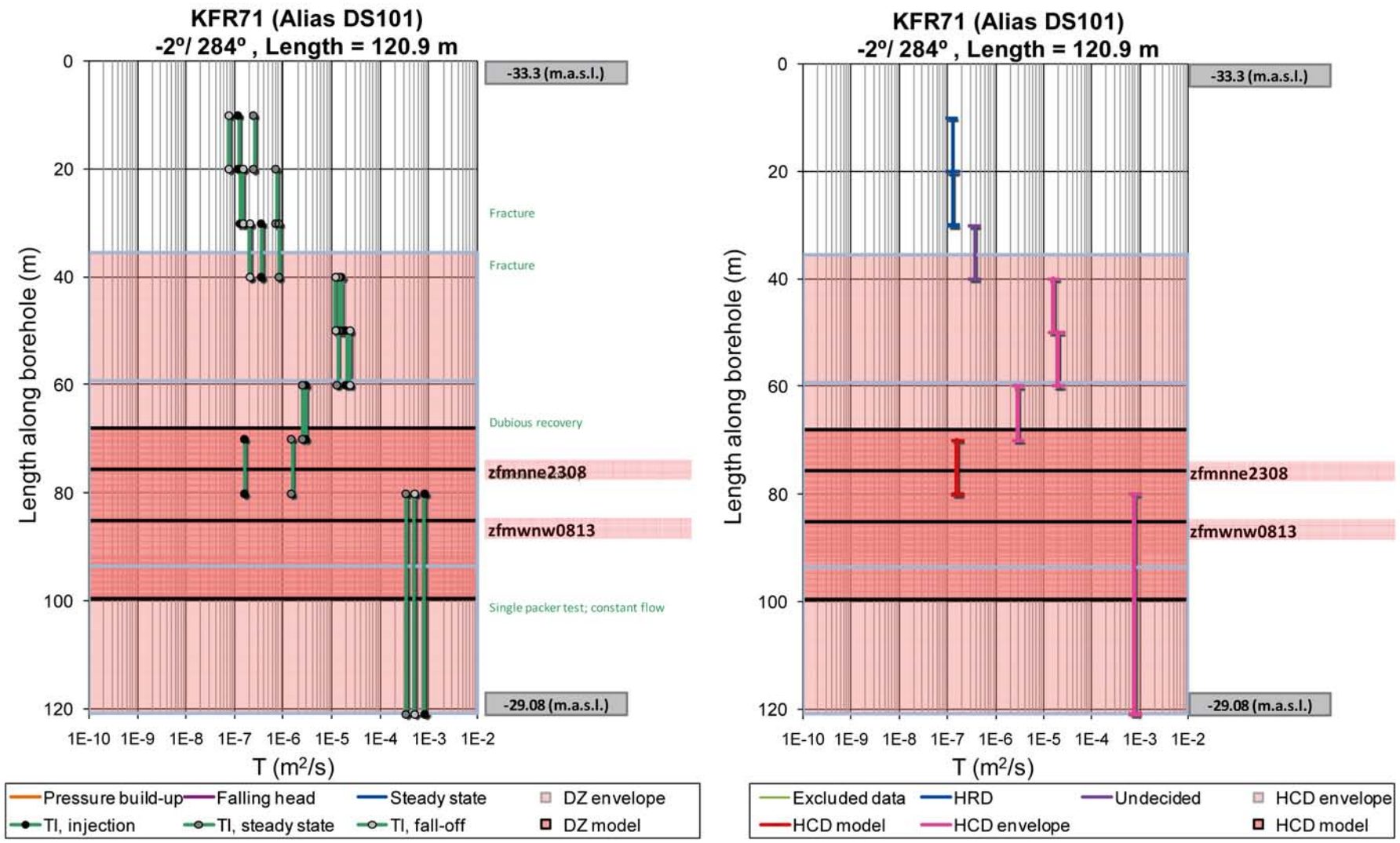

Figure B-51. *KFR71 raw data (left) and interpretation (right).*

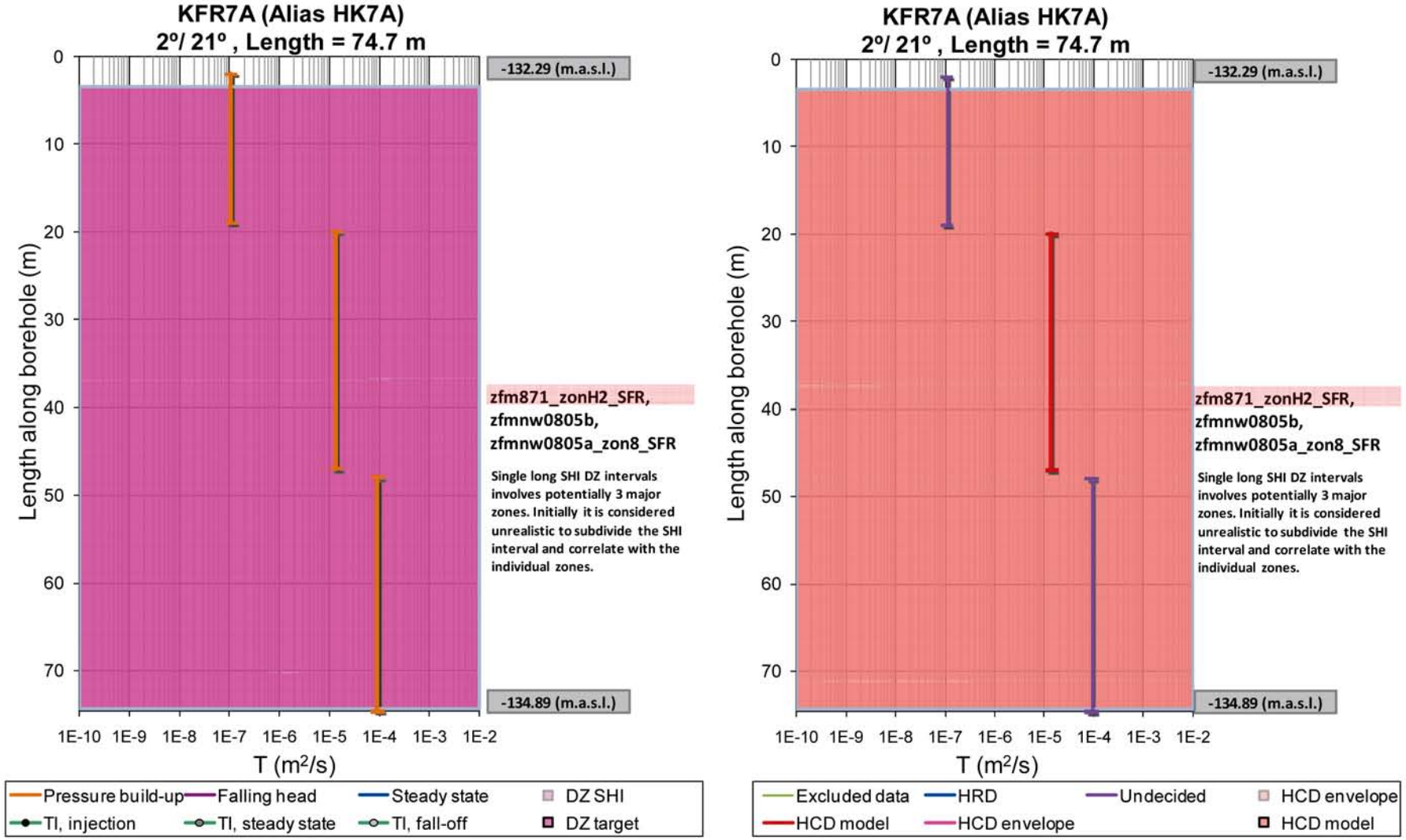

Figure B-52. *KFR7A raw data (left) and interpretation (right).*

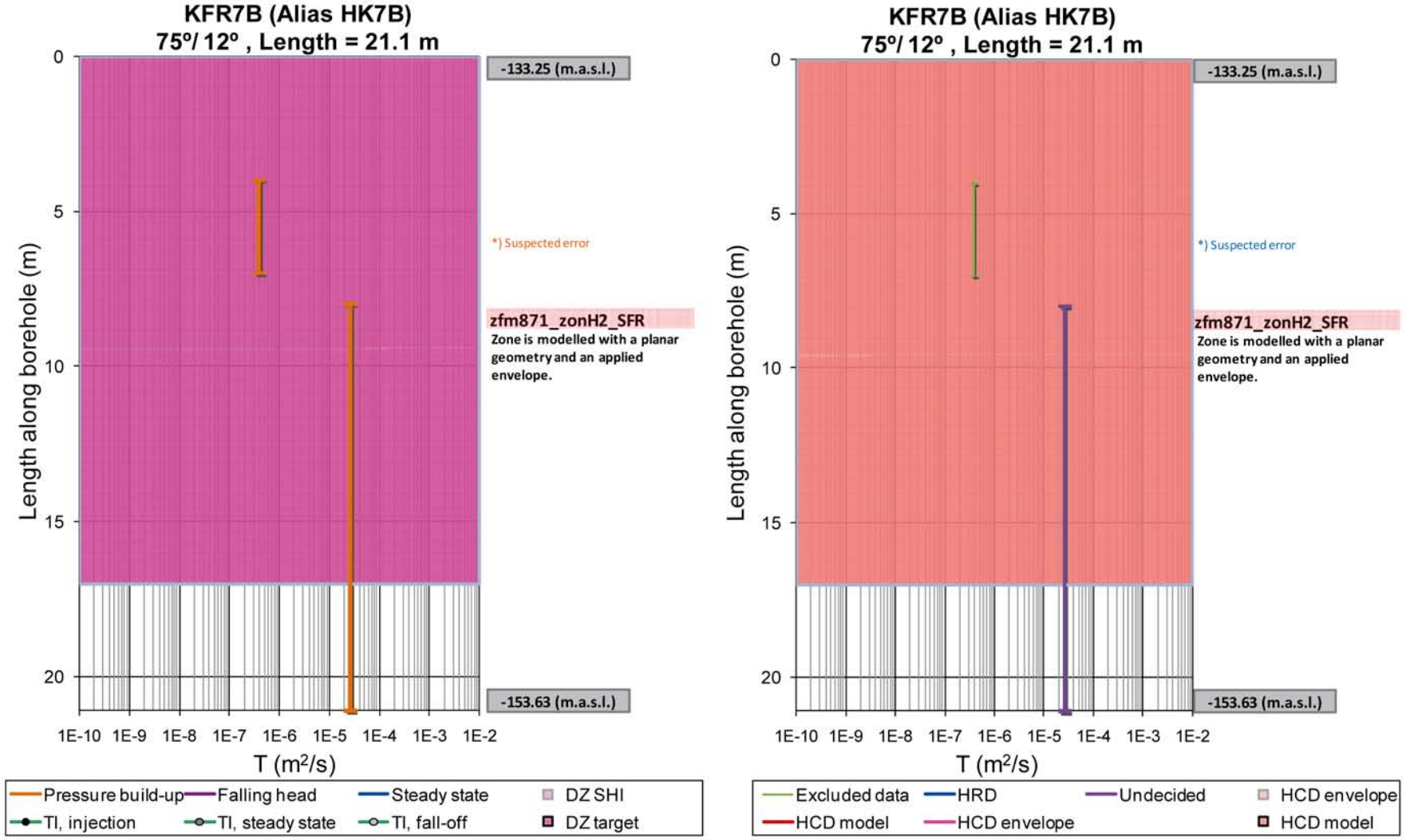

Figure B-53. *KFR7B raw data (left) and interpretation (right) . This borehole was chosen for an interference test (8–21.1 m) in ZFM871 (1985-12-26); due to instrumental failure, the test was later repeated with an expanded set of monitoring sections (1986-03-27; see Section 2.1.2).*

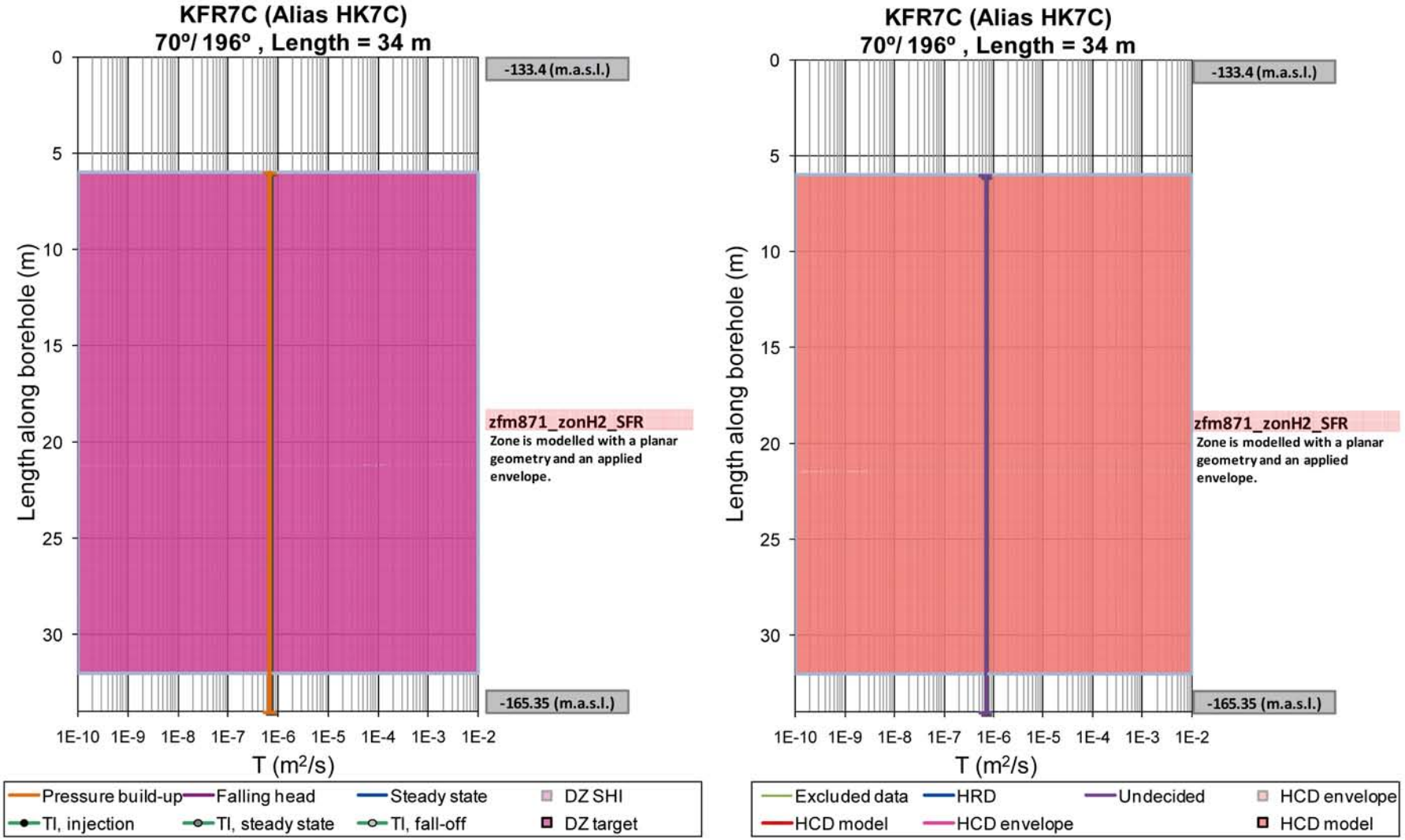

Figure B-54. *KFR7C raw data (left) and interpretation (right). A leaking packer in this borehole was interpreted as an unintentional interference test /Axelsson and Hansen 1997/ (Section 2.1.2).*

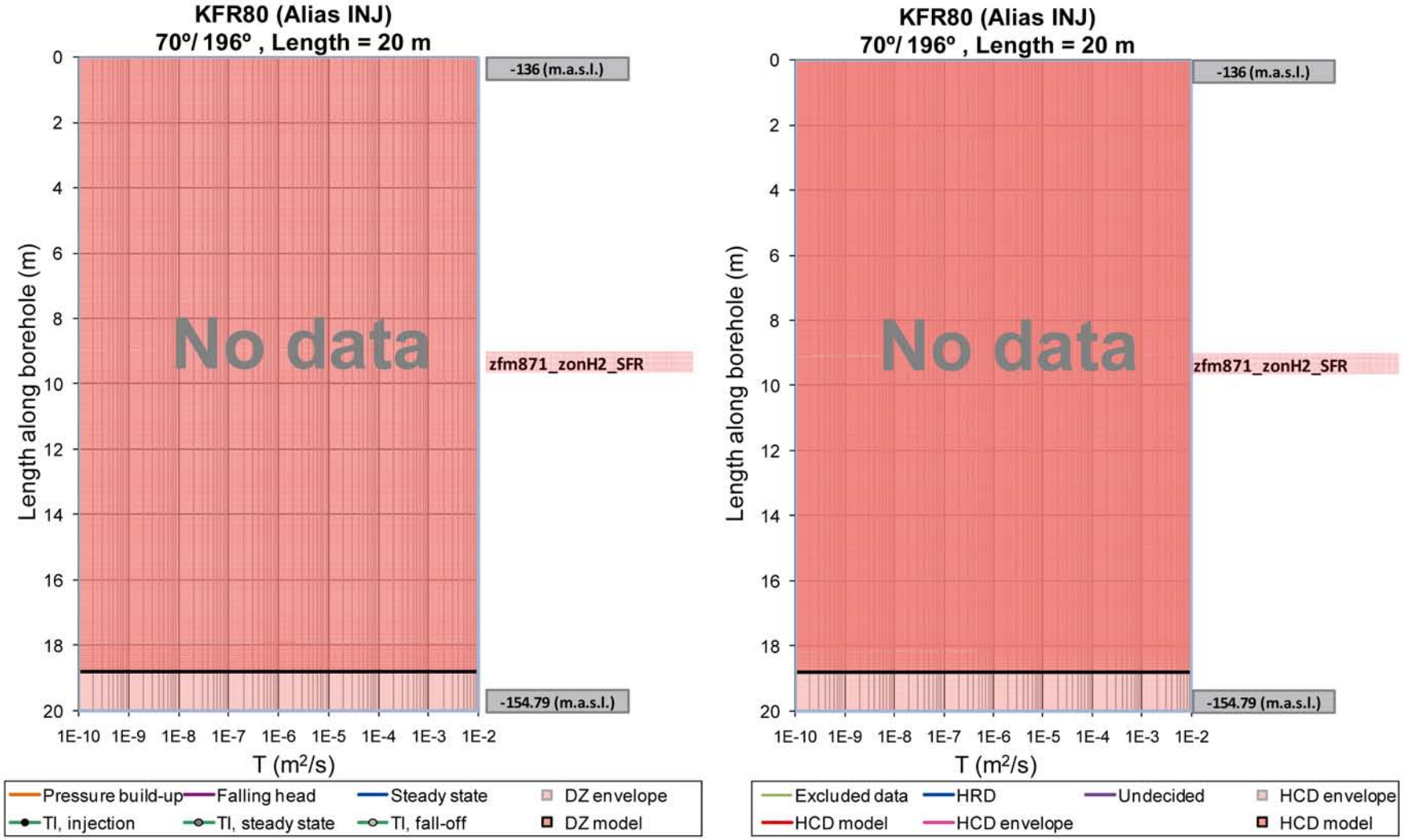

Figure B-55. *KFR80 raw data (left) and interpretation (right). No targeted tests performed in this borehole; it is part of the grouting fan that intersected ZFM871 during construction of NBT, and acted as the pumped borehole section in an unintentional interference test (Section 2.1.2).*

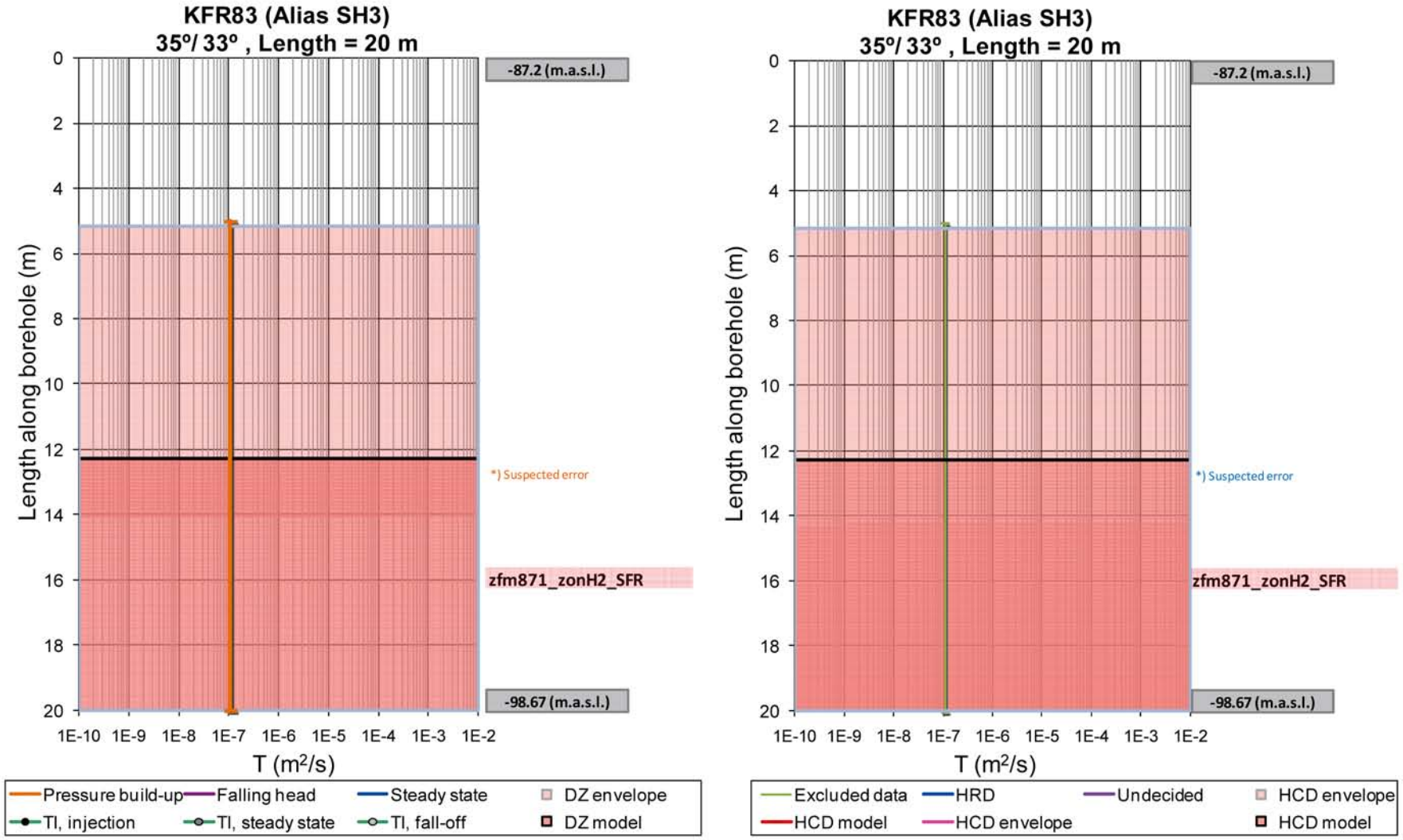

Figure B-56. *KFR83 raw data (left) and interpretation (right). An interference test (5–20 m) was performed in this borehole (Section 2.1.2).*

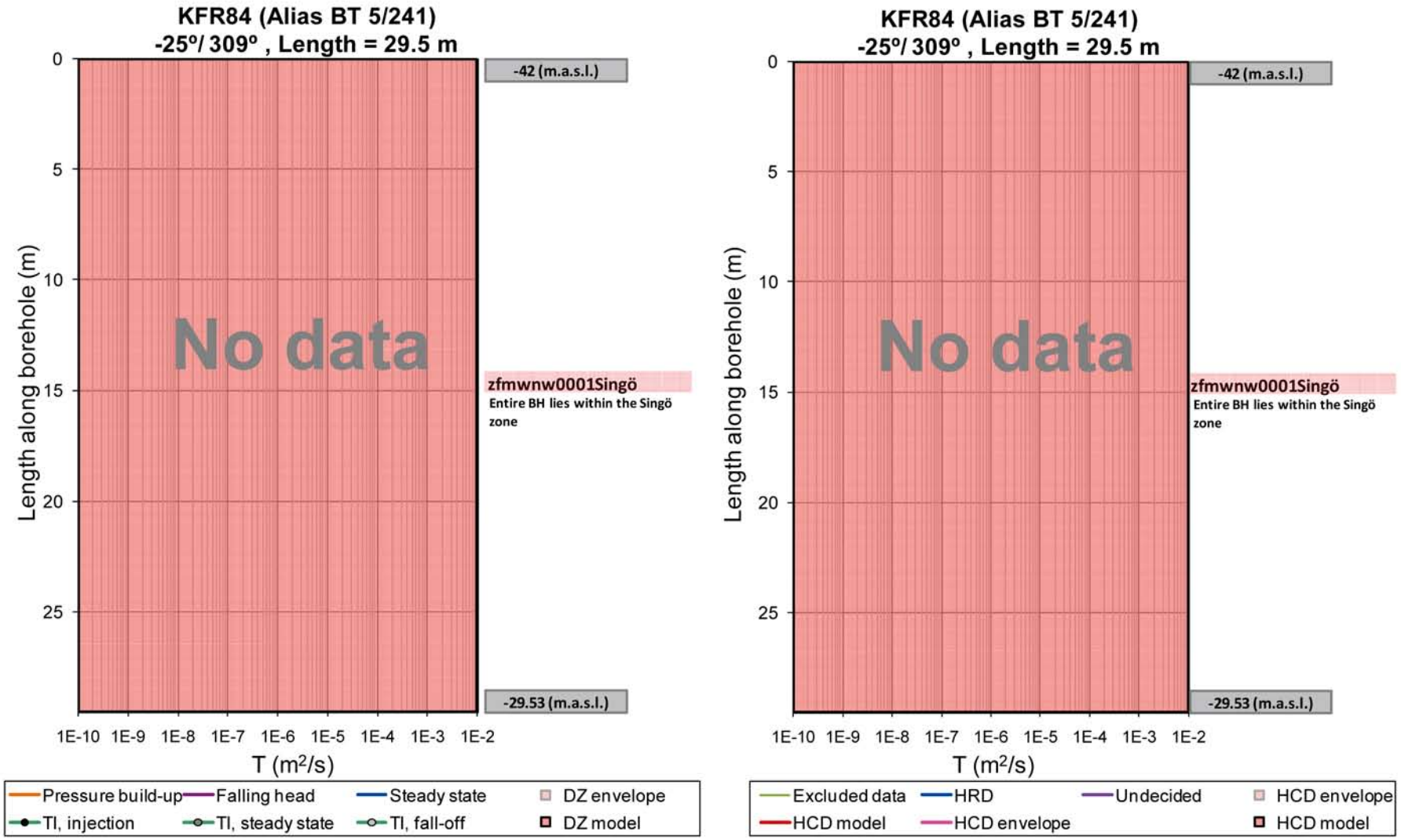

Figure B-57. *No data available in KFR84.*

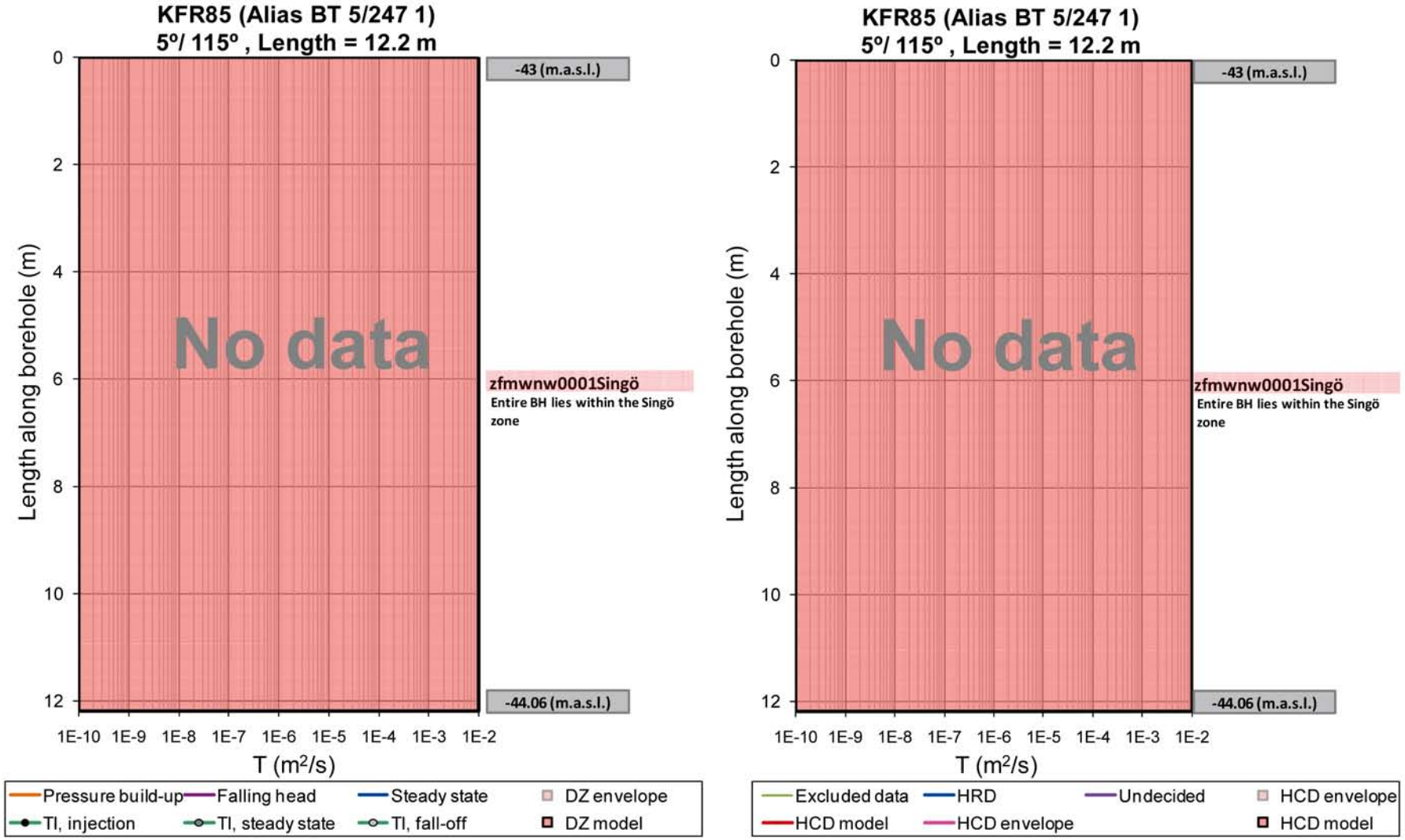

Figure B-58. *No data available in KFR85.*

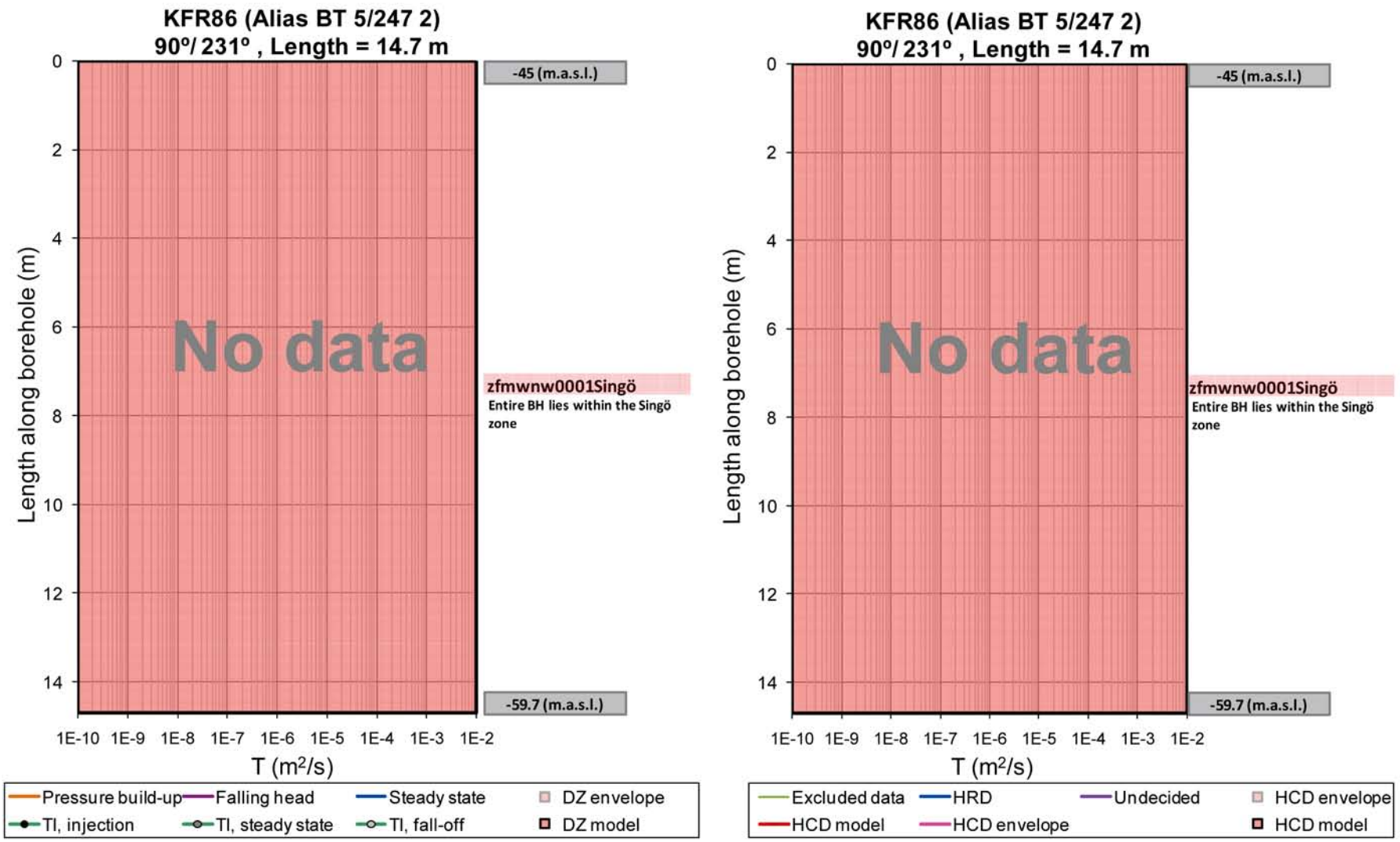

Figure B-59. *No data available in KFR86.*

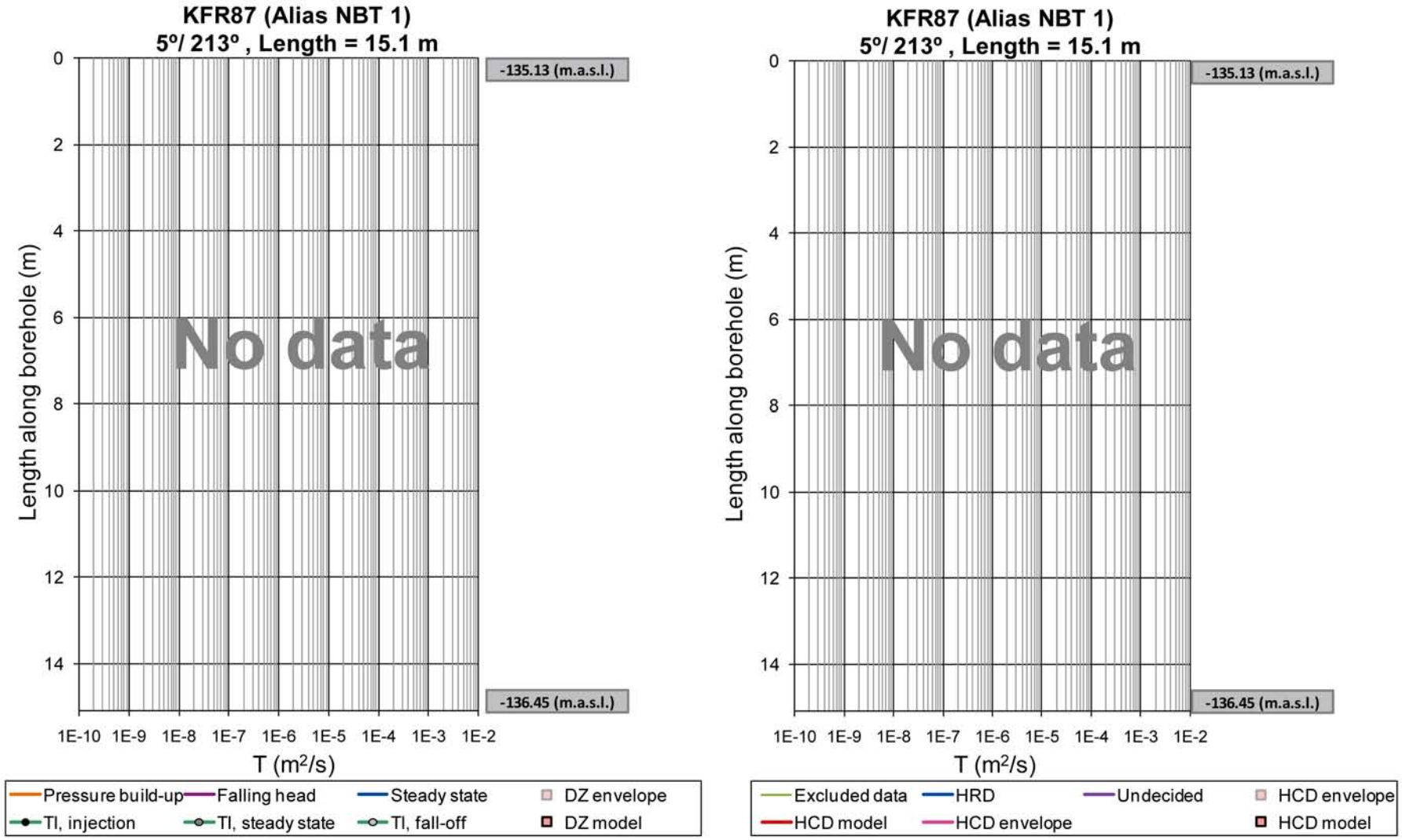

Figure B-60. *No data available in KFR87.*

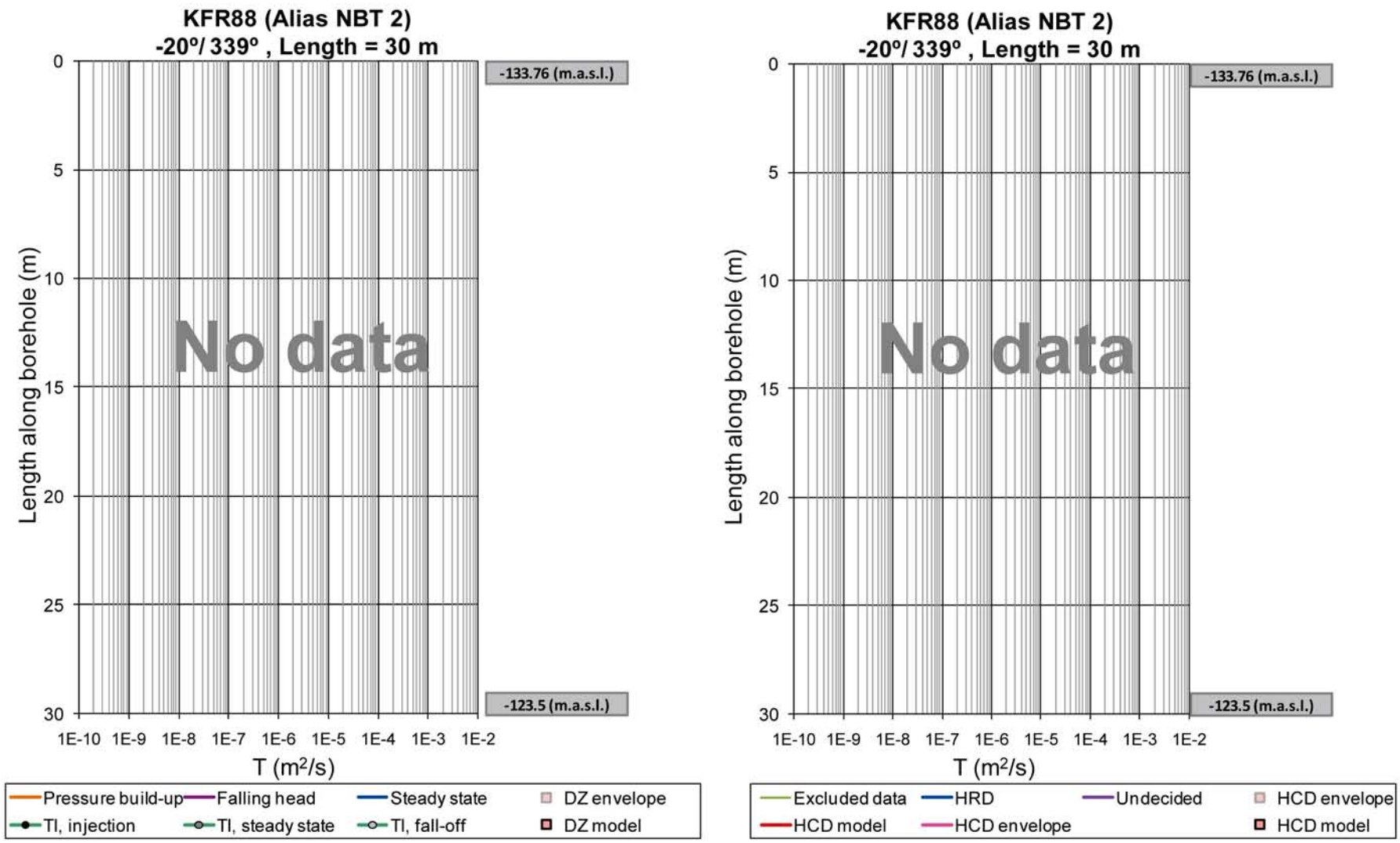

Figure B-61. *No data available in KFR88.*

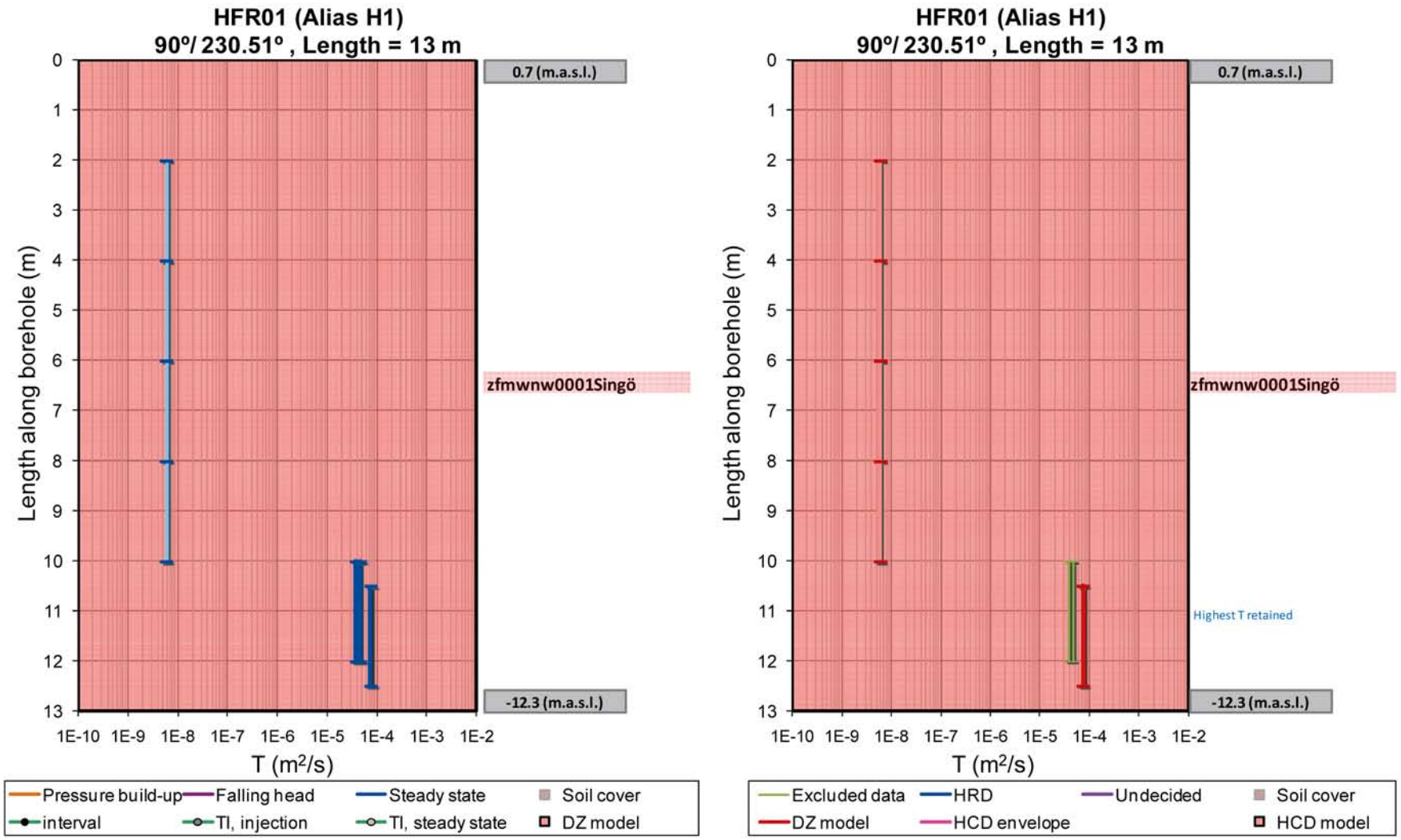

Figure B-62. *HFR01 raw data (left) and interpretation (right).*

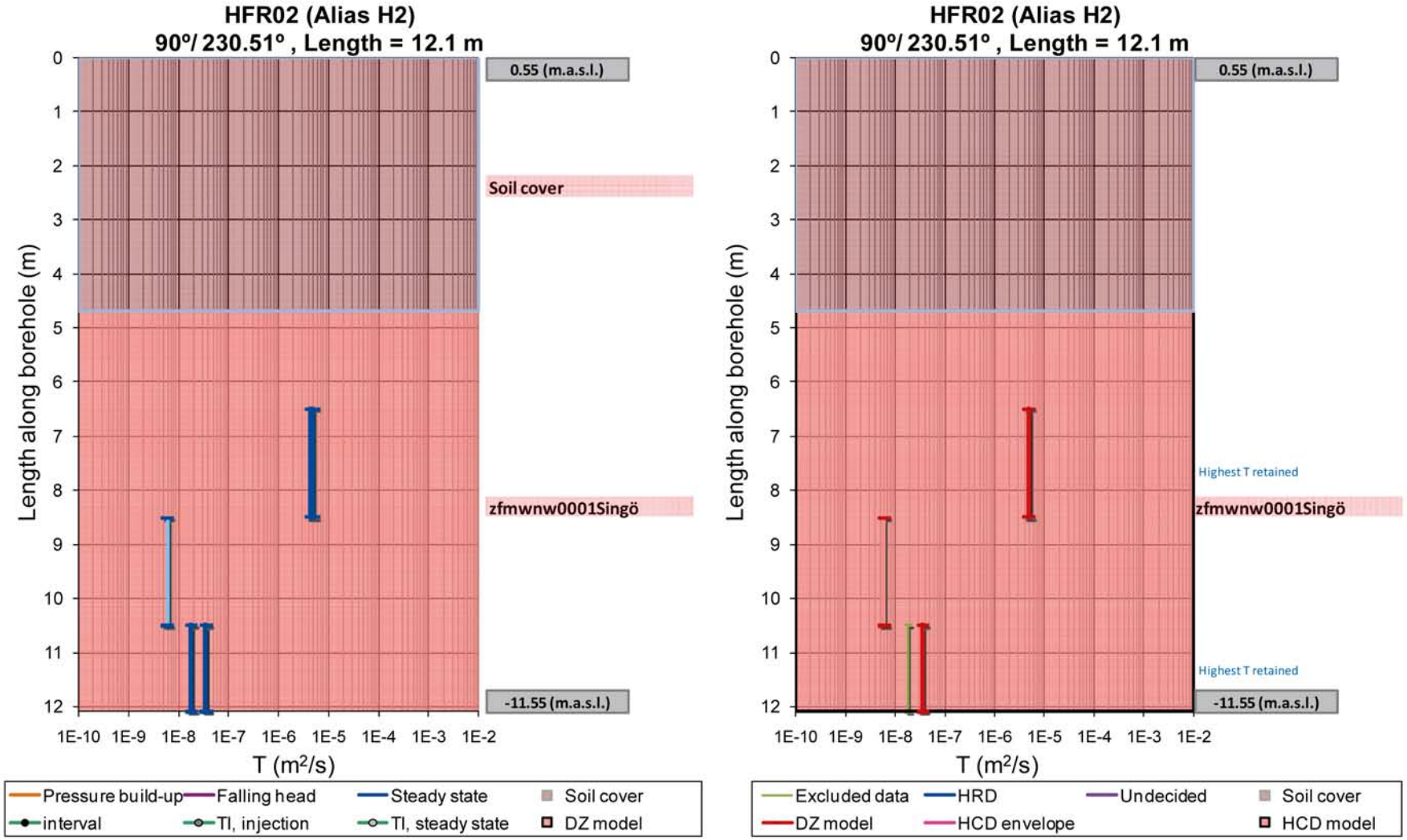

Figure B-63. *HFR02 raw data (left) and interpretation (right).*

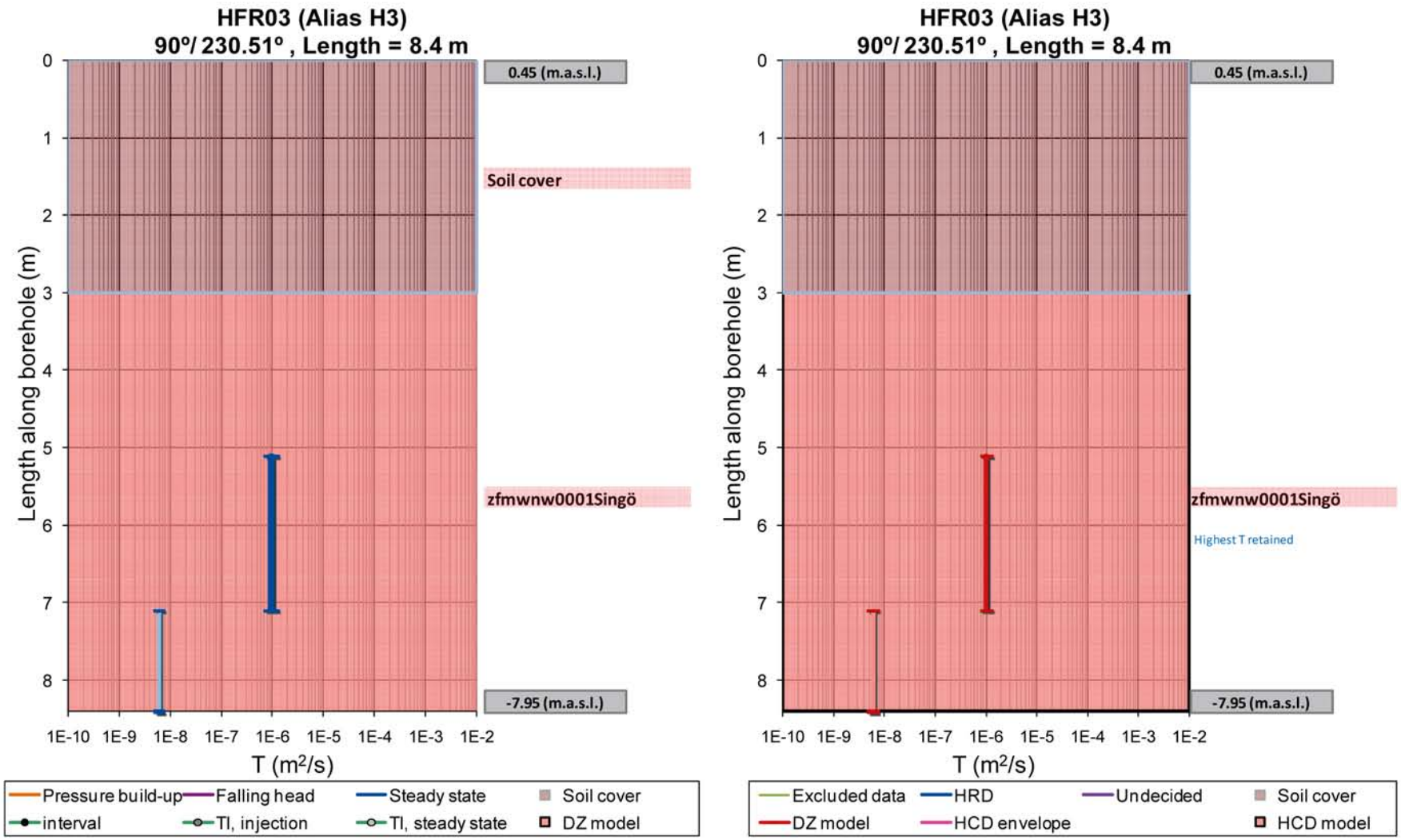

Figure B-64. *HFR03 raw data (left) and interpretation (right).*

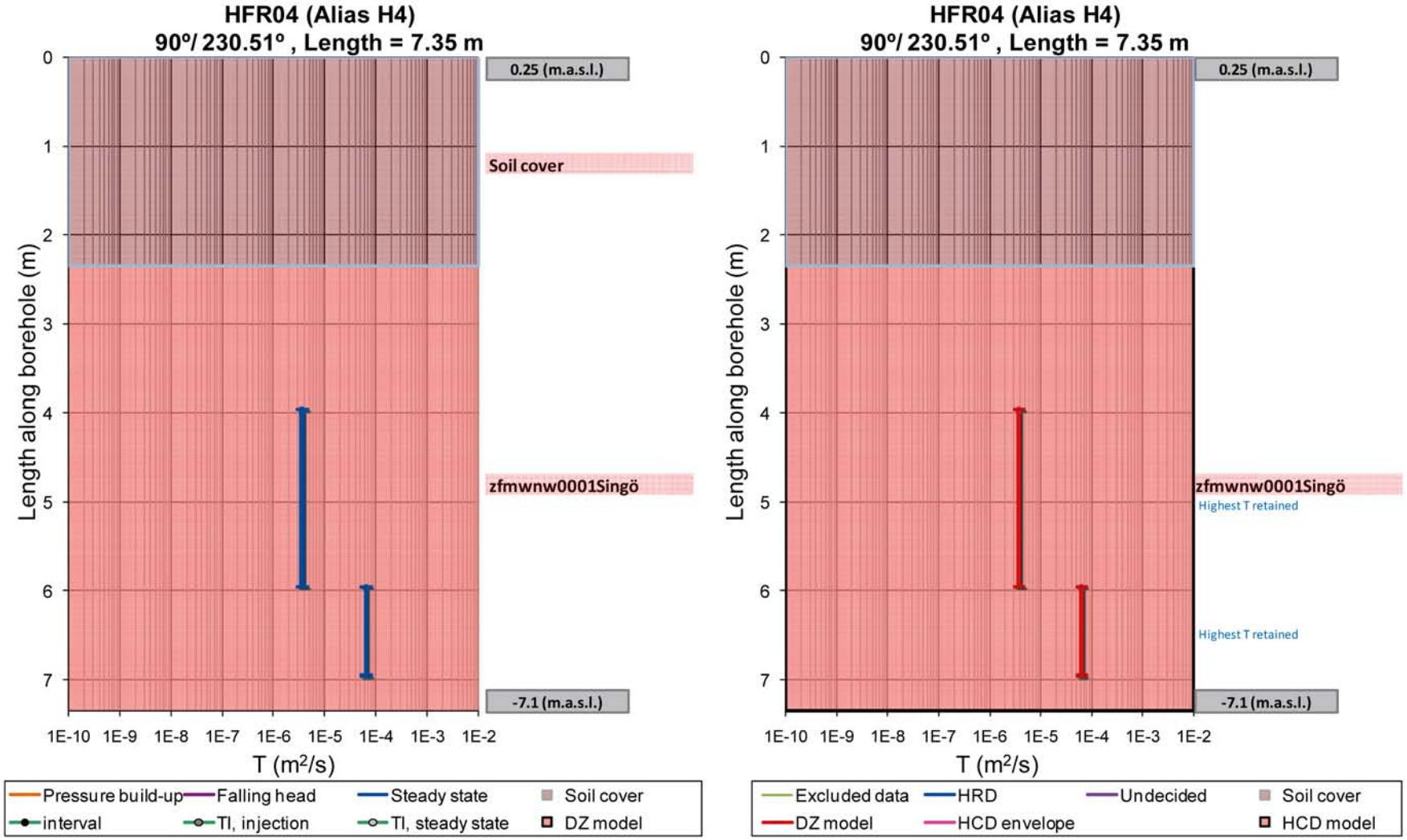

Figure B-65. *HFR04 raw data (left) and interpretation (right).*

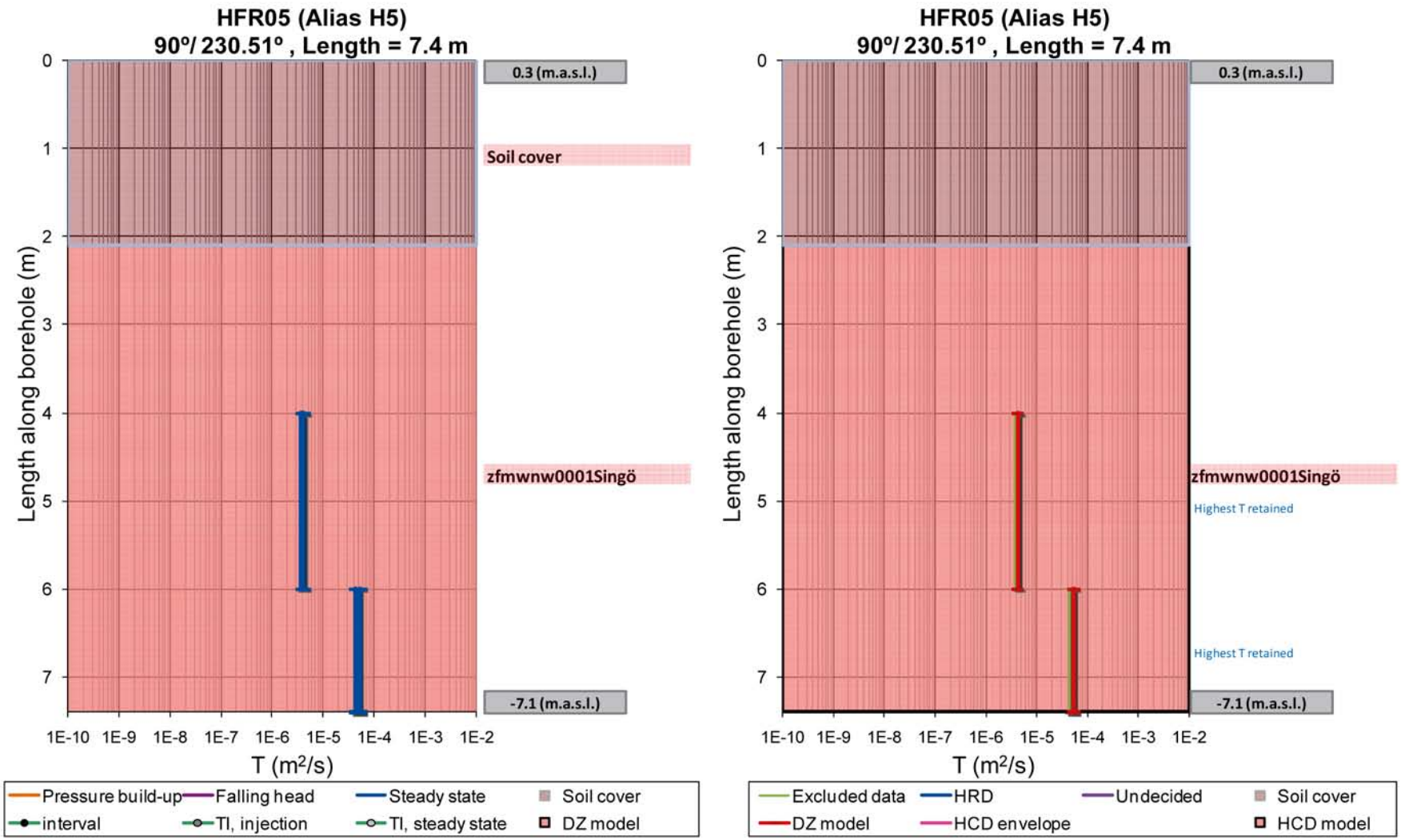

Figure B-66. *HFR05 raw data (left) and interpretation (right).*

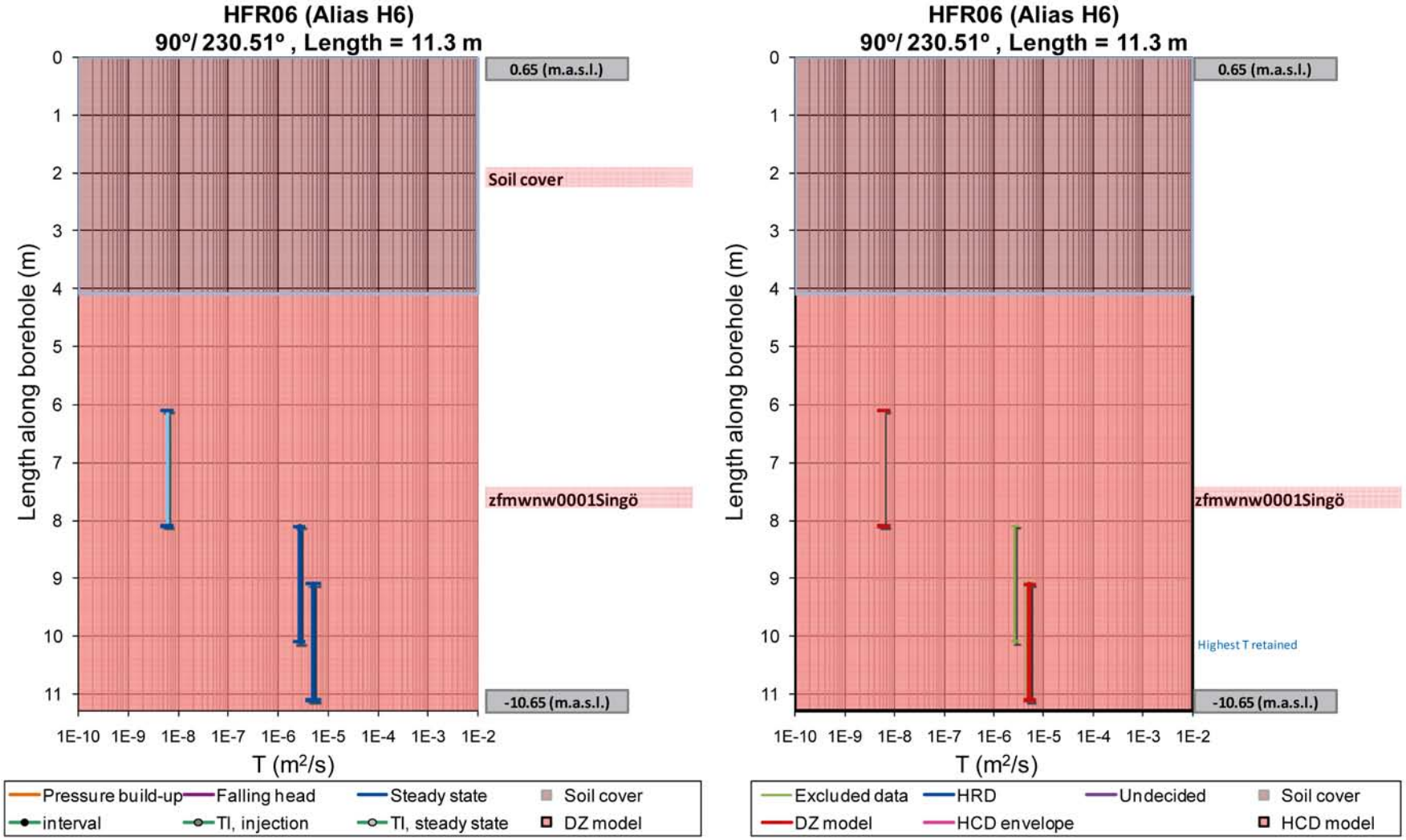

Figure B-67. *HFR06 raw data (left) and interpretation (right)*

Appendix C

Visualisation of interference test data

The geometric configuration of interference tests are visualised in this appendix (Figure C-1 to Figure C-12) and the interpretations are summarized (Table C-1 to Table C-10). The interpretation of responses is taken from /Axelsson and Mærsk Hansen 1997/ and the classification of borehole sections per HCD/HRD according to the geologic model SFR v.0.1 is taken from /Curtis et al. 2009/. Boreholes within brackets (Table C-1 to Table C-10), listed as response "None" imply that only some sections lack response.

The effective transmissivity values evaluated over a hydraulic path between tested borehole section and observed borehole section (with length L; Table C-1 to Table C-10) were evaluated with a type-curve matching of responses. This type-curve matching was based on the classical Theis curve, but it has been developed to account for the dual porosities of HCD/HRD. The documentation of this methodology is included in Appendix G. It is interesting to see how well the effective transmissivity of hydraulic paths within HCDs (Table C-1 to Table C-10) agree with the calculated intercept transmissivities in this report (see Chapter 6). However, it must be emphasised that the use of type-curves relies on the assumption of strongly idealized geometry, such as radial symmetric flow in a porous medium with infinite lateral extent (it is also assumed that $u<0.01$ is satisfied). The agreement between single-hole and cross-hole data, may either be coincidental – owing to simplifications made in the interpretation in both single- and cross-hole data, or it may actually indicate that HCDs are more homogenous than expected (i.e. less canalised; Section 3).

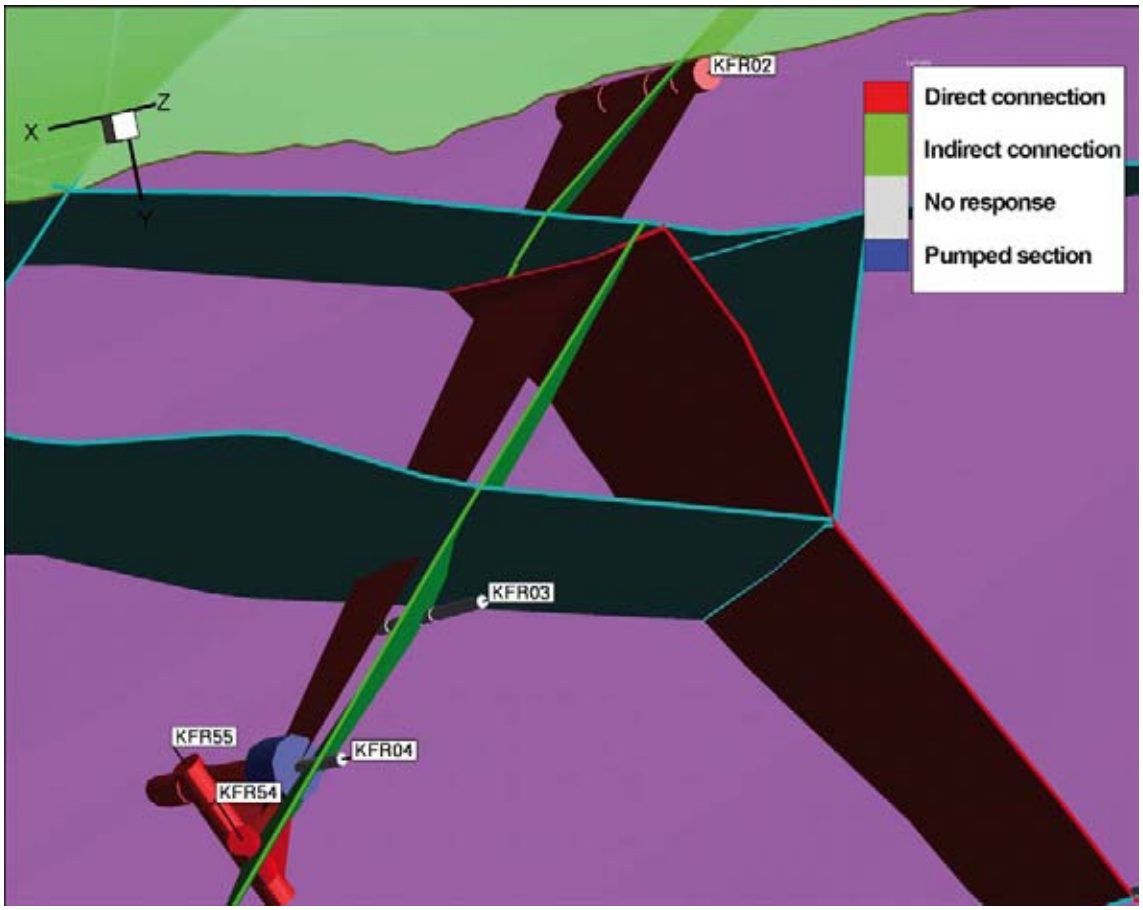

Figure C-1. *Interference test in KFR04 (28–43 m) covering 30% of hydraulic envelope for zfmne0870b (top view). Longest hydraulic path to KFR02 (also in zfmne0870a, 215 m).*

Table C-1. Interpretation of interference test in KFR04 (28–43 m).

RESPONSE	OBSHOLE	SECTION	CLASSED OBS SECTION	L (m)	Log T_0
Direct	KFR02	(2–20 m)	zfmne0870a	248	
		(21–42 m)	zfmne0870a	248	
		(43–80 m)	zfmne0870a	249	
		(81–116.8 m)	zfm871	255	
	KFR04	(44–83 m)	zfmne0870b	1	
		(84–110.5 m)	HRD	41	
	KFR54	(30–43 m)	zfmne0870b	28	–6.1
	KFR55	(8–21 m)	zfmne0870b	20	–6.1
		(22–39 m)	zfmne0870b	20	–6.3
		(40–48 m)	HRD	25	–6.3
		(49–61.9 m)	HRD	31	
None	KFR03, (KFR04)				

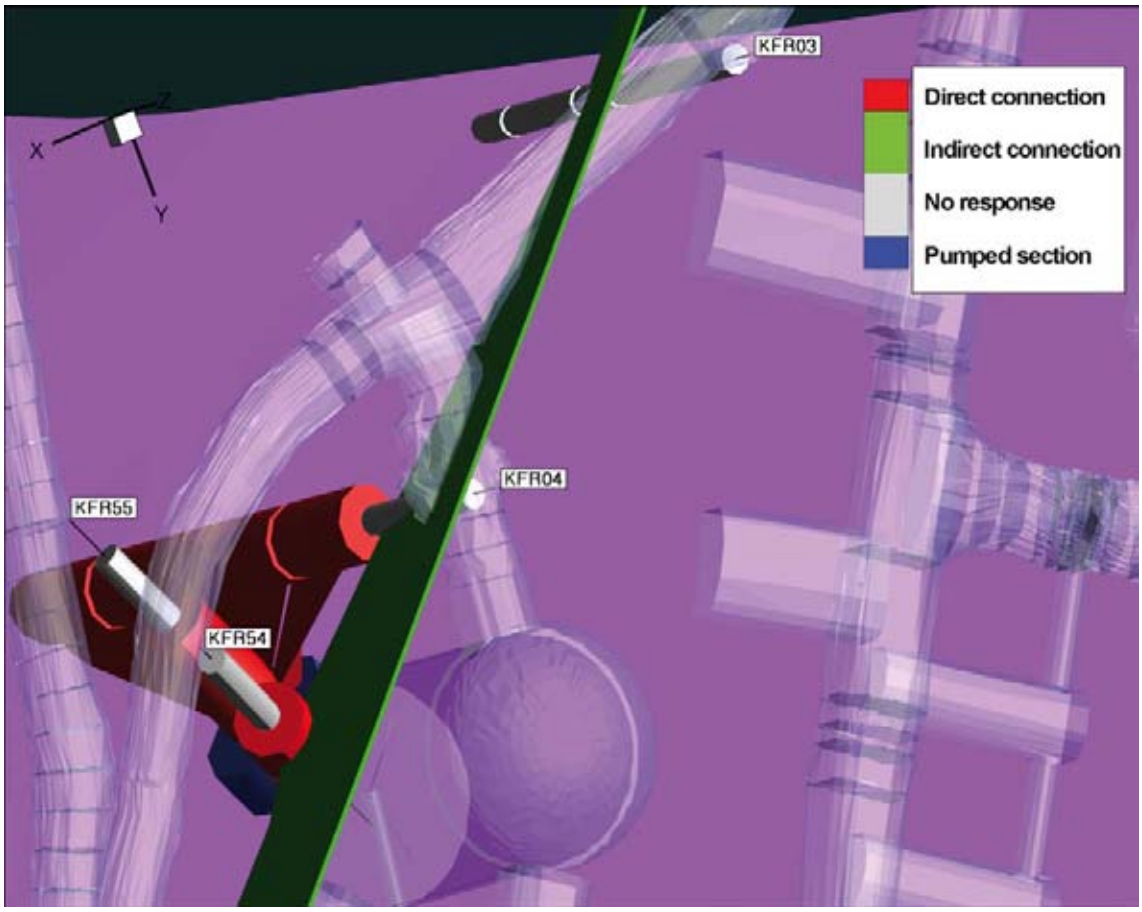

Figure C-2. *Interference test in KFR55 (40–48 m) located in HRD, just below zfmne0870 (top view). Longest hydraulic path 33 m. Note: no response in KFR03 (inside zfmne0870).*

Table C-2. Interpretation of interference test in KFR55 (40–48 m).

RESPONSE	OBSHOLE	SECTION	CLASSED OBS SECTION	L (m)	Log T_0
Direct	KFR04	(44–83 m)	zfmne0870b	25	
		(84–110.5 m)	HRD	33	–6.1
		(28–43 m)	zfmne0870b	25	–6.1
	KFR54	(30–43 m)	zfmne0870b	21	–6.1
	KFR55	(22–39 m)	zfmne0870b	1	
None	KFR02, KFR03, (KFR04)				

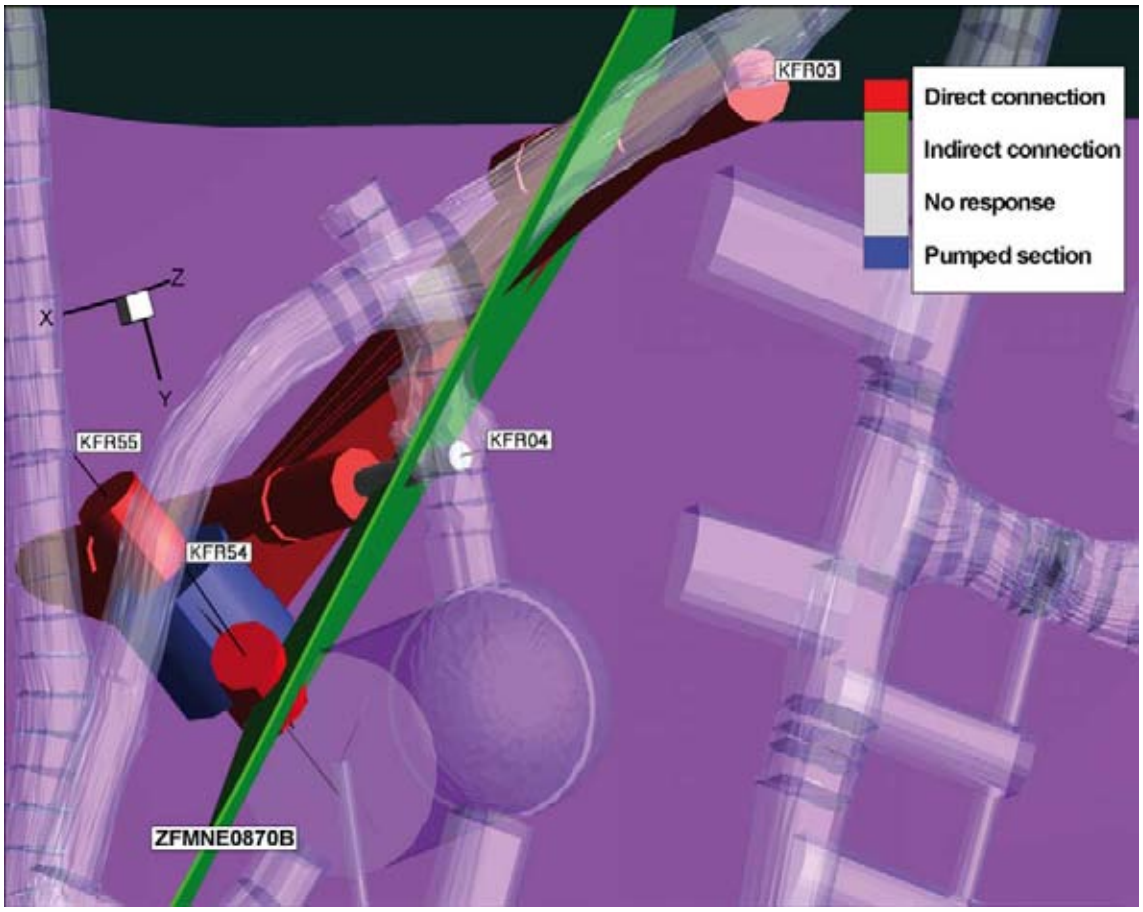

Figure C-3. *Interference test in KFR55 (22–39 m) covering 53% of hydraulic envelope for zfmne0870b (top view). Longest hydraulic path 100 m in KFR03 (in zfmne0870b/ZFM871). Compare to Figure C-2.*

Table C-3. Interpretation of interference test in KFR55 (22–39 m).

RESPONSE	OBSHOLE	SECTION	CLASSED OBS SECTION	L (m)	Log T_0
Direct	KFR03	(5–44 m)	zfmne0870b	94	
		(45–56 m)	zfmne0870b	94	
		(57–80 m)	zfm871 zfmne0870b	94	
		(81–101.6 m)	zfm871 zfmne0870b	99	
	KFR04	(44–83 m)	zfmne0870b	19	
		(84–110.5 m)	HRD	30	–6.1
		(28–43 m)	zfmne0870b	20	
	KFR54	(30–43 m)	zfmne0870b	21	–5.8
	KFR55	(8–21 m)	zfmne0870b	1	
		(40–48 m)	HRD		
None	KFR04	(5–27 m)	zfmne0870b	34	

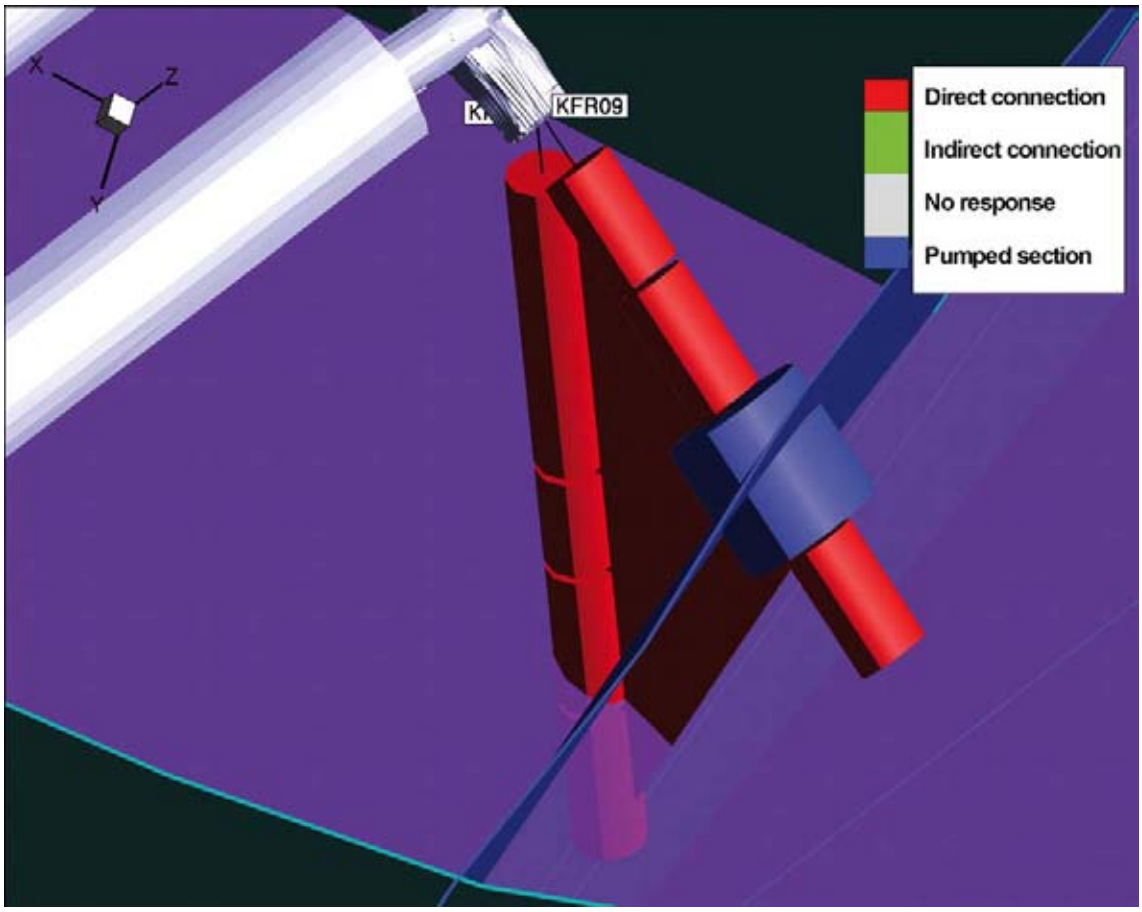

Figure C-4. *Interference test in KFR09 (43–62 m) covering 27% of the envelope of zfmnne0869 (top view). KFR09 is above ZFM871, while KFR10 extends below ZFM871. Longest hydraulic path 57 m.*

Table C-4. Interpretation of interference test in KFR09 (43–62 m).

RESPONSE	OBSHOLE	SECTION	CLASSED OBS SECTION	L (m)	Log T_0
Direct	KFR09	(7–23 m)	zfmnne0869	20	
		(24–42 m)	zfmnne0869	1	
		(63–80.3 m)	zfmnne0869	1	
	KFR10	(7–50 m)	HRD	33	
		(51–65 m)	zfm871 zfmnne0869	34	
		(66–86 m)	zfm871 zfmnne0869	44	
		(87–108 m)	zfm871 zfmnne0869	57	

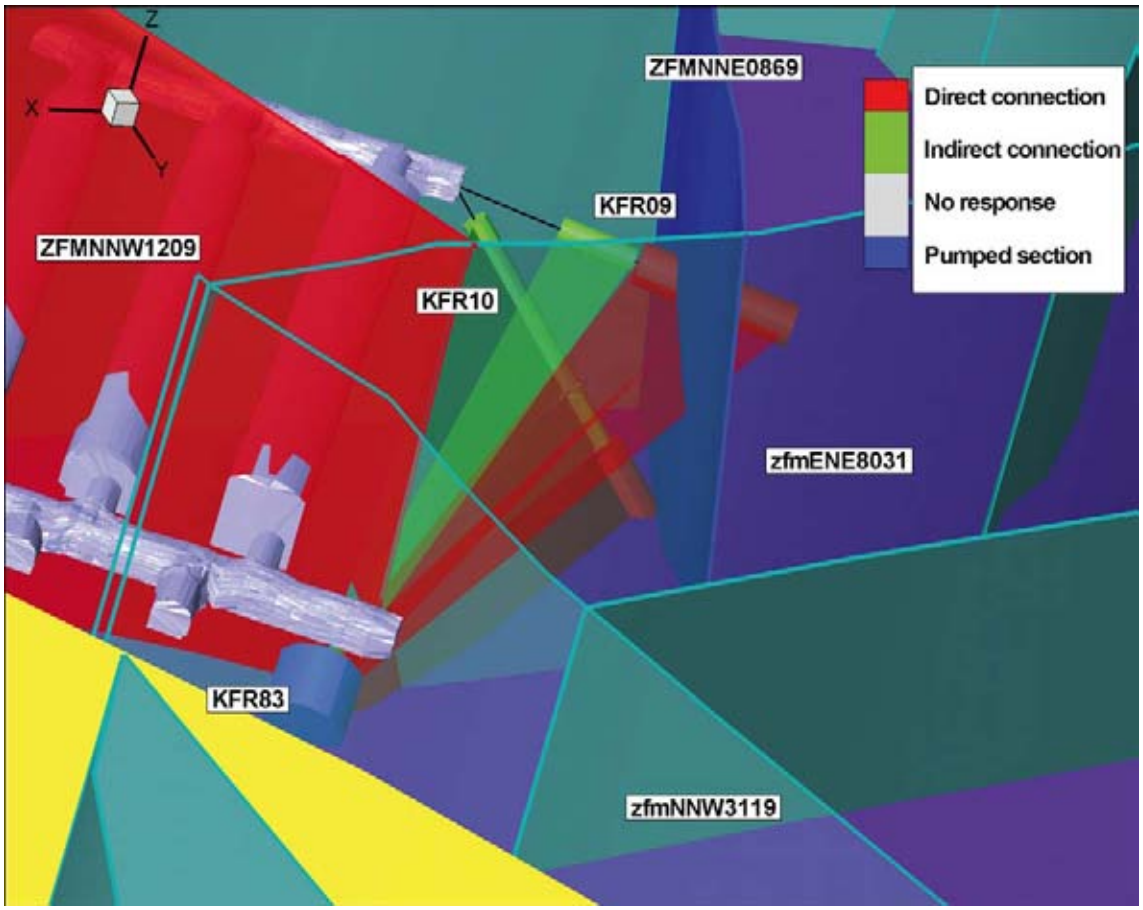

Figure C-5. *Interference test in KFR83 (5–20 m) covering entire hydraulic envelope for ZFM871 Hydraulic paths in ZFM871/ZFMNNE0869 (zon3) to KFR09 and KFR10 about 220 m, cf. Figure C-4.*

Table C-5. Interpretation of interference test in KFR83 (5–20 m).

RESPONSE	OBSHOLE	SECTION	CLASSED OBS SECTION	L (m)	Log T_0
Direct	KFR09	(43–62 m)	zfmnne0869	215	–3.1
		(63–80.3 m)	zfmnne0869	220	–3.1
	KFR10	(66–86 m)	zfm871 zfmnne0869	216	–3.5
		(87–108 m)	zfm871 zfmnne0869	222	–3.5
Indirect	KFR09	(24–42 m)	zfmnne0869	212	
	KFR10	(7–50 m)	HRD	210	
		(51–65 m)	zfm871 zfmnne0869	213	

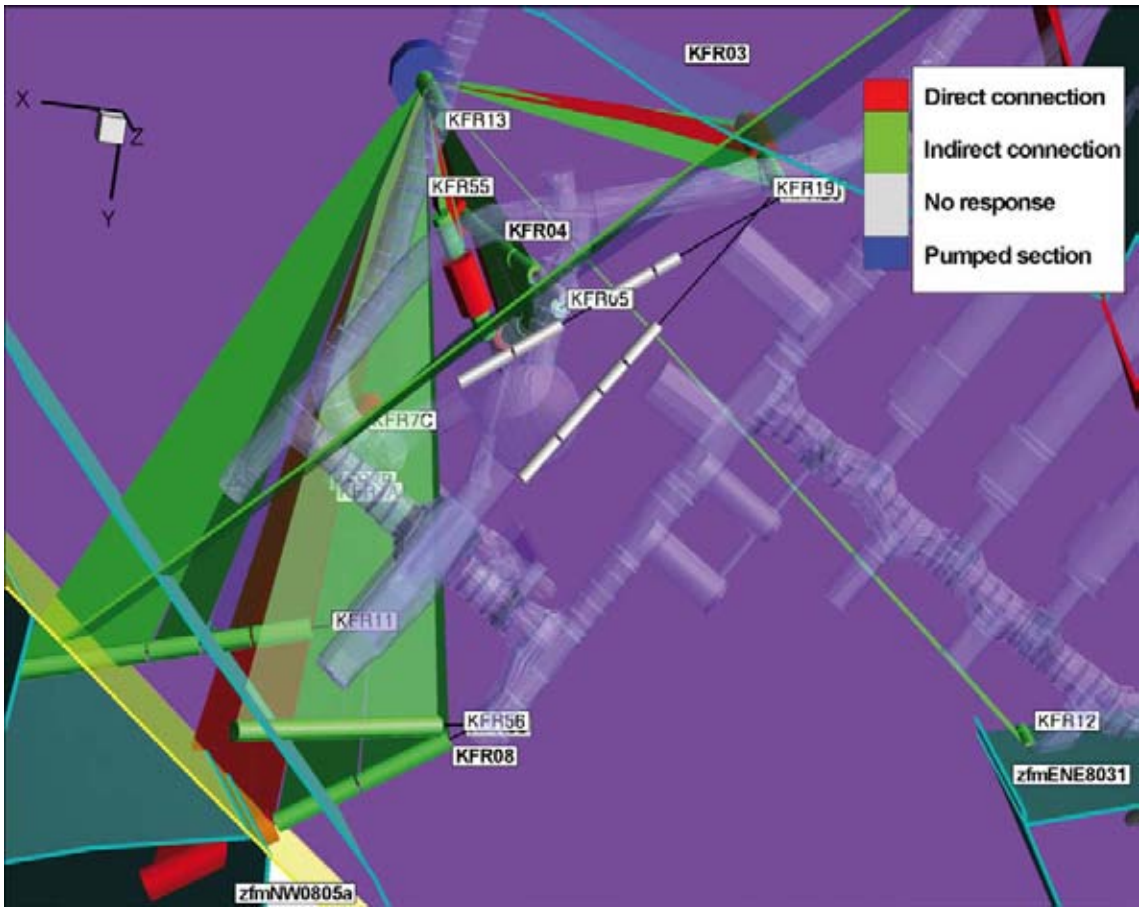

Figure C-6. *Interference test in KFR13 (54–76.6 m) covering 72% of the hydraulic envelope of ZFM871 (top view). Long distance observations KFR12 (250 m) and KFR08 (215 m).*

Table C-6. Interpretation of interference test in KFR13 (54–76.6 m).

RESPONSE	OBSHOLE	SECTION	CLASSED OBS SECTION	L (m)	Log T_0
Direct	KFR03	(45–56 m)	zfmne0870b	103	–4.3
		(57–80 m)	zfm871 zfmne0870b	96	–4.5
	KFR04	(84–110.5 m)	HRD	33	–4.8
	KFR05	(80–96 m)	zfm871 zfmne0870b	75	–4.4
	KFR08	(63–104 m)	zfmnnw0999 zfmnw0805a	215	–4.5
	KFR55	(22–39 m)	zfmne0870b	62	–4.9
	KFR7B	(4–7 m)	zfm871	117	–3.9
		(8–21.1 m)	zfm871	117	–3.6
	KFR7C	(3–5 m)	HRD	96	–4.5
		(6–34 m)	zfm871	79	–4.5
Indirect	KFR03	(5–44 m)	zfmne0870b	108	
		(81–101.6 m)	zfm871 zfmne0870b	95	
	KFR04	(44–83 m)	zfmne0870b	41	
		(28–43 m)	zfmne0870b	73	
	KFR05	(12–56 m)	zfmne0870b	80	
		(57–79 m)	zfm871 zfmne0870b	75	
		(97–131 m)	zfm871 zfmne0870b	76	
	KFR08	(6–35 m)	HRD	189	
		(36–62 m)	zfmnw0805a,b	201	
	KFR11	(7–24 m)	zfmnw0805b	167	
		(25–39 m)	zfmnw0805b	173	
		(40–55 m)	zfmnw0805a,b	179	
		(56–98.1 m)	zfmnw0805a	187	
	KFR12	(3–19 m)	zfm871	253	
		(20–33 m)	zfm871	249	
		(34–50.3 m)	zfm871	246	
	KFR13	(4–33 m)	HRD	21	
		(34–53 m)	zfm871	1	
	KFR55	(8–21 m)	zfmne0870b	57	
		(40–48 m)	HRD	72	
	KFR56	(10–81.7 m)	zfmnw0805b	187	
	KFR7A	(20–47 m)	zfm871 zfmnw0805a,b	138	
None	KFR01, KFR02, (KFR04), KFR09, KFR10, KFR19, KFR20, (KFR7A), KFR83				

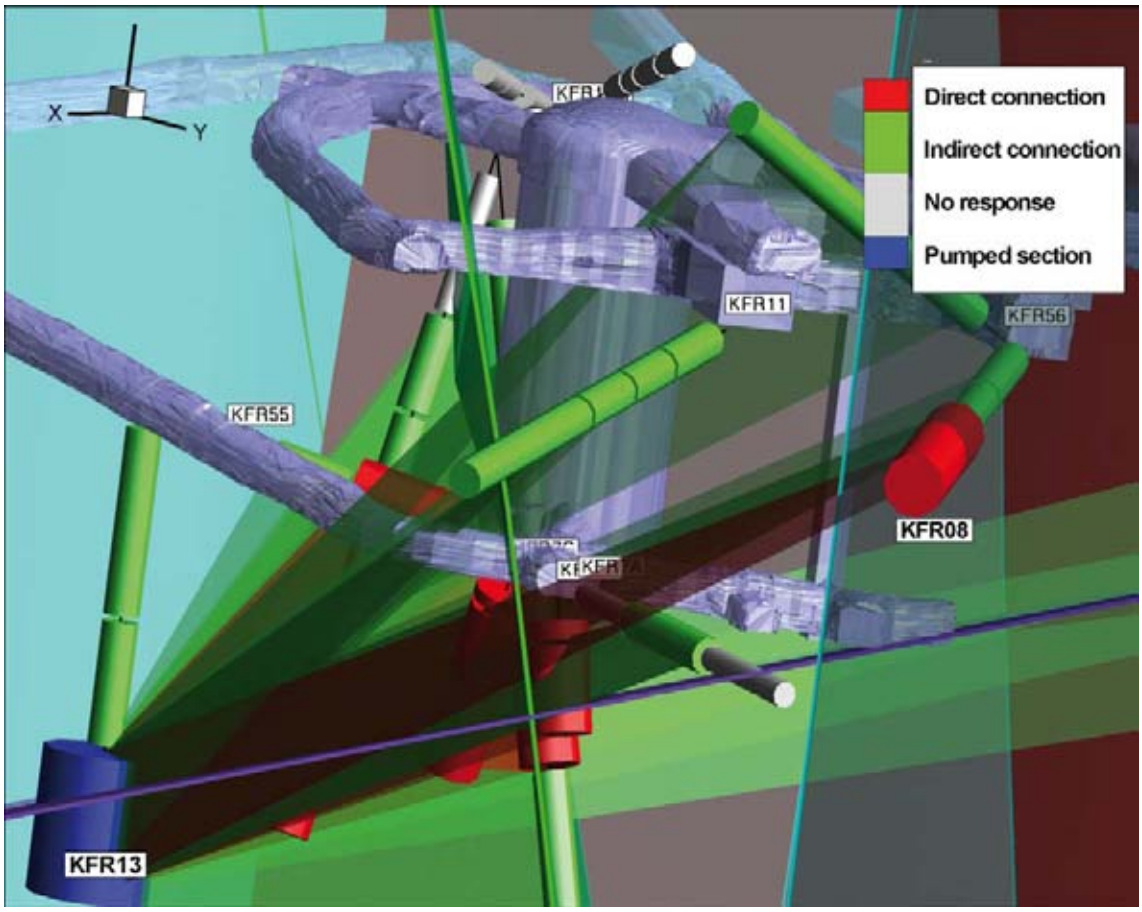

Figure C-7. *Interference test in KFR13 (54–76.6 m). Side view parallel to interception between ZFM871 and zfmne0870.*

Figure C-8. *"Unintentional interference test" in KFR80 (1.5–20 m) entirely inside ZFM871. Several direct responses in zfmne0870. Longest hydraulic paths to KFR02 (zfmne0870a; 300 m) and KFR01 (zfmwnw0001; 860 m).*

Table C-7. Interpretation of interference test in KFR80 (1.5–20 m).

RESPONSE	OBSHOLE	SECTION	CLASSED OBS SECTION	L (m)	Log T_0
Direct	KFR01	(11–44.5 m)	zfmwnw0001	851	
		(44.5–62.3 m)	zfmwnw0001	865	
	KFR02	(21–42 m)	zfmne0870a	303	
		(43–80 m)	zfmne0870a	302	
		(81–106.8 m)	zfm871	302	
	KFR03	(5–44 m)	zfmne0870b	129	
		(45–56 m)	zfmne0870b	127	
		(57–80 m)	zfm871, zfmne0870b	126	
		(81–101.6 m)	zfm871, zfmne0870b	126	
	KFR04	(5–27 m)	zfmne0870b	90	
		(44–83 m)	zfmne0870b	82	
		(28–43 m)	zfmne0870b	86	
	KFR05	(12–56 m)	zfm871, zfmne0870b	62	
		(57–79 m)	zfm871, zfmne0870b	49	
		(80–96 m)	zfm871, zfmne0870b	45	
		(97–131 m)	zfm871, zfmne0870b	45	
	KFR19	(77–94 m)	HRD	92	
		(95–110.2 m)	HRD	91	
	KFR20	(35–43 m)	HRD	116	
		(44–58 m)	HRD	110	
		(75–91 m)	HRD	101	
		(92–109.7 m)	HRD	101	
	KFR55	(8–21 m)	zfmne0870b	83	
		(22–39 m)	zfmne0870b	66	
None	(KFR02, KFR04, KFR19, KFR55)				

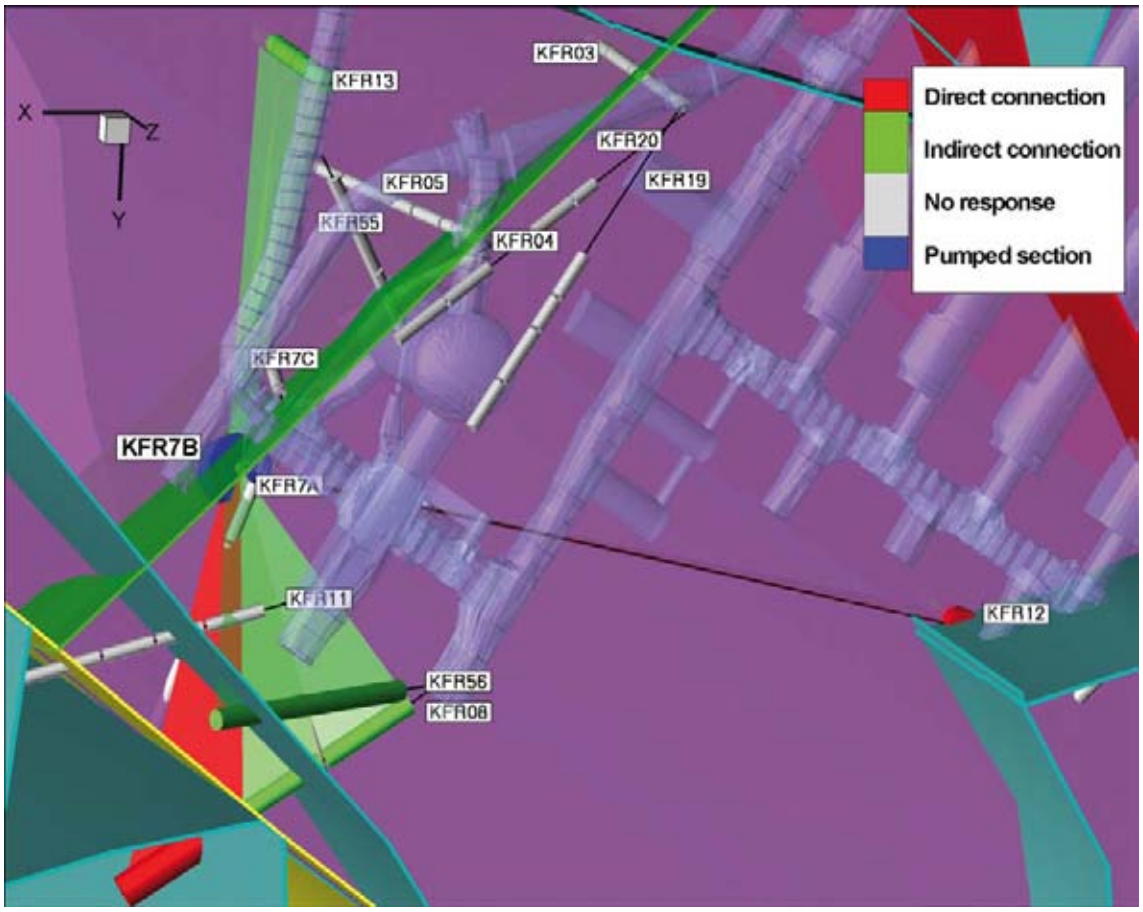

Figure C-9. *Interference test in KFR7B (8–21.1 m) covering 53% of hydraulic envelope for ZFM871. Longest hydraulic paths in KFR12 (215 m) and KFR08 (100 m).*

Table C-8. Interpretation of interference test in KFR7B (8–21.1 m).

RESPONSE	OBSHOLE	SECTION	CLASSED OBS SECTION	L (m)	Log T_0
Direct	KFR05	(80–96 m)	zfm871 zfmne0870b	68	–4.4
	KFR08	(63–104 m)	zfmnnw0999 zfmnw0805a	100	–4.2
	KFR11	(56–98.1 m)	zfmnw0805a	82	–4.2
	KFR12	(20–33 m)	zfm871	215	–4.2
	KFR7A	(48–74.7 m)	zfm871 zfmnw0805a,b	48	
	KFR7C	(3–5 m)	HRD	24	–4.5
		(6–34 m)	zfm871	25	–4.3
Indirect	KFR04	(44–83 m)	zfmne0870b	85	
		(84–110.5 m)	HRD	85	
		(28–43 m)	zfmne0870b	89	
	KFR05	(12–56 m)	zfmne0870b	75	
		(57–79 m)	zfm871 zfmne0870b	69	
		(97–131 m)	zfm871 zfmne0870b	67	
	KFR08	(6–35 m)	HRD	86	
		(36–64 m)	zfmnw0805a,b	89	
	KFR11	(7–24 m)	zfmnw0805b	61	
		(25–39 m)	zfmnw0805b	65	
		(40–55 m)	zfmnw0805a,b	72	
	KFR12	(34–50.3 m)	zfm871	214	
	KFR13	(4–33 m)	HRD	112	
		(34–53 m)	zfm871	112	
		(54–76.6 m)	zfm871	117	
	KFR55	(8–21 m)	zfmne0870b	77	
		(22–39 m)	zfmne0870b	67	
		(40–48 m)	HRD	64	
	KFR56	(10–81.7 m)	zfmnw0805b	86	
	KFR7A	(2–19 m)	zfm871 zfmnw0805a,b	9	
		(20–47 m)	zfm871	21	
	KFR7B	(4–7 m)	zfm871	1	
None	KFR01, KFR02, KFR03, (KFR04), KFR09, KFR10, (KFR12), KFR19, KFR20, KFR83				

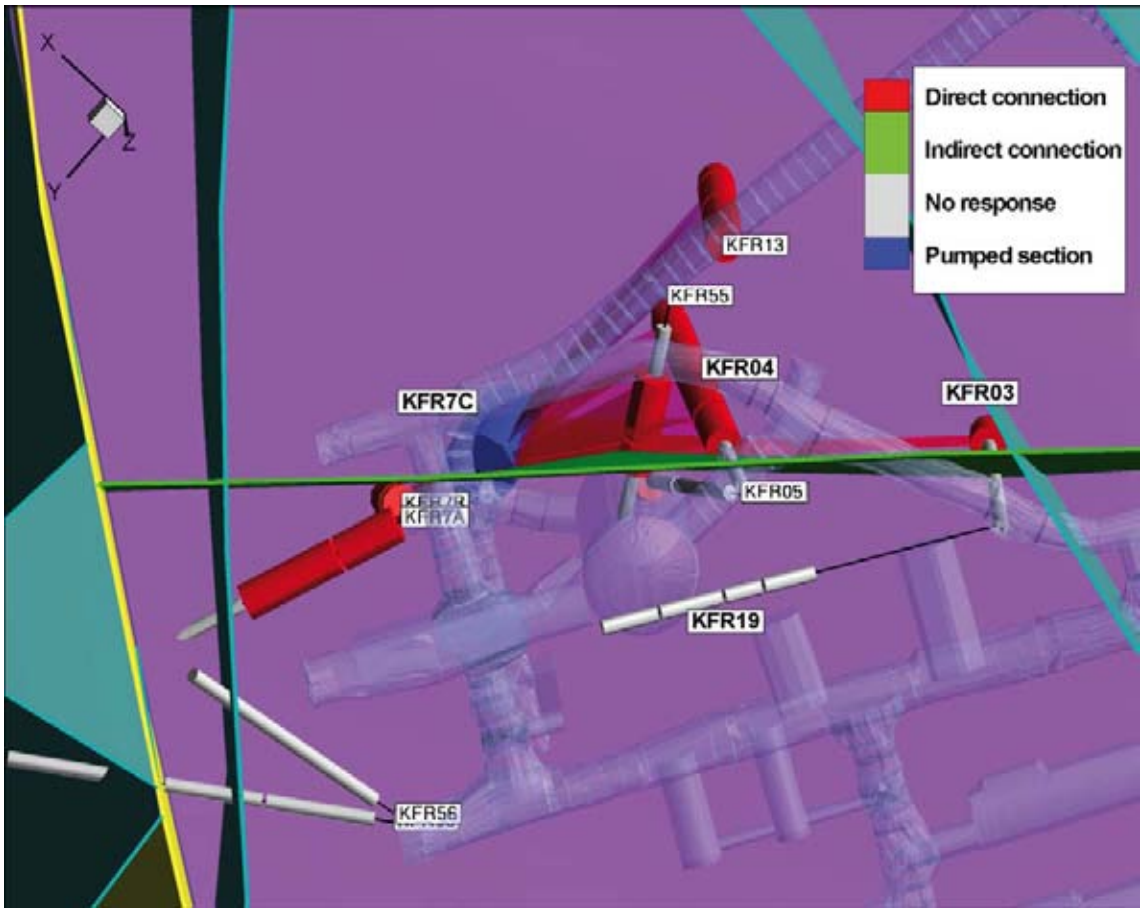

Figure C-10. *Interference test in KFR7C (3–34 m) covering entire hydraulic envelope for ZFM871, close to zfmne0870 (top view). Longest hydraulic path 33 m.*

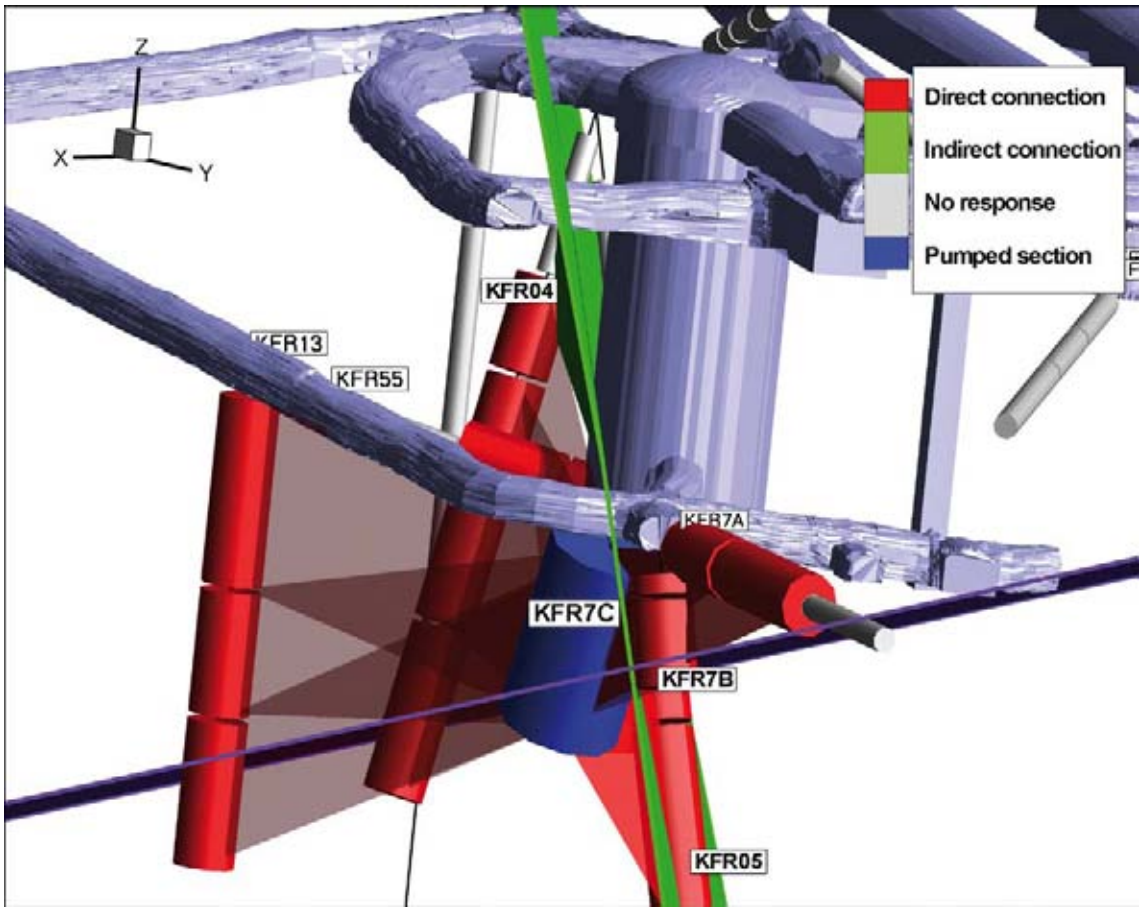

Figure C-11. *Interference test in KFR7C (3–34 m) covering entire hydraulic envelope for ZFM871, close to zfmne0870. Side view, along intersection between ZFM871 and zfmne0870.*

Table C-9. Interpretation of interference test in KFR7C (3–34 m).

RESPONSE	OBSHOLE	SECTION	CLASSED OBS SECTION	L (m)	Log T_0
Direct response	KFR03	(81–101.6 m)	zfm871 zfmne0870b	127	
	KFR04	(44–83 m)	zfmne0870b	50	
		(84–110.5 m)	HRD	50	
		(28–43 m)	zfmne0870b	66	
	KFR05	(80–96 m)	zfm871 zfmne0870b	37	
		(97–131 m)	zfm871 zfmne0870b	37	
	KFR13	(4–33 m)	HRD	78	
		(34–53 m)	zfm871	78	
		(54–76.6 m)	zfm871	79	
	KFR55	(22–39 m)	zfmne0870b	44	
		(40–48 m)	HRD	41	
	KFR7A	(2–19 m)	zfm871 zfmnw0805a,b	25	
		(20–47 m)	zfm871 zfmnw0805a,b	43	
	KFR7B	(4–7 m)	zfm871	22	
		(8–21.1 m)	zfm871	24	
None	KFR01, KFR02, (KFR03, KFR04, KFR05), KFR08, KFR19, (KFR55), KFR56, (KFR7A)				

Figure C-12. *Interference test in KFR08 (63–104 m) covering 50% of hydraulic envelope for zfmnw0805a and the entire zfmnnw0999. Longest hydraulic paths in ZFM871 and zfmne0870a =400 m.*

Table C-10. Interpretation of interference test in KFR08 (63–104 m).

RESPONSE	OBSHOLE	SECTION	CLASSED OBS SECTION	L (m)	Log T_0
Direct	KFR11	(56–98.1 m)	zfmnw0805a	61	–3.9
	KFR7A	(48–74.7 m)	zfm871 zfmnw0805a,b	49	–4.8
	KFR7B	(8–21.1 m)	zfm871	100	–3.6
Indirect	KFR02	(43–80 m)	zfmne0870a	409	
		(81–118 m)	zfm871	414	
		(137–170.3 m)	HRD	428	
	KFR03	(57–80 m)	zfm871 zfmne0870b	236	
	KFR08	(6–35 m)	HRD	28	
		(36–62 m)	zfmnw0805a,b	1	
	KFR11	(7–24 m)	zfmnw0805b	54	
		(25–39 m)	zfmnw0805b	54	
		(40–55 m)	zfmnw0805a,b	55	
	KFR19	(66–76 m)	HRD	160	
		(77–94 m)	HRD	144	
		(95–110.2 m)	HRD	130	
	KFR7A	(2–19 m)	zfm871 zfmnw0805a,b	80	
		(20–47 m)	zfm871 zfmnw0805a,b	60	
	KFR7B	(4–7 m)	zfm871	99	
	KFR7C	(3–5 m)	HRD	118	
		(6–34 m)	zfm871	120	
None	KFR01, (KFR02, KFR03), KFR04, KFR05, KFR09, KFR10, KFR12, KFR13, (KFR19), KFR20, KFR55				

Appendix D

Reproduction of the original Table 4-4 in /Axelsson and Mærsk Hansen 1997/

All interference test data presented in this report are based on the revised interpretations by /Axelsson and Mærsk Hansen 1997/. Unfortunately, Table 4-4 in /Axelsson and Mærsk Hansen 1997/, which defines the revised interpretations for all interference tests performed in zfmnne0869 (zone 3) was accidentally replaced by another table, and is therefore not included in the published report. Fortunately, this Table (*Figure D-1*) was found in original draft report (97-04-28). This Table is therefore published in this report to meet the requirements on traceability and referability of SICADA data. According to these revised interpretations, some responses in the KFR83-test (SH3) discarded, and the entire KFR10-test (HK10:1) was disqualified, owing to disturbances.

Table 4 Zone 3. Hydraulic connections - interference tests

Flow Site (Test)	Flow (l/min)	Test length (hours)	Zones in FS	Obs. hole (OH)	Zones in OH	Hydr path [m]	Draw down [m]	T (m^2/s)	K (m/s)	Indirect response	No response	Ref.
HK9:2	1.1	69	3	HK9:1		38	0.24					1
(B)				HK9:3		20	0.11					1
				HK9:4		19	-					1
				HK10:1	3,H2 ?	68	0.24					1
				HK10:2		50	0.24					1
				HK10:3		39	0.23					1
				HK10:4		36	0.09					1
				SH3	H2	223	-					1
SH3	25.8	458	Parallell	HK7A:1	H2,8 ?	269	0.15 *					2
(D)			with 6	HK7B:1	H2	257	0.17 *					2
				HK7C:1	H2	254	0.16 *					2
				HK7C:2	H2 ?	251	0.23 *					2
				HK9:1		228	0.41	3.5E-04				2
				HK9:2	3	223	0.49	3.6E-04	7.6E-05			2, 3
				HK9:3		220	0.24			Indirect		2
				HK10:1	3,H2 ?	230	0.31	1.5E-04	2.3E-05			3
				HK10:2		223	0.67	9.0E-05				2
				HK10:3		219	0.61			Indirect		2
				HK10:4		216	0.31			Indirect		2
				HK11:1	H1,8 ?	319	0.25 *					2
HK10:1	0.8	156	3,H2 ?	**								4
(H)												

* Drawdown caused by activities in tunnel NBT

** Reported drawdown in boreholes HK1, HK2, HK3, HK4, HK5, HK7A, HK7B, HK7C, HK8, HK9, HK11, HK12, HK13, Kb19, Kb20, Kb25, Kb26, SH3 interpreted as not due to test

References

1) IRAP 86403, Table 5.7
2) IRAP 86403, Tables 5.8, 5.9
3) SFR 86-03, Table 6.4.5
4) IRAP 86403, pg 58-59

Figure D-1. *The intended "Table 4-4" in /Axelsson and Mærsk Hansen 1997/, which defines the revised interpretations for all interference tests performed in zfmnne0869 (zone 3).*

Depth trend comparison

Alternative depth dependence models for extrapolating HRD conductivity to greater depths than the range of available hydraulic data (approximately z = 0 to –200 m.a.s.l.) are presented in Chapter 6. On the other side of the Singö-zone, there is plenty hydraulic data available at greater depths from the Site Investigation Forsmark. The Singö-zone divides SFR and the Forsmark domains into two separate geologic units, and it is therefore questionable whether relations and concepts can be transferred across the Singö-zone without evidence from supporting data. As an example, the depth trend models for HRD conductivity suggested in /Axelsson 1986/ fitted to data on either side of the Singö zone are compared.

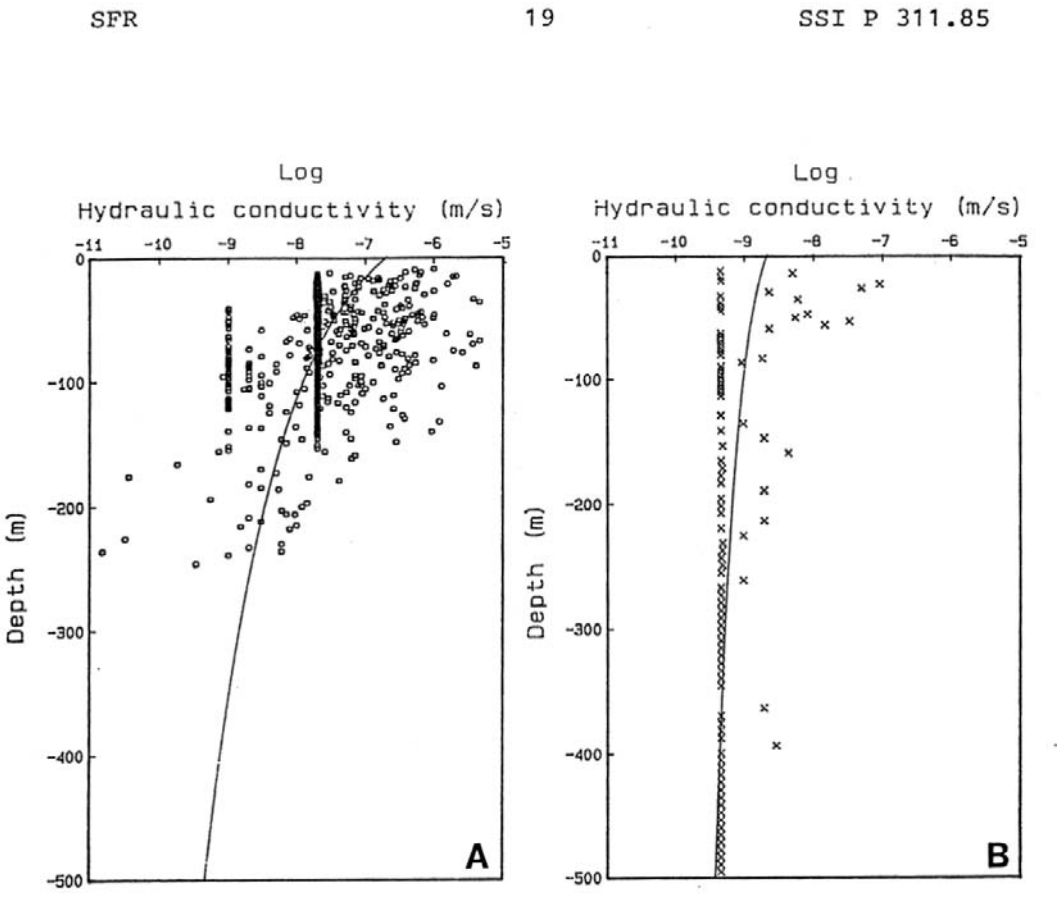

Figure 4.2. Measured hydraulic conductivity of the rock mass with fitted curves.
A Investigation boreholes at the repository site, SFR.
B Research borehole, DBT-1, at the Forsmark power plant.

Figure E-1. *Modelled depth dependence in HRD conductivity as fitted to hydraulic data, for SFR (left) and DBT-1 at the Forsmark power plant (right). Taken from /Axelsson 1986/.*

Appendix F

Main changes between the preliminary v 0.1 model delivery and the 'final' post review model delivery

By Phillip Curtis, Golder Associates AB

No lineaments or the deformation zone ground surface traces have been modified. Estimates of the span of various properties have been removed from the property tables since it was judged that sufficient information is lacking.

Deformation zone ID	Parameter	Preliminary v0.1	Final v0.1	Comment
ZFM871	Orientation	070 / 19	071 / 19	
	Thickness	20 m	24 m	
	Length	1,400 m	1,200 m	There is still no associated lineament, only a change in the estimated projected length
	Bh intercepts		Additional intercepts have been included from KFR24, KFR25 and KFR57	Additional intercepts based on /Axelsson and Mærsk Hansen 1997/
	Tunnel intercepts		Very minor adjustments to RVS contol point intercepts, no change in interpretation	
ZFMNE0870B	Orientation	227 / 74	227 / 73	Adjustment in position interpreted in KFR09 and added intercept position from KFR36
	Tunnel intercepts		Very minor adjustments to RVS contol point intercepts, no change in interpretation	
ZFMNNE0869	Orientation	200 / 80	201 / 86	
	Thickness	50 m	60 m	More weight given to SHI thickness estimates.
	Tunnel intercepts		Very minor adjustments to RVS contol point intercept, no change in interpretation	
ZFMNNW0999	Confidence	High	Medium	There is a geometrical intercept with KFR08 SHI DZ2. However, this interval is now inferred as being dominated by ZFMNW0805A and no exclusive evidence for the existence of ZFMNNW0999 has been identified
	Thickness	20 m	5 m	Return to a default thickness due to reinterpretation of the KFR08 intercept (see above)
ZFMNW0805A	Orientation	134 / 90	314 / 83	Steep dip to the NE (leads to a 180° change in strike notation) based on adjusted intercept position with SHI DZ2 in KFR08.
	Thickness	20 m	60 m	Adjusted to correspond to the entire extent of SHI DZ2 in KFR08
	Bh intercepts			Adjusted position in KFR08. Very minor adjustment to position in KFR7A
ZFMNW0805B	Bh intercepts			No significant change in zone geometry. However, target intercepts in KFR7A and KFR08 are no longer quoted since the respective intervals are inferred as being dominated by other zones and no exclusive evidence for the existence of ZFMNW0805B has been identified
ZFMNW0002	Name	ZFMWNW0804	ZFMNW0002	The preliminary model name of zone ZFMWNW0804 has been replaced by ZFMNW0002
	Thickness	40 m	58 m	Change based on a reassessment of tunnel mapping results

Appendix G

Methodology for evaluating conductivity from interference tests.

This appendix shows the methodology for interpreting conductivity from cross-hole tests used in /Carlsson et al. 1987/. The text is scanned from /Arnefors and Carlsson 1985, pp 28–32/.

5.2 Mellanhålstester

Kristallin berggrund kan betraktas som ett matrix genom vilket zoner av hydrauliskt konduktiva sprickor förekommer. I matrixet, som också benämns bergmassa (Carlsson et al 1983), förekommer sprickor vilka ej har motsvarande högkonduktiva egenskaper men vilka dock kan innehålla stora mängder vatten. Berggrunden kan, i enlighet med internationell fackterminologi, beskrivas som ett dubbel-poröst medium (jämför avsnitt 4.4.2). Vid utvärdering av mellanhålstester i sådant medium måste hänsyn tas till det flöde som inträffar mellan bergmassa och sprickzoner och som innebär att så kallad konventionell utvärdering med utnyttjande av ekv (4-1) och (4-8) leder till en överskattning av formationens hydrauliska konduktivitet och magasinskoefficient (Streltsova 1983 och 1984).

I den följande utvärderingen av de tre mellanhålstesterna har de teorier och matematiska behandlingar som presenterats av Streltsova (1983 och 1984) utnyttjats. Sålunda har primärt beaktats inom vilka sektioner som påverkan från respektive mellanhålstest utgör en påverkan längs en primär konduktiv sprickzon (i första hand sprickzon 9). I de sektioner som uppvisar påverkan men som geologiskt tolkats att ej innefatta någon primär sprickzon, har utvärderingen baserats på teorier gällande för bergmassa omgivande en eller flera sprickzoner. I de fall tryckförändringsförloppet uppvisar att en primär påverkan föreligger har dock en sådan tolkning i första hand utförts.

Figur 5.9 visar vattentrycksförändringen i en sprickzon som funktion av tid vid olika förhållanden mellan sprickzonens och bergmassans hydrauliska egenskaper. Parametern beta i figuren uttryckes genom ekv (5-1).

$$\text{beta} = \frac{r}{4\varepsilon}\sqrt{\frac{K_m}{K_f}\frac{S_{sm}}{S_{sf}}} \qquad (5\text{-}1)$$

där 2E = avståndet mellan hydrauliskt konduktiva sprickzoner.

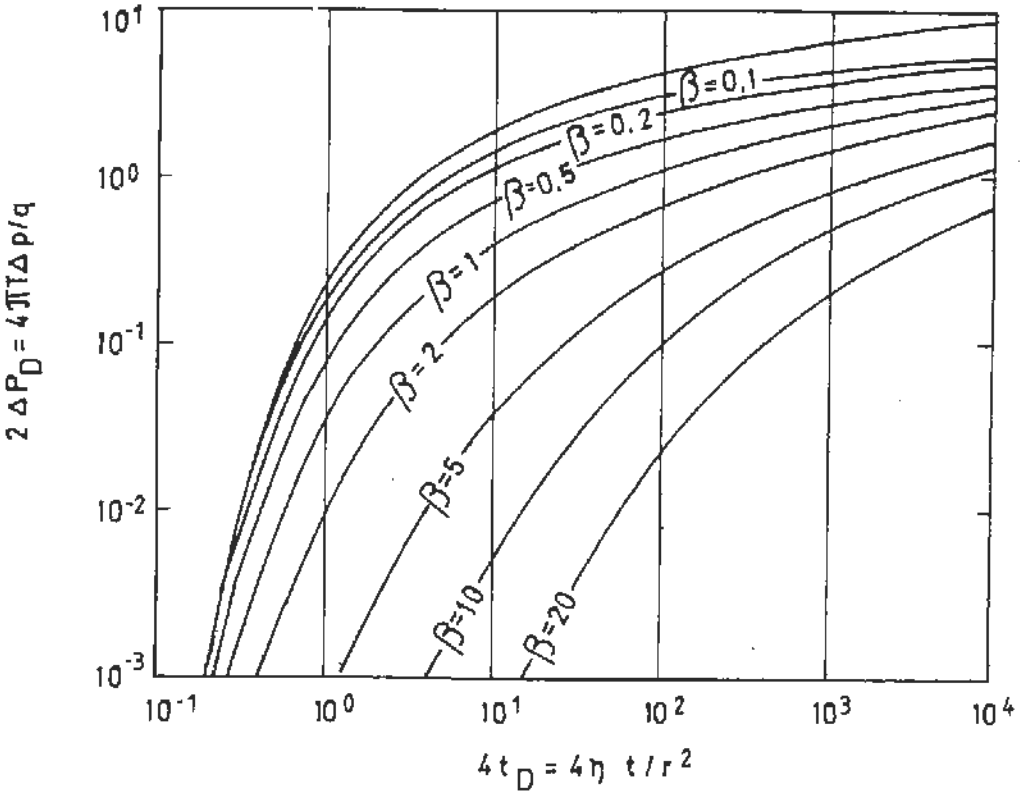

Fig.5.9. Vattentrycksförändring som funktion av tid, uttryckt i dimensionlösa enheter, för en sprickzon vid olika förhållanden mellan sprickzonens och omgivande bergmassas egenskaper (Streltsova 1983).

Kurvornas utseende är således beroende både av förhållandet mellan bergmassans och sprickzonens hydrauliska konduktiviteter samt mellan deras specifika magasinskoefficienter. Figurerna 5.10 och 5.11 visar renodlat inverkan av de båda nämnda förhållandena där r_D är given av ekv (5-2).

$$r_D = \frac{r}{H}\sqrt{\frac{K}{K_f}m-} \qquad (5\text{-}2)$$

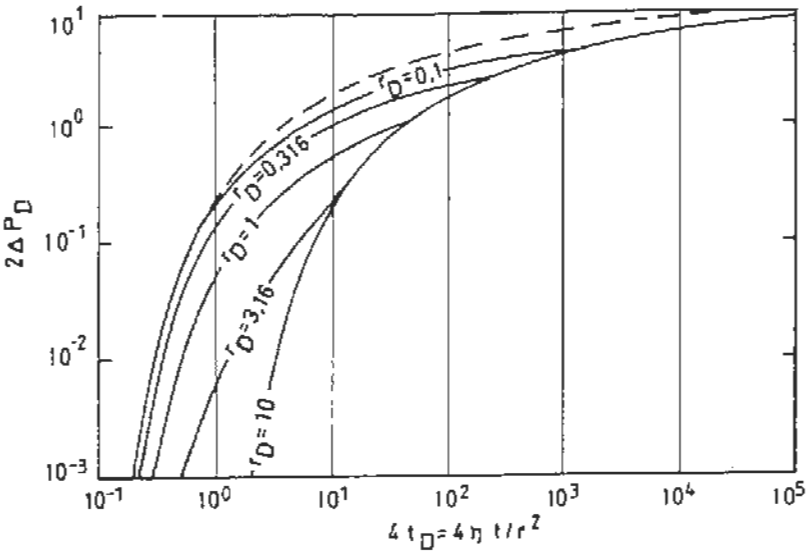

Fig.5.10. Vattentrycksförändring som funktion av tid, uttryckt i dimensionlösa enheter, för en sprickzon vid olika förhållanden mellan sprickzonens och omgivande bergmassas hydrauliska konduktiviteter, S_{sm}/S_{sf} = 10 (Streltsova 1983).

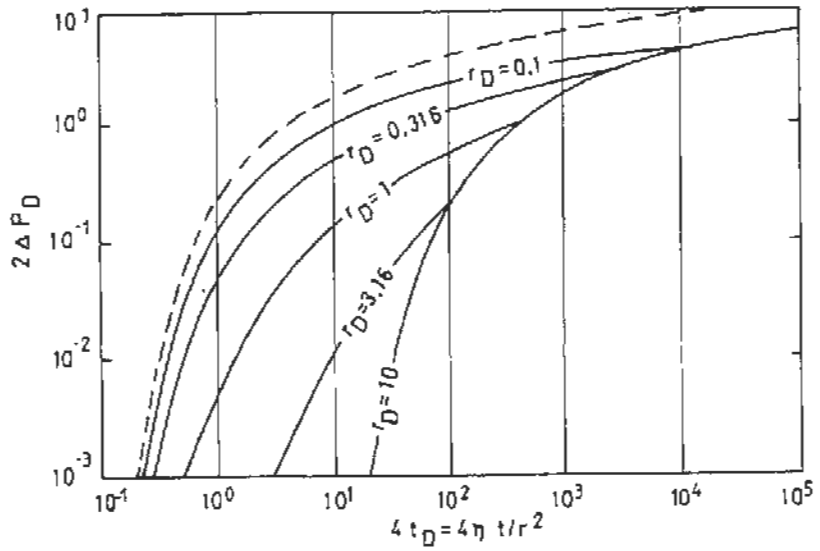

Fig.5.11. Vattentrycksförändring som funktion av tid, uttryckt i dimensionlösa enheter, för en sprickzon vid olika förhållanden mellan sprickzonens och omgivande bergmassas hydrauliska konduktiviteter, S_{sm}/S_{sf} = 100 (Streltsova 1983).

Vattentrycksförändringen i bergmassan omgivande en eller flera hydrauliskt konduktiva sprickzoner har ett avvikande förlopp från det i sprickzonerna. I figurerna 5.12 och 5.13 visas detta förlopp för olika värden på r_D och på förhållandena mellan de specifika magasinskoefficienterna. De visade förloppen avser en tryckförändring som utgör ett medelvärde genom hela det betraktade bergmatrix-blocket. Den fysikaliska förklaringen till lutningen 1:2 av tryckförändringen är den linjära diffusionsmekanismen som styr flödet mellan bergmassa och sprickzoner. En tryckförändringsregistrering i en punkt inom ett block kommer dock att visa ett förhållande som liknar Theis-kurvan enligt ekv (4-8), dock med kraftig förskjutning i horisontell led.

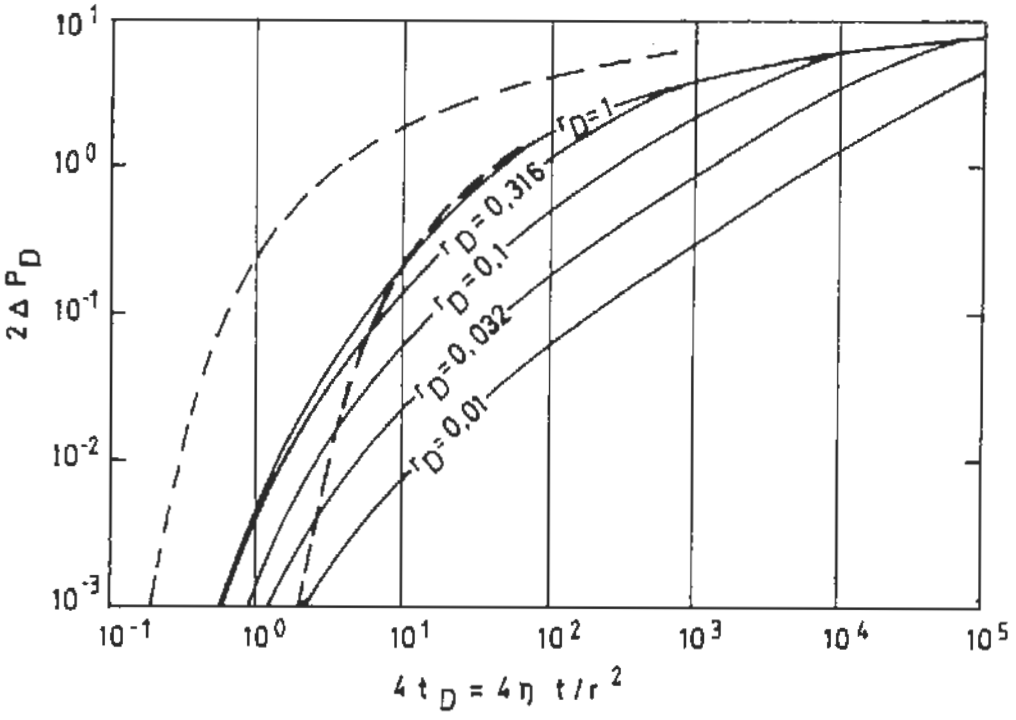

Fig.5.12. Vattentrycksförändring som funktion av tid, uttryckt i dimensionslösa enheter, i en bergmassa som omger en sprickzon vid olika förhållanden mellan bergmassans och sprickzonens hydrauliska konduktiviteter, $S_{sm}/S_{sf} = 10$ (Streltsova 1983)

Erhållna värden på hydraulisk konduktivitet från mellanhålstesterna beräknade enligt ekv (5-1) och (5-2) redovisas under avsnitt 6. I detta avsnitt redovisas och diskuteras också beräknade värden på specifika magasinskoefficienten. Erhållna sambandskurvor mellan tryck och tid redovisas i bilaga 3 för de registreringar som utförts medelst datalogger. Bilagorna 4 - 6 visar sambandskurvorna för övriga manuellt registrerade sektioner.

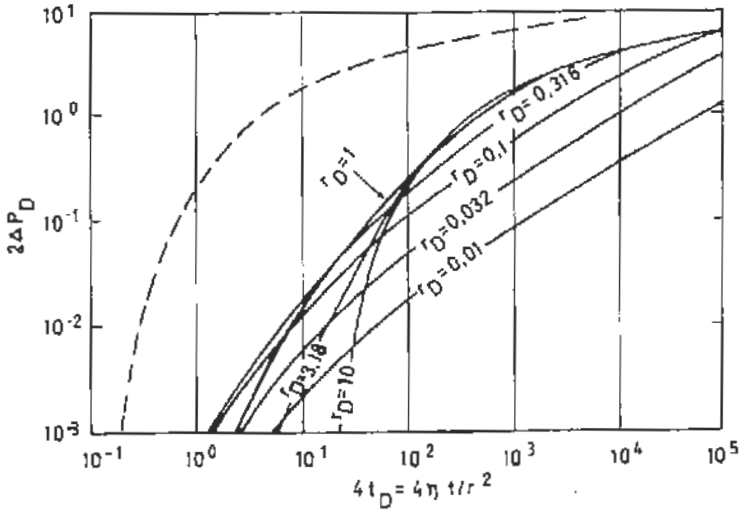

Fig.5.13. Vattentrycksförändring som funktion av tid, uttryckt i dimensionslösa enheter, i en bergmassa som omger en sprickzon vid olika förhållanden mellan bergmassans och sprickzonens hydrauliska konduktiviteter,
$S_{sm}/\ S_{sf}$ = 100 (Streltsova 1983)

Vid utvärderingarna har observerats att erhållna tryckavsänkningar under slutskedet av testernas flödesperiod är mindre än teoretiskt beräknade, (Diagram F, bilaga 3). Detta torde bland annat bero på det med tiden avtagande flödet under testernas flödesfas. Detta verkar också reducerande på tryckavsänkningen. Vidare har under samtliga testers genomförande bergarbeten pågått inom SFR. Dessa har medfört att en långvarig transient förändring av grundvattentryck pågår inom hela området, vilket bland annat registreras i pågående långtidsobservationer av grundvattentryck (Carlsson et al 1985).